Structural and functional analysis of *Syn*Cph2(1-2), a non-canonical phytochrome from *Synechocystis* sp. PCC 6803

Kumulative Dissertation

zur Erlangung des Doktorgrades der Naturwissenschaften

(Dr. rer. nat.)

dem

Fachbereich Chemie

der Philipps-Universität Marburg

vorgelegt von

Katrin Anders

aus Karl-Marx-Stadt

Marburg an der Lahn, 2014

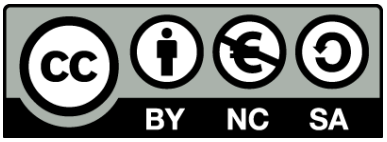

Structural and functional analysis of *Syn*Cph2(1-2), a non-canonical phytochrome from *Synechocystis* sp. PCC 6803

Kumulative Dissertation

zur Erlangung des Doktorgrades der Naturwissenschaften

(Dr. rer. nat.)

dem

Fachbereich Chemie

der Philipps-Universität Marburg

vorgelegt von

Katrin Anders

aus Karl-Marx-Stadt

Marburg an der Lahn, 2014

Vom Fachbereich Chemie der Philipps-Universität Marburg (Hochschulkennziffer 1180) als Dissertation am _____ angenommen.

Erstgutachter:	Prof. Dr. Lars-Oliver Essen Fachbereich Chemie, Philipps-Universität Marburg
Zweitgutachter:	Prof. Dr. Alfred Batschauer Fachbereich Biologie, Philipps-Universität Marburg

Tag der mündlichen Prüfung:

Publications:

Katrin Anders, David von Stetten, Jo Mailliet, Stephan Kiontke, Vitaly A. Sineshchekov, Peter Hildebrandt, Jon Hughes and Lars-Oliver Essen. **Spectroscopic and Photochemical Characterization of the Red-Light Sensitive Photosensory Module of Cph2 from *Synechocystis* PCC 6803.** Photochemistry and Photobiology. 2011; 87:160-173.

Philipp Savakis, Sven De Causmaecker, Veronika Angerer, Ulrike Ruppert, Katrin Anders, Lars-Oliver Essen and Annegret Wilde. **Light-induced alteration of c-di-GMP level controls motility of *Synechocystis* sp. PCC 6803.** Molecular Microbiology. 2012; 85:239-251.

Katrin Anders, Grazia Daminelli-Widany, Maria Andrea Mroginski, David von Stetten and Lars-Oliver Essen. **Structure of the cyanobacterial phytochrome 2 photosensor implies a tryptophan switch for phytochrome signaling.** The Journal of Biological Chemistry. 2013; 288:35714-35725.

Katrin Anders, Alexander Gutt, Wolfgang Gärtner and Lars-Oliver Essen. **Phototransformation of the red-light sensor Cph2 from *Synechocystis* sp. depends on its tongue motifs.** This research was submitted on 03.03.2014 to The Journal of Biological Chemistry.

Special achievements:

First poster prize at the International Conference of Tetrapyrrole Photoreceptors of Photosynthetic Organisms (ICTPPO) 2011, Berlin

The structure of *Syn*Cph2(1-2) was assigned “Structure of the month -December 2013”, Helmholtz Zentrum Berlin

"Die Neugier ist die mächtigste Antriebskraft im Universum, weil sie die beiden größten Bremskräfte im Universum überwinden kann: die Vernunft und die Angst."

Walter Moers

Table of contents

1 Summary

Phytochromes are photoreceptors that incorporate a bilin chromophore and can be found in plants, bacteria and fungi. Upon photoconversion between the red light (P_r) and far red light (P_{fr}) absorbing state the chromophore undergoes a $Z \rightarrow E$ double bond isomerization that triggers conformational changes within the protein environment. *Syn*Cph2 from *Synechocystis* sp. PCC 6803 comprises the domain architecture GAF1-GAF2-GGDEF1*-EAL-GAF3-GGDEF2, which indicates that it is a hybrid of a GAF-GAF bidomain phytochrome and a cyanobacteriochrome, represented by the GAF3 domain.

This work provides a detailed analysis of the N-terminal GAF1-GAF2 module. *Syn*Cph2(1-2) retains the red/far red photochemistry of canonical phytochromes, therefore, the GAF2 domain is able to substitute for the PHY domain in the latter. The PCB chromophore is covalently attached to Cys-129 in the GAF1 domain. In cooperation with the group of *P. Hildebrandt* we showed that all four pyrrole nitrogens are protonated in both P_r and P_{fr} states that comprise a *ZZZssa* and *ZZEssa* conformation, respectively. Accordingly, near UV/vis CD spectra of both states closely resemble *Syn*Cph1. Far UV CD data reveal an increase of the α-helical content of at least 3% in the $P_r \rightarrow P_{fr}$ transition which goes along with an increased hydrodynamic diameter of P_{fr} observed in size exclusion chromatography.

We solved the crystal structure of *Syn*Cph2(1-2) in the P_r conformation at a resolution of 2.6 Å. The knotless protein crystallizes as an antiparallel dimer, whereby the GAF1 domain connects to GAF2 *via* a long α-helical linker. The GAF2 domain mimics the overall organization of the PHY domain in protruding a tongue-like extension that covers the chromophore binding pocket of GAF1. The PCB chromophore in the *ZZZssa* conformation is non-planar and exhibits a high tilt between the B- and C- as well as C- and D-rings. UV/vis and RR spectroscopical studies as well as a QM/MM approach in cooperation with the group of *M. A. Mroginski* show that this conformation is not caused by radiation damage but is enforced by the protein matrix. Based on the structural data we performed a mutagenesis study involving the D-ring environment, the propionate interactions of the chromophore and the tongue region. We showed that the B-ring propionate interactions differ in *Syn*Cph2(1-2) compared to canonical phytochromes and seem to vary depending on the type of effector domain. Based on the observed α-helical increase in P_{fr} and the data for the amino acids in the conserved tongue motifs, we suggested a model for the structural changes during photoconversion. Here, a conformational switching of the tongue

region is supposed *via* swap of the tryptophans from the $W^G/_AG$ and WxE motifs that act as anchors in the P_{fr} structure. Upon photoconversion the Asp-Arg salt bridge between GAF1 and the tongue is broken, the PRxSF motif is reoriented and maybe structurally reorganized to an α-helical structure establishing a new Asp-Ser interaction.

We analyzed the photoconversion in *Syn*Cph2(1-2) and further illuminated the influence of the conserved PRxSF and WxE motifs. *Syn*Cph2(1-2) comprises four and three intermediates in the $P_r \rightarrow P_{fr}$ and $P_{fr} \rightarrow P_r$ photoconversion, respectively. Ser-385 of the PRxSF and Trp-389 of the WxE motif in the tongue region are ~13 Å and ~15 Å distant from the chromophore's D-ring, respectively, but they affect the formation of the P_{fr} state as S385A and W389A variants comprise an altered spectrum after red light illumination. The S385A mutation affects the last intermediate of the $P_r \rightarrow P_{fr}$ photoconversion and the first of the back reaction. The W389A mutation has major implications on the photocycle compared to S385A. It already affects the third intermediate that directly decays to a degenerated red light adapted state. The three intermediates of the back reaction to P_r all differ from *Syn*Cph2(1-2). In contrast, a phenylalanine substitution of Trp-389 results in wild type behavior, implying that the bulky and/or aromatic character of the tryptophan is important for its function as switch. Based on these results we concluded that during the $P_r \rightarrow P_{fr}$ photoconversion only the chromophore and its nearest surroundings are altered in the first two intermediates. During formation of intermediate R2 conformational changes occur in the tongue region, involving the tryptophan-switch. Formation of the last intermediate triggers the movement of Ser-385 and the formation of the hydrogen bond network involving the aspartate of GAF1 and Ser-385.

In a work performed with *P. Savakis*, *S. De Causmaecker* and *V. Angerer* and in cooperation with the group of *A. Wilde* we illuminated the role of the C-terminal GAF3-GGDEF2 module. *Syn*Cph2(5-6) comprises a photoconversion between a blue (P_b) and green light absorbing (P_g) state. It covalently attaches PCB to Cys-1022 and to Cys-994 and is able to isomerize the chromophore to PVB. The module can produce c-di-GMP in the GGDEF2 domain in a light dependent manner with P_g as the signaling state. *In vivo* studies in *Synechocystis* sp. confirmed these observations. Under blue light conditions the c-di-GMP production of *Syn*Cph2(5-6) leads to an inhibition of phototaxis as the type IV pili-dependent twitching motility of *Synechocystis* sp. is inhibited by large amounts of c-di-GMP. Nevertheless, only a coproduction of *Syn*Cph2(5-6) with *Syn*Cph2(1-4) can restore the wild type phenotype under white light thus proving the enzymatic activity of *Syn*Cph2(1-4) that is mediated by the EAL domain in degrading c-di-GMP.

Overall, the here presented studies on *Syn*Cph2 show the interplay between the photochemical and structural properties in the P_r / P_{fr} and P_b / P_g interconverting modules as well as their implications *in vivo*. Future studies will benefit from the enhanced knowledge about intramolecular signaling in phytochromes including the tryptophan switch hypothesis.

2 Zusammenfassung

Phytochrome sind Bilin-bindende Photorezeptoren, die in Pflanzen, Bakterien und Pilzen zu finden sind. Im Rahmen der Phototransformation aus einer Rotlicht- (P_r) in eine Dunkelrotlicht-absorbierende Form (P_{fr}) findet im Chromophor eine $Z \rightarrow E$ Doppelbindungsisomerisierung statt, die konformationelle Änderungen in der Proteinumgebung hervorruft. *Syn*Cph2 aus *Synechocystis* sp. PCC 6803 weist einen GAF1-GAF2-GGDEF1*-EAL-GAF3-GGDEF2 Domänenaufbau auf, was darauf hindeutet, dass es sich um ein Hybrid aus einem GAF-GAF-Bidomänen-Phytochrom und einem Cyanobakteriochrom (GAF3) handelt.

Diese Arbeit enthält eine detaillierte Analyse des N-terminalen GAF1-GAF2 Moduls. *Syn*Cph2(1-2) weist eine rot/dunkelrote Photochemie auf; somit ist die GAF2 Domäne in der Lage, die kanonische PHY Domäne zu ersetzen. Der Chromophor PCB ist kovalent an Cys-129 in der GAF1 Domäne gebunden. In Kooperation mit der Gruppe von *P. Hildebrandt* konnten wir zeigen, dass alle vier Pyrrolstickstoffe sowohl in P_r (*ZZZssa*) als auch in P_{fr} (*ZZEssa*) protoniert sind. Demzufolge ähneln die Nah-UV/Vis CD Spektren beider Zustände denen von *Syn*Cph1. In der Nah-UV CD Spektroskopie konnte ein 3%iger Anstieg des α-Helix Gehaltes in der $P_r \rightarrow P_{fr}$ Phototransformation festgestellt werden. Desweiteren erhöht sich in P_{fr} der hydrodynamische Durchmesser von *Syn*Cph2(1-2), was mittels Größenausschlusschromatographie festgestellt werden konnte.

Die Kristallstruktur von *Syn*Cph2(1-2) in der P_r Konformation konnte bei einer Auflösung von 2,6 Å gelöst werden. Das Protein kristallisiert als antiparalleles Dimer, wobei die GAF1 und GAF2 Domänen durch einen α-helikalen Linker verbunden sind. Die GAF2 Domäne ahmt den strukturellen Aufbau der kanonischen PHY Domäne nach, indem sie mit einem Zungen-ähnlichen Vorsprung die Chromophorbindungstasche in GAF2 abdeckt. Der Chromophor PCB in seiner *ZZZssa* Konformation ist nicht planar, sondern zeigt eine Verkippung der B-/C- sowie der C-/D-Ringe gegeneinander. In UV/Vis- und RR-spektroskopischen Untersuchungen sowie QM/MM Berechnungen in Kooperation mit der Gruppe von *M. A. Mroginski* konnten wir zeigen, dass diese Konformation nicht durch Strahlenschaden ausgelöst, sondern von der Proteinumgebung erzwungen wird. Basierend auf der Kristallstruktur führten wir eine Mutagenesestudie durch, die die D-Ringumgebung und Propionatinteraktionen des Chromophors sowie die Zungenregion umfasste. Dabei unterscheiden sich die B-Ringpropionatinteraktionen von kanonischen Phytochromen und scheinen vom Typ der Effektordomäne abzuhängen. Die Analyse konservierter Motive in

der Zungenregion führte zu einem Modell, das die strukturellen Änderungen während der Photokonversion beschreibt. Dabei wird die Zungenregion durch einen Trp-Positionstausch in den W$^{G}/_{A}$G und WxE Motiven verdreht, die als Anker die P_{fr} Struktur stabilisieren. Desweiteren bricht die Asp-Arg Salzbrücke, das PRxSF Motiv wird reorientiert und wahrscheinlich α-helikal, wodurch sich die neue Asp-Ser Interaktion ausbilden kann.

Eine nähere Untersuchung der Photokonversion in *Syn*Cph2(1-2) ergab, dass sich vier Intermediate in der $P_r \rightarrow P_{fr}$ und drei in der $P_{fr} \rightarrow P_r$ Photokonversion bilden. Trotz ihrer Distanz von ~13 Å und ~15 Å zum D-Ring des Chromophors, beeinflussen Ser-385 aus dem PRxSF und Trp-389 aus dem WxE Motiv die Bildung des P_{fr} Zustandes. Die S385A Mutation wirkt sich auf das letzte Intermediat der $P_r \rightarrow P_{fr}$ Photokonversion und das erste der Rückreaktion aus. Die W389A Mutation zeigt größere Auswirkungen auf den Photozyklus als S385A. Sie beeinflusst schon das dritte Intermediat, das direkt in einen degenerierten Rotlicht-adaptierten Zustand zerfällt. Die drei $P_{Deg} \rightarrow P_r$ Intermediate unterscheiden sich alle von *Syn*Cph2(1-2). Ein Austausch von Trp-389 mit Phenylalanin stellt das Wildtyp-ähnliche Verhalten wieder her, was auf die Bedeutung der sterischen Ausdehnung und/oder Aromatizität des Tryptophans für seine Funktion als Schalter hinweist. Wir schlussfolgern, dass in den ersten zwei Intermediaten nur der Chromophor und seine nächste Umgebung von Veränderungen betroffen sind. Während der Bildung von Intermediat R2 treten die strukturellen Änderungen in der Zungenregion auf, die den oben postulierten Tryptophanwechsel beinhalten. Die Bildung des letzten Intermediates leitet die Reorientierung von Ser-385 und die Ausbildung des Wasserstoffbrückennetzwerkes ein, das das Aspartat der GAF1 Domäne sowie Ser-385 einschließt.

Im Rahmen einer Arbeit, die mit *P. Savakis*, *S. De Causmaecker* und *V. Angerer* in Kooperation mit der Gruppe von *A. Wilde* ausgeführt wurde, konnten wir die Rolle des C-terminalen GAF3-GGDEF2 Moduls beleuchten. *Syn*Cph2(5-6) photokonvertiert zwischen einer Blau- (P_b) und Grünlicht-absorbierenden (P_g) Form. PCB ist kovalent an Cys-1022 und Cys-994 gebunden und wird zu PVB autoisomerisiert. Das Modul ist in der Lage, lichtabhängig c-di-GMP in der GGDEF2 Domäne herzustellen, wobei der Signalzustand P_g auch in *in vivo* Studien in *Synechocystis* sp. bestätigt wurde. Unter Blaulichtbedingungen führt die c-di-GMP Herstellung von *Syn*Cph2(5-6) zu einer Inhibierung der Phototaxis, da die Motilität von *Synechocystis* sp. von hohen c-di-GMP Konzentrationen inhibiert wird. Durch Koproduktion von *Syn*Cph2(5-6) und *Syn*Cph2(1-4) konnte der Wildtypphenotyp unter Weisslicht wiederhergestellt werden, was zeigt, dass *Syn*Cph2(1-4) eine enzymatische Aktivität aufweist, die durch die c-di-GMP-abbauende EAL Domäne verursacht wird.

Die hier dargelegten Studien von *Syn*Cph2 zeigen das Zusammenspiel von photochemischen und strukturellen Eigenschaften in den P_r / P_{fr} und P_b / P_g interkonvertierenden Modulen sowie ihre Bedeutung *in vivo*. Zukünftige Studien profitieren von den Einblicken in die Signaltransduktion in Phytochromen und insbesondere von der Trp-Schalterhypothese.

3 Introduction

The sun radiates $63.29 \cdot 10^3 \frac{kW}{m^2}$ [1], representing 10^{21} times the power of the 434 nuclear power plants on earth [2]; $1.36 \frac{kW}{m^2}$ [3] reach the surface of our planet. Already in earth's early history the arising life used this energy to perform metabolic processes. Cyanobacteria are among the first organisms that carried out photosynthesis. They appeared in the precambrian 2.8 billion years ago [4] and needed to adapt to their environment. For organisms that utilize light as an energy source, sensing of parameters, such as light quantity (intensity) and quality (wavelength composition), is of paramount importance. As a result, photoreceptor proteins evolved. Because organisms utilize different parts of the electromagnetic spectrum, this protein class exhibits a high diversity respective composition and functionality (Fig. 3.1). Reaching from UVR8 (**UV**-light **R**esistance locus **8**), a UV-B (**U**ltra**V**iolet-**B**) photoreceptor that absorbs intrinsically *via* tryptophan residues, over rhodopsines, PYP- (**P**hotoactive **Y**ellow **P**rotein), LOV- (**L**ight **O**xygen **V**oltage) or BLUF (sensors of **B**lue-**L**ight **U**sing **F**AD)-domain proteins, cryptochromes, photolyases to phytochromes [5,6] that all bind an organic molecule as light absorbing chromophore, the whole light spectrum from UV to IR light is covered.

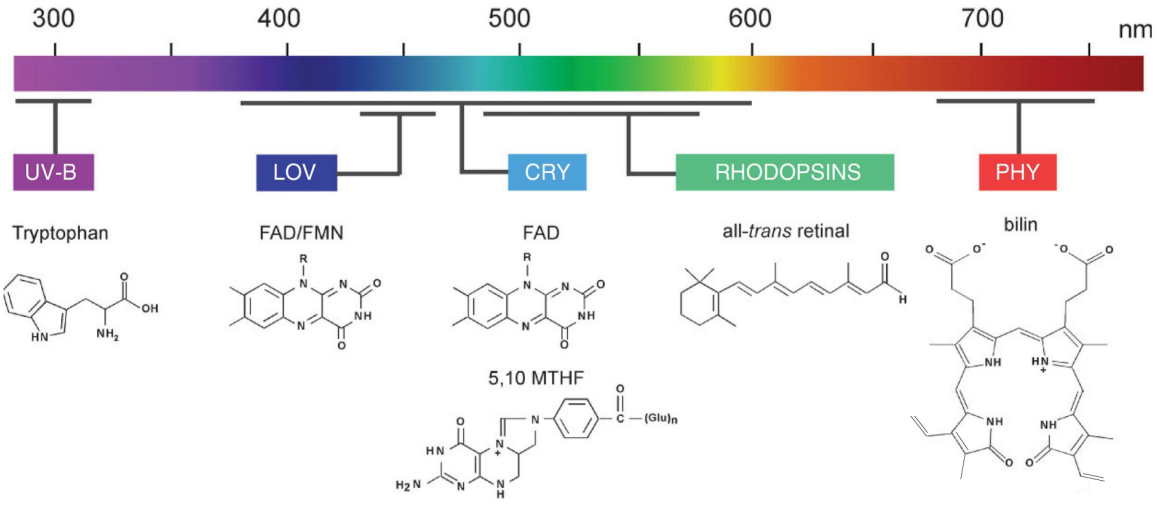

Figure 3.1: The different photoreceptors and their light absorption preferences. Chromophore structures of the respective photoreceptors are shown below (figure modified after Ref. [5]). UV-B: UV receptors as UVR8; LOV: **L**ight **O**xygen **V**oltage domain containing proteins; CRY: **cry**ptochromes; PHY: **phy**tochromes; FAD: **F**lavin **A**denine **D**inucleotide; FMN: **F**lavin **M**ono**N**ucleotide; 5,10-MTHF: 5,10-**M**ethenyl**T**etra**H**ydro**F**olate.

3.1 Phytochromes

Phytochromes are red / far red light photoreceptors with an incorporated bilin chromophore These proteins can be found in photosynthetic organisms such as plants, bacteria, cyanobacteria and in non-photosynthetic organisms like fungi[7], respectively. They exist in two stable conformations that can be photointerconverted: the red light absorbing P_r conformation can be transferred to the far red light absorbing P_{fr} state *via* red light illumination. Conversion of P_{fr} to P_r can be achieved through irradiation with far red light. Furthermore, conversion can happen in a light-independent process, known as dark reversion[7]. Rockwell *et. al.*[8] divided the biliprotein photoreceptors into three families based on their photosensory domain architecture. Group I includes the canonical phytochromes that possess a PAS-GAF-PHY (PAS: **P**er-**A**RNT-**S**im, GAF: c**G**MP phosphodiesterase/**A**denyl cyclase/**F**hlA, PHY: **phy**tochrome) domain architecture in their sensor region. Firstly discovered in plants[9] this domain organization can also be found in bacterial and other eukaryotic phytochromes[7]. Biliverdin (BV) binding phytochromes from bacteria are called bacteriophytochromes (Bphs or BphPs), fungal and diatom phytochromes Fphs or Dphs, respectively[7,8]. Group I phytochromes comprise a PAS and GAF domain that have a backbone conformation forming a knot, in which the N-terminus protrudes through a loop region of the GAF domain[10–13].

Phytochromes of Group II and III are exclusively found in cyanobacteria. Cyanobacterial phytochromes 2 (Cph2), that build Group II, lack the N-terminal PAS domain and are thus unknotted; their photosensory region consists of a GAF-bidomain. Group III consists of a family of biliprotein photoreceptors that does not only possess a red / far red light photochemistry but covers the whole spectrum of light with its different representatives. These cyanobacteriochromes (CBCRs)[14] are GAF-only photoreceptors where the GAF domain suffices to attach the chromophore and performs functional photochemistry in contrast to other phytochromes[8].

All members of the three families incorporate a bilin cofactor that is covalently bound *via* a thioether linkage. The domain composition in phytochrome sensory regions is limited to GAF, PAS and PHY domains. The N-terminal extensions however show some variability among the organisms. GAF domains are named after the three proteins where they were first described, a vertebrate cGMP-specific phosphodiesterase[15], a cyanobacterial adenylate cyclase and the bacterial formate hydrogen lyase transcription activator FhlA[16]. They can also be found in guanylyl cyclases, in phytochromes and CBCRs as well as in other bacterial enhancer binding proteins such as NifA, a transcriptional activator for operons involved in nitrogen fixation[17]. GAF domains are about 150 amino acids in length and often bind small, planar, aromatic ligands including tetrapyrroles, flavins, flavonoids and nucleotides[16].

PAS domains were first identified by sequence homology in the *Drosophila* proteins **P**eriod and **S**ingle-minded as well as in the vertebrate **A**ryl hydrocarbon receptor nuclear transporter (ARNT). They occur in all kingdoms of life[18]. PAS domains are sensory modules of signal transduction proteins, typically sensing oxygen tension, redox potential or light intensity. They also bind small ligands and mediate protein-protein interactions[19]. The majority of PAS containing proteins are sensor histidine kinases of the prokaryotic two-component signaling systems. PAS domains can also often be found in serine/threonine kinases, guanylate cyclases, phosphodiesterases, transcription factors, ion channels and chemotaxis proteins. Typically, they are linked to the N-terminus of the effector domains in the given systems[18].

PAS domains are composed of 100-120 amino acids and vary in their primary sequence though they share a conserved three-dimensional fold. This fold consists of a PAS and PAC motif which are linked by a flexible region that can adopt different conformations depending on the bound ligand[20]. The central antiparallel β-sheet consists of five strands in the topological order of 2-1-5-4-3 which are flanked by several α-helices whose number, length and orientation deviate[18]. Special PAS domains that bind flavin nucleotides and show phototropin-like photochemistry are called LOV domains.

PAS domains share a high structural similarity with GAF domains that are composed of a six-stranded antiparallel β-sheet with strand topology 3-2-1-6-5-4. This corresponds to an additional strand inserted between strand 2 and 3 of the PAS domain. The structural similarities and the fact that PAS and GAF domains are linked to the same classes of effector domains confirm that they might share a common evolutionary origin[18,21].

The phytochrome (PHY) domain was found to be structurally related to a GAF domain and is exclusively found in phytochromes[10,11,16]. This domain stabilizes the photoexcited state of phytochromes[22,23].

3.2 Chromophores of phytochromes and other biliproteins

Photoreceptor chromophores exhibit high diversity. In contrast to tryptophan residues in a UV light receptor, flavins in blue light receptors or retinal in opsins, phytochromes and CBCRs bind a cofactor that allows them to cover an enormous spectral range: a bilin. These molecules have an intense absorption, which is even more enhanced by the protein environment, are stable, offer long-lived excited states[24] and are non-toxic to the cell. Bilins are linear tetrapyrroles with three additional double bonds at the carbon bridges between the pyrrols and therefore possess 11 double bonds in total that make up a conjugated system. Tetrapyrroles can be also found in chlorophyll breakdown, where the toxic chlorophyll is converted to a fully reduced linear tetrapyrrole that cannot absorb

light anymore. They can also be found in cyanobacterial light harvesting complexes, the phycobilisomes. These complexes are located on the outer surface of the thylakoid membrane and consist of different types of phycobiliproteins. They are arranged to a central core with hexamers stacked over another forming rod-shaped extensions [25]. According to this organization of phycobiliproteins with different bilins and absorption maxima, the excitation energy is transferred from the periphery with proteins of the highest to the core region with proteins of the lowest excitation energy. From the core the energy is transferred to the membrane bound photosystem II. Phycobiliproteins are highly fluorescent and have antioxidative properties; they are used in applications like foods, cosmetics, biotechnology, diagnostics and medicine [26]. Phycobiliproteins can covalently bind the bilin chromophore, but depend on lyases for this process. This is in contrast to GAF domains, which can attach their chromophore autocatalytically. Although phycobiliproteins have completely different functions in light harvesting, compared to the phytochrome photoreceptors and are phylogenetically only distantly related to them, they possess similar chromophores, the same mode of covalent binding of these and similar interactions to the apoproteins [24].

The biosynthesis of all bilin chromophores (see Fig. 3.2) starts with the precursor pro-

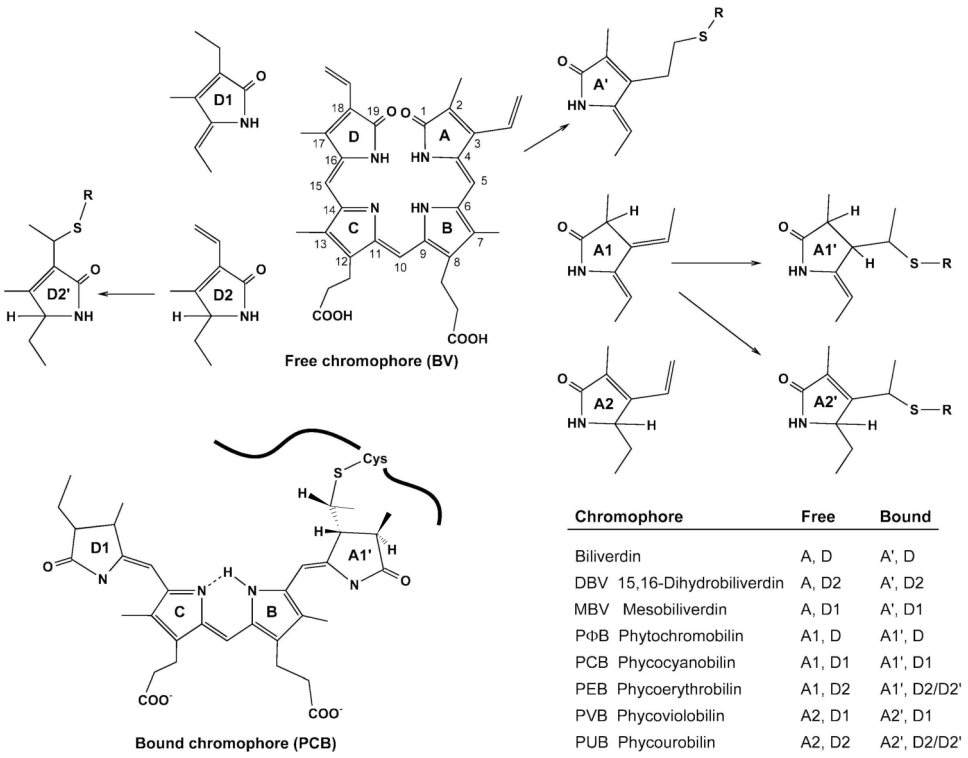

Chromophore	Free	Bound
Biliverdin	A, D	A', D
DBV 15,16-Dihydrobiliverdin	A, D2	A', D2
MBV Mesobiliverdin	A, D1	A', D1
PΦB Phytochromobilin	A1, D	A1', D
PCB Phycocyanobilin	A1, D1	A1', D1
PEB Phycoerythrobilin	A1, D2	A1', D2/D2'
PVB Phycoviolobilin	A2, D1	A2', D1
PUB Phycourobilin	A2, D2	A2', D2/D2'

Figure 3.2: Free and covalently attached bilins. The full structures show biliverdin (BV) as unbound and phycocyanobilin (PCB) as protein bound chromophore. The partial structures display the modified rings A and D in other biliprotein chromophores where rings B and C remain unchanged. Protein-linked rings are marked by a prime. The table includes the name and constitution of bilin chromophores found in phytochromes and phycobiliproteins (figure modified after Ref. [24]).

toheme, a macrocycle that is also present in hemoglobin and myoglobin. Protoheme is cleaved by the enzyme heme oxygenase (HO1) at the α-methine bridge. The resulting biliverdin IXα (BV) is attached as chromophore without further modifications in bacteriophytochromes and fungal phytochromes[7]. Reduction of BV at one or two out of three possible positions by ferredoxin-dependent bilin reductases yields all other phytobilins[24]. The ferredoxin-dependent biliverdin reductase HY2 is responsible for the biosynthesis of phytochromobilin (PΦB), a chromophore exclusively found in plant phytochromes[27]. The PCB:ferredoxin oxidoreductase (PcyA) synthesizes phycocyanobilin (PCB), which can be found in cyanobacterial phytochromes and CBCRs, *via* a regio-specific reduction of the *exo* vinyl group of ring D and the *endo* vinyl group of ring A of BV using four electrons from reduced ferredoxin[28]. Phycoerythrobilin (PEB), a chromophore in phycobiliproteins, is synthesized from BV either in two sequential reactions of two reductases, PebA and PebB with the intermediate dihydrobiliverdin (DBV), that is present in cryptophyte biliproteins[24], or by the cyanoviral bifunctional enzyme PebS, that combines both activities on one polypeptide chain[29]. The reductase which catalyzes the reduction from BV to mesobiliverdin (MBV) in cryptophyte biliproteins is unknown[24]. Apart from PCB and PEB, phycobiliproteins harbor phycourobilin (PUB) and phycoviolobilin (PVB) chromophores, which are synthesized from PEB and PCB, respectively. Interestingly, the lyases that perform the isomerization also attach the matured chromophores to the corresponding apo-protein[30]. In CBCRs that also bind PVB, no additional lyase or isomerase is needed, the GAF domains itself are able to isomerize PCB to PVB. In green algae and non-vascular plants an additional reductase, PubS, was discovered recently, that catalyzes the conversion of BV to PUB. The function of PUB in plants remains elusive; the authors suggest a reversible binding of PUB to apo-phytochromes[31].

3.3 Phytochrome photoconversion

The quantum yield of phytochrome photoconversion is quite low (Φ= 0.16)[32] in comparison to the antenna pigment C-phycocyanin, where the energy transfer to the reaction center is above 90%[33]. This difference is due to the chromophore embedding. Rigid embedding results in good energy transfer, whereas in phytochromes the chromophore is loosely held, thus vibrations compete with the primary photochemical process[34].

P_r to P_{fr} kinetics are completed within milliseconds up to seconds, while the first intermediate appears in the pico second range[35]. In the primary photochemical process a $Z \rightarrow E$ double bond isomerization between C15 and C16 of the chromophore (see Fig. 3.2) takes place, forming the first intermediate I_{700}, which is also called Lumi-R according to the nomenclature of rhodopsins[35]. All the following spectroscopical intermediates result from relaxation processes of the chromophore or the protein surroundings, where the

protein adapts to the new energetic conditions and needs no further light input. The first intermediate within these thermal reactions shows very weak absorbance and is therefore named I_{bl} (bl = bleached) or Meta-R[35]. The subsequent intermediates are P_{fr}-like with only minor absorbance changes[35].

Interestingly, the native phytochrome A (phyA) exhibits a primary photoproduct that is composed of two thermally metastable components I^1_{700}, I^2_{700}[34]. They convert with two different time constants into I_{bl}.

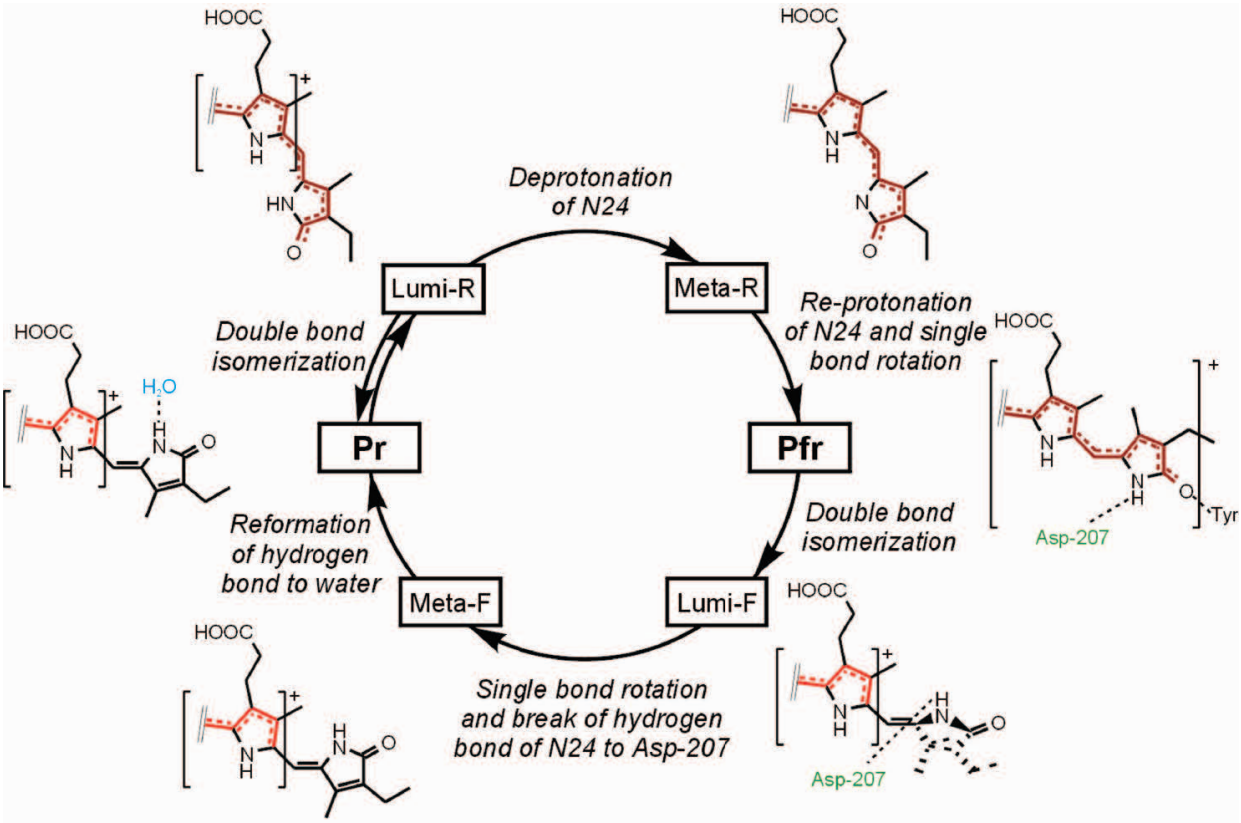

Figure 3.3: Phytochrome photocycle. The changes of the chromophore during photoconversion are highlighted by the display of the rings C and D. N24 refers to the D-ring nitrogen, Asp-207 to the *Syn*Cph1 numbering[36]. Intermediates are shown in thin lettering.

The photocycle intermediates have been studied by optical and vibrational spectroscopic methods, the intermediates of the $P_r \rightarrow P_{fr}$ reaction are solely characterized by these techniques. For the reverse $P_{fr} \rightarrow P_r$ reaction also NMR data exists[37]. After the primary photoisomerization process from P_r to Lumi-R including the $Z \rightarrow E$ photoisomerization of the C-D methine bridge (Lumi-R) the following thermal relaxation process involves a transient deprotonation in the Meta-R state[38]. It takes place at the D-ring nitrogen N24, where the proton is transferred to a nearby water molecule resulting in a neutral chromophore. During the transformation of Meta-R to P_{fr} this D-ring nitrogen is reprotonated[36,37].

The backward photoconversion $P_{fr} \rightarrow P_r$ undergoes different intermediates than the

forward reaction[39]. According to the nomenclature, they are called Lumi-F and Meta-F. In contrast to the $P_r \rightarrow P_{fr}$ photoconversion, all pyrrole nitrogens remain protonated during the whole process. After double bond isomerization at C15/C16 leading to Lumi-F a partial single bond rotation at C14/C15 takes place resulting in the Meta-F intermediate. The last step to P_r is a pure relaxation process involving the formation of a hydrogen bond between the ring D-nitrogen and a water molecule[36] (see Fig. 3.3).

Both photochemical reactions use different mechanisms. In the $P_r \rightarrow P_{fr}$ phototransformation the reaction is driven protonically after double bond isomerization. In the backward reaction $P_{fr} \rightarrow P_r$ the mechanical force of the partial single bond rotation initiates the change of the hydrogen bond partner. The different trigger in the two conversion reactions makes this photocycle unidirectional[36].

3.4 Group I: PAS-GAF-PHY phytochromes

Phytochromes with a sensor module comprised of a PAS, GAF and PHY domain are the most widespread family members. They are found in plants, fungi, but also in bacteria including cyanobacteria, where they perform red / far red photochemistry. The chromophore attachment site varies from the PAS domain in bacterial and fungal phytochromes binding BV to the GAF domain in plant and cyanobacterial phytochromes that attaches PΦB or PCB (see Fig. 3.4). All crystal structures of Group I members show that the N-terminal helix of the PAS domain threads through a loop region of the GAF domain thus creating a figure-of-eight knot within the protein backbone[10,11]. Although the PAS-GAF-PHY archi-

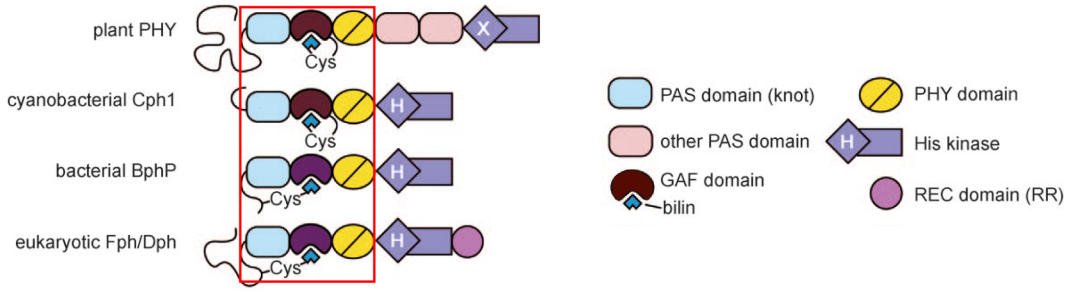

Figure 3.4: Domain architecture of Group I phytochromes following[8]. Fph and Dph refers to fungal and diatom phytochromes, respectively. The chromophore attachment site with the conserved cysteine as well as the N-terminal extension from the PAS domains are presented. The red frame indicates the PAS-GAF-PHY domain photosensory module that is characteristic for Group I phytochromes. Plant phytochromes have additional PAS domains in their C-terminal effector module as well as a HK-related domain (X) without a conserved histidine residue. In contrast to other phytochromes Fphs and Dphs have C-terminal response regulator receiver domains (RR).

tecture is conserved throughout the different organisms, the length of the N-terminal extensions varies considerably, and the C-terminal effector module utilizes different architectures, too.

3.4.1 Plant phytochromes

Phytochromes regulate seed germination, greening, stem extension, flowering and other processes in plants[40] and can be seen as estimator of spectral changes within plant communities. Daylight exhibits a red to far red light ratio of 1.2 to 1 which decreases throughout the vegetation layers because photosynthetic pigments like chlorophyll absorb red light but not far red light[41]. Plant phytochromes absorb with $\lambda_{max}\sim$ 660 nm in the P_r ground state and $\lambda_{max}\sim$ 705-730 nm in the P_{fr} conformation[40] and can thus sense the ratio of red and far red light. The latter is a signal for the proximity of neighbors and community density[41].

In contrast to prokaryotes, P_{fr} is always the physiologically active state in plants and triggers photomorphogenesis[40]. Plant phytochromes bind PΦB with only a few exceptions (see section 3.7). *Arabidopsis thaliana* possesses the five different phytochromes PhyA-E, which diverge by up to 50% from each others sequence[42]. The phytochrome genes involve three main clades: *phyA*, *phyB* and *phyC*. Some species have additional phytochrome genes which are included in the *phyB* lineage[43]. PhyA is supposed to be the primary photoreceptor for mediating far red light regulation of gene expression. It is very photolabile; upon red light illumination and transition into P_{fr} PhyA is proteolytically degraded *in vivo* whereas PhyB is relatively stable in the light[44].

The architecture of plant phytochromes is shown in figure 3.4. Notable features are the long N-terminal extension (NTE) and the effector module consisting of two PAS domains, called PAS repeat, and a histidine kinase-related domain. This module is important for dimerization and downstream signaling[42]. Figure 3.5 represents a relative assignment of functions to the domains. The NTE was shown to be important for biological activity. Its N-terminal serine-rich sequence is involved in channeling downstream signaling *via* high or low fluence pathways in different cellular contexts, as shown for PhyA from *Avena sativa*[46]. The diverse NTEs of PhyA and B are thought to be responsible for the different photosensing specificities[47]. In the effector module, the PAS repeat is crucial for signaling *via* interactions with the phytochrome-interacting factor 3 (PIF3)[42]. The histidine kinase-related domain lacks the conserved histidine phosphoacceptor site though it is related to bacterial histidine kinase domains. Nevertheless, biochemical studies suggest that phytochromes are light-regulated kinases as phytochromes from *Avena sativa* and the green alga *Mesotaenium caldariorum* showed serine / threonine kinase activity[48].

Plant phytochrome signaling is very complex because it occurs in the cytoplasm as well as in

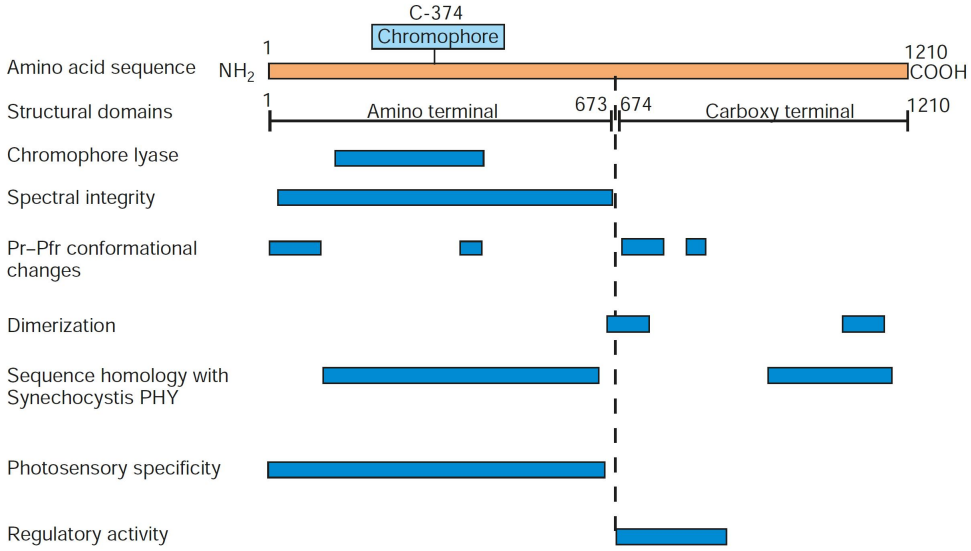

Figure 3.5: Molecular map of plant phytochromes with an assignment of the different functions to protein regions. The numbering relates to *Arabidopsis* PhyB. The "amino terminal" correlates to the photosensory region consisting of the N-terminal extension and the PAS-GAF-PHY domains as well as the chromophore attached to Cys-374. The "carboxy terminal" refers to the PAS repeat and the HK-related domain ([41] with simplifications; originally from [45]).

the nucleus and involves different pathways [40,49] (see Fig. 3.6). In the dark, phytochromes are localized mainly in the cytoplasm. After red light illumination PhyA and PhyB accumulate in the nucleus. PhyB contains a nuclear localization signal (NLS) in its C-terminal effector module that is masked by the N-terminal photosensory module in P_r. In P_{fr} the interaction is less strong leading to the unmasking of the NLS. PhyA does not contain an NLS; it is shuttled by two NLS containing proteins, FHY1 (**F**ar red elongated **Hy**pocotyl **1**) and FHL (**FH**Y1-**L**ike), into the nucleus [49]. There, the phytochromes form local protein clusters, called phytochrome speckles, nuclear bodies or photobodies [50]. Early speckles containing PhyA and B can be detected after 1-2 min of red light illumination after darkness. They disappear after 1 h of light exposure. Also FHY1, FHL and PIF3 and PIF7 can be found in these early speckles. After 2 h of red light the phytochrome speckles reappear and linger in the light. Because PhyA is rapidly degraded in the light, these late speckles contain mainly PhyB. The function of the speckles is still under discussion involving several theories. One refers to speckles as storage depots for activated phytochromes without being sites of signaling events, another one sees them as sites of phytochrome signaling because there is a close correlation between the localization of PhyB in speckles and PhyB-mediated responses [51]. A third model supposes speckles as sites for degradation of photolabile proteins [49].

PhyA and PhyB concentrations are down regulated from dark to red light, PhyA levels 50-100-fold, PhyB five-fold [49]. The P_{fr} conformation of PhyA is degraded ubiquitin-

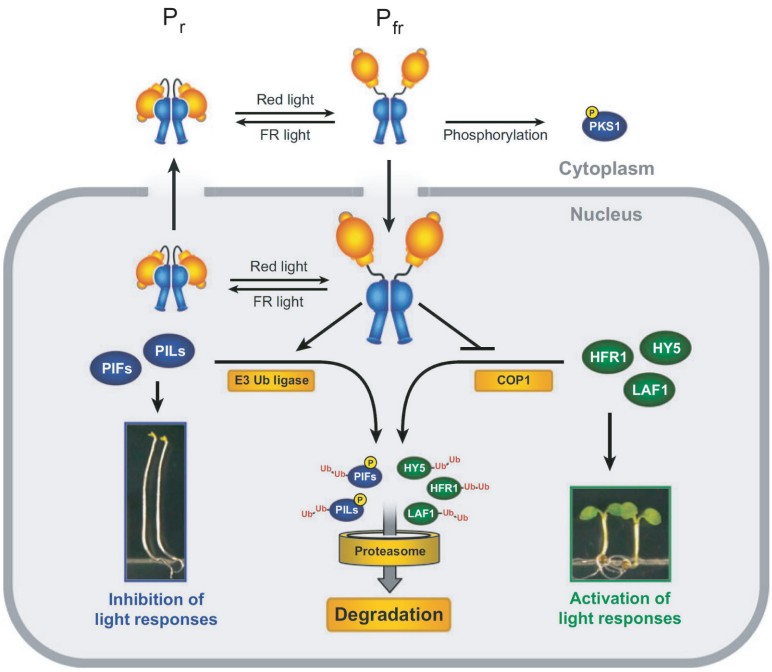

Figure 3.6: Simplified model of plant phytochrome signal transduction[52]. In the dark phytochromes are accumulated in the P_r conformation. Upon red light illumination the P_{fr} state is built including huge conformational changes. In the cytoplasm the phytochrome binds and phosphorylates phytochrome kinase substrate 1 (PKS1) and interacts with nucleoside phosphate dikinase 2 (NDPK2). Furthermore, the phytochromes enter the nucleus, PhyA with the help of two proteins, PhyB because of its intrinsic nuclear localization signal (NLS). In the nucleus light responses are repressed in the dark because negative transcription components like phytochrome-interacting factors (PIFs) and PIF3-like proteins (PILs) inhibit light responses whereas positive components like HFR1 (long **H**ypocotyl in **F**ar **R**ed **1**), LAF1 (**L**ong **A**fter **F**ar-red light **1**) and HY5 (long **Hy**pocotyl **5**) are degraded dependent on the *constitutive photomorphogenic 1* (COP1). When the phytochrome in its P_{fr} conformation enters the nucleus, it activates the degradation of PIFs and PILs and excludes COP1 from the nucleus, thus inhibiting the degradation of HFR1, LAF1 and HY5.

proteasome-dependent. It is bound by a E3 ubiquitin ligase complex where COP1 (**Co**nstitutive **P**hotomorphogenic **1**) with other proteins builds the substrate receptor for the E3 ubiquitin lyase. Phosphorylation of PhyA enhances the binding to this complex and thus the degradation of the protein. As PhyA and COP1 are both localized on speckles, the degradation seems to be located there. PhyB degradation is also mediated by COP1[49].

In the dark, PIFs and PIF3-like proteins (PILs) that are transcription factors which negatively regulate photomorphogenesis, inhibit light responses. Positive transcription factors like HFR1 (long **H**ypocotyl in **F**ar **R**ed **1**), LAF1 (**L**ong **A**fter **F**ar red light **1**) and HY5 (long **Hy**pocotyl **5**) are degraded in a COP1-dependent manner in the dark[52]. Upon irradiation phytochromes in the P_{fr} state directly reverse this by inducing a rapid degradation of the PIFs and PILs[53] (see Fig. 3.6). PIFs bind the phytochromes in their

photo activated P_{fr} conformation and are phosphorylated and degraded by the ubiquitin-proteasome system[49]. Phytochromes also inhibit the COP1-dependent degradation of HFR1, LAF1 and HY5 by excluding it from the nucleus[52].

Phytochrome signaling in the cytoplasm is much faster, it occurs within minutes or even seconds[40]. Although the knowledge about signaling in the nucleus is more advanced, some interaction partners of phytochromes in the cytoplasm are known. Within the cytosolic phytochrome kinase substrate (PKS) family PKS1 is bound and phosphorylated by PhyA and B[54]. PhyA also interacts with nucleoside phosphate dikinase 2 (NDPK2) whose enzymatic activity is enhanced by P_{fr} binding[40]. The formation of P_{fr} is followed supposedly by activation of heterotrimeric G-proteins leading to changes in the cytosolic cGMP and Ca^{2+} levels[55]. The phytochrome signal in the cytoplasm seems to provide directional information thus the mechanism is not settled at the moment. In higher plants an interaction between phytochrome and phototropin seems to take place at the plasma membrane enabling the steering of directional responses[40,56].

3.4.2 Fungal phytochromes

Fungi are non-photosynthetic eukaryotic organisms that have both plant and animal photoreceptors[57]. Though they are not in need to adjust their growth and development for better light usage, fungi must sense their surrounding environment[58]. Soil-living fungi may reach the surface and find completely different conditions like dangerous ultraviolet irradiation, temperature shifts, lowered humidity and higher oxygen concentrations, to which adjustment might be desirable. Light is a fast indicator for the change in habitat and is thus an important sensing parameter. Fungi also need photoreceptors for their reproduction, for example sessile fungi want to escape the substrate to produce and spread spores[57]. A number of different photoreceptors were found in fungi including members of the phytochrome family. In *Aspergillus nidulans* phytochromes repress sexual development and promote asexual development under red light conditions[59].

Fungal phytochromes exhibit red / far red photochemistry like a typical phytochrome with P_r as ground state, but the P_r and P_{fr} maxima are red shifted compared to plant phytochromes with maxima of 707 nm and 754 nm, respectively[59,60]. They attach BV at a cysteine in the PAS domain which may explain the red shift of the maxima. However, a heme oxygenase for the biosynthesis of BV in fungi could not be identified yet[57]. Phylogenetically, fungal phytochromes are more related to bacterial than to plant phytochromes and share their domain architecture (see Fig. 3.4). They have a canonical sensor module consisting of PAS, GAF and PHY as well as a long N-terminal extension. This NTE is sufficient to stabilize the P_{fr} state of FphA, because dark reversion could only be observed after removal of the NTE[60]. The C-terminal effector module consists of a histidine kinase

(HK) domain and a response regulator domain (RR). Proteins with a RR are involved in phosphotransfer pathways and signal transduction. RR domains can be found in two contexts, either as part of a two-component system [61], often found in prokaryotes or in a more complex phosphorelay system, which is predominantly found in eukaryotes [57]. Two-component systems are composed of a HK and a RR that often acts as transcription factor. In phosphorelay systems the sensory protein, that means the first part in the signal transduction chain, is called hybrid kinase as it harbors a HK domain and a C-terminal RR receiver domain in one protein. In contrast to two-component systems this RR has no effector domain. It accepts and transmits a phosphoryl group from its N-terminal HK domain to a histidine-containing phosphotransfer protein (HPt) that connects the hybrid kinase with another RR, that possesses an effector domain. RR domains catalyze a transfer of a phosphoryl group from a conserved histidine in the kinase domain to a conserved aspartate in the RR receiver domain. Fungal phytochromes are hybrid kinases that are presumptively part of a phosphorelay system. In contrast, bacteriophytochromes and cyanobacterial phytochromes are almost exclusively classical two-component systems [57].

The HK domain of FphA from *Aspergillus nidulans* shows red-light dependent autophos-

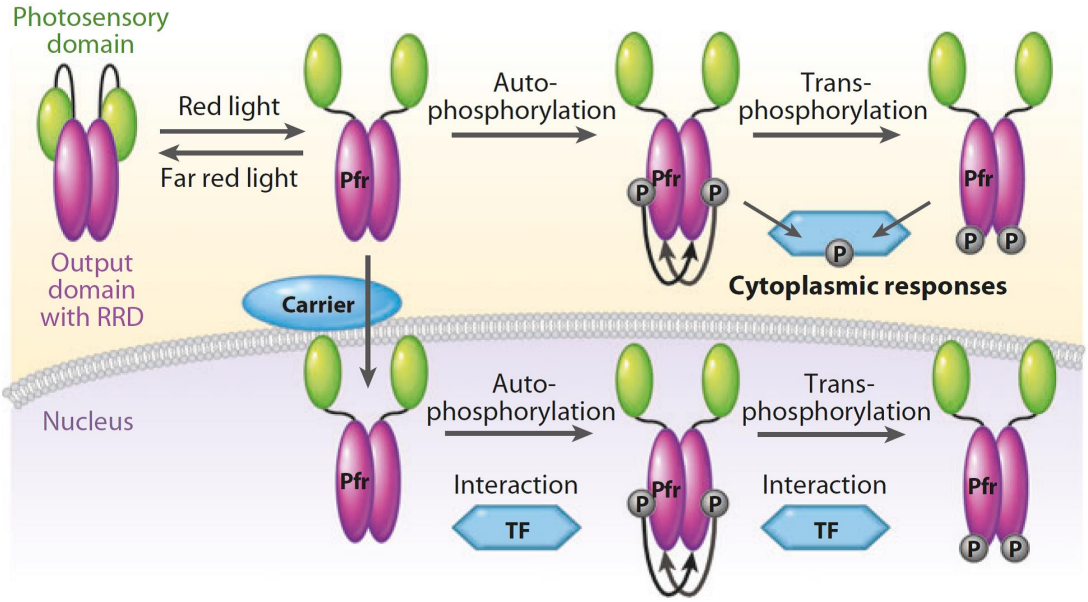

Figure 3.7: Hypothetical model of phytochrome signaling in fungi. After red light illumination the P_{fr} state is generated including large conformational changes. P_{fr} is supposed to be the active state. The protein in P_{fr} is autophosphorylated at a conserved histidine residue in the HK domain and can transphosphorylate a conserved aspartate residue in the RR domain (RRD) of its dimerization partner. The downstream histidine-containing phosphotransfer protein (HPt) that is phosphorylated (P) by the RR as well as the terminal RR is not known yet. The mechanism of nuclear import is unclear and might include carrier proteins. In the nucleus FphA interacts with transcription factors (TF); also signal transduction chains in the cytosol are possible [57].

phorylation activity at the histidine phosphoacceptor site and no phosphorylation activity in P_r. Since this red light dependent autophosphorylation occurred only when the conserved aspartate in the RR domain was mutagenized, the authors suggest that the RR domain of FphA is blocked under red light-sensing conditions[60]. Regarding the whole wild type protein, autophosphorylation occurred in both photochemical states. As fungal phytochromes are hybrid kinases which usually contain multiple phosphodonor and -acceptor sites, trans-phosphorylation also occurs at the conserved aspartate residue in the RR domain, which was proven by mutagenesis experiments. This trans-phosphorylation between two FphA molecules, including the histidine autophosphorylation site and the aspartate trans-phosphorylation site in the RR, occurred in the P_r state of the donor molecule and was independent from the conformation of the acceptor molecule (see Fig. 3.7). Some interaction partners of FphA were described like VeA (**Ve**lvet **A**) and LreB (**L**ight **re**sponse **B**) which are a regulator of different developmental and metabolic pathways and a part of the blue-light receptor system, respectively. The interaction with both proteins occurs on the C-terminal effector module of the phytochrome and is located in the nucleus so a nuclear shuttle of the phytochrome must be present[57,62].

3.4.3 Bacteriophytochromes

Phytochromes can be found in photosynthetic and non-photosynthetic bacteria and are called bacteriophytochromes or Bphs[63,64]. In the non-photosynthetic eubacterium *Deinococcus radiodurans* Bph seems to regulate the synthesis of carotenoids, which are thought to protect against UV light[63]. In the photosynthetic bacterium *Rhodopseudomonas palustris*, phytochromes regulate the biosynthesis of the photosynthetic apparatus[65]. They covalently attach BV at a conserved cysteine residue in the N-terminus of the PAS domain. The binding of BV and thus an additional double bond in the π-system of the chromophore compared to PCB or PΦB leads to a red shifted spectrum of *Deinococcus radiodurans* Bph with absorption maxima of 698 nm (P_r) and 750 nm (P_{fr})[66]. One exception was found in the aerobic photosynthetic bacterium *Bradyrhizobium* sp. where a phytochrome with a short C-terminal effector region, that has no homology to known effector domains, binds PCB with a cysteine in the GAF domain thus exhibiting a P_o (orange, max. 610 nm) / P_r photochemistry. This atypical bacteriophytochrome was supposedly acquired *via* lateral gene transfer[67].

The thermodynamical ground state of bacteriophytochromes varies so that they can be divided into two families: the first has P_r as ground state, the second P_{fr}. Phytochromes of the latter are called bathy-Bphs[64]. The domain architecture of Bphs (see Fig. 3.4) resembles fungal phytochromes although the C-terminal module shows more variability. In anoxygenic photosynthetic bacteria, phytochromes possessing a HK domain can be found, where the auto-phosphorylation of the histidine kinase motif triggers a phosphotransfer to a

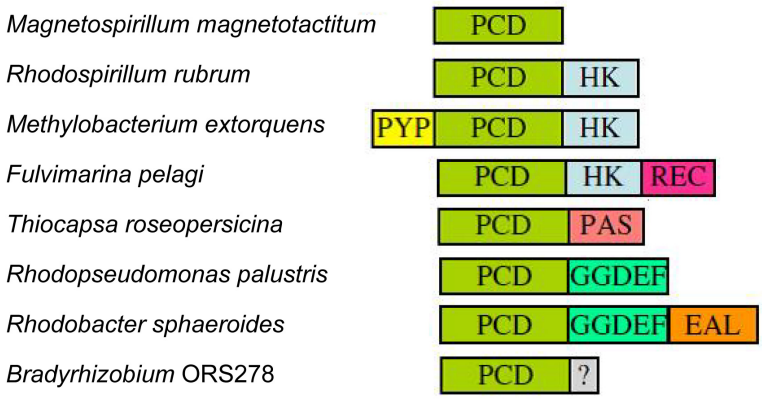

Figure 3.8: Bacteriophytochrome domain architectures in anoxygenic photosynthetic bacteria, following the phylogenetic analysis published by Giraud *et al.*[64]. PCD: **P**hotosensory **C**ore **D**omain consisting of PAS, GAF and PHY; HK: histidine kinase domain, REC: response regulator domain; GGDEF: domain containing a conserved motif of Gly/Gly/Asp/Glu/Phe; EAL: domain with a conserved Glu/Ala/Leu motif; PAS: Per/ARNT/Sim domain; PYP: photoactive yellow protein.

response regulator[61]. The active state for the phosphorylation depends on the Bph and is either P_r or P_{fr}[64]. Interestingly, the gene encoding for the response regulator is often found in the phytochrome operon[68]. The domain combination PAS-GAF-PHY-HK also occurs with an N-terminal PYP domain or like in fungal phytochromes with a C-terminal RR domain. Furthermore, architectures with a C-terminal PAS domain, a C-terminal GGDEF domain or GGDEF-EAL module (see subsection 3.5.2) can be found. In addition, Bphs with a stand-alone PAS-GAF-PHY module or a C-terminal effector domain that cannot be assigned, are also present within the bacteriophytochrome family (see Fig. 3.8)[64]. GGDEF and EAL domains are involved in the turnover of c-di-GMP (cyclic diguanylate), variants of Bphs with PAS domains are believed to bind directly to a repressor, thus preventing it to interact with DNA[69].

3.4.4 Cyanobacterial phytochromes

Cyanobacteria are prokaryotic organisms that perform oxygenic photosynthesis, some can also fix nitrogen. They are very specialized but exhibit a high biodiversity, so that they adapted to vastly different habitats like terrestrial, glacial, aerial, marine, brackish and fresh water environments[70]. Cyanobacteria produce bioactive compounds which could be used in products with applications in food, nutritional, cosmetic and pharmaceutical industries[71]. They are also an interesting tool for synthetic biology because they grow fast and are easy to manipulate genetically, thus promising to be sources for biofuels, chemicals and nutritional products[72].

The first prokaryotic phytochrome was discovered in the model cyanobacterium, *Synechocystis* sp. PCC 6803, and was named as cyanobacterial phytochrome 1 (Cph1)[73]. *Synechocystis* sp. is a unicellular cyanobacterium that was isolated from a freshwater lake[74]. It can grow either phototrophically *via* oxygenic photosynthesis in the light or heterotrophically on glucose[75,76]. Cyanobacterial phytochromes 1 have plant-like domain architectures with a canonical sensory module but a shortened C-terminal effector module consisting of a histidine kinase (see Fig. 3.4). *Syn*Cph1, which is the most studied cyanobacterial phytochrome, and CphA from *Calothrix* sp. PCC7601 (also called *Fremyella diplosiphon*) bind PCB at a conserved cysteine in the GAF domain[77,78]. There are also Bph-type proteins in cyanobacteria. CphB from *Calothrix* binds BV at Cys24 in the N-terminal PAS domain[79,80]. All three proteins exhibit a regular red / far red photoconversion. The PCB binding *Syn*Cph1 and CphA absorb at 654 nm and 702 nm as well as 663 nm and 707 nm in their P_r and P_{fr} conformation, respectively and are thus slightly blue-shifted compared to plant phytochromes[79,81]. The BV binding CphB absorbs in a red-shifted manner at 704 nm and 750 nm because of its chromophore[79]. Bathyphytochromes have not been found in cyanobacteria so far, in all known cyanobacterial Group I phytochromes P_r is the ground state. Interestingly, *Syn*Cph1 exhibits no significant dark reversion of P_{fr} to P_r[81] and also P_{fr} of CphA and B remains stable in the dark for several days[79]. Being prokaryotic histidine kinases, cyanobacterial phytochromes of Group I like *Syn*Cph1 and CphB are involved in two-component signaling. Both show kinase activity in P_r thus establishing the P_r conformation as signaling state in contrast to plant phytochromes. In both proteins the kinase autophosphorylation as well as the phosphotransfer to the respective response regulator is strictly P_r dependent, the P_{fr} state is enzymatically inactive[80,82]. The physiological role of cyanobacterial phytochromes of Group I is still unclear.

3.4.5 Group I Phytochrome structures

Phytochrome structures were not available for a long time until the canonical phytochromes of Group I could be crystallized and their structures solved. However, a structure of a plant phytochrome is still elusive so that only bacterial and cyanobacterial phytochrome structures provide currently three-dimensional information for this group. The first structure available was from *Deinococcus radiodurans*, the *Dr*BphP (see Fig. 3.9), a bacteriophytochrome in the P_r conformation[12,13]. The structure confirmed the chromophore attachment of BV at the N-terminus of the PAS domain in the *ZZZssa* conformation. In addition, an unusual figure-of-eight knot was discovered that stabilizes the PAS - GAF interaction. It consists of the N-terminus of the PAS domain which is passing through a loop region in the GAF domain. Unfortunately, this construct lacks the PHY domain and exhibits only a bleached P_{fr} spectrum[12]. An analog structure with the same features of *Rhodopseu-*

*domonas palustris Rp*BphP3 in the P_r state was also published[83]. This biliverdin binding bacteriophytochrome exhibits a new type of photoconversion because it photoconverts between P_r and a **n**ear-**r**ed light absorbing P_{nr} state. A single leucine to tyrosine mutation in the GAF domain reverts the photochemistry to classical P_r / P_{fr} behavior.

The first structure of a the complete sensory module in the P_r conformation was provided from *Syn*Cph1, a cyanobacterial phytochrome[10] (see Fig. 3.9). Here, the PCB chromophore is attached covalently to the conserved cysteine in the GAF domain and exhibits a *ZZZssa* conformation. Like in *Dr*BphP, *Syn*Cph1 provides the knotted interface as well as the relative orientations of the PAS and GAF domains. Interestingly, although the N-terminus is not the attachment site of the chromophore like in bacteriophytochromes, the N-terminal helix of the PAS domain is located near the chromophore and seals the binding pocket. The additional PHY domain in the *Syn*Cph1 structure is connected *via* a long α-helical linker to the GAF domain. It bears a long, tongue-like protrusion that reaches out to the GAF domain and seals the chromophore binding pocket. The tongue-GAF interaction is stabilized by a salt bridge. The arginine of the conserved PRxSF motif of the tongue reaches into the binding pocket and interacts with a conserved aspartate of the GAF domain. Also, the conserved $W^G/_AG$ and WxE motifs were found in the tongue region[10].

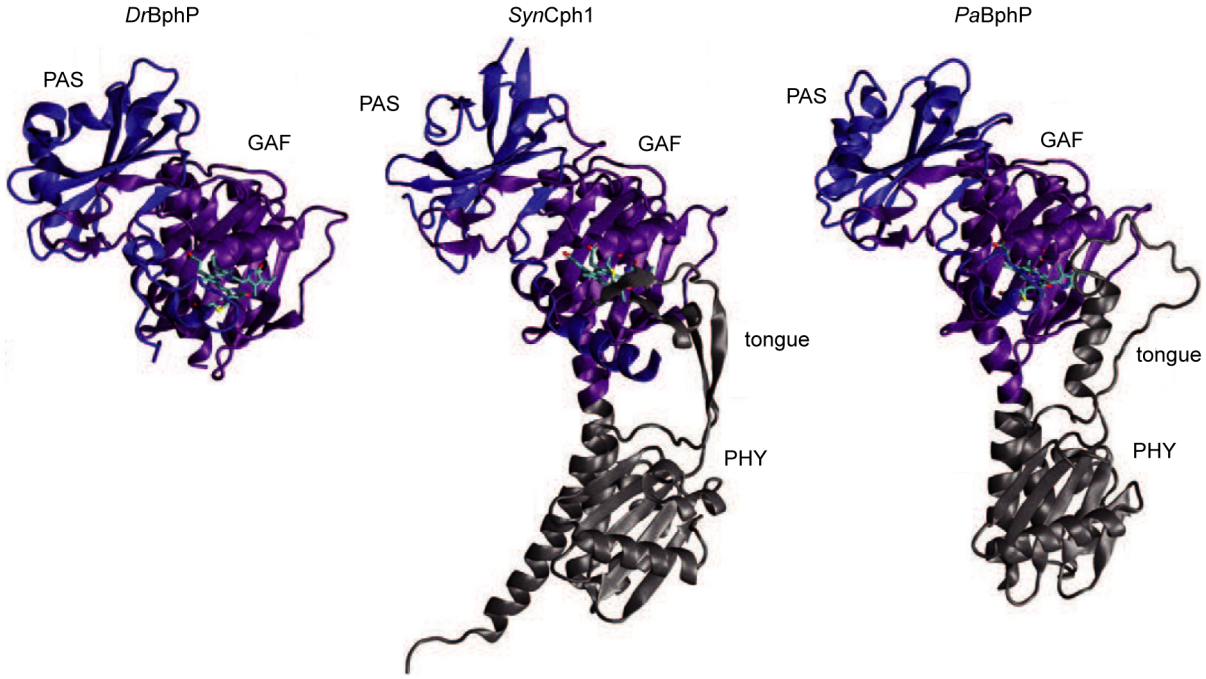

Figure 3.9: Structures of Group I phytochrome sensory modules (figure modified from Ref.[8]). PAS, GAF and PHY domains are displayed in blue, purple and black, respectively. The structure of *Dr*BphP in the P_r state includes only the PAS and GAF domain, thus lacking the PHY domain (PDB code: 2O9C)[13]. The photosensory module of *Syn*Cph1 (PDB code: 2VEA)[10] crystallized in the P_r state whereas the module of *Pa*BphP (PDB code: 3C2W)[11], a bathyphytochrome, is in the P_{fr} state.

A tyrosine mutant of *Syn*Cph1 was crystallized[84] whose relative position of the PHY domain is shifted by 17° relative to the wild type, reflecting structural plasticity between the PAS-GAF module and the PHY domain.

The crystal structure of the thermally unstable P_{fr} state is still a challenge. In 2008, the crystal structure of *Pseudomonas aeruginosa Pa*BphP, a bathyphytochrome in its ground state P_{fr}, was crystallized[11]. The overall structure with the tongue-like protrusion and the knot-forming loop resembles the *Syn*Cph1 structure. The BV chromophore in its *ZZEssa* conformation is attached at the N-terminus. A Q188L mutant of this phytochrome crystallized with two different chromophore conformations that the authors assigned to the P_r and P_{fr} state[85]. Cryo trapping experiments with the wild type protein led to crystal structures from three early intermediates of the P_{fr} to P_r transition[86].

Another structure of a bathyphytochrome in its P_{fr} ground state was published: *Rp*BphP1 of *Rhodopseudomonas palustris*[69], It contains not only the photosensory module of the phytochrome but also the majority of the effector module. The latter consists of a PAS domain with a PAC motif and a novel domain which the authors call 2-helix output sensor (HOS) domain. Protein dimers are arranged in an anti-parallel fashion within the crystal structure, which is essential for the activation of the HOS domain.

Single particle cryoelectron microscopy studies[87] of the *Deinococcus radiodurans Dr*BphP full length protein in the P_r conformation consisting of the PAS-GAF-PHY photosensory module with a C-terminal HK revealed parallel dimers. The dimerization interface is built not only by the HK domain but also by the photosensory module. The authors suggest a different PHY domain conformation than in the X-ray structures because a 30° rotation of the PHY domains was required to fit the model phytochrome structure in the cryoEM map.

3.5 Group II: Cph2 phytochromes

Cyanobacteria harbor canonical Group I phytochromes as well as non-canonical phytochromes of Group II. They occur only in cyanobacteria, accordingly, these phytochromes are called cyanobacterial phytochromes II (Cph2).

Cph2 phytochromes lack the N-terminal PAS domain of canonical Group I phytochromes and are therefore knotless. The photosensory domain consists of the chromophore binding GAF domain and an additional GAF or PHY domain. Cph2 family members often contain multiple GAF domains, which may have additional conserved cysteine residues, and HK domains as effector modules[16] (see Fig. 3.10). They bind PCB *via* a conserved cysteine in the N-terminal GAF domain. The known members of this family exhibit a red / far red photocycle with blue shifted maxima compared to plant phytochromes[88,89]. The P_r

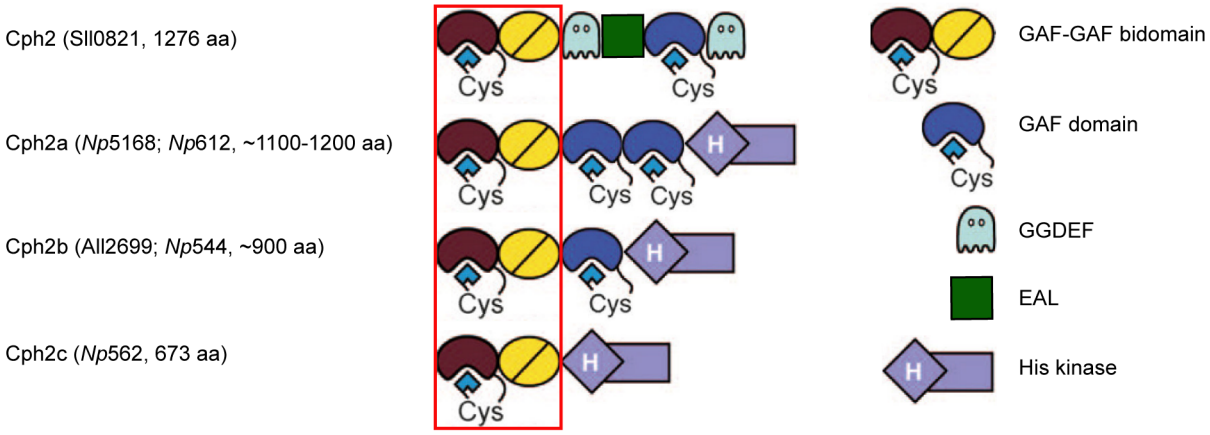

Figure 3.10: Domain organization in the Cph2 family. The red frame indicates the GAF-GAF bidomain photosensory module that is characteristic for Group II phytochromes. Blue squares indicate the bilin chromophore attached to a conserved cysteine (Cys). GGDEF and EAL domains are involved in the turnover of c-di-GMP. Protein names in parentheses relate to the following species: *Synechocystis* sp. PCC 6803: Sll; *Anabaena* sp. PCC7120: All (is also *Nostoc* sp.); *Nostoc punctiforme*: *Np*. Also, the protein length is displayed in parentheses (figure modified after Ref.[16], symbols after Ref.[8]).

conformation is the ground state[88]. In Group II three proteins are so far well characterized: *Syn*Cph2 from *Synechocystis* sp. PCC 6803 and *Sy*A as well as *Sy*B from *Synechococcus* sp. OS-A and OS-B, respectively.

3.5.1 *Sy*A and *Sy*B

*Sy*A and *Sy*B from *Synechococcus* sp. exhibit a GAF-PHY-GAF-HK architecture in which the N-terminal GAF domain and the PHY domain build up the Cph2-module. The second GAF domain also contains a conserved cysteine, that could bind a bilin chromophore[88]. The GAF-PHY construct of both proteins exhibits absorbance maxima of 630 nm and 704 nm in P_r and P_{fr}, respectively. A three-dimensional NMR structure (see Fig. 3.11) from a GAF construct of *Sy*B in the P_r conformation revealed a knot-less GAF domain very similar to known Group I crystal structures[90]. The chromophore PCB is bound covalently in the *ZZZssa* conformation like in canonical phytochrome structures[10]. The lowest-energy conformers in the NMR study reveal a high flexibility for the chromophore especially at the B- and C-ring propionates[90].

The GAF-only construct exhibits photoconversion into P_{fr} according to an absorbance spectrum. However, in the Resonance Raman spectrum the domain does not show wild type behavior after red light illumination suggesting a non-native conformation different from P_{fr}[88]. Nevertheless, the same group published a P_{fr}-NMR structure from the GAF domain of *Sy*B in which the pyrrole ring A and not ring D of the chromophore is rotated[91]

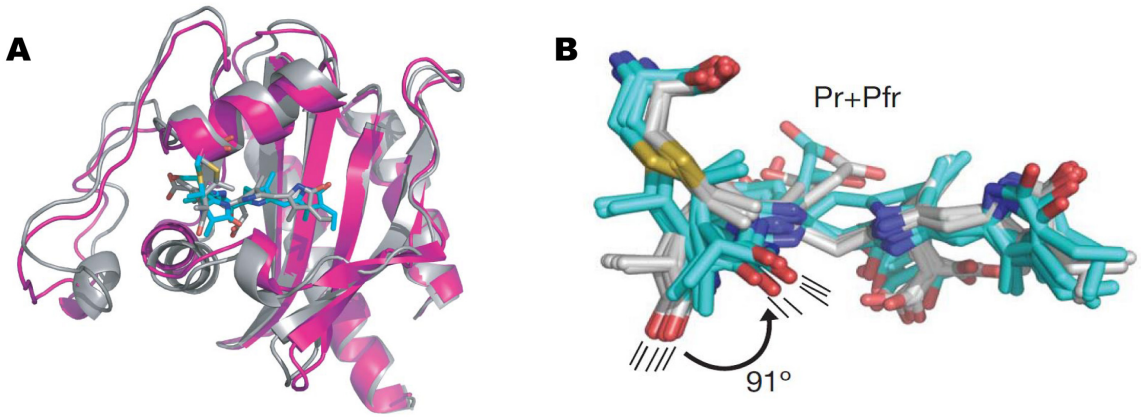

Figure 3.11: Structures of the P_r conformation and the red light adapted state of the *Sy*B GAF-only construct. **A**: Superimposition of the protein backbone from the lowest-energy conformer of the NMR structures for P_r (gray, PDB code: 2K2N) and the state after red light illumination (magenta, PDB code: 2KLI). **B**: A-ring rotation in the PCB chromophore shown by the five lowest-energy conformers of the NMR structures in the P_r conformation (gray) and the state after red light (cyan). For the A-ring a 91° rotation was derived[91].

(see Fig. 3.11). The validity of this structure has been subject of much debate.

3.5.2 *Syn*Cph2

*Syn*Cph2 from *Synechocystis* sp. (see Fig. 3.10, upper protein domain organization) contains three GAF domains of which the first two N-terminal GAF domains build the Cph2-module. The third GAF domain (GAF3) that also harbors a conserved cysteine is framed by a GGDEF-EAL module and a C-terminal GGDEF domain.

GGDEF and EAL domains are involved in synthesis and hydrolysis of the second messenger c-di-GMP,[92] which is discovered only since 1987[93]. The name of the domains refer to the conserved amino acids in the important motifs for catalysis. GGDEF and EAL domains can be found in bacteria but are absent in archaea and eukarya. They are usually part of multidomain proteins. Typically, these effector domains are located at the C-termini of one or multiple, sensory and signal transduction domains. The sensor domains can detect a wide range of signals as for example phosphorylation, binding of small molecule ligands, protein binding, binding of gaseous molecules and light (see Fig 3.12). Some GGDEF and EAL domains are linked to N-terminal periplasmic or integral membrane sensory domains[92]. The GGDEF domain is a diguanylate cyclase (DGC) that produces c-di-GMP from two GTP (**G**uanosine **T**ri**P**hosphate) molecules. The GGDEF structure is very close to eukaryotic adenylate cyclases. The first structure of the PleD DGC from *Caulobacter crescentus*[94] includes a GGDEF domain with its two receiver domains. C-di-GMP formation takes place by the use of two GGDEF domains that each

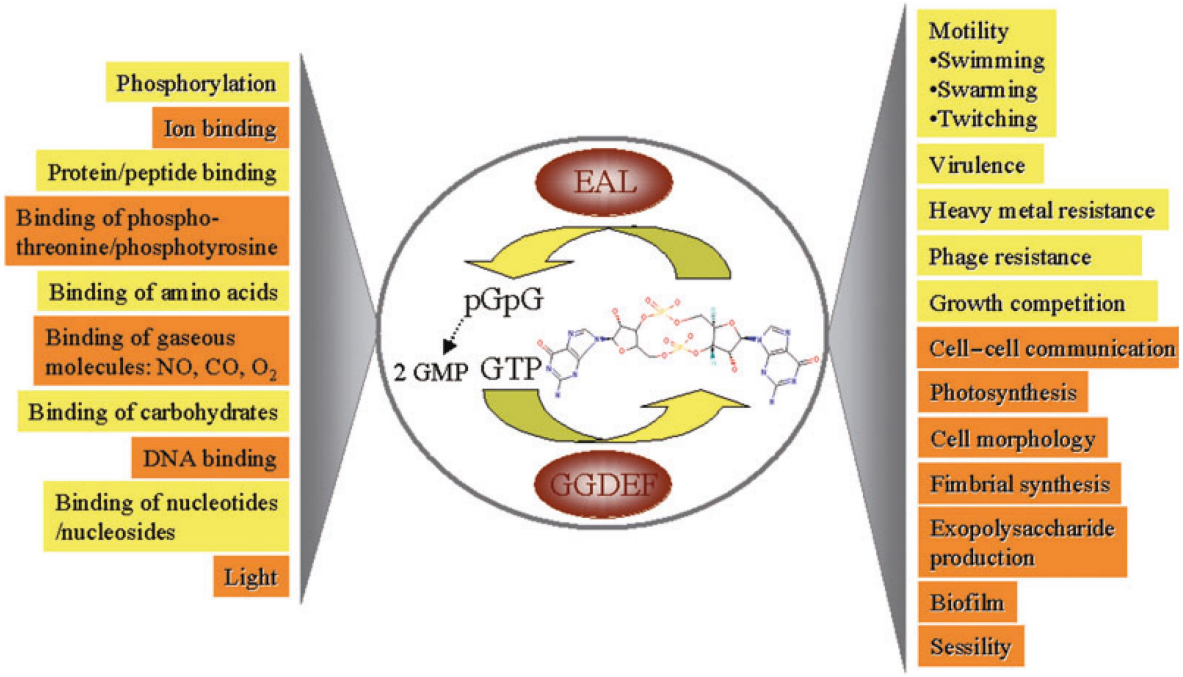

Figure 3.12: Input and output signals of the c-di-GMP metabolism. On the left side the various input signal are displayed, the output behavior by variation of the c-di-GMP concentration is on the right [92]. C-di-GMP is produced from two GTP molecules by the GGDEF domain and the EAL domain degrades c-di-GMP to dinucleotide 5´-phosphoguanylyl-(3´-5´)-guanosine (pGpG).

bind one GTP substrate. Thereby, the highly conserved GGDEF motif is folded into a β-hairpin and is part of the active half-site. The formation of the catalytically active homodimer is controlled by the N-terminal domains that form a dimer in a signal-dependent manner [95] (see Fig 3.13).

For PleD and other GGDEF proteins, a non-competitive product inhibition could be shown [94,96] that sets an upper limit for the concentration of c-di-GMP in the cell. Dimeric base-intercalated c-di-GMP molecules act as an interdomain cross-linker between the GGDEF domain and the sensory module thus preventing the GGDEF domain to move and build the active site out of the two half-sites from the two GGDEF domains. This phenomenon is called inhibition by domain immobilization [95].The primary inhibition site I_P has a conserved RxxD motif located opposite to the substrate binding site in the GGDEF domain. This is linked to the secondary inhibition site I_S that lies within the effector domains [95].

Phosphodiesterase (PDE) activity for the degradation of c-di-GMP can be found in EAL and HD-GYP domains (named after conserved amino acids) [97]. EAL-containing PDEs catalyze the opening of the c-di-GMP molecule by hydrolysis of an ester bond yielding the linear dinucleotide 5´-phosphoguanylyl-(3´-5´)-guanosine (pGpG). They are highly substrate specific and require Mg^{2+} or Mn^{2+} for their catalytic activity which is acid-

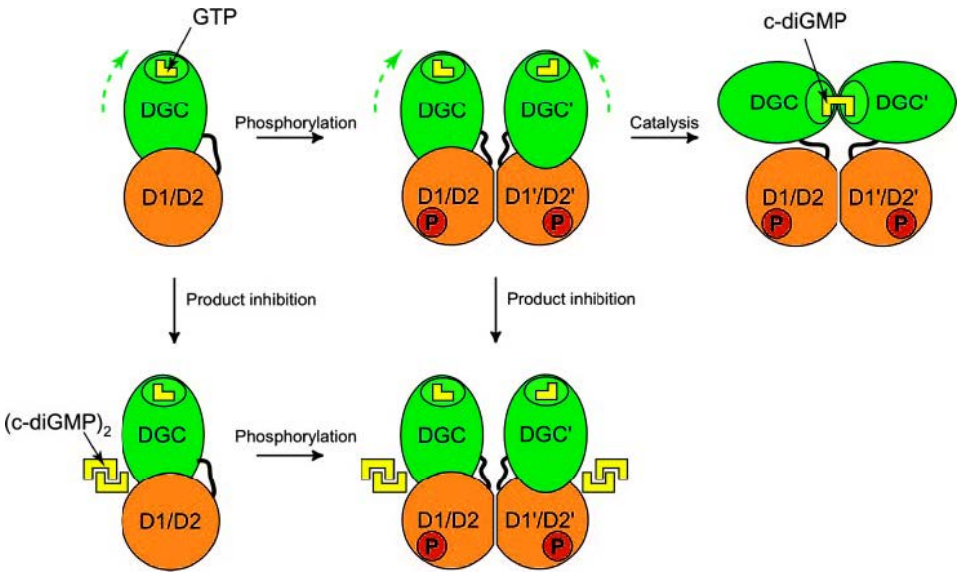

Figure 3.13: Model for the regulation of PleD, a GGDEF domain-containing protein. The GGDEF domain (here abbreviated with DGC = diguanylate cyclase) is attached *via* a flexible linker to the D1/D2 input domains which build the stem. Green arrows indicate the mobility of the GGDEF domain. PleD is activated by the phosphorylation (P) of the D1 domain which induces dimerization and puts the two substrate binding sites (displayed as small ellipses in the GGDEF domain) in close contact so that the c-di-GMP synthesis can occur. The GTP and c-di-GMP molecules are displayed in yellow. Allosteric product inhibition can occur by binding a c-di-GMP dimer at the I-site of the GGDEF domain - stem interface. The GGDEF domain remains immobilized and cannot rearrange anymore to build the two-part binding site (below) [94].

base regulated [95]. EAL domains can also hydrolyze pGpG into two GMP (**G**uanosine **M**ono**P**hosphate) molecules but the reaction is very slow and probably not physiologically relevant [92]. EAL domains exhibit a TIM (**T**riosephosphate **I**so**M**erase) barrel fold in their crystal structure which is composed of a central β-barrel and flanking α-helices. The catalytic divalent cation, Mg^{2+} or Mn^{2+}, is placed at the bottom of the substrate binding pocket and is coordinated by four conserved amino acids including the glutamate of the EAL motif, which is the general base, and a substrate oxygen from a phosphate group. A further coordinating water molecule is thought to donate a proton to the glutamate residue [95]. The regulation of the PDE activity must be due to the sensory domains. In full length protein crystal structures of EAL-containing proteins, the antiparallel dimers form an interface only consisting of the EAL domains. A signaling route was suggested that includes a rearrangement in quaternary organization upon signal reception and a subsequent change in the EAL-EAL interface that affects the active site geometry [98].

Approximately one third of all known GGDEF and EAL containing proteins comprise both domains in the order GGDEF-EAL, mostly at the C-terminus [95]. This group of proteins seems to have different tasks. Several composite proteins have either PDE or DGC function.

The PDE activity of PdeA from *Caulobacter crescentus* is strongly stimulated by GTP binding to the GGDEF domain[99], but bifunctional composite proteins have been reported as well[100].

C-di-GMP controls a wide range of cellular functions and interferes with cellular signaling on several levels, including transcription, protein activity, translation, protein secretion and protein stability[95]. One example for c-di-GMP-specific acceptors are PilZ-containing proteins that often comprise regulatory, catalytic or transport domains. It is also suggested, that catalytically inactive EAL or GGDEF domains are c-di-GMP receptors and control the effector module[95]. Also c-di-GMP binding to a transcription factor from *Pseudomonas aeruginosa*, that is a master regulator of flagellar gene expression, was reported. The binding inhibits its association to the promoter and leads to the derepression of the operon[101].

*Syn*Cph2 contains a GGDEF-EAL module as well as a single C-terminal GGDEF domain. The full length *Syn*Cph2 protein, which was produced as an intein-fusion protein with a PCB chromophore[89], exhibited red / far red light dependent photoreversibility with difference spectrum extrema at 643 nm and 690 nm. Cys129, located in the first GAF domain of the Cph2-module was confirmed to be the chromophore binding amino acid[89]. Another study could corroborate that in addition the GAF3 domain has bilin lyase activity and can bind a PCB chromophore[102]. A construct comprising GAF3 exhibits blue light absorption but was supposed to be photochemically silent in this study[102]. The N-terminal Cph2-module was produced as well as a GAF1-only construct. The authors could show that GAF1 is sufficient to bind PCB and is therefore a bilin lyase domain. GAF2 is needed to stabilize the P_{fr} conformation in accordance with the function of PHY domains in canonical phytochromes[102].

In vivo studies of *Syn*Cph2 revealed that *Syn*Cph2-deficient mutant strains exhibit a reduced growth under red light suggesting P_{fr} as the active state[103]. In contrast to this finding a DNA microarray approach investigating the expression of different genes in *Synechocystis* sp. showed that the absence of *Syn*Cph2 changed the far red light response of genes implying P_r as active state[104]. The affected genes are involved in nitrogen metabolism, stress adaption and secretion of proteins. The authors furthermore reason, that phytochromes do not exclusively act on the transcription level, because the affected genes cannot explain the reduced growth of *Syn*Cph2-deficient mutants under red light[104].

In phototaxis experiments *Syn*Cph2-deficient cells move towards blue-light, in contrast to wild type cells that do not move[105]. Mutagenesis studies with a Cys1022 to valine substitution in GAF3 indicated that *Syn*Cph2 itself is the blue-light photoreceptor since the mutated cells moved towards blue light exhibiting the same phenotype as *Syn*Cph2-deficient cells. Interestingly, both conserved cysteines, Cys129 as well as Cys1022 are needed for the inhibition of phototaxis towards blue light, because also a C129A mutant showed positive phototaxis towards blue light[106]. This was confirmed in another study where

it was shown that *Syn*Cph2 inhibits phototaxis towards UV-A light. The C129S and C1022S mutants exhibited the same phenotype, positive phototaxis towards UV-A light like *Syn*Cph2-deficient cells[107].

3.6 Group III: Cyanobacteriochromes

Group III of the bilin-binding photoreceptors consists of cyanobacteriochromes, stand-alone GAF domains that are sufficient to achieve fully reversible photochemistry[8]. CBCRs are related to phytochromes and share the bilin lyase activity to attach the linear tetrapyrrole

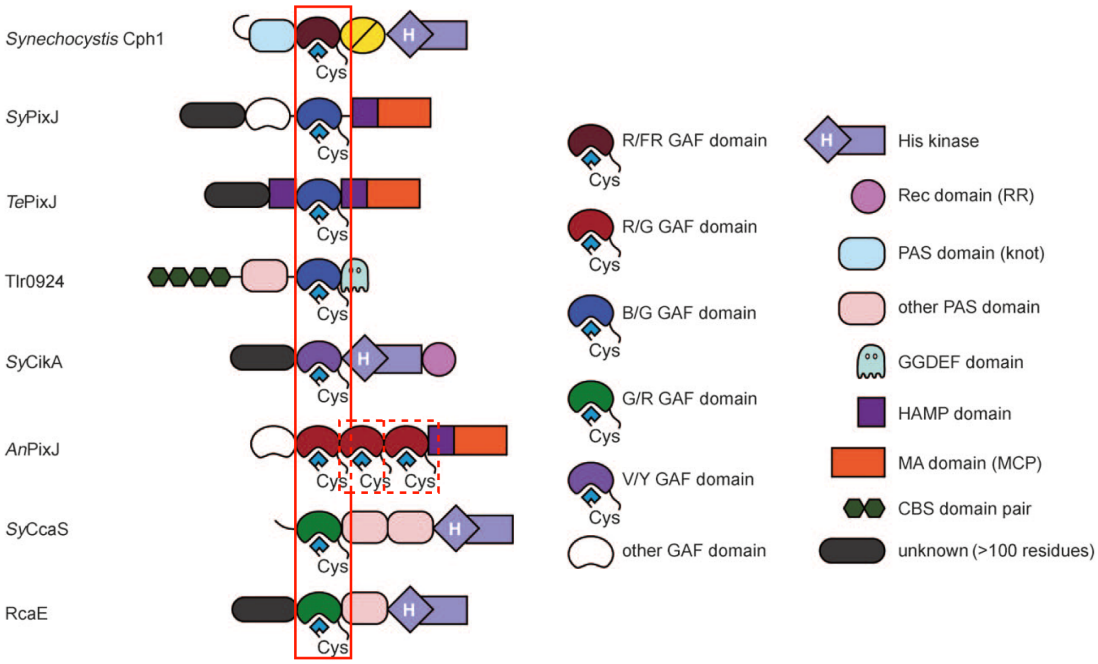

Figure 3.14: Domain architecture of characterized cyanobacteriochromes including their photochemical properties. The red frame indicates the single GAF domain photosensory module that is characteristic for CBCRs, dashed frames additional CBCR domains in *An*PixJ. R/FR refers to a red / far red photocycle, G to a green, B to a blue, V to a violet, Y to a yellow photoproduct, respectively. *Synechocystis* Cph1 is not a CBCR but a canonical Group I phytochrome from *Synechocystis* sp.[8]. In the same organism, *Sy*PixJ[14], *Sy*CikA[108] and *Sy*CcaS[109] can be found. *Te*PixJ[110,111] and Tlr0924[112] originate from *Thermosynechococcus elongatus*. *An*PixJ is from *Anabaena* (*Nostoc*) sp.[108] and RcaE from *Fremyella diplosiphon*[113]. Blue squares indicate the bilin chromophore attached to a conserved cysteine (Cys). MCP = **M**ethyl-accepting **C**hemotaxis **P**rotein domain; HAMP = present in **H**istidine kinases, **A**denyl cyclases, **M**ethyl-accepting proteins and **P**hosphatases; is a linker domain, that connects sensory with signaling domains; CBS = can be found in **C**ystathionine **B**eta-**S**ynthases, tandem pairs act as sensors of cellular energy status in binding adenosine derivatives[114].

to conserved cysteine residues. They also share a cognate photocycle that implies the photoisomerization of the chromophore between a *15Z*- and *15E*-state and an accompanying rotation of the D-ring[115]. In contrast to phytochromes the absorption properties of CBCRs are extremely diverse and cover the whole light spectrum. CBCRs often occur in multiple copies within one protein that allows various light signals to affect one single effector domain[116]. The domain architecture of CBCR proteins (see Fig. 3.14) is manifold and involves C-terminal effector domains as HKs but also GGDEF and other output domains.

Although CBCRs were discovered only a few years ago[117], the biological role of some CBCRs is known. RcaE from *Fremyella diplosiphon* is involved in complementary chromatic adaption (CCA)[113] that regulates the relative concentration of the light harvesting proteins phycocyanin (red light-absorbing) and phycoerythrin (green light-absorbing) in response to the red and green light ratio in cyanobacteria[118]. *Sy*PixJ from *Synechocystis* sp. is participating in the positive phototaxis of the cells. The light signal perceived from *Sy*PixJ is supposed to lead finally to retraction and extension of pili for phototaxis[119,120], as the motility of *Synechocystis* is type VI-like pili-dependent[121]. For *Sy*CikA from *Synechocystis* sp. an involvement in the circadian rhythm was proposed[124].

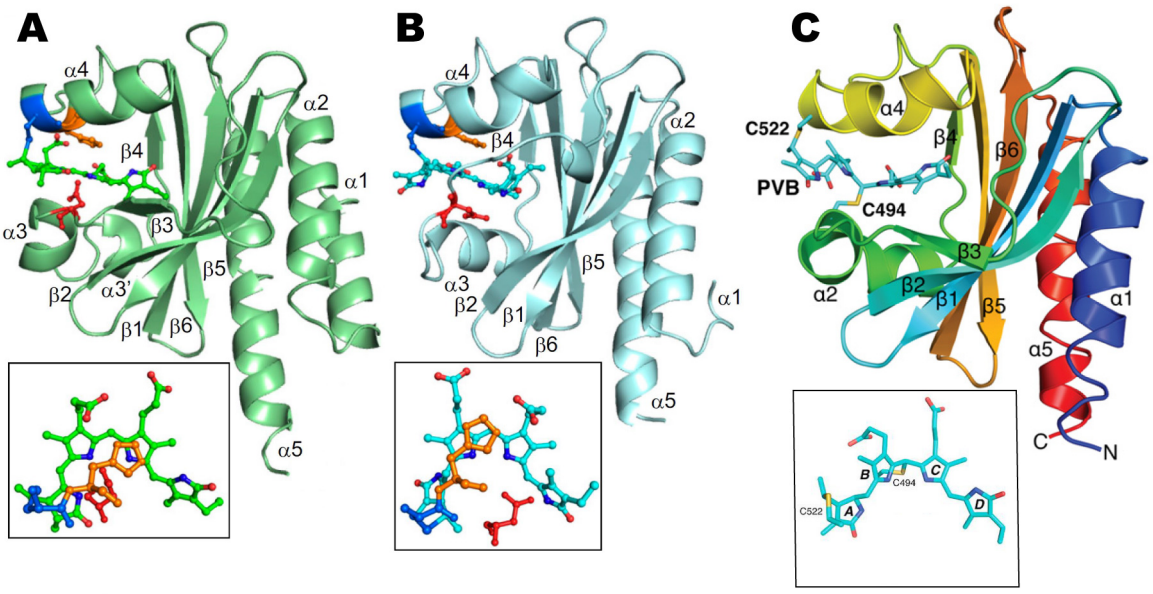

Figure 3.15: Xray crystallographic structures of **A**: second GAF domain of *An*PixJ in P_r (*15Z*) (PDB code: 3W2Z)[122], **B**: *Te*PixJ in P_g (*15E*) (PDB code: 3VV4)[122] and **C**: *Te*PixJ in P_b (*15Z*) (PDB code: 4GLQ)[123]. The chromophores along with the key residues are shown in boxes below the structure. In **A** and **B** histidine and aspartate residues are displayed in yellow and red, respectively. Covalent attachment to cysteine residues is shown in dark blue in **A** and **B** and cyan in **C**. α-helices and β-sheets are numbered. *An*PixJ binds PCB as chromophore, *Te*PixJ contains a mix of PCB and PVB. Here, only PCB containing structures are shown, but there also exists a *Te*PixJ P_b structure with PVB (PDB-code: 4FOF)[123].

CBCRs can be divided into four subfamilies according to their photochemistry. Two of these subfamilies have opposite photocycles[115]. The absorbance characteristics of the photochemical states as shown in Fig. 3.14 are defined by listing first the *15Z* and then the *15E* conformation[8]. Green/red (G/R) CBCRs have a green-absorbing (*15Z*) ground state and a red-absorbing (*15E*) photoproduct[109], whereas red/green (R/G) CBCRs have a red-absorbing (*15Z*) ground state and a green-absorbing (*15E*) photoproduct[108]. This shows that CBCRs do not necessarily feature the *15E*-state as the long-wavelength state. The G/R CBCR *Sy*CcaS exhibits phosphorylation activity under green light and thus in the red-absorbing (*15E*) state[125], so it shares the physiologically active conformation with plant phytochromes. The other two subfamilies are called insert-Cys and DxCF CBCRs and use a second conserved cysteine residue for chromophore attachment[126]. Their *15Z*-ground state exhibits an absorbance at shorter wavelengths in the near-UV to blue light,

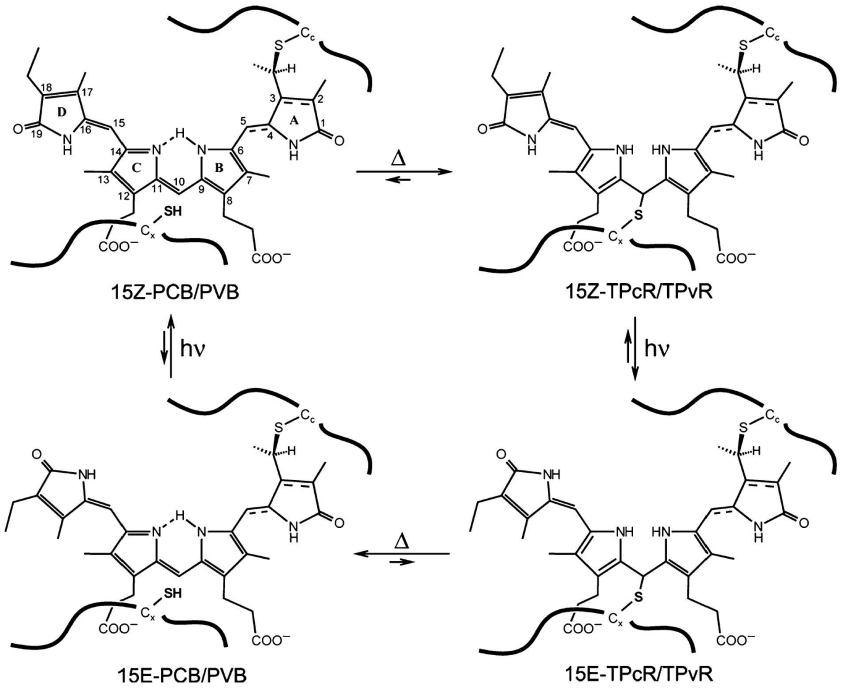

Figure 3.16: Supposed photocycle of DxCF CBCRs. The chromophore in the *15Z*-conformation is attached to one cysteine. In a thermal process (Δ), a second conserved cysteine can bind to C10 thus forming a TPcR (10-thio-phycocyanorubin) or TPvR (10-thio-phycoviolorubin) chromophore. Upon light irradiation ($h\nu$) D-ring rotation occurs within the chromophore. The backward reaction from the *15E* to *15Z* chromophore first includes the elimination and rebuilding of the unbound cysteine residue and upon light illumination the ring-D rotation. PCB and PVB differ at ring A, which is presented with dashed lines (see Fig. 3.2). The bold wavy lines indicate the protein, C_C and C_X are canonical and additional chromophore-binding cysteines, respectively. Horizontal arrows display equilibria between once or twice attached chromophores, vertical arrows equilibria between *15Z*- and *15E*-states[127].

whereas the *15E*-state absorbs at longer wavelengths from blue to orange[115]. All CBCRs bind PCB as chromophore. In addition, DXCF CBCRs can autocatalytically isomerize PCB into PVB, thus changing the spectral behavior of the (*15E*) state to an absorbance between teal and orange light[111,128,129].

Crystal structures of two different CBCRs exist that are representatives of two different subclasses, covering both the (*15Z*) as well as the (*15E*) conformation (see Fig. 3.15). The second GAF domain of *An*PixJ from *Anabaena* sp. PCC 7120, a R/G CBCR, could be crystallized in the P_r (*15Z*) ground state including its chromophore PCB in the *ZZZssa* conformation[122]. *Te*PixJ from *Thermosynechococcus elongatus* is a B/G absorbing DxCF CBCR. Interestingly, recombinant CBCRs contains a mix of PCB and PVB[111]. Crystal structures of the PVB binding protein in the P_b (C10-*Zs*/C15-*Za*)[123] and P_g (C10-*Zs*/C15-*Ea*) state[122] as well as the PCB binding form in the P_b[123] conformation exist. In all structures the CBCRs adopt the canonical GAF fold. The chromophore is bound in a cleft formed by the six-stranded antiparallel β-sheet and three helices; three other helices are located on the opposite side of the sheet. The chromophore remains solvent-exposed on ring A and B because of the missing PAS and PHY domain. Just like in phytochromes, key protein-chromophore interactions are also conserved in CBCRs: A conserved histidine or tyrosine residue forms a hydrogen bond to the carbonyl oxygen of ring D in the *15Z*-state in both structures. In the *15E*-state a conserved aspartate hydrogen-bonds to the amide nitrogen of ring D[115]. Another conserved aspartate, responsible for a salt bridge to an arginine of the PHY domain in *Syn*Cph1[10] directly interacts with the rings A, B and C in the *15Z* CBCRs structures. *An*PixJ exhibits a single-linked chromophore in the (*15Z*) state, the crystal structure of a green-absorbing (*15E*) photoproduct has not been solved yet. In contrast, crystal structures in both states of *Te*PixJ exist, which elucidate the mechanism of the photocycle. The P_b (*15Z*) state exhibits a second thioether linkage to the chromophore which involves the C10 carbon and the cysteine within the conserved DxCF sequence characteristic for that subfamily[123]. This results in a rubinoid species with a smaller π-system, which explains the blue-light absorbance[8]. In the P_g state (*15E*) of *Te*PixJ this thioether linkage is broken[122] (see Fig. 3.15).

3.7 Evolution of phytochromes

Phytochromes are widely distributed photoreceptors. Even in the archaebacterium *Methanosarcina acetivorans* a gene for a putative phytochrome-type protein (gene ID: 1476455, protein: NP_619420.1) was postulated in the genome[68]. Most of the phytochromes have a conserved, canonical N-terminal photosensory module. The chromophore, which is attached, varies among plant, fungal and bacterial phytochromes. Nearly all plant phytochromes incorporate PΦB, with some rare exceptions like the phytochrome from

the moss *Physcomitrella patens* that presumably harbors PUB as chromophore[31] or the phytochrome from the green algae *Mesotaenitum caldariorum* that incorporates PCB[130] like phytochromes from cyanobacteria. Plant and most of the cyanobacterial phytochromes, as well as phytochrome-like proteins share a conserved cysteine in the GAF domain as chromophore binding residue[131]. Bacterial phytochromes exhibit a different location of the chromophore binding cysteine. It is located N-terminal in the PAS domain and seems to be exclusive and required for BV binding. The cysteine in this position is conserved in all those phytochromes that are lacking the cysteine conservation in the GAF domain[131].

BV seems to be the more ancient type of chromophores, as implied by the high distribution of bilin synthases among organisms. The biosynthesis enzyme, heme oxygenase (HO, see section 3.2), is present in most organisms, whereas PCB and PΦB synthases are restricted to plants, cyanobacteria and red algae[131]. Furthermore in chromophore synthesis it is the only one that is synthesized from heme in a one-step reaction. It is also the precursor of all the other bilin chromophores. The evolutionary chromophore switch from BV to other chromophores could be due to adaption to the chlorophyll environment. PCB and PΦB adducts have blue shifted absorbance maxima of $\Delta\lambda$= 30-40 nm[131] leading to a P_r absorption spectrum that is closer to the one from chlorophyll. This provides a more accurate measurement of the available photosynthetic wavelengths[68].

In two phylogenetic studies of *Lamparter*[131] and *Karniol et al.*[68] comparable phylogenetic trees where observed but the authors suggest different evolutionary hypotheses that are presented hereafter.

Phylogenetic analyses of PΦB and PCB binding phytochromes of *Lamparter* could confute the assumption that plant phytochromes were inherited from the cyanobacterial endosymbiont that gave rise to plant plastids[131]. They were performed with protein sequences of the photosensory module (Fig. 3.17 A) or the histidine kinase module of phytochromes. Both phylogenetic analyses show that plant and cyanobacterial sequences are not clustering in a common subbranch. In both phylogenetic trees plant, fungal and cyanobacterial phytochromes form separate branches indicating that members of each group evolved from a single progenitor[131]. The plant branch does not originate from a position close to the cyanobacterial group. So plant-like phytochromes were most likely already present in the cell when the cyanobacterial endosymbiont appeared. Phylogenetic analyses of HOs came to the same conclusion as plant HOs are closer related to animal than to cyanobacterial HOs[132].

Lamparter[131] suggested a possible scenario for the evolution of PCB and PΦB binding phytochromes. It stated that cyanobacteria developed BV-reducing enzymes like PcyA, PebA and B but not the phytochrome or HO which were inherited from a proteobacterial predecessor. Gene duplication resulted in two phytochromes from which one achieved a switch of the chromophore attachment site from the N-terminal PAS domain to the GAF

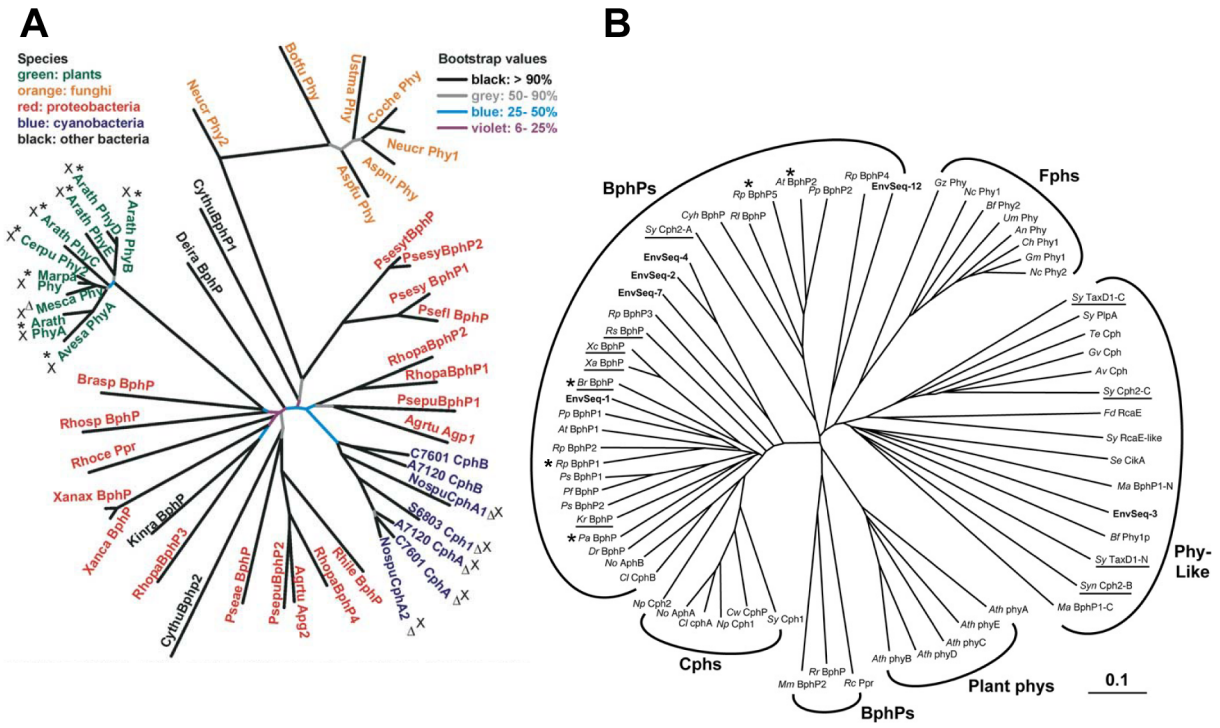

Figure 3.17: Phylogenetic trees of two studies **A:** Phylogenetic tree of phytochromes using the N-terminal photosensory module[131]. Chromophores: *: PΦB, Δ: PCB, all others: BV; x: is the binding site in the GAF domain, all others in the PAS domain. The bootstrap value corresponds to the reliability of the assignment. For the protein and organism abbreviations see *Lamparter*[131]. **B:** Phylogenetic tree using the GAF domain sequences (figure modified from Ref.[68]). Underlined proteins lack an obvious HK domain, asterisks indicate members of bathy-BphP subfamily. The protein and organism abbreviations are shown in Ref.[68].

domain and a preference of PCB over BV. Both types can still be found in cyanobacteria[77,133]. Phytochrome-like proteins including RcaE and CikA may have evolved in cyanobacteria by combination of phytochrome domains with other domains.

The eukaryotic predecessor of plants already had a phytochrome before it acquired a cyanobacterium as endosymbiont. Since HOs were already present in the cells this phytochrome had BV as chromophore. After the cyanobacterial endosymbiosis BV reducing enzymes became available from which one developed to the PΦB synthase and the others were lost as well as the cyanobacterial phytochromes in the chloroplast. With the new chromophore available, the chromophore attachment site changed to a position in the GAF domain. The development into different types of plant phytochromes occurred later, probably after the loss of BV-binding phytochromes[131]. The problem of this hypothesis of convergent evolution is the chromophore attachment site as it would be surprising that the covalent binding to a cysteine residue occurs in exactly the same position in cyanobacterial and plant phytochromes.

Another study of *Karniol et al.* used GAF domains for a phylogenetic analysis and came to a comparable clustering of the families[68] (Fig. 3.17 B). Interestingly, this study included four bathyphytochromes, which stabilize P_{fr} as ground state. These four do not cluster together on a tree but are placed on two branches, suggesting that sequences outside the GAF domain are responsible for this spectral behavior.

This study generated a different scenario for phytochrome evolution. Here, the bacteriophytochrome family is the progenitor for all bilin-containing photochromic pigments. This precursor may have been a GAF containing protein that changed its heme-binding pocket to bind linear bilins and added a PAS domain as chromophore attachment site. The evolving PHY region may have helped to establish P_r/P_{fr} photochemistry. Relatives of this phytochromes then emerged during the evolution of the other clades. Fungal phytochromes probably evolved directly from bacterial phytochromes. They kept BV as chromophore and added their target response regulator directly to the photoreceptor. The change of the bilin binding site to the GAF domain in PCB binding cyanobacterial phytochromes is then the reaction to a need for discrimination of PCB from its precursor BV. The new position of the cysteine in the three-dimensional structure allows only the binding to the ethylidene side chain of PCB instead of the vinyl side chain of BV[68].

Although this study found the same distant relation of plant and cyanobacterial phytochromes the authors suggest the derivation of plant phytochromes from cyanobacterial phytochromes during chloroplast endosymbiosis. After establishment of PΦB instead of PCB two additional PAS domains were added to help with the signal output. In this context, the cyanobacterial HK domain was modified to change HK activity, too[68].

The evolution of phytochromes went on, even in a non-photoreceptory direction. In *Rhodopseudomonas palustris* two different types of bacteriophytochrome-related proteins exist depending on the strain. The first one is a canonical BV-binding bacteriophytochrome. In other strains this protein does not bind a chromophore but established a redox sensing ability[134]. Interestingly, both use the same signal transduction pathway. The redox-sensing proteins phylogenetically form two sister clades related to the phytochrome family. The authors suggest that an ancestor evolved from a light sensor to a redox sensor. The redox sensing is mediated by two conserved cysteines located in the PHY and in the histidine kinase domains, respectively. The cysteines are involved in the reversible redox-dependent formation of aggregates *via* intermolecular disulfide bonds.

Genetically, phytochromes can be often found in operons where they are incorporated with other elements of their sensory transduction chain. Genes of bacterial phytochromes are often in the same operon like genes encoding factors important for two-component histidine-kinase signal transduction. Cyanobacterial and bacteriophytochromes are incorporated with response regulators and sometimes other histidine-kinases. Some bacterial phytochrome operons include a HO gene needed for BV synthesis[68].

4 Objective of the thesis

Plant phytochromes are known since 1959, only in 1997 prokaryotic phytochromes like *Syn*Cph1 were discovered[73]. The knowledge about these red/far red photoreceptors is mainly focussed on Group I phytochromes on the one hand because they were the first known, on the other hand because the findings can be easily transferred to plant phytochromes thus leading to possible agricultural applications. Only a few publications focus on Group II phytochromes that include only head characterizations. *Syn*Cph2 was an interesting target because of its intriguing molecular architecture. It does not include a HK effector module but c-di-GMP producing and degrading domains that are assembled within one chromoprotein. In addition, *Syn*Cph2 contains another photoreceptor module, a CBCR domain, and the interplay of the two photoreceptors fused in one protein was elusive.

In preliminary work I was able to establish the production and purification of *Syn*Cph2(1-2), a stable protein in high yields and purity. I performed first spectral characterizations and initial crystallization attempts[135]. In addition, *in vivo* data of *Syn*Cph2 were already published.

The main objective for my PhD thesis was increasing the knowledge about Group II phytochromes and especially about *Syn*Cph2(1-2). It should be established as a model system, also as minimal model for plant phytochromes, and should be completely spectroscopically characterized. Based on these data, a mechanistic comparison of Group II and Group I phytochromes should become feasible. A crystal structure of *Syn*Cph2(1-2) was aspired, because a complete structure of a Group II photosensory module was not available and should provide further insights into this subfamily. Based on the structural and spectroscopical data and the advantage of a sensory module that only contains two domains, other important questions that concern all phytochromes should be addressed. For example, the route of intramolecular signal transduction in phytochromes is still elusive. Using these structural data mutagenesis studies should reveal the importance and function of conserved residues and motifs, also in comparison to Group I photoreceptors. The knowledge about signaling in phytochromes can be utilized in applications like optogenetics where a sensory module fused to an effector module can be applied to control biological processes either in research, medical, nutritional or other applications.

5 Publications

5.1 Spectroscopic characterization of *Syn*Cph2(1-2)

This research was originally published in Photochemistry and Photobiology. *Katrin Anders, David von Stetten, Jo Mailliet, Stephan Kiontke, Vitaly A. Sineshchekov, Peter Hildebrandt, Jon Hughes and Lars-Oliver Essen.* **Spectroscopic and Photochemical Characterization of the Red-Light Sensitive Photosensory Module of Cph2 from *Synechocystis* PCC 6803.** Photochemistry and Photobiology. 2011; 87:160-173.
 Some preliminary results were already presented in the diploma thesis[135].

Summary

The phytochrome *Syn*Cph2 contains three GAF domains with two chromophore-binding cysteines. Whereas GAF3 is a CBCR domain, the first two GAF domains correspond to a Group II phytochrome module. Here we present the first spectroscopic and photochemical studies of this module. We characterized *Syn*Cph2(1-2) as well as two mutants, Y47H and R383D. The latter mutant is predicted to affect the conserved salt bridge between the arginine in the tongue region of GAF2 and the aspartate of the DIP motif in the GAF1 domain. The equivalent variant of Y47H in *Syn*Cph1 exhibits a reduced P_r to P_{fr} photoconversion and is highly fluorescent, which is attributed to the formation of a salt bridge between the histidine and the C-ring propionate group. The same mutation in BV-binding phytochromes leads to a non-fluorescent protein with functional photochemistry.

We were able to heterologously produce and purify the proteins assembled with PCB. *Syn*Cph2(1-2) exhibits $P_r \rightarrow P_{fr}$ photoconversion; P_{fr} is thermally instable and converts to P_r in the dark. The absorbance maxima are blue shifted relative to *Syn*Cph1. The quantum yield for the $P_r \rightarrow P_{fr}$ photoconversion is 0.12, in the back reaction 0.19, the first value is lower and the latter higher than in *Syn*Cph1 and plant phytochromes. At photoequilibrium conditions a portion of 60% P_{fr} could be formed. The spectral behavior of *Syn*Cph2(1-2) corresponds closely to Group I phytochromes despite the absence of a PAS domain, so that the PHY domain-replacing GAF2 domain seems to function analogously,

including the predicted tongue region. This is further proven by the R383D mutant that remains arrested in an intermediate state upon red-light illumination. *Syn*Cph2(1-2) near UV/vis CD spectra revealed differences in the spectra of P_r and P_{fr} that arise from a large change in the asymmetric environment of the chromophore. Nevertheless, the spectra closely resemble the states of *Syn*Cph1. The Y47H mutant shows the spectroscopic behavior characteristic of *Syn*Cph2(1-2) with a reduced P_{fr} content at the photoequilibrium. Fluorescence measurements revealed a 40% lower fluorescence quantum yield for the Y47H mutant as for the wild type. This behavior resembles more BV-binding phytochromes like *Pa*BphP than *Syn*Cph1 and can be attributed to higher structural flexibility in the chromophore binding pocket including the B-ring propionate. This may be caused by the missing PAS domain that in *Syn*Cph1 seals the pocket with its N-terminal α-helix.

Size exclusion chromatography revealed an earlier elution of P_{fr}, possibly because of a global conformational change of P_{fr} compared to P_r. Circular dichroism (CD) measurements proved an increase of the α-helical content of at least 3% during the P_r to P_{fr} photoconversion. This might be caused by adaptions in the tongue region or by an adjustment of the GAF1 and GAF2 domains relative to each other.

We could prove the covalent attachment of the chromophore to Cys129 by mass spectrometry analysis. The *ZZZssa* chromophore conformation in P_r and *ZZEssa* in P_{fr} could be confirmed by Resonance Raman (RR) measurements that indicate a torsional twisting of the C-D methine bridge and show high resemblance to the spectra of *Syn*Cph1. All four pyrrole nitrogens are protonated in both conformations. The RR spectra of Y47H are essentially identical to *Syn*Cph2(1-2), indicating almost the same chromophore conformations. CD and RR measurements suggest slight differences of the electrostatic interactions in the chromophore binding pocket in the P_r state when compared to *Syn*Cph1, whereas P_{fr} exhibits very similar chromophore structures and protein-cofactor interactions. Also, the direction of D-ring rotation during photoconversion can be assigned by near UV/vis CD spectra[136]. According to this hypothesis the CD spectra of *Syn*Cph2(1-2) indicate a counter-clockwise rotation of the D-ring upon $P_r \rightarrow P_{fr}$ conversion.

Contributions

K. Anders designed experiments, cloned the wild type plasmids, produced and purified proteins, performed absorbance, CD and fluorescence spectroscopical measurements, analyzed the data and wrote the manuscript. D. von Stetten performed RR experiments, J. Mailliet performed fluorescence spectroscopical measurements, S. Kiontke cloned the Y47H and R383D plasmids, V. A. Sineshchekov helped with fluorescence data analysis, P. Hildebrandt wrote the RR result part in the manuscript. J. Hughes gave fruitful discussions and L.-O. Essen designed experiments, wrote and revised the manuscript.

Photochemistry and Photobiology, 2011, 87: 160–173

Spectroscopic and Photochemical Characterization of the Red-Light Sensitive Photosensory Module of Cph2 from *Synechocystis* PCC 6803

Katrin Anders[1], David von Stetten[2], Jo Mailliet[3], Stephan Kiontke[1], Vitaly A. Sineshchekov[4], Peter Hildebrandt[5], Jon Hughes[3] and Lars-Oliver Essen*[1]

[1]Department of Chemistry, Philipps University, Marburg, Germany
[2]European Synchrotron Radiation Facility, Grenoble, France
[3]Department of Plant Physiology, Justus Liebig University, Giessen, Germany
[4]Biology Department, M.V. Lomonosov Moscow State University, Moscow, Russia
[5]Institute for Chemistry, Technical University of Berlin, Berlin, Germany

Received 21 July 2010, accepted 19 October 2010, DOI: 10.1111/j.1751-1097.2010.00845.x

ABSTRACT

Cyanobacterial phytochromes are a diverse family of light receptors controlling various biological functions including phototaxis. In addition to canonical *bona fide* phytochromes of the well characterized Cph1/plant-like clade, cyanobacteria also harbor phytochromes that absorb green, violet or blue light. The *Synechocystis* PCC 6803 Cph2 photoreceptor, a phototaxis inhibitor, is unconventional in bearing two distinct chromophore-binding GAF domains. Whereas the C-terminal GAF domain is most likely involved in blue-light perception, the first two domains correspond to a Cph1-like photosensory module lacking the PAS domain. Biochemical and spectroscopic studies show that this region switches between red (P_r) and far-red (P_{fr}) absorbing states. Unlike Cph1, the P_{fr} state of Cph2 decays rapidly in darkness. Mutations close to the PCB chromophore further destabilize the P_{fr} state without drastically affecting the spectroscopic features such as the quantum efficiency of $P_r \rightarrow P_{fr}$ conversion, fluorescence, or the Resonance-Raman signature of the chromophore. Overall, the PAS-less photosensory module of Cph2 resembles Cph1 including its mode of isomerisation, but the P_{fr} state is unstable.

INTRODUCTION

For efficient energy collection photosynthetic organisms possess various photosensors to regulate the synthesis of their photosynthetic apparatus, their movement as well as differentiation. One such group of photosensors is the red/far-red sensitive phytochrome family that universally exists in plants, most algae, many cyanobacteria and even in certain other eubacteria and fungi. The latter two groups of organisms show that phytochromes are not restricted to photosynthetic organisms (1). Signaling as mediated by most phytochromes involves absorption of red and far-red light which leads to two stable conformations, P_{fr} and P_r, respectively. The ability to absorb light is conferred by a covalently linked open-chain tetrapyrrole cofactor which is bound to a conserved cysteine *via* a thioether linkage. This cofactor differs slightly among various organisms (1). While plant phytochromes use phytochromobilin, their relatives in cyanobacteria such as Cph1 (2,3) utilize phycocyanobilin (PCB). Alternatively, biliverdin (BV), directly generated from heme, is found as chromophore in eubacterial as well as in fungal phytochromes (4). Although all phytochrome-like photoreceptors utilize a GAF domain to incorporate autocatalytically their cognate tetrapyrrole chromophores, cyanobacteria have up to three different phytochrome subfamilies which differ in their overall domain organization. The Cph1 subfamily resembles plant phytochromes in comprising an N-terminal sensory module consisting of PAS, GAF and PHY domains that shows a fully competent photochemistry (1). In the P_r state, the PCB chromophore adopts a *ZZZssa* conformation, that undergoes a $Z \rightarrow E$ double bond isomerization of the methine bridge between rings C and D upon red light absorption. A first ground state intermediate, lumi-R, could be identified for several phytochromes including Cph1 (5), before after several relaxation steps, during which the protein conformation changes due to protein–cofactor interactions, the photoactivated P_{fr} state is generated.

The second cyanobacterial phytochrome subfamily, exemplified by Cph2 (6), has a different domain organization as they lack the N-terminal PAS domain and replace the PHY domain by at least one additional GAF domain (GAF2) that probably adopts the function of the PHY domain. Whereas the globular regions of the PHY domain of Cph1 and the GAF2 domain of Cph2 are only weakly similar (sequence identity $< 16\%$), the tongue-like protrusion between the secondary structure elements $\beta 16$ and $\alpha 15$ is remarkably well conserved (7). In Cph1, the tongue uses the conserved PRxSF motif together with the N-terminal α-helix to form a part of the complex binding site for the chromophore. Two additional motifs within the tongue, the WG^AG and $W^{F,Y}xE$ regions, which generate a kink (7), are likewise preserved in the GAF2 domain of Cph2.

The Cph2 phytochrome from *Synechocystis* PCC 6803 (*Syn*Cph2, Fig. 1) differs from other Cph2-like phytochromes such as those from *Nostoc punctiforme* (6) in two aspects: First, it lacks a histidine kinase-like region as C-terminal transmitter module that is commonly found in phytochromes.

*Corresponding author email: essen@chemie.uni-marburg.de (Lars-Oliver Essen)

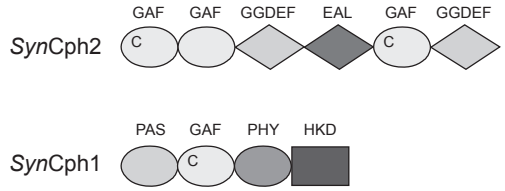

Figure 1. Domain organization of *Syn*Cph2 and *Syn*Cph1. Photosensory (oval symbols) and regulatory domains (angled symbols) differ in both phytochromes. GGDEF and EAL domains are involved in the turnover of c-di-GMP; *Syn*Cph1 contains a histidine kinase domain (HKD). The tetrapyrrole is covalently linked to a conserved cysteine (denoted C) in the GAF domain.

After the two N-terminal GAF domains (GAF1, GAF2) forming a P_r/P_{fr} switchable photosensory module, *Syn*Cph2 bears a GGDEF and an EAL domain. GGDEF domains usually act as bis-(3′-5′)-cyclic dimeric guanosine monophosphate (c-di-GMP) cyclases to increase the cellular c-di-GMP concentration, whereas in many cases EAL domains act as phosphodiesterases to decrease c-di-GMP content. As a second messenger in bacteria, c-di-GMP is known to regulate motility and biofilm formation (8). The second feature of *Syn*Cph2 is the presence of a third GAF domain, GAF3, which comprises a putative chromophore binding site and is followed by a second GGDEF domain. The GAF3 domain shows homology to other tetrapyrrole-binding proteins, which can be considered as third subfamily of phytochromes called cyanobacteriochromes (9,10). Unlike phytochromes belonging to the Cph1 and Cph2 subfamilies these phytochrome-like proteins absorb blue light. It can thus be supposed that *Syn*Cph2 additionally acts as a blue light receptor (11,12).

Recently, the key step of the generally accepted mechanism of the P_r/P_{fr} phototransformation, *i.e.* the *Z/E* photoisomerization of the C-D methine bridge, was questioned by an NMR study of the minimal chromophore-binding GAF domain derived from a thermophilic representative of the Cph2-subfamily. In that study it was claimed that instead a 90° flip of ring A caused the conformational changes required for down-stream signaling (13). Given that previous structural studies on phytochromes, which included the PHY domain, showed that the tetrapyrrole chromophore is intimately buried within the GAF domain by the sealing action of the tongue region (7,14), we wondered whether the N-terminal photosensory module of *Syn*Cph2 (GAF1-GAF2) shows marked differences to Cph1-like phytochromes due to its lack of an N-terminal PAS domain. Accordingly, we extended previous studies (15,16) on *Syn*Cph2 (GAF1-GAF2) utilizing mutants known from Cph1 to affect photoisomerisation as well as tongue–GAF domain interactions.

MATERIALS AND METHODS

Molecular cloning of Cph2(1,2), Y47H and R383D. The first 1272 bases from the gene *sll0821* from *Synechocystis* sp. PCC 6803 coding for M1-T424 of *Syn*Cph2 were amplified *via* PCR from genomic DNA by using a polymerase with exonuclease activity (Phusion, Finnzymes). Primers were designed to enable a ligation into the vector pCDFDuet-1 (Novagen). The upstream primer 5′-CGAGCGGCG*TCATGA*G**CAACCCTAATCGATCCTTAGAAG**-3′ includes a *Bsp*HI restriction site and the template ORF (bold), adding a serine codon after the start-methionine codon. The downstream primer was 5′-GAT*AAGCTT*AG TGGTGATGATGGTGATGGCTAGC**AGTCACAAACTGTTGGG TAATG-**3′; by this an additional *Hind*III restriction site and six histidine codons were included, and also an alanine and serine-coding codon between the template ORF and the his_6-tag.

The corresponding gene products were amplified by PCR and cloned into the vector pCR 2.1-TOPO (Invitrogen). The colonies were selected by 35 μg mL^{-1} kanamycin and blue/white screening. After sequencing, inserts were cloned into pCDFDuet-1 using 50 μg mL^{-1} streptomycin for selection.

The mutant Y47H was produced by QuikChange site-directed mutagenesis (Stratagene) of the pCDFDuet-1/Cph2(1,2) plasmid using the primer pair 5′-CCGGGTAAAAATTCACAAATTTG-CTAGCGATGGCAGCGG-3′ and 5′-CCGCTGCCATCGCTAG-CAAATTTGTGAATTTTTACCCGG-3′ (analytical restriction sites are underlined). The R383D mutant was generated using the primer pair 5′-GACCGCCGCAATATTCTGCCCGATCTAAGCTTCGAG GCTTGGG-3′ and 5′-CCCAAGCCTCGAAGCTTAGATCGGGCA GAATATTGCGGCGGTC-3′. The vectors were verified by dideoxy sequencing and cotransformed into BL21 Gold (DE3) (Novagene) with the p171 coexpression vector that harbors the genes *pcyA* and *ho1* coding for the enzymes supplying the cofactor PCB (17).

Recombinant overproduction of Cph2(1,2). Cultures with 1 L TB media (and antibiotics, final concentrations of 50 μg mL^{-1} streptomycin and 100 μg mL^{-1} ampicillin) were grown in 5 L flasks to OD_{595nm} 0.3 at 310 K and 150 rpm. After decreasing the temperature to 291 K, the expression was induced at OD_{595nm} 0.5 by 0.05 mM isopropyl β-D-thiogalactoside (Gerbu). After 22 h the cells were pelleted at ~8600 ***g*** for 15 min, resuspended in about 15–20 mL PB buffer (50 mM NaH_2PO_4, 300 mM NaCl, 10 mM imidazole, pH 8.0) per liter cell culture and frozen at 193 K. After slowly thawing the cells 0.1 mM EDTA (final concentrations), 0.02 mM PMSF and 40 μg mL^{-1} lysozyme (Serva) were added. Subsequent to 10 min incubation the cells were lysed *via* two passages through an emulsifier C5 (Avestin) at 50000–100000 kPa. The cell debris was pelleted at ~40000 ***g*** for 30 min. While stirring the supernatant, ammonium sulfate was slowly added up to a final concentration of 13.5%. After incubation overnight the protein was pelleted by centrifugation for 15 min at ~20000 ***g*** and resuspended in about 8–10 mL PB buffer per original liter cell culture. The solution was then clarified at 13000 rpm for 15 min (Beckman, JA20 rotor). The supernatant was added to a pre-equilibrated nickel affinity column (Ni^{2+}-NTA agarose matrix [Qiagen]), diameter 1.5 cm, height 4.8 cm, flow rate 1 mL min^{-1}). After washing with three column volumes of PB buffer, the protein was eluted by a gradient of PB and EB (50 mM NaH_2PO_4, 300 mM NaCl, 500 mM imidazole, pH 8.0). The final purification step removing most of the apoprotein was carried out by size exclusion chromatography (SEC). The column (Superdex 200 26/60, GE Healthcare, volume 318 mL, flow rate 2 mL min^{-1}) was equilibrated with SEC buffer (50 mM Tris/HCl, 300 mM NaCl, 5 mM EDTA, pH 8.0) prior to loading the protein solution. The eluate was concentrated with an Amicon-Ultra concentrator (10 kDa membrane cut-off, Millipore). Protein concentrations were determined by UV measurements at 280 nm. The binding of the cofactor was shown by zinc-induced fluorescence. After SDS-PAGE the gel was incubated for 30 min in 2 mM zinc acetate. The bilin coordinates the zinc ion (18), such that under UV radiation (312 nm) the resulting bright fluorescence could be detected. Afterwards the gel was stained with Coomassie blue.

Mass spectrometry. To identify the bound cofactor the protein was digested with chymotrypsin, the fragments separated by reversed-phase HPLC and detected by FT-ICR (Bruker).

UV/vis spectroscopy. UV/Vis absorbance spectra were measured with a modified Agilent 8453 UV/vis diode detector-array spectrophotometer using an integration time of 100 ms and 1 nm resolution at room temperature. Irradiation of the sample for 30 s with red or far-red LED sources (B5-436-30D, λ_{max} 664 nm and SMC735, λ_{max} 735 nm; both 40 nm FWHM, Roithner, Vienna) at a distance of 0.5–1 cm was found to be sufficient for saturation as further illumination did not change UV/vis spectra. A cell of 1 cm path length was used. The extinction coefficients at 280 nm were calculated by ProtParam (ExPASy) taking into account the chromophore absorbance at this wavelength. Extinction coefficients at the P_r maximum were determined as triplicates from UV/vis data of a protein sample in SEC buffer solution and in 8 M urea pH 2.7. As the protein concentrations under both conditions were the same and the

extinction coefficient of urea-denatured peptide-bound PCB is known (19), the extinction coefficients at the P_r maximum could be calculated.

Dark reversion in the temperature range of 295–311 K was detected *via* a spectropolarimeter J-810 (Jasco) used for recording the time-dependent absorbance. After irradiating the sample for 30 s with light of 656 ± 10 nm the absorbance at 644 nm was determined with a 2 mm path length cell in time intervals of 1–20 min.

The half lives $t_{1/2}$ and thus the rate constant k of the dark reversion could be calculated from the resulting mono-exponential curves. Each value is the average of at least three measurements. Determining the rate constant k as function of the temperature allows calculation of the activation energy ΔE_A on the basis of Arrhenius plots.

Fluorescence spectroscopy. Different types of fluorescence measurements were carried out with a FluoroMax 4 spectrofluorometer (Horiba Jobin Yvon). Emission spectra were measured at an excitation wavelength of 600 nm after 30 s red or far-red (λ_a = 656, 735 nm) irradiation of the sample and were averaged over three scans. Excitation light of 600 nm, which is weakly absorbed, was chosen to minimize photoconversion effects during the measurement. The fluorescence quantum yield of Cph2(1,2) φ_F^{Cph2} was determined by comparison with the fluorescence of chlorophyll *a* (in acetone) for which the quantum yield φ_F^{Chla} is known (20). The integral fluorescence F^{Chla} of chlorophyll *a* and F^{Cph2} of Cph2(1,2) is given by

$$F^{Chla} = I_0^{600nm} \cdot (1 - T)^{Chla} \cdot K \cdot \varphi_F^{Chla}, \quad (1)$$

and by

$$F^{Cph2} = I_0^{600nm} \cdot (1 - T)^{Cph2} \cdot K \cdot \varphi_F^{Cph2} \quad (2)$$

where I_0^{600} is the intensity of the light source at 600 nm, K an apparatus-specific constant and T^{Chla} and T^{Cph2} the transmittance of chlorophyll *a* and Cph2(1,2), respectively, at 600 nm. Then φ_F^{Cph2} is obtained according to

$$\frac{\varphi_F^{Cph2} = (1 - T)^{Chla} \cdot \varphi_F^{Chla} \cdot F^{Cph2}}{(1 - T)^{Cph2} \cdot F^{Chla}} \quad (3)$$

Emission spectra of Cph2(1,2) were also measured with excitation wavelengths of 590 or 610 nm to elucidate a possible dependence of the spectra on the wavelength of excitation and thus to detect other possible fluorescent species in the sample. Excitation spectra were measured with an emission wavelength of 720 nm.

Variable P_r fluorescence connected with its photoconversion into a photoproduct stable at low temperature (presumably lumi-R) and into P_{fr} at ambient temperature was taken as a measure of its photochemical activity. The extent of the P_r photoconversion at low and ambient temperatures, γ_1 and γ_2, characterized the initial P_r photoreaction and operation of the P_r–P_{fr} photocycle, respectively (21). More specifically, for testing the P_r–P_{fr} photoconversion at ambient temperatures, variable fluorescence of P_r connected with its photoconversion by actinic/exciting light at a wavelength of 644 nm was monitored and six measurements were averaged. From this measurement the P_{fr} content under photostationary conditions and the photoconversion rate constant k_1^{Cph2} could be calculated. The latter quantity was obtained by a linear fit to the data gained within the first 20 s. The rate constant can be taken from the slope of the linear fit and shows the initial turnover rate of P_r. This was used to calculate the quantum yield of photoconversion φ_P^{Cph2} according to

$$\varphi_P^{Cph2} = \frac{k_1^{Cph2} \cdot \varepsilon_{660}^{Cph1\Delta2} \cdot I_0^{Cph1\Delta2,660} \cdot \varphi_P^{Cph1\Delta2}}{k_1^{Cph1\Delta2} \cdot \varepsilon_{644}^{Cph2} \cdot I_0^{Cph2,644}} \quad (4)$$

using the quantum yield for Cph1Δ2 $\varphi_P^{Cph1\Delta2}$ as a reference (22). In Eq. (4), $\varepsilon_{660}^{Cph1\Delta2}$ and ε_{644}^{Cph2} refer to the extinction coefficients of Cph1Δ2 and Cph2(1,2) at the absorption maximum, respectively. The corresponding actinic light intensities are denoted by $I_0^{Cph1\Delta2,660}$ and $I_0^{Cph2,644}$, whereas the photoconversion rate constant is given by $k_1^{Cph1\Delta2}$.

The extent of the $P_r \rightarrow P_{fr}$ photoconversion under saturating red light (λ_a = 644 nm) at ambient temperatures was determined by the ratio of the variable P_r fluorescence

$$\gamma_2 = \frac{\Delta F}{F_0} = \frac{(F_0 - F_1)}{F_0}, \quad (5)$$

where F_0 denotes the fluorescence intensity in the far-red illuminated state, and F_1 denotes photostationary conditions, given the fact that P_{fr} does not fluoresce (23).

Evaluation of γ_2 from the fluorescence measurements allows determination of the P_{fr} absorption spectrum from the initial P_r spectrum and the spectrum at the photoequilibrium as a difference:

$$spectrum(P_{fr}content) = spectrum(P_r + P_{fr}) - spectrum(P_r) \cdot (1 - \gamma_2). \quad (6)$$

Knowing γ_2 and the quantum yield of the direct photoreaction $P_r \rightarrow P_{fr}$ ($\varphi_P^{Pr \rightarrow Pfr}$) the quantum yield of the reverse $P_{fr} \rightarrow P_r$ photoreaction can be calculated because the rates of the photoconversion at photoequilibrium in both directions are the same (24,25):

$$v_{Pr \rightarrow Pfr} = v_{Pfr \rightarrow Pr}. \quad (7)$$

The rate of the photoconversion for low OD (< 0.1) is

$$v_{Pr \rightarrow Pfr} = I_0 \cdot \frac{S}{V} \cdot 2.3 \cdot OD_{Pr} \cdot \varphi_P^{Pr \rightarrow Pfr}, \quad (8)$$

$$v_{Pfr \rightarrow Pr} = I_0 \cdot \frac{S}{V} \cdot 2.3 \cdot OD_{Pfr} \cdot \varphi_P^{Pfr \rightarrow Pr}, \quad (9)$$

where I_0 is the actinic light intensity, S the illuminated area, and V the illuminated volume. OD_{Pr} and OD_{Pfr} are the individual optical densities for P_r and P_{fr} under photostationary conditions at the wavelength of the red actinic light. With Eq. (7) one can conclude

$$OD_{Pr} \cdot \varphi_P^{Pr \rightarrow Pfr} = OD_{Pfr} \cdot \varphi_P^{Pfr \rightarrow Pr}, \quad (10)$$

$$\varphi_P^{Pfr \rightarrow Pr} = \frac{OD_{Pr}}{OD_{Pfr}} \cdot \varphi_P^{Pr \rightarrow Pfr}. \quad (11)$$

OD_{Pfr} can be obtained from the absorption spectrum calculated by Eq. (6). For the determination of OD_{Pr} the initial P_r spectrum needs to be reduced in agreement with the extent of the phototransformation at the P_r–P_{fr} photoequilibrium after red light illumination γ_2:

$$spectrum(P_r content) = spectrum(P_r) \cdot (1 - \gamma_2). \quad (12)$$

The optical density of the samples was low (< 0.1 OD) practically excluding screening effects, self-absorption of fluorescence and deviation from linearity in the equations for the determination of the photoconversion quantum yields.

The extent of P_r photoconversion of R383D under photostationary conditions was determined by measurements with a cuvette precooled at 273 K because of the fast reversion of the red light phototransformation product to P_r.

Low temperature spectra of P_r and P_{fr} were carried out after irradiating the sample with red or far-red light at room temperature and subsequent cooling to 77 K. At this temperature thermal relaxation processes of the photoinduced reaction cycle are blocked (23) such that irradiation of the sample should, if at all, only induce the transition of P_r to the primary photoproduct lumi-R (26). Low-temperature emission spectra were measured with an excitation wavelength of 600 nm. To verify the possibility of the $P_r \rightarrow$ lumi-R photoconversion at this temperature, the frozen sample was illuminated with saturating actinic light at 656 nm monitoring the decrease of the P_r fluorescence ($\Delta F/F_0$) and concomitant increase of intensity at the emission maximum of lumi-R (27). Likewise, excitation spectra were measured at 77 K at the emission wavelength of 720 nm to examine formation of a lumi-R-like state.

Furthermore, temperature-dependent emission spectra were measured from 100 to 269 K by increasing temperature in intervals of 25 K. These measurements allowed for determining the temperature dependence of φ_F^{Cph2}. Linearization of this dependence in the Arrhenius coordinates allowed the determination of ΔE_A for the P_r fluorescence decay and of the activation barrier for the reaction of $P_r \rightarrow$ lumi-R in the electronically excited state (23,26).

Circular dichroism spectroscopy. Circular dichroism (CD) spectra were measured with a spectropolarimeter J-810 (Jasco) at room temperature after 30 s irradiation with 656 ± 10 nm or 735 ± 10 nm light using a cell of 1 mm path-length. After baseline corrections, for which the same cell filled with buffer was used, the data were averaged over three scans.

Resonance Raman spectroscopy. Resonance Raman (RR) spectra were recorded with 1064 nm excitation using a RFS 100/S (Bruker Optics, Ettlingen, Germany) Fourier-transform Raman spectrometer (4 cm^{-1} spectral resolution). The near-IR excitation line was close enough to the first electronic transition to generate a sufficiently strong preresonance enhancement of the chromophoric vibrational bands such that Raman bands of the protein matrix remained very weak in the spectra of the parent states. Typical sample volumes were 5 μL of a 1–2 mM protein solution in 50 mM NaH_2PO_4 (pH 8.0) and 300 mM NaCl. All spectra were measured at 133 K using a liquid-nitrogen cooled cryostat (Linkam, Waterfield, Surrey, UK). The laser power at the sample was set to 300 mW, which did not damage the chromoproteins as checked by comparing spectra of the samples obtained before and after RR data acquisition. The total accumulation time was about 2 h for each spectrum. For all RR spectra, the background was subtracted manually. To obtain the P_{fr} spectra, the samples were irradiated at room temperature with 656 nm and then rapidly frozen to 133 K. Red light-emitting diodes were used for photoconversion (*vide supra*).

RESULTS

*Syn*Cph2 (*sll0821*) from *Synechocystis* PCC6803 includes two likely PCB-binding cysteines, Cys129 and Cys1022, in two of its three GAF-like domains (Fig. 1). Together with the subsequent GAF2 domain only the first PCB-binding site in GAF1 confers P_r–P_{fr}-like photochromicity (15). The GAF domains 1 and 2 share some sequence identity with the GAF and PHY domain region of the well-characterized photosensory module from the cyanobacterial phytochrome Cph1 (Cph1Δ2). Accordingly, to get a photochemically functional protein, an N-terminal *Syn*Cph2 variant comprising the residues M1–T424 and covering the GAF1 and GAF2 domains (molecular mass 49.8 kDa, Cph2(1,2)) together with a C-terminal histidine affinity tag was constructed that, according to the structure of the Cph1Δ2 module (7), is terminated 24 amino acids after the tongue region.

The Y176H mutant of the Cph1 GAF domain was found to exhibit a strong fluorescence and a severely reduced $P_r \rightarrow P_{fr}$ photoconversion (28,29). The equivalent mutant Y276H of phyB from *Arabidopsis thaliana* is photochemically arrested in the P_r state but imitates physiologically the P_{fr} signaling state (29,30). Interestingly, this mutant is not fluorescent in biliverdin-binding phytochromes, allowing the two phytochrome subtypes to be distinguished (31).

Accordingly, together with the R383D mutant predicted to affect a conserved salt bridge between the tongue region and the GAF1 domain, the analogous Y47H mutant of Cph2(1,2) was constructed to allow an assignment of Cph2 to either the Cph1/plant-like or BV-like class of phytochromes.

Expression, purification and characterisation of the holoprotein

Cph2(1,2) was overproduced in *Escherichia coli* with typical yields of 30–35 mg L^{-1} culture. After induction, the culture slowly became deep-green with bacteria pellets exhibiting an intense blue color. SDS-PAGE analysis showed the recombinant protein at an apparent molecular mass of 50 kDa, of which about 60% was soluble in the cell extract. Zn^{2+}-induced fluorescence revealed the binding of the cofactor PCB (Fig. 2) in nearly 90% of the soluble protein. Initial purification *via* Ni-NTA affinity chromatography led to a homogeneity of Cph2(1,2) of 90–95% for the holoprotein. The final purification step was based on SEC. The wildtype Cph2(1,2), Y47H and R383D mutants showed only slightly different elution profiles indicating a predominantly monomeric species eluting at an apparent mass of 46.8 kDa. P_{fr} eluted only slightly earlier than P_r, possibly because of a slight conformational change (Fig. 3). P_{fr} could however, not be separated from P_r by SEC, in contrast to Cph1Δ2 (32). Nevertheless, SEC allowed PCB-bound Cph2(1,2) to be separated from apoprotein since the Cph2(1,2) apoprotein aggregated.

Cph2(1,2) contains one cysteine in each GAF domain. To prove that the cofactor is PCB and exclusively linked to GAF1 in the *E. coli* assembled Cph2(1,2), a mass spectrometry

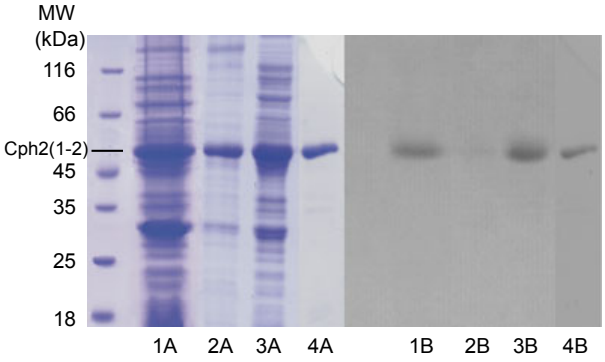

Figure 2. A: 12% SDS-PAGE gel of BL21 Gold cells expressing Cph2(1,2) (1: whole culture; 2: pellet; 3: supernatant; 4: purified protein; MW = molecular mass marker) after Coomassie staining. B: Zinc staining of the same gel.

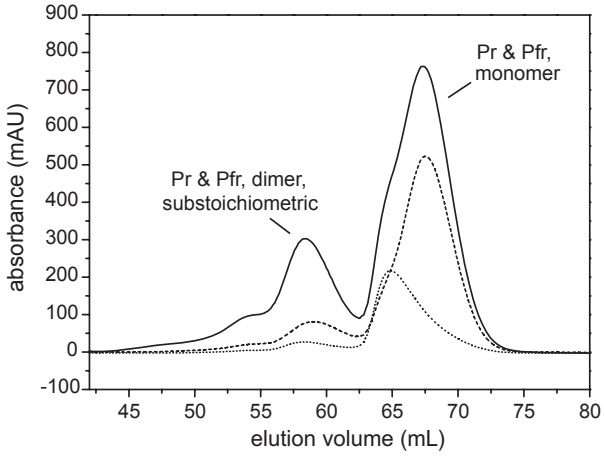

Figure 3. Elution profile of size exclusion chromatography for Cph2(1,2) (SAR = 0.8) measured at 280 nm (solid curve), 644 nm (dashed curve) for indicating P_r conformation and 700 nm (dotted curve) for P_{fr} conformation; Y47H and R383D exhibit the same elution profile (not shown).

analysis was carried out. Chymotryptic fragments of Cph2(1,2) were separated by RP-HPLC and analyzed by ESI-MS. The fragment (T124–Y133) that is predicted to carry the cofactor PCB at C129 was detected as a PCB-adduct at *m/z* 876.8975 ($[M + 2H]^{2+}$ ion; calculated *m/z*: 876.9005). Further MS-MS analysis of this peak (Fig. 4) showed a set of signals that proved binding of PCB to Cys129. The bond between the cysteine and the cofactor is scissile due to fragmentation. Accordingly, the spectrum also showed peaks of the single PCB (M^+; *m/z*: 587.4), PCB with a remaining thiol moiety (M^+; *m/z*: 619.3), the peptide with an intact cysteine without PCB (M^+; *m/z*: 1166.5) and the peptide without PCB and sulfur (M^+; *m/z*: 1132.5).

UV/vis absorption spectroscopy

The absorption spectra of Cph2(1,2) and its Y47H mutant show the characteristics of P_r and P_{fr} states known from Cph1 (Figs. 4 and 5, Table 1). The photoproduct of R383D after red-light irradiation displays a broadened absorption spectrum in the red region in comparison with the wildtype and Y47H, suggesting that R383D remains in an intermediate state (Fig. 5).

The absorption maxima of the P_{fr} state of the wildtype are red-shifted with respect to P_r, the effect being largest between 550 and 750 nm (Max P_r: 644 nm, P_{fr}: 695 nm). Compared with Cph1, the maxima of P_r and P_{fr} display a blue shift of 8–19 nm (Table 1). In comparison with wildtype Cph2(1,2), the Y47H and R383D mutants show a further blue shift of the minima in the difference spectra (4–7 nm; WT: 696 nm, Y47H: 689 nm, R383D: 692 nm) corresponding to a *ca* 25 nm blue shift of their P_{fr} maxima. Interestingly, an N-terminal *Syn*Cph2 fragment truncated at N390, *i.e.* within the tongue region (shorter by 34 amino acids than Cph2(1,2) [15]) shows a similar behavior to these Cph2(1,2) mutants. The smaller red shift of the P_{fr} state is, therefore, attributed to either a

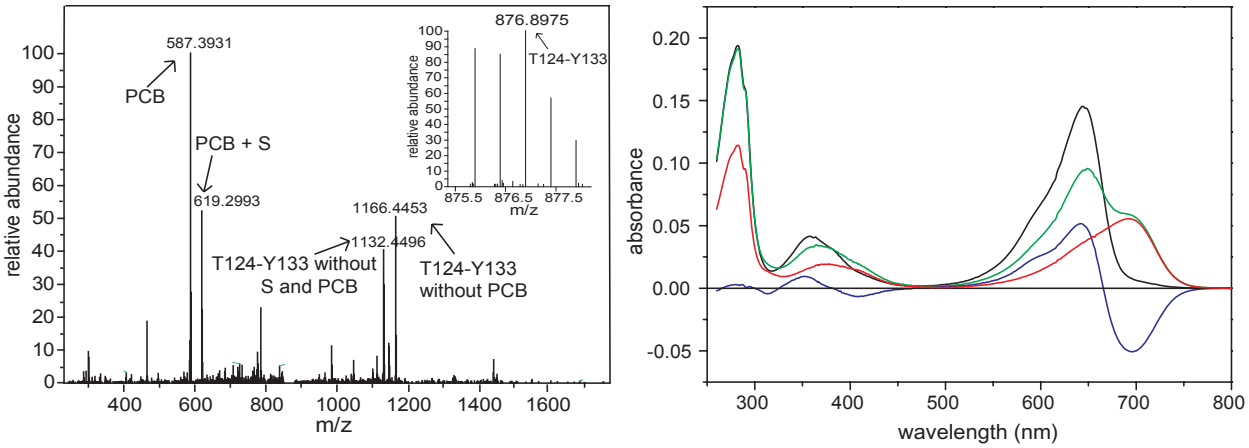

Figure 4. Characterization of PCB-bound Cph2(1,2): MS-MS analysis *via* FT-ICR of the protein fragment *m/z* 876.9 (left). The fragmentation occurs at the bond between the cofactor and the protein. The T124-Y133 peptide and PCB fragments are detected with and without the sulfur of the cofactor-binding cysteine. Inlay, mass spectrum of the chymotryptically obtained T124-Y133 peptide prior to fragmentation. UV/vis absorption spectra of Cph2(1,2) (right) in 50 mM Tris-buffer pH 8.0 after far-red (black curve, P_r) and red (green curve, P_{fr} + P_r) irradiation; the difference spectrum ($A[P_r]-A[P_{fr}]$) and the P_{fr} spectrum calculated from the spectrum after red irradiation are shown in the blue and the red curve, respectively.

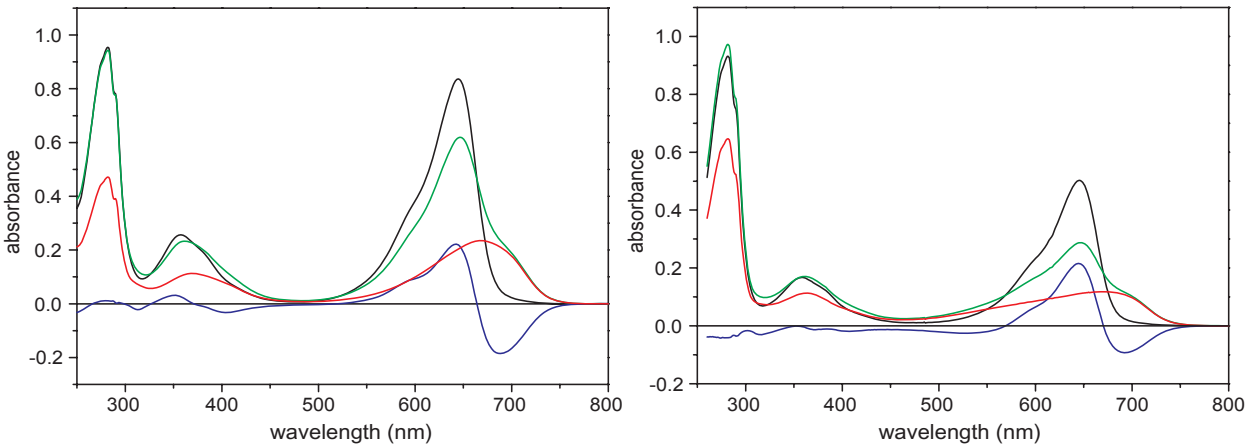

Figure 5. UV/vis absorption spectra of Y47H (left) and R383D (right) in 50 mM Tris-buffer pH 8.0 after irradiation with far-red (black curve, P_r) and red (green curve, P_{fr} + P_r) light; the difference spectrum ($A[P_r]-A[P_{fr}]$) is shown in the blue curve, the calculated P_{fr} (or intermediate) spectrum in the red curve.

Table 1. UV/vis absorption maxima and minima of the Cph2(1,2) wildtype and its Y47H and R383D mutants in comparison with full length Cph1 and Cph2 and an N-terminal Cph2 construct (N-390) which ends within the tongue region.

	Maximum P_r (nm)	Minimum P_{fr} (nm)	Maximum difference spectrum (nm)	Minimum difference spectrum (nm)	Isosbestic point (nm)
Cph2(1,2)	644, 358	695, 376	642.5	696	665.5
Y47H	644, 357	670, 370	642.5	689	664
R383D	646, 358	*ca* 670, 364	644	692	666
Cph2-N390 (15)			642	690	
Full length Cph2 (16)			643	690	
Full length Cph1 (17,53)	663	703	660	705	680

distorted interaction between the tongue region and the PCB that increases solvent accessibility of the chromophore, or to a perturbed chromophore conformation.

The extinction coefficient at 280 nm for the protein moiety was predicted by ProtParam (ExPASy). Taking into account the absorption of the chromophore at this wavelength (ε_{280nm} = 5mM^{-1} cm^{-1} [33,34]), the overall extinction coefficient of the Cph2(1,2) holoprotein was thus calculated to be $\varepsilon_{280nm}^{Cph2} = 90mM^{-1} \cdot cm^{-1}$. $\varepsilon_{644nm}^{Cph2}$ was determined using the PCB extinction coefficient of C-phycocyanin in 8 M acidic urea (19,35) where PCB is bound to a denatured peptide chain. Also the maximum 644 nm/280 nm specific absorbance ratio (SAR; Table 2) was calculated using UV/vis data. The extinction coefficients obtained at 280 nm reflected the higher number of tryptophans in the photosensory module of Cph2(1,2) than in Cph1Δ2 (13 *vs* 7) whereas the latter has a higher extinction coefficient at the P_r maximum (33). Accordingly, the SAR values of Cph2(1,2) are lower than of Cph1Δ2.

The Y47H mutant—expected to affect ring D rotation of the chromophore during photoisomerisation—showed photoconversion behavior similar to the wildtype except for a lower portion of P_{fr} content at photoequilibrium. Analogous mutants in Cph1Δ2 (28,29), phyA and phyB (29,30) displayed extremely reduced or fully blocked photoconversion, indicating that a structural change near ring D partially or completely prevents methine bridge isomerization. The R383D mutant—predicted to destroy the salt bridge between the arginine of the PRxSF motif of the tongue region and a conserved aspartate in the DIP motif of the GAF1 domain—also exhibited photoconversion, but unlike the Cph2(1,2) wildtype and the Y47H mutant, the spectrum of the R383D photoproduct was unusually broadened in the red/far-red region reflecting conformational heterogeneity of the bound PCB cofactor in a P_{fr}-like state or formation of a red-shifted state other than P_{fr}.

P_r was the stable state of Cph2(1,2) wildtype, Y47H, and R383D, as P_{fr} and the intermediate state of R383D completely reverted to P_r in the dark. To determine the rate constants for this reaction, the absorbance was monitored at the P_r maximum. The absorbance changes of P_r indicate first-order kinetics for dark reversion. At 303 K, where *Synechocystis* shows maximal growth (36), the half life of P_{fr} in the dark was 54 min. With a half life of 11.8 ± 0.6 min at the same temperature Y47H showed five-fold faster dark reversion, implying a destabilized P_{fr} state. R383D exhibits an even further accelerated dark reversion. At 293 K the half life of the photoproduct was 6.4 ± 0.1 min, almost 40-fold faster than in the wildtype at that temperature ($t_{½}$:238 min). From the half lives obtained for wildtype Cph2(1,2) (Table 3), a linear Arrhenius plot (Fig. 6) could be generated, yielding an activation energy of ΔE_a = 112.4 ± 4.8 kJ mol^{-1}.

Whereas in plants the dark reversion of P_{fr} is well known (26,37), Cph1Δ2 showed no dark reversion even after 2 weeks at room temperature (2,33) in contrast to Cph2(1,2). It should

Table 2. Extinction coefficients and absorbance ratios.

	ε_{280nm} (mM^{-1} cm^{-1})	ε_{max} (mM^{-1} cm^{-1})	SAR (A_{max}/A_{280nm})
Cph2(1,2)	90	78 ± 2 (644 nm)	0.8
Y47H	89	77 ± 1 (644 nm)	0.9
R383D	90	78 ± 1 (646 nm)	0.6
Cph1Δ2 (33)	64	82 (654 nm)	1.3

Table 3. Half lives of the P_{fr}-state of Cph2(1,2) determined by UV/vis absorption measurements.

Temperature (K)	Half life (min)
295	159.9 ± 11.7
299	92.3 ± 7.1
303	53.9 ± 1.3
307	24.5 ± 1.8
311	16.0 ± 1.5

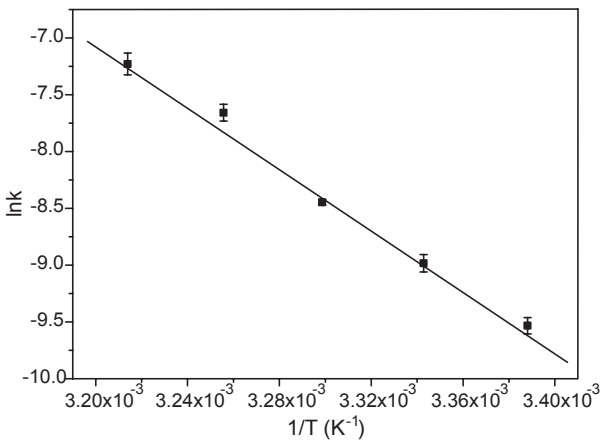

Figure 6. Arrhenius plot of the $P_{fr} \rightarrow P_r$ dark reversion determined by UV/vis measurements.

be noted in this context that the process in plants also proved to be complex: it depends on species and tissues (in monocots it is not observed), on phytochrome type (phyA or phyB), and their native state (phyA, for instance, reveals no dark reversion in yeast) (21).

Fluorescence spectroscopy

The fluorescence emission spectra of the P_r states of Cph2(1,2) and the Y47H mutant (Fig. 7) show maxima at 667 nm. A variation of the maximum of the emission wavelength on the excitation wavelength was not observed, implying that the sample was homogenous. Similarly, the maximum of the excitation spectrum at 644 nm (Fig. 7) coincides with the absorption maximum of P_r. Like other phytochromes (26), the P_{fr} states show no measurable fluorescence. From the emission spectra of the P_r states, fluorescence quantum yields for the wildtype protein, Y47H, and R383D were determined to be $\varphi_F^{Cph2} = 3.2 \cdot 10^{-2}$, $\varphi_F^{Y47H} = 2.0 \cdot 10^{-2}$, and $\varphi_F^{R383D} = 3.3 \cdot 10^{-2}$, respectively. These values were in the same range as determined for Cph1Δ2 which has a fluorescence quantum yield of $\varphi_F^{Cph1\Delta2} = 2.3 - 2.5 \cdot 10^{-2}$ (J. Hughes, unpublished). Plant phytochromes have a significantly lower fluorescence quantum yield at room temperature, characteristically in the range $1.5 - 5.0 \times 10^{-3}$ for phyA from different plant species in different laboratories (26).

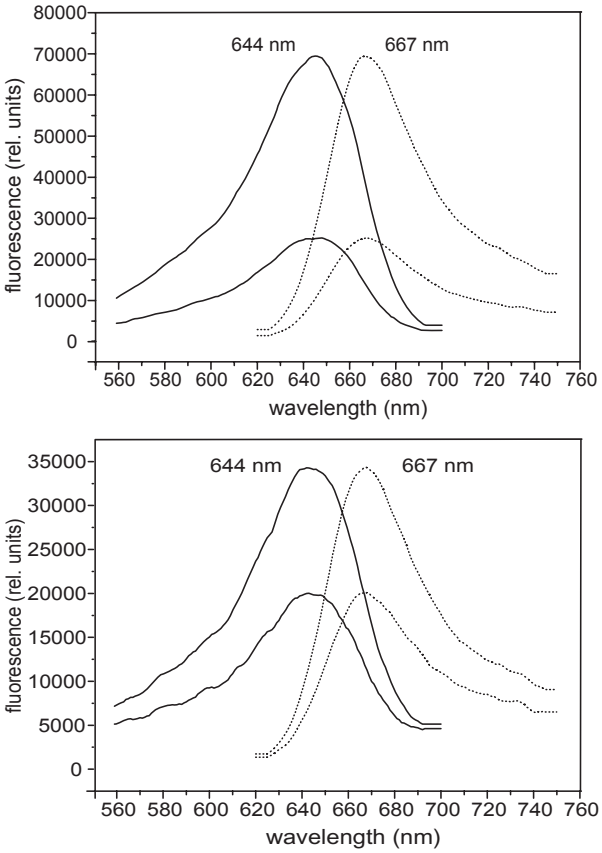

Figure 7. Room temperature fluorescence excitation (solid) and emission spectra (dotted curves) for Cph2(1,2) (top) and Y47H (bottom) after far-red (P_r, upper curves) and red irradiation (P_{fr}, lower curves) in 50 mM Tris-buffer pH 8.0; excitation wavelength of emission spectra λ_{ex} = 600 nm, emission wavelength of excitation spectra at λ_{em} = 720 nm (emission spectra were scaled to the same maximum as excitation spectra). The mutant R383D exhibits the same fluorescence characteristics with an emission maximum of 668 nm and an excitation maximum of 646 nm.

Unlike to Cph1 and the plant phytochromes phyA and phyB (28,29), where the analogous Y → H mutation induces strong fluorescence (*e.g.* Cph1: $\varphi_F^{Y176H} = 0.145$ ([29] and J. Hughes, unpublished), the Y47H mutant of Cph2(1,2) shows 40% lower fluorescence than the wildtype protein. This finding is in agreement with the results for the analogous Y163H mutant of PaBphP, a biliverdin-binding phytochrome from *Pseudomonas aeruginosa* (29).

The kinetic of the $P_r \rightarrow P_{fr}$ photoconversion of Cph2(1,2) shows a mono-exponential decrease at room temperature (Fig. 8). At photoequilibrium, the fluorescence levels at 40% relative to P_r. Thus, we obtained a photostationary equilibrium portion of the P_{fr} state of 60% ($\gamma_2^{WT} = 0.60$) which agrees with the results reported for the 58% *in vivo* portion of P_{fr} of *Syn*Cph2 (38). The destabilization of the P_{fr} state observed for the mutant Y47H of Cph2(1,2) was reflected by a P_{fr} portion of 51% ($\gamma_2^{Y47H} = 0.51$). The nonfluorescent intermediate generated after red-light illumination of R383D was determined to be 59% ($\gamma_2^{R383D} = 0.59$). This value represents a lower limit because of the rapid reversion to P_r. A more accurate value of $\gamma_2^{R383D} = 0.63$ was calculated to achieve a reasonable continuous profile for the UV/vis intermediate spectrum (Fig. 5).

Under these experimental conditions the rate constants of photoconversion during the first 20 s were determined to be 0.0054, 0.0055 and 0.0043 s^{-1} for the Cph2(1,2) wildtype, Y47H, and R383D, respectively. Interestingly, the quantum yield of the $P_r \rightarrow P_{fr}$ photoconversion was 0.12 for Cph2(1,2) and 0.13 for Y47H and thus rather lower than for other phytochromes. Cph1Δ2, for example, has a quantum yield of 0.16 (22). Values of 0.07–0.21 for plant phytochromes of different size and from different plant species have been reported (26). Analogously, the quantum yield of the P_r conversion of R383D is 0.10. The quantum yields for the conversion from P_{fr} to P_r are 0.19 for the wildtype and 0.26 for

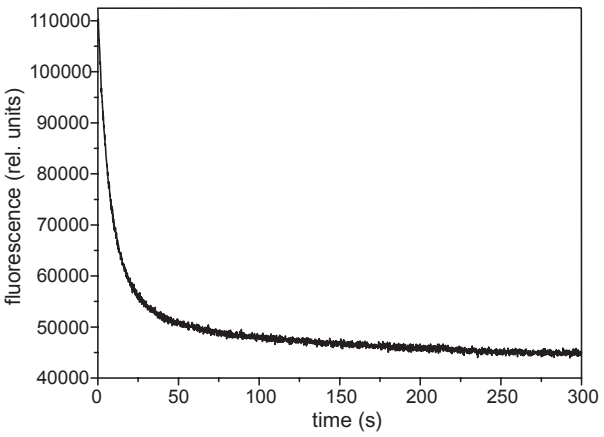

Figure 8. P_r–P_{fr} photoconversion by irradiation at 644 nm and measuring emission at λ_{em} = 720 nm.

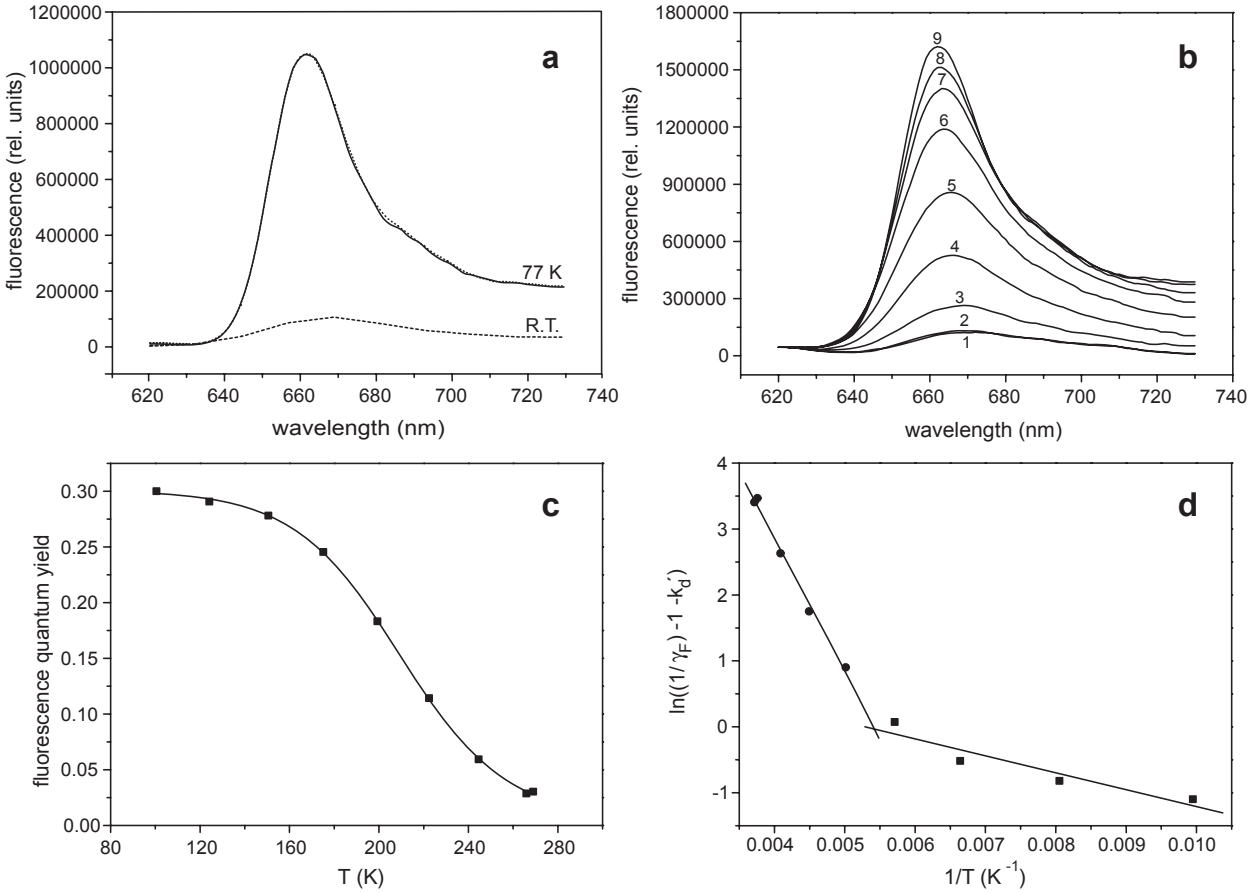

Figure 9. (a) Emission spectra of Cph2(1,2) in the P_r state in 50 mM Tris buffer pH 8.0; solid line: at 77 K, dotted line: after red light illumination at 77 K, dashed line: P_r at room temperature. (b) Temperature-dependent emission spectra from 269 K (1) down to 100 K (9) in 25 K steps. (c) Temperature dependence of the fluorescence quantum yield with a sigmoidal course; the fluorescence yield at 100 K was assumed to be 0.3. (d) Fluorescence yields in Arrhenius coordinates; k_d' temperature-independent excitation deactivation constant normalized to the fluorescence constant (k_d/k_f) is taken as 2; evaluation of k_d' see Ref. (54).

Y47H. These values, on the contrary, are higher than those of Cph1 and plant phytochromes (22,26).

Low-temperature measurements of Cph2(1,2) (Fig. 9a) showed a 10-fold increase of fluorescence intensity at 77 K, whereas for full-length Cph1 the increase was 15 to 20-fold at 85 K (39). Irradiation of P_r with red light at 77 K did not cause any photoconversion in analogy to Cph1 (Fig. 9a) and also to moss CP2, fern *Adiantum capillus-veneris* phy1, phyB and the minor pool of phyA′ that do not exhibit photoconversion up to 160–170 K ($\rightarrow P_r'$ photochemical type) and in contrast to major phyA′ photoactive at these temperatures ($\rightarrow P_r'$ photochemical type) (21). This finding indicates that the energy barrier which leads to lumi-R might be too high to allow for cryo-trapping of this state. Alternatively, if the lumi-R state is formed at 77 K the yield of the reverse lumi-R $\rightarrow P_r$ photoreaction should be much higher than the direct one, resulting in a shift of the photoequilibrium to the inital P_r state. The emission maximum exhibited a red shift of 8 nm at higher temperatures (Fig. 9b). An analogous phenomenon, albeit in the opposite direction, was noted for Cph1 and the moss phytochrome CP2, where blue shifts of the maximum of up to 7 nm were observed (23,39,40). In contrast to the emission spectra, the maximum of excitation spectra did not reveal any temperature dependence and were identical in this temperature range.

The temperature-dependent relative quantum yield of Cph2(1,2) (Fig. 9c) shows a sigmoidal decrease with increasing temperature. At *ca* 210 K, the maximum decrease of the quantum yield was observed. In Arrhenius coordinates the temperature dependence shows two linear regions between 269–185 K and 185–100 K (Fig. 9d). The activation energies of the P_r fluorescence decay and thus of the P_r photoreaction are ΔE_a = 16.7 kJ mol^{-1} and ΔE_a = 2.1 kJ mol^{-1}, respectively. The activation energies for the Cph1Δ2 fluorescence decay are ΔE_a = 12.6 kJ mol^{-1} and ΔE_a = 6.5 kJ mol^{-1} in the range 210–273 K and 210–85 K (23) and thus smaller at higher temperatures and larger at lower temperatures.

ΔE_a values of the mutants are represented in Table 4. Although the activation energies resemble the wildtype, the mutant R383D has a two-fold larger activation energy at higher temperatures. The ΔE_a breaking points of the mutants are shifted to higher temperatures compared to the wildtype.

Table 4. Fluorescence properties of Cph2(1,2) wildtype and its Y47H and R383D mutants; *corrected for P_{fr} instability: 0.63, **quantum yield of the $P_r \rightarrow$ intermediate photoconversion, ***not detected.

	Wildtype	Y47H	R383D
λ_{max} of the P_r emission spectrum (nm)	667	667	668
λ_{max} of the P_r excitation spectrum (nm)	644	644	646
Fluorescence quantum yield φ_F^{Pr}, 293 K	3.2×10^{-2}	2.0×10^{-2}	3.3×10^{-2}
Extent of the photoconversion γ_1 at 77 K	0	0	0
Extent of the photoconversion γ_2 at 293 K	0.60	0.51	0.59*
Quantum yield of the P_r photoconversion $\varphi_P^{Pr \rightarrow Pfr}$	0.12	0.13	0.10**
Quantum yield of the P_r photoconversion $\varphi_P^{Pfr \rightarrow Pr}$	0.19	0.26	n.d.***
Activation energies ΔE_a of the fluorescence decay (kJ mol^{-1})	269–185 K:16.7 185–100 K: 2.1	270–200 K: 18.8 200–97 K: 3.0	270–214 K: 29.8 214–97 K: 2.2

CD spectroscopy

Far-UV CD spectra (Fig. 10) revealed a major conformational change during the $P_r \rightarrow P_{fr}$ photoconversion. At 208 nm, P_r shows a 5% larger ellipticity than P_{fr}. Between 224 and 240 nm the ellipticity of P_r was lower, at 229 nm even by 10%. This spectral change reflects an increase of α-helical structures by at least 3% during the $P_r \rightarrow P_{fr}$ conversion. Because CD spectra of the P_{fr} state were recorded with a sample still containing *ca* 40% P_r, the increase of the α-helical content of Cph2(1,2) in the P_{fr} conformation is probably even higher. These results are corroborated by earlier investigations of plant phytochromes which reported a 3–5% increase of α-helical content upon $P_r \rightarrow P_{fr}$ photoconversion (26,41,42). These differences in P_r and P_{fr} spectra are in contrast to the results obtained for the Y47H and R383D mutants for which essentially the same α-helical content was calculated in the respective P_r and P_{fr} states.

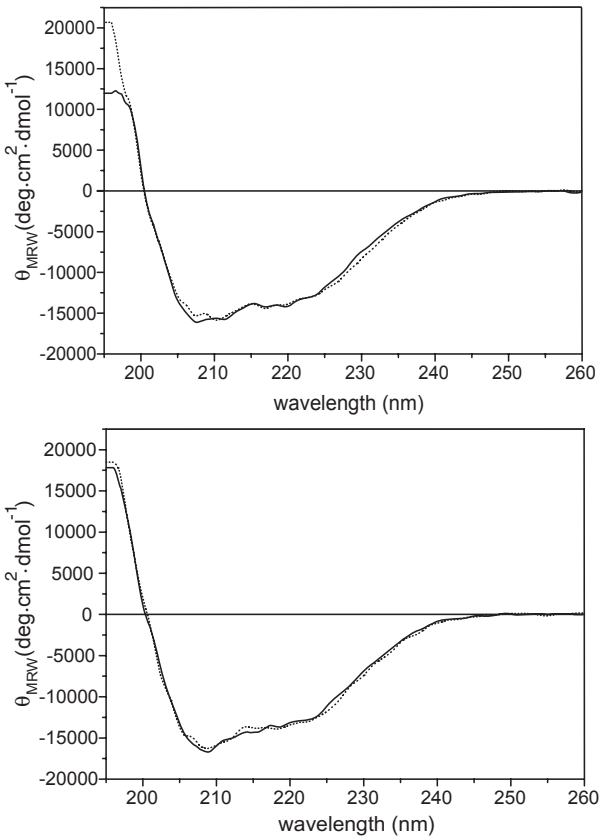

Figure 10. Far-UV CD spectrum of Cph2(1,2) (top) and Y47H (bottom) in 5 mM Tris-buffer; solid line: P_r, dashed line: P_{fr}; CD measurements revealed a melting point of 327.4 K for Cph2(1,2).

A large change of the asymmetric environment of the PCB cofactor was shown by near-UV/vis CD spectra (Fig. 11). The CD signal of the protein-bound tetrapyrrole arises from asymmetric, electric dipole–dipole interactions between the chromophore and the surrounding amino acids in the PCB binding pocket (43). The spectra of the two states of Cph2(1,2) are quite different but resemble closely the respective states of Cph1 (31,44). These findings suggest that the cofactors experience similar environments in the two subfamilies of cyanobacterial phytochromes.

The P_r spectrum of Cph2(1,2) is characterized by three extrema, two major bands at 350 and 640 nm and a small negative band at 277 nm. As mentioned above, the spectrum measured for P_{fr} includes contributions also from the P_r state present under photostationary conditions. A pure P_{fr} spectrum could be calculated showing a strong positive band at 701 nm, a weaker band at 418 nm and a negative band at 370 nm. Both states exhibit a negative band at 303 nm, a wavelength at which the ellipticity is the same for both states. Interestingly, the mutants Y47H and R383D show very similar spectra (apart from the P_{fr} state of R383D, due to the fast dark reversion), implying that the respective amino acid substitutions do not significantly distort the immediate protein environment of the cofactor.

The CD signals between 250 and 290 nm are mostly due to aromatic amino acid side chains that are in a chiral environment (44,45). The large CD change between P_r and P_{fr} conformation in this region indicates a major conformational change of the protein during photoconversion. The different CD spectra at larger wavelengths imply that the cofactor environment is substantially altered during the photoconversion. Only the CD signal at 303 nm remains unaffected.

Resonance Raman spectroscopy

The RR spectra of Cph2(1,2) display a vibrational band pattern that is, in general, very similar to that of Cph1Δ2 (Fig. 12a). In both the parent states of Cph2(1,2), all four pyrrole nitrogens are protonated such that the chromophore exists in a cationic form as indicated by the characteristic N-H in-plane bending modes of the rings B and C at 1572 (P_r) and

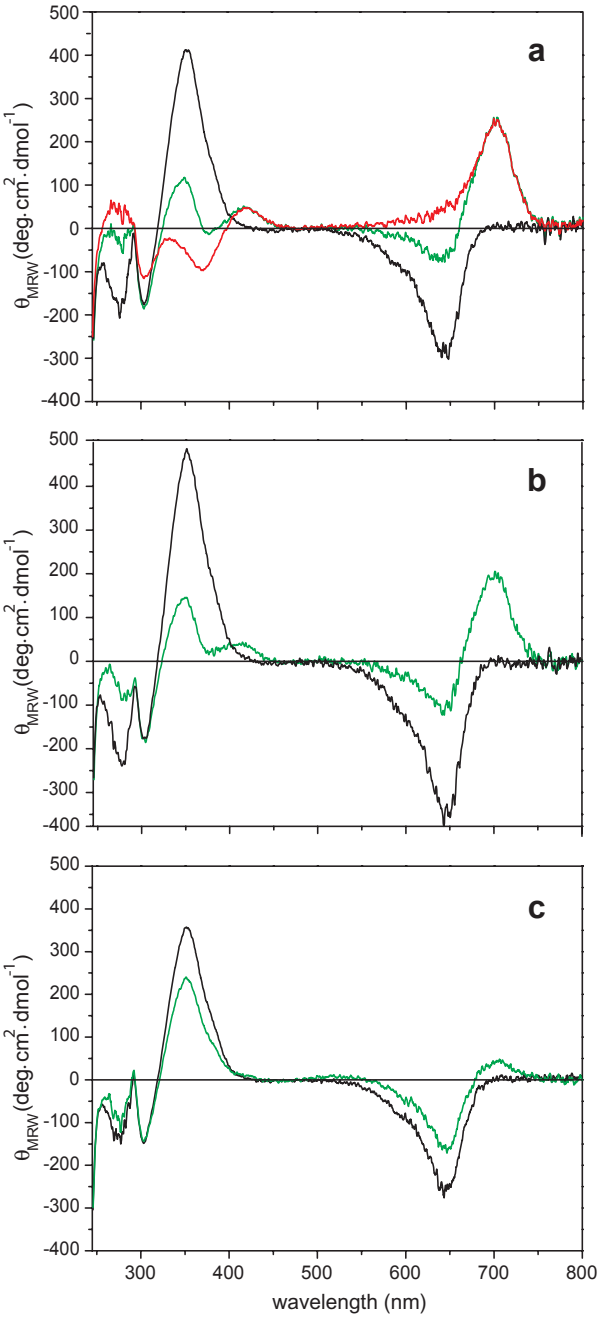

Figure 11. Near UV/vis CD spectrum of Cph2(1,2) (a), Y47H (b) and R383D (c) in 50 mM Tris-buffer pH 8.0 after irradiation with far-red (black curve, P_r) and red (green curve, P_{fr} + P_r) light; red curve: the calculated P_{fr} spectrum of Cph2(1,2). Differences in the spectral intensities of P_r result from an increased proportion of apoprotein in the sample. The spectrum of the photoproduct of R383D exhibits a larger contribution from the P_r-like spectrum due to the very fast dark reversion.

1552 cm^{-1} (P_{fr}) (Fig. 12a,c), which disappear upon H/D exchange (data not shown). The frequencies are nearly the same as in the corresponding states of Cph1Δ2 (46) pointing to very similar hydrogen bond interactions of the inner pyrrole rings in both proteins. However, there are some notable differences in the region between 1600 and 1670 cm^{-1} (Fig. 12c), which is dominated by vibrational modes with strong contributions from C=C stretchings of the methine bridges (46–48). Among them, the C=C stretching of the C-D methine bridge (CD stretching) exhibits the highest RR intensity and thus it was attributed to the 1612 cm^{-1} band of P_{fr} in both Cph2(1,2) and Cph1Δ2. The somewhat weaker band on the high frequency side at 1639 cm^{-1} in Cph2(1,2) and 1642 cm^{-1} in Cph1Δ2 originates from the C=C stretching of the A-B methine bridge (AB stretching). Frequencies and relative intensities of the AB and CD stretchings display considerable variations in various PCB-phytochrome adducts including phytochromes from cyanobacteria (SyB-Cph1), bacteria (V249C from Agp1), and plants (phyA from oat) (49,50). In this respect, the RR spectrum of the P_{fr} state of Cph2(1,2) is very similar to that of Cph1Δ2, despite the slightly lower relative intensity and the small 3 cm^{-1} frequency downshift of the AB stretching. Conversely, the spectral differences of these bands are much larger for the P_{fr} state of SyB-Cph1 which, compared with Cph1Δ2 shows a downshift of the AB and CD stretchings by 26 and 5 cm^{-1}, respectively (49).

In the P_r state of Cph2(1,2), however, the RR spectrum in the C=C stretching region is more closely related to that of SyB-Cph1: in both cases, a frequency upshift of the CD stretching and a downshift of the AB stretching cause the two bands to coincide leading to a nearly symmetrically shaped single peak, in contrast to the two-banded profile in the P_r spectrum of Cph1Δ2 (51). As the AB stretching is especially sensitive to subtle changes of the methine bridge geometry (51), the spectral differences between Cph2(1,2) and Cph1Δ2 may be attributed to different electrostatic interactions in the chromophore binding pocket. Accordingly, this may cause slight perturbations of the tetrapyrrole structure beyond the level of methine bridge Z/E configuration and s/a conformation changes. This conclusion is supported by the even larger frequency variations of the CD and AB stretching modes in the P_r state of Cph1Δ2 which occur under preservation of the *ZZZssa* configuration of the tetrapyrrole upon changing the pH from 6.5 to 7.8 (P. Hildebrandt, unpublished, [51]).

Minor structural differences between respective parent states in Cph1Δ2 and Cph2(1,2) are further reflected in the spectral region between 1200 and 1400 cm^{-1} and between 600 and 850 cm^{-1}. The latter region involves bands arising from torsional modes of the tetrapyrrole and C-H out-of-plane (HOOP) modes of its methine bridges, among which the HOOP coordinate of the CD methine provides the largest contribution to the strongest bands around 800 cm^{-1} (Fig. 12b). In P_{fr}, we note a remarkable up-shift of the 802 cm^{-1} band in Cph1Δ2 to 817 cm^{-1} in Cph2(1,2). A closer inspection of this peak indicates that it exhibits a shoulder on the low-frequency side of the 817 cm^{-1} band of Cph2(1,2) and, conversely, on the high frequency side of the 802 cm^{-1} band of Cph1Δ2. Thus, the spectral differences between Cph1Δ2 and Cph2(1,2) in this region can also be understood in terms of an intensity redistribution among two closely spaced bands (*ca* 802 and 817 cm^{-1}) in Cph2(1,2) compared with Cph1Δ2. The underlying molecular origin is not clear but it might be due to a structural heterogeneity of the cofactor which is specifically reflected by the HOOP mode of the CD methine bridge (50). Such an explanation may also hold for comparing the doublet of the nearly equally intense bands at 792 and

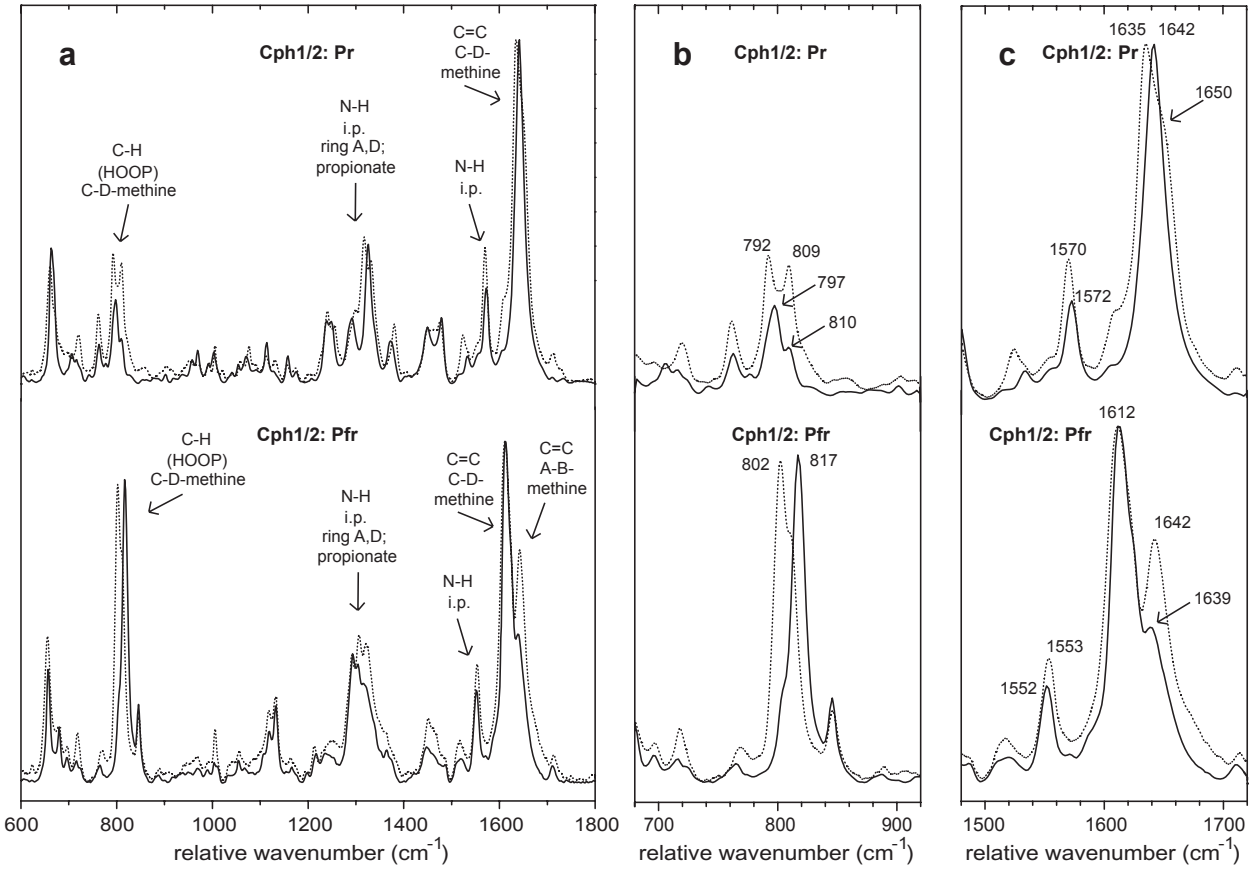

Figure 12. Resonance Raman spectra of Cph2(1,2) (solid) and Cph1Δ2 (dotted) in the P_r (top) and P_{fr} (bottom) state in 50 mM NaH_2PO_4 buffer pH 8.0. Experimental details are given in the text.

809 cm^{-1} in the P_r state of Cph1Δ2 with the 797 cm^{-1} band and its shoulder at *ca* 810 cm^{-1} in Cph2(1,2).

The bands in the region between 1200 and 1400 cm^{-1} originate from modes including, *inter alia*, the N-H in-plane bending modes of the pyrrole rings A and D as well as coordinates of the propionate side chains. Deviations between the corresponding spectra may thus reflect different electrostatic interactions of the chromophore in Cph1Δ2 and Cph2(1,2), both in the P_r and the P_{fr} state.

The RR spectra of the Y47H mutant of Cph2(1,2) in the P_r and P_{fr} state are essentially identical to those of the corresponding states of the wildtype protein, indicating that there are almost no conformational differences between the chromophores of both proteins (Fig. 13). Only a 7 cm^{-1} shift of the CD stretching is noted for the P_{fr} state that reflects altered protein-cofactor interactions due to the Y → H exchange close to ring D.

DISCUSSION

In terms of domain organization, cyanobacterial phytochromes of the Cph2 subfamily are intermediate between bacteriophytochromes and the Cph1/plant-type phytochromes on the one hand and the cyanobacteriochromes on the other hand. Whereas the sensory module of the former group comprises PAS-GAF-PHY domains, phytochromes of the Cph2 subfamily miss the N-terminal PAS domain but possess two consecutive GAF domains such that representatives can even be considered as a unique type of PAS-less Cph1 phytochromes (10). In contrast, the cyanobacteriochrome subfamily corresponds to stand-alone chromophore-binding GAF domains with their photoconversion characteristics shifted to the green–violet range of the visible spectrum (6,9). Structural studies of Cph1 revealed a tripartite organization of its tetrapyrrole-binding site (7). Here, complete sealing of the GAF-bound chromophore is achieved by the tongue protruding from the PHY domain and by an N-terminal, mostly helical region preceding the PAS domain. This region forms a figure-of-eight knot in the peptide chain by passing through a 33-residue lasso-like insertion between the β9-strand and α8-helix of the GAF domain. In *Syn*Cph2 the GAF2 domain functions analogously to the related PHY domain on account of its predicted tongue-like extension. Interestingly, although the N-terminal PAS domain seen in Cph1 is missing, the lasso-like insertion is still seen in the GAF1 domain (V97-D127), thus raising questions as to its function there and the degree to which the Cph1 and Cph2 subfamilies share common photochemical behavior signaling patterns.

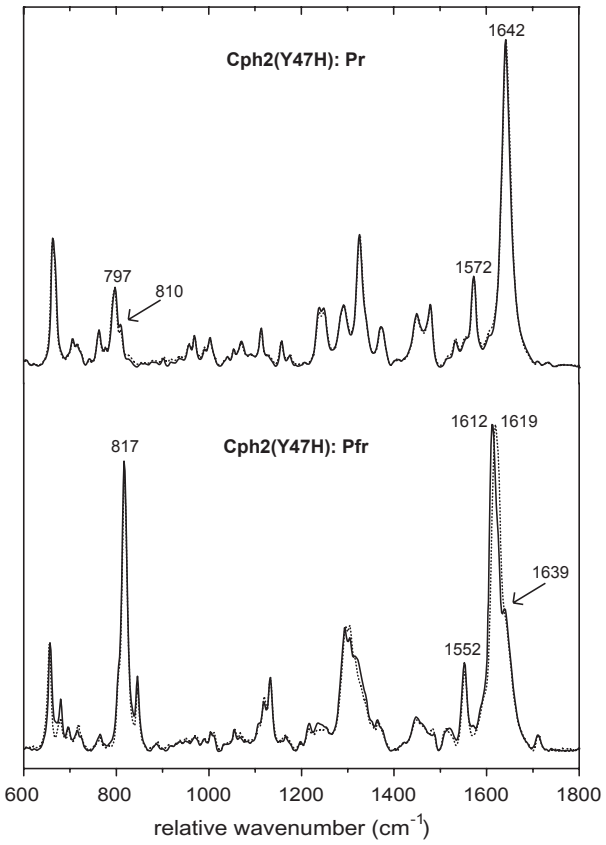

Figure 13. Resonance Raman spectra of Cph2(1,2) wild type (solid) and Y47H mutant (dotted) in the P_r (top) and P_{fr} (bottom) state. Experimental details are given in the text.

Photochemical and thermal conversion between P_r and P_{fr}

Following assembly with the PCB cofactor, the first two GAF domains of *Syn*Cph2 resemble Cph1 in forming a module capable of reversible photoconversion between P_r and P_{fr} states. Other features shared with Cph1 include: (1) the attachment site of the tetrapyrrole chromophore at a conserved cysteine within the GAF1 domain; (2) a similar fluorescence quantum yield in the P_r state and the lack of fluorescence in the P_{fr} state (1,26); (3) the inability to undergo the $P_r \rightarrow$ lumi-R photoreaction at low temperatures (P_r'' photochemical type like CP2, phyB and phyA″ [21,40]) in contrast to the photochemically active P_r' type of phyA (phyA′), (4) the asymmetric environment of the cofactor as revealed by near-UV/vis CD data, and (5) the fully protonated *ZZZssa* and *ZZEssa* conformations of the chromophore in the P_r and P_{fr} state, respectively, as shown by RR spectroscopy.

On the other hand, there are remarkable differences between Cph2(1,2) and Cph1: First, Cph2(1,2) undergoes a fast $P_{fr} \rightarrow P_r$ dark reversion. The large activation energy ΔE_a of the $P_{fr} \rightarrow P_r$ dark reversion is not unusual for a photoreceptor (52) and may cause an interdependence of temperature and light controlling the Cph2-mediated biological response. Furthermore, Cph2(1,2) lacks any changes of the quaternary arrangement unlike Cph1Δ2, where the $P_r \rightarrow P_{fr}$ transition is associated with an altered tendency for dimerisation (32). Independent of its state, the Cph2(1,2) fragment is predominantly monomeric at all concentrations that were examined. However, the data obtained from size-exclusion chromatography and far-UV CD spectroscopy indicate some global conformational changes of Cph2 upon $P_r \rightarrow P_{fr}$ photoconversion, where the P_r state adopts a more globular form. It may be that these changes are related either to conformational adaptations in the tongue region or to rearrangements of the GAF1 and GAF2 domains relative to each other. Such an involvement of the tongue in transmitting conformational changes is corroborated by the R383D mutant, where the salt bridge between the PRxSF motif of the tongue and the aspartate of the DIP motif within the GAF domain has been disrupted (7). This mutant is unable to reach a wild type-like P_{fr} state after red light illumination, has an increased sterical hindrance for the $P_r \rightarrow$ lumi-R photoreaction and could be hence stalled in an alternative, red-shifted state. Accordingly, R383D exhibits a nearly 40-fold faster dark reversion to P_r than wildtype Cph2(1,2) and is much faster than the Y47H mutation next to ring D of the chromophore. Similar to these mutants, a disruption of the tongue, as in the *Syn*Cph2 variant comprising only the N-terminal 390 amino acids, causes a blue shift of the P_r and P_{fr} spectra by about 6 nm (15).

Another intriguing difference between Cph2(1,2) and Cph1/plant-type phytochromes concerns the spectral characteristics of the Y47H mutant, which forms a P_{fr} state spectrally similar to that of the Cph2(1,2) and Cph1 wildtypes, whereas the equivalent mutant in Cph1 and plant-type phytochromes is photochemically dysfunctional and strongly fluorescent (28–30). Apart from a faster dark reversion and the lower rate of P_{fr} formation at photoequilibrium, the Y47H mutant undergoes a $P_r \rightarrow P_{fr}$ photoconversion even though the P_r fluorescence quantum yield is slightly lower, suggesting an altered chromophore-protein interaction compared to Cph1 (28,29). Interestingly, the Y47H variant with its substitution close to the D-ring of the chromophore highly resembles the BV-binding phytochromes such as PaBphP from *P. aeruginosa* (29,31), where the $Y \rightarrow H$ mutation does not exert major effects on photoconversion.

The structure of the chromophore pocket in P_r and P_{fr}

Structural details of the chromophore binding pocket can be derived from the CD and RR spectra. The prominent CD signal in the red spectral region is a negative and a positive band in the P_r and P_{fr} states, respectively. The reversal of the sign of the ellipticity, which is common to phycobilin-binding phytochromes like Cph1 and plant phytochromes (31), suggests a counter-clockwise rotation of ring D upon the $P_r \rightarrow P_{fr}$ transition. Whereas in the P_{fr} state the CD spectrum in the region of the electronic transitions of the chromophore is, in general, closely related to those of Cph1/plant-like phytochromes, the P_r spectrum lacks the small, but significant positive and negative CD on the long wavelength side of the lowest energy transition, similar to BV-binding phytochromes but in contrast to Cph1/plant-like phytochromes. These findings are consistent with the RR spectroscopic results that indicate alterations of the electrostatic interactions in the chromophore binding pocket of the P_r state compared to Cph1, which could well account for the changes in the CD spectrum.

In the P_{fr} state, the RR spectra imply very similar protein–cofactor interactions and chromophore structures. The only remarkable spectral difference between Cph2(1,2) and Cph1Δ2 refers to the intensity re-distribution between the two closely spaced bands between 800 and 820 cm^{-1}, which is tentatively attributed to a shift of an equilibrium of conformational substates that differ only in subtle details of the tetrapyrrole structure.

Despite these spectral differences in the RR spectra, however, the gross chromophore conformation in the respective parent states, *i.e*. *ZZZssa* in P_r and presumably *ZZEssa* in P_{fr}, is the same in Cph2(1,2) and Cph1Δ2.

Implications for the mechanism of photoconversion

Substitution of Tyr47 by a histidine has been suggested to increase the fluorescence yield at the expense of the photochemical reaction channel of the excited state of P_r in PCB-binding phytochromes. The molecular basis is thought to lie in the formation of a salt bridge between the histidine residue and the propionate group of the C-ring. Accordingly, the analogous substitution in BV-binding phytochromes should not impair the photoisomerization which for this chromophore proceeds via clockwise rotation of ring D, in contrast to the opposite direction of the rotation of PCB-binding phytochromes (31). In Cph2(1,2) the conformational constraints around ring D may be softer as the local environment of the B- and C-ring propionates is altered due to the missing PAS domain that in other phytochromes is in close vicinity to this region of the chromophore binding pocket. The lack of the PAS domain may thus increase the structural flexibility in this region of the cofactor such that formation of an otherwise chromophore-locking histidine-propionate salt bridge is hindered. This effect on the cofactor structure appears to be reflected by the frequency upshift of the CD stretching in the RR spectrum of the P_{fr} state, *i.e*. a mode that is localized in close vicinity to the mutation site.

Recently, the mechanism of photoconversion itself has come into scope proposing a mode of photoconversion other than the D-ring flip as postulated before. NMR-studies on the isolated GAF-domain of the Cph2-like phytochrome from *Synechococcus* sp. OS-B (49) have been interpreted to show a large conformational change for the orientations of the A-B ring but not of the C-D ring (13) as indicated previously in crystal structures and from other data. Interestingly, the C-H out-of-plane modes of the C-D methine bridge of Cph2(1,2) have an upshift of 20 cm^{-1} and show a large intensity increase upon $P_r \rightarrow P_{fr}$ conversion that may be caused by torsional twisting of the C-D methine bridge. A similar upshift of about 18 cm^{-1} was observed for OS-B (49). This predominant feature was almost lost in the RR spectrum of the GAF-only variant of this phytochrome used for NMR spectroscopy. Given the lack of conformational constraints by the tongue and the absence of large changes in the HOOP region associated with $P_r \rightarrow P_{fr}$ transitions, it remains questionable whether such dramatic A-B ring reorientations as suggested in (13) also occur in intact chromophore environments. We hope that structural analyzes of intact Cph2-like photosensory modules such as Cph2(1,2) will reveal the true chromophore conformation in this subgroup of phytochromes.

Acknowledgements—This work was supported by DFG grants ES152/6-1 to L.-O.E., HU702/6 to J.H. and RFFI grant 08-04-01453 to V.S. The authors are very grateful to Uwe Linne for mass-spectrometric analysis and for technical support provided by Tina Lang and Petra Gnau and the students Julia Schlereth, Katrin Back and Michael Kock.

REFERENCES

1. Rockwell, N. C., Y. S. Su and J. C. Lagarias (2006) Phytochrome structure and signaling mechanisms. *Annu. Rev. Plant Biol.* **57**, 837–858.
2. Yeh, K. C., S. H. Wu, J. T. Murphy and J. C. Lagarias (1997) A cyanobacterial phytochrome two-component light sensory system. *Science* **277**, 1505–1508.
3. Hughes, J., T. Lamparter, F. Mittmann, E. Hartmann, W. Gärtner, A. Wilde and T. Börner (1997) A prokaryotic phytochrome. *Nature* **386**, 663.
4. Rockwell, N. C. and J. C. Lagarias (2010) A brief history of phytochromes. *Chemphyschem* **11**, 1172–1180.
5. van Thor, J. J., K. L. Ronayne and M. Towrie (2006) Formation of the early photoproduct lumi-R of cyanobacterial phytochrome Cph1 observed by ultrafast mid-infrared spectroscopy. *J. Am. Chem. Soc.* **129**, 126–132.
6. Montgomery, B. L. and J. C. Lagarias (2002) Phytochrome ancestry: Sensors of bilins and light. *Trends Plant Sci.* **7**, 357–366.
7. Essen, L. O., J. Mailliet and J. Hughes (2008) The structure of a complete phytochrome sensory module in the Pr ground state. *Proc. Natl. Acad. Sci. U.S.A.* **105**, 14709–14714.
8. Romling, U., M. Gomelsky and M. Y. Galperin (2005) C-di-GMP: The dawning of a novel bacterial signalling system. *Mol. Microbiol.* **57**, 629–639.
9. Ikeuchi, M. and T. Ishizuka (2008) Cyanobacteriochromes: A new superfamily of tetrapyrrole-binding photoreceptors in cyanobacteria. *Photochem. Photobiol. Sci.* **7**, 1159–1167.
10. Ulijasz, A. T., G. Cornilescu, D. von Stetten, C. C. Cornilescu, F. Velazquez Escobar, J. Zhang, R. J. Stankey, M. Rivera, P. Hildebrandt and R. D. Vierstra (2009) Cyanochromes are blue/green light photoreversible photoreceptors defined by a stable double cysteine linkage to a phycoviolobilin-type chromophore. *J. Biol. Chem.* **284**, 29757–29772.
11. Fiedler, B., T. Borner and A. Wilde (2005) Phototaxis in the cyanobacterium *Synechocystis* sp. PCC 6803: Role of different photoreceptors. *Photochem. Photobiol.* **81**, 1481–1488.
12. Wilde, A., B. Fiedler and T. Borner (2002) The cyanobacterial phytochrome Cph2 inhibits phototaxis towards blue light. *Mol. Microbiol.* **44**, 981–988.
13. Ulijasz, A. T., G. Cornilescu, C. C. Cornilescu, J. Zhang, M. Rivera, J. L. Markley and R. D. Vierstra (2010) Structural basis for the photoconversion of a phytochrome to the activated Pfr form. *Nature* **463**, 250–254.
14. Yang, X., J. Kuk and K. Moffat (2008) Crystal structure of *Pseudomonas aeruginosa* bacteriophytochrome: Photoconversion and signal transduction. *Proc. Natl. Acad. Sci. U.S.A.* **105**, 14715–14720.
15. Wu, S. H. and J. C. Lagarias (2000) Defining the bilin lyase domain: Lessons from the extended phytochrome superfamily. *Biochemistry* **39**, 13487–13495.
16. Park, C. M., J. I. Kim, S. S. Yang, J. G. Kang, J. H. Kang, J. Y. Shim, Y. H. Chung, Y. M. Park and P. S. Song (2000) A second photochromic bacteriophytochrome from *Synechocystis* sp. PCC 6803: Spectral analysis and down-regulation by light. *Biochemistry* **39**, 10840–10847.
17. Landgraf, F. T., C. Forreiter, A. Hurtado Pico, T. Lamparter and J. Hughes (2001) Recombinant holophytochrome in *Escherichia coli*. *FEBS Lett.* **508**, 459–462.
18. Berkelman, T. R. and J. C. Lagarias (1986) Visualization of bilin-linked peptides and proteins in polyacrylamide gels. *Anal. Biochem.* **156**, 194–201.
19. Stadnichuk, I. N. (1995) Phycobiliproteins: Determination of chromophore composition and content. *Phytochem. Anal.* **6**, 281–288.

20. Losev, A. P., E. I. Sagun, G. A. Kochubeev and I. N. Nichiporovich (1986) Fluorescence quantum yields, lifetimes, and critical distances for energy transfer for Chlorophyll *a* and its Pheophytin in solutions. *J. Appl. Spectrosc.* **45**, 798–803.
21. Sineshchekov, A. V. (2004) Phytochrome A: Functional diversity and polymorphism. *Photochem. Photobiol. Sci.* **3**, 596–607.
22. Lamparter, T., F. Mittmann, W. Gärtner, T. Börner, E. Hartmann and J. Hughes (1997) Characterization of recombinant phytochrome from the cyanobacterium *Synechocystis*. *Proc. Natl. Acad. Sci. U.S.A.* **94**, 11792–11797.
23. Sineshchekov, V., L. Koppel', B. Esteban, J. Hughes and T. Lamparter (2002) Fluorescence investigation of the recombinant cyanobacterial phytochrome (Cph1) and its C-terminally truncated monomeric species (Cph1Δ2): Implication for holoprotein assembly, chromophore–apoprotein interaction and photochemistry. *J. Photochem. Photobiol. B, Biol.* **67**, 39–50.
24. Butler, W. L., S. B. Hendricks and H. W. Siegelman (1964) Action spectra of phytochrome *in vitro*. *Photochem. Photobiol.* **3**, 521–528.
25. Pratt, L. H. (1975) Photochemistry of high molecular weight phytochrome *in vitro*. *Photochem. Photobiol.* **22**, 33–36.
26. Sineshchekov, V. A. (1995) Photobiophysics and photobiochemistry of the heterogeneous phytochrome system. *Biochim. Biophys. Acta* **1228**, 125–164.
27. Sineshchekov, V. A. and A. V. Sineshchekov (1990) Different photoactive states of the red phytochrome form in the cells of etiolated pea and oat seedlings. *J. Photochem. Photobiol. B, Biol.* **5**, 197–217.
28. Fischer, A. J. and J. C. Lagarias (2004) Harnessing phytochrome's glowing potential. *Proc. Natl. Acad. Sci. U.S.A.* **101**, 17334–17339.
29. Fischer, A. J., N. C. Rockwell, A. Y. Jang, A. Ernst, S. Waggoner, Y. Duan, H. Lei and J. C. Lagarias (2005) Multiple roles of a conserved GAF domain tyrosine residue in cyanobacterial and plant phytochromes. *Biochemistry* **44**, 15203–15215.
30. Su, Y. and J. C. Lagarias (2007) Light-independent phytochrome signaling mediated by dominant GAF domain tyrosine mutants of *Arabidopsis* phytochromes in transgenic plants. *Plant Cell* **19**, 2124–2139.
31. Rockwell, N. C., L. Shang, S. S. Martin and J. C. Lagarias (2009) Distinct classes of red/far-red photochemistry within the phytochrome superfamily. *Proc. Natl. Acad. Sci. U.S.A.* **106**, 6123–6127.
32. Strauss, H. M., P. Schmieder and J. Hughes (2005) Light-dependent dimerisation in the N-terminal sensory module of cyanobacterial phytochrome 1. *FEBS Lett.* **579**, 3970–3974.
33. Hahn, J., H. M. Strauss, F. T. Landgraf, H. F. Gimenez, G. Lochnit, P. Schmieder and J. Hughes (2006) Probing protein-chromophore interactions in Cph1 phytochrome by mutagenesis. *FEBS J.* **273**, 1415–1429.
34. Lamparter, T., B. Esteban and J. Hughes (2001) Phytochrome Cph1 from the cyanobacterium *Synechocystis* PCC6803. *FEBS J.* **268**, 4720–4730.
35. Glazer, A. N. and S. Fang (1973) Chromophore content of blue-green algal phycobiliproteins. *J. Biol. Chem.* **248**, 659–662.
36. Inoue, N., Y. Taira, T. Emi, Y. Yamane, Y. Kashino, H. Koike and K. Satoh (2001) Acclimation to the growth temperature and the high-temperature effects on photosystem II and plasma membranes in a mesophilic cyanobacterium, *Synechocystis* sp. PCC6803. *Plant Cell Physiol.* **42**, 1140–1148.
37. Braslavsky, S. E., W. Gartner and K. Schaffner (1997) Phytochrome photoconversion. *Plant Cell Environ.* **20**, 700–706.
38. Fiedler, B., D. Broc, H. Schubert, A. Rediger, T. Börner and A. Wilde (2004) Involvement of cyanobacterial phytochromes in growth under different light qualities and quantities. *Photochem. Photobiol.* **79**, 551–555.
39. Sineshchekov, V., J. Hughes, E. Hartmann and T. Lamparter (1998) Fluorescence and photochemistry of recombinant phytochrome from the cyanobacterium *Synechocystis*. *Photochem. Photobiol.* **67**, 263–267.
40. Sineshchekov, V., L. Koppel', J. Hughes, T. Lamparter and M. Zeidler (2000) Recombinant phytochrome of the moss *Ceratodon purpureus* (CP2): Fluorescence spectroscopy and photochemistry. *J. Photochem. Photobiol. B, Biol.* **56**, 145–153.
41. Chen, E., W. Parker, J. W. Lewis, P. S. Song and D. S. Kliger (1993) Time-resolved UV circular dichroism of phytochrome A: Folding of the N-terminal region. *J. Am. Chem. Soc.* **115**, 9854–9855.
42. Chai, Y. G., P. S. Song, M. M. Cordonnier and L. H. Pratt (1987) A photoreversible circular dichroism spectral change in oat phytochrome is suppressed by a monoclonal antibody that binds near its N-terminus and by chromophore modification. *Biochemistry* **26**, 4947–4952.
43. Bjorling, S. C., C. F. Zhang, D. L. Farrens, P. S. Song and D. S. Kliger (1992) Time-resolved circular dichroism of native oat phytochrome photointermediates. *J. Am. Chem. Soc.* **114**, 4581–4588.
44. Borucki, B., H. Otto, G. Rottwinkel, J. Hughes, M. P. Heyn and T. Lamparter (2003) Mechanism of Cph1 phytochrome assembly from stopped-flow kinetics and circular dichroism. *Biochemistry* **42**, 13684–13697.
45. Kelly, S. M. and N. C. Price (2000) The use of circular dichroism in the investigation of protein structure and function. *Curr. Protein Pept. Sci.* **1**, 349–384.
46. Mroginski, M. A., D. H. Murgida and P. Hildebrandt (2007) The chromophore structural changes during the photocycle of phytochrome: A combined resonance Raman and quantum chemical approach. *Acc. Chem. Res.* **40**, 258–266.
47. Mroginski, M. A., D. H. Murgida, D. von Stetten, C. Kneip, F. Mark and P. Hildebrandt (2004) Determination of the chromophore structures in the photoinduced reaction cycle of phytochrome. *J. Am. Chem. Soc.* **126**, 16734–16735.
48. Andel, F., J. T. Murphy, J. A. Haas, M. T. McDowell, I. van der Hoef, J. Lugtenburg, J. C. Lagarias and R. A. Mathies (2000) Probing the photoreaction mechanism of phytochrome through analysis of resonance Raman vibrational spectra of recombinant analogues. *Biochemistry* **39**, 2667–2676.
49. Ulijasz, A. T., G. Cornilescu, D. von Stetten, S. Kaminski, M. A. Mroginski, J. Zhang, D. Bhaya, P. Hildebrandt and R. D. Vierstra (2008) Characterization of two thermostable cyanobacterial phytochromes reveals global movements in the chromophore-binding domain during photoconversion. *J. Biol. Chem.* **283**, 21251–21266.
50. Von Stetten, D. (2008) Investigation of the Chromophore Structure in Plant and Bacterial Phytochromes by Comparison of Experimental and Calculated Raman Spectra. Ph.D. thesis, Technische Universität Berlin.
51. Mroginski, M. A., D. von Stetten, F. V. Escobar, H. M. Strauss, S. Kaminski, P. Scheerer, M. Günther, D. H. Murgida, P. Schmieder, C. Bongards, W. Gärtner, J. Mailliet, J. Hughes, L.-O. Essen and P. Hildebrandt (2009) Chromophore structure of cyanobacterial phytochrome Cph1 in the Pr state: Reconciling structural and spectroscopic data by QM/MM calculations. *Biophys. J.* **96**, 4153–4163.
52. Schroeder, C., K. Werner, H. Otten, S. Krätzig, H. Schwalbe and L. O. Essen (2008) Influence of a joining helix on the BLUF domain of the YcgF photoreceptor from *Escherichia coli*. *Chembiochem* **9**, 2463–2473.
53. Park, C.-M., J.-Y. Shim, S.-S. Yang, J.-G. Kang, J.-I. Kim, Z. Luka and P.-S. Song (2000) Chromophore-apoprotein interactions in *Synechocystis* sp. PCC6803 phytochrome Cph1. *Biochemistry* **39**, 6349–6356.
54. Turoverov, K. K. (1969) Analytical method of determination of the fluorescence decay constants. *Optika i spectroskopiya (Russ)*. **26**, 564–570.

5.2 *In vivo* and *in vitro* characterization of *Syn*Cph2(5-6)

This research was originally published in Molecular Microbiology. *Philipp Savakis, Sven De Causmaecker, Veronika Angerer, Ulrike Ruppert, Katrin Anders, Lars-Oliver Essen and Annegret Wilde.* **Light-induced alteration of c-di-GMP level controls motility of *Synechocystis* sp. PCC 6803.** Molecular Microbiology. 2012; 85:239-251.

Summary

The C-terminal photosensory module of *Syn*Cph2 (*Syn*Cph2(5-6)) consists of a CBCR and a C-terminal GGDEF domain (GAF3-GGDEF2). GGDEF domains catalyze the synthesis of the second messenger c-di-GMP from two GTP molecules. In the N-terminal photosensory module a c-di-GMP degrading EAL domain can be found in combination with an inactive GGDEF* domain (GAF1-GAF2-GGDEF*1-EAL). In bacteria, c-di-GMP regulates the transition between sessile and motile lifestyles. To ensure beneficial conditions for photosynthesis, *Synechocystis* can move along a light gradient, *i.e.* exhibits phototaxis. Twitching motility of *Synechocystis* is dependent on type IV pili. *Synechocystis* cells do not move towards blue light but *cph2*-deficient cells (△*cph2*) show positive phototaxis under these conditions[105]. In this study we analyzed the role of *Syn*Cph2(5-6) *in vivo* as well as its spectral characteristics and the *in vitro* light-controlled c-di-GMP production. *In vivo* studies showed that △*cph2/cph2(5-6)* mutant cells were non-motile under white light, whereas wild type cells showed positive phototaxis. Under green light conditions △*cph2/cph2(5-6)* mutant cells as well as the wild type exhibit positive phototaxis, whereas in blue lights, no movement can be detected for either strain. *Syn*Cph2(5-6) therefore suffices to complement the △*cph2* phenotype under blue light. However, it cannot replace *Syn*Cph2 under white light conditions, the mutant remains immobile because of the blue light content of the light. An alanine mutation of the second covalent attachment site from the chromophore C994A leads to a photochemically inactive protein that is arrested in a P_r-like state. Interestingly, this mutant shows constitutive DGC activity, it inhibits phototaxis also under green light. Another mutant of △*cph2/cph2(5-6)* cells with mutations in the GGDEF motif itself and therefore without enzymatic activity showed no phototaxis under white and blue light. This indicates that the Cph2(5-6) module of *Syn*Cph2 produces c-di-GMP in the GGDEF2 domain mainly under blue light conditions, which leads to the inhibition of phototaxis. We could demonstrate, that in *Synechocystis*, large amounts of c-di-GMP inhibit motility. The expression of a stand-alone EAL domain in the △*cph2/cph2(5-6)* mutant cells leads to a suppression of the non-motile phenotype, *i.e.* to phototaxis, under blue light caused by the hydrolysis of c-di-GMP. A coproduction of the △*cph2/cph2(5-6)* mutant cells with the N-terminal *Syn*Cph2(1-4) module restores

the wild type phenotype including the phototaxis towards white light where *Syn*Cph2(1-4) counteracts the inhibitory activity of the *Syn*Cph2(5-6) module. Thereby, the activity of the *Syn*Cph2(1-4) module is mediated by the EAL domain. A mutation of the strain leading to a catalytically inactive EAL domain causes the loss of function of the module.

We were able to recombinantly produce and purify *Syn*Cph2(5-6). The protein exhibits reversible photoconversion between a blue and green light absorbing P_b and P_g state, respectively. The GGDEF2 domain is catalytically active and *Syn*Cph2(5-6) is able to produce c-di-GMP from GTP in a light-dependent manner. Higher enzymatic activity was observed under blue light revealing P_g as signaling state. For P_b, a high background activity was observed, which can be attributed to an amount of a photochemically inactive P_r-like state in the sample that also shows an enzymatic activity. With the variant C994A we could prove that this species lacks photoconversion and light-dependent c-di-GMP enzymatic production, but is constitutively active. Mass spectrometry analysis revealed the covalent binding of PCB or its isomer PVB to Cys-1022. A possible fragment of the chromophore linked to both, Cys-1022 and Cys-994, could be found, however with a mass difference of -2, presumably consisting of DBV, an intermediate in the PCB biosyn-thesis. In further denaturation experiments a mixture of PCB and PVB could be detected, corroborating the noted autoisomerization ability and chromophore promiscuity of CBCRs[111].

This is the first study that identified c-di-GMP as a functional second messenger in *Synechocystis* and *Syn*Cph2 as its light-regulated modulator. The EAL domain as well as the GGDEF2 domain is catalytically active, in contrast to the GGDEF1 domain that contains a degenerated GGDEF motif. The modular architecture of the protein hints to a hybrid composition of a Cph2-type phytochrome and a CBCR. The GAF3-GGDEF2 module is widespread among cyanobacteria and is part of different multi-domain proteins. The *Syn*Cph2(1-4) module is only found in five cyanobacterial species (07/2012), three of them harbor the *Syn*Cph2 architecture.

Contributions

P. Savakis wrote the manuscript, designed, performed and analyzed the *in vitro* experiments including plasmid cloning, protein production and purification, spectroscopy, c-di-GMP assays and mass-spectrometry analysis, S. De Causmaecker and V. Angerer performed the *in vivo* experiments and analyzed the data, V. Angerer purified protein, performed c-di-GMP assays and analyzed the data, U. Ruppert cloned the plasmids for *in vivo* measurements, K. Anders designed experiments, cloned the wild type plasmid for the *in vitro* experiments and established expression conditions, L.-O. Essen designed experiments, revised the manuscript and A. Wilde designed the *in vivo* experiments as well as wrote and revised the manuscript.

Molecular Microbiology (2012) 85(2), 239–251 ■
doi:10.1111/j.1365-2958.2012.08106.x
First published online 12 June 2012

Light-induced alteration of c-di-GMP level controls motility of *Synechocystis* sp. PCC 6803

Philipp Savakis,[1‡] Sven De Causmaecker,[1,2‡] Veronika Angerer,[1] Ulrike Ruppert,[2] Katrin Anders,[1] Lars-Oliver Essen[1] and Annegret Wilde[2*]**
[1]*Department of Chemistry, Philipps-University Marburg, 35032 Marburg, Germany.*
[2]*Institute of Microbiology and Molecular Biology, Justus-Liebig University Giessen, 35392 Giessen, Germany.*

Summary

Cph2 from the cyanobacterium *Synechocystis* sp. PCC 6803 is a hybrid photoreceptor that comprises an N-terminal module for red/far-red light reception and a C-terminal module switching between a blue- and a green-receptive state. This unusual photoreceptor exerts complex, light quality-dependent control of the motility of *Synechocystis* sp. PCC 6803 cells by inhibiting phototaxis towards blue light. Cph2 perceives blue light by its third GAF domain that bears all characteristics of a cyanobacteriochrome (CBCR) including photoconversion between green- and blue-absorbing states as well as formation of a bilin species simultaneously tethered to two cysteines, C994 and C1022. Upon blue light illumination the CBCR domain activates the subsequent C-terminal GGDEF domain, which catalyses formation of the second messenger c-di-GMP. Accordingly, expression of the CBCR-GGDEF module in Δ*cph2* mutant cells restores the blue light-dependent inhibition of motility. Additional expression of the N-terminal Cph2 fragment harbouring a red/far-red interconverting phytochrome fused to a c-di-GMP degrading EAL domain restores the complex behaviour of the intact Cph2 photosensor. c-di-GMP was shown to regulate flagellar and pili-based motility in several bacteria. Here we provide the first evidence that this universal bacterial second messenger is directly involved in the light-dependent regulation of cyanobacterial phototaxis.

Accepted 17 May, 2012. For correspondence. *E-mail annegret.wilde@mikro.bio.uni-giessen.de; Tel. (+49) 641 99 35545; Fax (+49) 641 99 35549; **E-mail essen@chemie.uni-marburg.de; Tel. (+49) 6421 2822032; Fax (+49) 6421 2822191. ‡These authors contributed equally to this work.

Introduction

The ability to perceive and react to light quality, quantity and direction is of paramount importance for phototrophic organisms. Cyanobacterial genomes consequently encode a wealth of various photoreceptors. Photoreceptor proteins bind chromophores, organic molecules that can absorb photons of different wavelengths. Precise wavelength sensitivity is achieved by specific interactions between the chromophore and the apoprotein. In cyanobacteria, several members of the cryptochromes (Hitomi *et al.*, 2000), phototropins (Narikawa *et al.*, 2006; Cao *et al.*, 2010), BLUF [Blue Light Using FAD (flavin adenine dinucleotide)] domain proteins (Okajima *et al.*, 2006) and rhodopsins (Jung *et al.*, 2003) have accordingly been identified and characterized. The best studied photoreceptors in cyanobacteria, however, are bilin-containing photoreceptors of the phytochrome family (Rockwell and Lagarias, 2010). These photoreceptors switch between red (P_r) and far-red (P_{fr}) absorbing states by utilizing a tetrapyrrole chromophore that is covalently bound to a cysteine residue. Like in plants, several fungi and other eubacteria, cyanobacterial phytochromes (e.g. Cph1) harbour an N-terminal PAS-GAF-PHY (Per ARNT Sim, cGMP phosphodiesterase Adenylyl cyclase FhlA, Phytochrome) photosensory module (Hughes *et al.*, 1997; Yeh *et al.*, 1997). The related Cph2-type phytochromes [named after *Synechocystis* sp. PCC 6803 (hereafter *Synechocystis* 6803) Cph2 (Park *et al.*, 2000; Wu and Lagarias, 2000)] lack the PAS domain but can support P_r/P_{fr} photoconversion by utilizing at least two GAF domains (Montgomery and Lagarias, 2002). Finally, cyanobacterial genomes also encode a third, distinct class of bilin-binding photoreceptors, namely the cyanobacteriochromes (CBCRs) (Ikeuchi and Ishizuka, 2008). The CBCRs are characterized by stand-alone GAF domains that are sufficient for photoconversion between either green (P_g) and red (Terauchi *et al.*, 2004; Hirose *et al.*, 2008; 2010; Narikawa *et al.*, 2008), blue (P_b) and green (Yoshihara *et al.*, 2004; Ishizuka *et al.*, 2006; Rockwell *et al.*, 2008), UV and blue, or violet and orange (Rockwell *et al.*, 2011) absorbing states. To date, CBCRs have been associated with processes as diverse as chromatic adaptation (Kehoe and Grossman, 1996; Hirose *et al.*, 2008; 2010) and phototaxis (Yoshihara *et al.*, 2000). Aside from the common histidine kinase signal

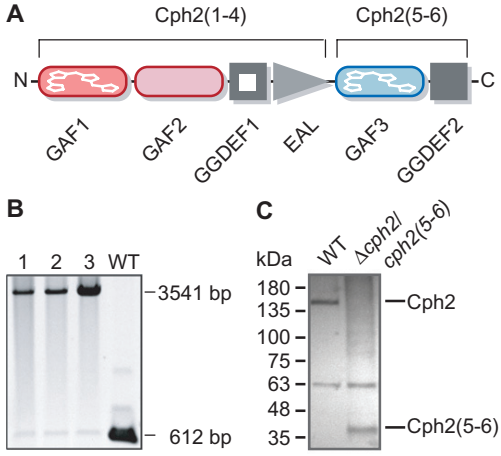

Fig. 1. Construction of the *Synechocystis* 6803 Δ*cph2/cph2(5-6)* mutant.
A. Domain organization of Cph2 from *Synechocystis* 6803 showing a bimodular architecture with an N-terminal red/far-red light sensor (Cph2(1-4)) and a C-terminal blue/green light sensor, the Cph2(5-6) module. Only the GGDEF1 domain is predicted to be catalytically inactive.
B. Colony PCR with primers binding to the genomic integration platform of three independently generated Δ*cph2/cph2(5-6)* clones, which show segregation of mutant gene copies as compared to WT.
C. Western blot analysis of cell lysates from the Δ*cph2/cph2(5-6)* mutant (clone 1) and the WT grown in copper-free medium using a gradient SDS-PAGE (4–16%). A polyclonal α-Cph2(5-6) antibody was used for detection of Cph2.

output domains, a few bacterial phytochromes employ a set of different output domains, such as MCP domains (methyl-accepting chemotaxis protein) (Bhaya, 2004) or GGDEF and EAL domains (Tarutina *et al.*, 2006). The latter two domain types were named after prominent sequence motifs essential for catalytic activity and mediate turnover of c-di-GMP, a second messenger that occurs exclusively in eubacteria. GGDEF domains catalyse the synthesis of c-di-GMP from two GTP molecules (Paul *et al.*, 2004), while proteins with active EAL domains catalyse cleavage of c-di-GMP to linear 5′-pGpG (Schmidt *et al.*, 2005).

Cph2 from *Synechocystis* 6803 (1276 residues, 144.7 kDa) comprises six domains in the order GAF-GAF-GGDEF-EAL-GAF-GGDEF (Fig. 1A). While the N-terminal GAF1-GAF2 bidomain autocatalytically binds a phycocyanobilin (PCB) chromophore to yield a P_r/P_{fr}-switching photosensory module (Anders *et al.*, 2011), the C-terminal GAF3 (CBCR) domain binds a tetrapyrrole chromophore, forming a species that absorbs blue light (Park *et al.*, 2000; Wu and Lagarias, 2000). Based on its molecular architecture Cph2 can hence be considered a composite phytochrome with a Cph2-type phytochrome module (domains 1–2) at its N-terminus and a CBCR module at its C-terminus (domain 5) (Fig. 1A). Sequence comparisons reveal that the N-terminal GGDEF1 domain exhibits mutations in residues essential for catalysis and therefore is predicted to lack diguanylate cyclase (DGC) activity. The pairing of GGDEF and EAL domains on the same polypeptide is a well-known phenomenon and proteins with one or two (Christen *et al.*, 2005; Cao *et al.*, 2010) inactivated domains have been described. In the CC3396 protein of *Caulobacter crescentus* the active site of the GGDEF domain is likewise mutated, rendering it catalytically inactive but retaining its ability to bind GTP. Accordingly, Christen *et al.* (2005) demonstrated that addition of GTP allosterically stimulates phosphodiesterase (PDE) activity of the EAL domain located downstream. Catalytically inactive GGDEF domains can thus exert a regulatory function.

In bacteria, c-di-GMP mainly acts in the regulation of the transition between a motile and a sessile lifestyle (Simm *et al.*, 2004; Jenal and Malone, 2006; Römling and Amikam, 2006). So far, light-dependent regulation of either DGC or PDE activity was demonstrated in a few photosensory proteins bearing GGDEF and EAL output domains (Tarutina *et al.*, 2006; Barends *et al.*, 2009; Cao *et al.*, 2010). In *Rhodobacter sphaeroides*, the biliverdin-binding protein BphG1 harbours an N-terminal PAS-GAF-PHY photosensory module followed by a C-terminal GGDEF-EAL output module. Interestingly, full-length BphG1 exhibits light-independent PDE activity. Only upon removal of the EAL domain light-dependent DGC activity could be detected prompting a regulatory model in which the EAL domain is cleaved off to yield two distinct BphG1 fragments. Autocatalytic cleavage of BphG1, however, was observed only in *Escherichia coli*, but not yet in *R. sphaeroides* (Tarutina *et al.*, 2006). Another example is the six-domain protein SL2 from *Synechococcus elongatus* [REC (CheY-homologous receiver domain)-PAS-PAS-LOV-GGDEF-EAL]. Upon irradiation with blue light, doubling of PDE activity was shown for the three C-terminal domains (Cao *et al.*, 2010). Finally, the PDE activity of the homodimeric BLUF-EAL protein BlrP1 of *Klebsiella pneumoniae* is upregulated fourfold when irradiated with blue light. Light activation is postulated to occur by allosteric action of the BLUF domain of one monomer onto the EAL domain of the other (Barends *et al.*, 2009). Interestingly, for none of these photoreceptors a biological function has been delineated.

Synechocystis 6803 exhibits flagellar-independent 'twitching motility' that allows movement over moist surfaces using type IV pili. Mutants devoid of type IV pili are non-motile (Bhaya *et al.*, 2000). In order to ensure optimal conditions for photosynthesis, *Synechocystis* 6803 cells move along a light gradient. Regulation of phototactic motility is complex and involves a variety of gene products, including different photoreceptors (Fiedler *et al.*, 2005; Narikawa *et al.*, 2008; Song *et al.*, 2011), the RNA chaperone Hfq (Dienst *et al.*, 2008) and adenylate cycla-

ses (Bhaya *et al*., 2006). Wild-type (WT) *Synechocystis* 6803 cells do not move towards blue light, whereas Δ*cph2* mutant cells show positive, blue light-dependent phototaxis. Accordingly, in *Synechocystis* 6803 Cph2 is responsible for inhibiting phototaxis towards blue light (Wilde *et al*., 2002). In addition, Moon *et al*. (2011) investigated the further wavelength dependency of Cph2 activity and found that *cph2* mutant cells also respond to UV-A light with positive phototaxis, whereas the WT is non-motile under these conditions.

Its complex domain architecture indicates that Cph2 can sense a broad range of the visible light spectrum to regulate motility. The mechanism by which two functional modules, the Cph2 domains 1–4 and 5–6 (Fig. 1A), respectively, assess, balance and ultimately integrate different light qualities into an output signal has remained elusive. To address these questions we analysed the recombinant C-terminal CBCR-GGDEF2 (5–6) module with respect to its spectral characteristics and light-controlled c-di-GMP production *in vitro*. In addition, we show that expression of the CBCR-GGDEF2 module in the *Synechocystis* 6803 Δ*cph2* mutant strain restores blue light-regulated, c-di-GMP-dependent inhibition of motility, whereas additional expression of genes encoding PDEs complements this phenotype.

Results

Previous studies on the role of Cph2 in phototactic motility of *Synechocystis* 6803 failed to unambiguously assign the blue light sensory activity to a specific GAF domain (Fiedler *et al.,* 2005). As sequence analyses strongly suggested that the CBCR (GAF3) domain of Cph2 belongs to the subfamily of blue/green-absorbing CBCRs, we hypothesized that this domain causes blue light perception of Cph2. Expression of the C-terminal CBCR-GGDEF2 module (Cph2(5-6)) alone would then be sufficient to generate a WT-like phenotype under blue light in *cph2*-deficient mutants.

In vivo *studies of Cph2 function*

We transformed a Δ*cph2* mutant strain of *Synechocystis* 6803 (Wilde *et al*., 2002) with a plasmid that allows for integration of the *cph2(5-6)* DNA fragment into a neutral site of the *Synechocystis* 6803 genome by means of double homologous recombination. The fragment was placed under the control of the *petJ* promoter, which is repressed by copper (Tous *et al*., 2001). Segregation was verified by colony-PCR (Fig. 1B). We then analysed the phototactic behaviour of the mutant in order to assess the role of Cph2(5-6) *in vivo*. Cellular production of the Cph2(5-6) module was ascertained by Western blot analysis using an antibody specific to Cph2(5-6) (Fig. 1C). Whole protein extracts from Δ*cph2/cph2(5-6)* cells grown in BG-11 medium supplemented with either 1.0, 0.3 or 0 μM $CuSO_4$ were compared to the WT and the Δ*cph2* mutant grown in copper-free BG-11. Only cytosolic extracts from the Δ*cph2/cph2(5-6)* mutant grown in inducing, copper-free medium showed a protein band corresponding to the *cph2(5-6)* gene product (Fig. S1A).

Phototactic behaviour of the Δ*cph2/cph2(5-6)* mutant was studied on agar plates (Fig. 2). Whereas the WT and Δ*cph2* mutant cells exhibited positive phototaxis towards white light, Δ*cph2/cph2(5-6)* mutant cells were non-motile under induced conditions (Fig. 2A). This shows that Cph2(5-6) is a functional module that inhibits phototaxis in *Synechocystis* 6803. To address the wavelength dependency of this inhibitory effect, phototaxis of the Δ*cph2/cph2(5-6)* mutant towards blue and green light was analysed (Fig. 2A). Whereas the WT showed no phototaxis under blue light illumination, the Δ*cph2* mutant moved towards the light source as shown by Wilde *et al*. (2002). Under green light illumination, both the WT and the Δ*cph2* mutant showed phototaxis towards the light source. Under non-induced conditions the Δ*cph2/cph2(5-6)* mutant behaved like the Δ*cph2* mutant, whereas under conditions that induce Cph2(5-6) expression this mutant exhibited wavelength-dependent phototaxis (Fig. 2A). Like in WT cells no movement was observed under blue light illumination while green light restored motility. This shows a clear wavelength dependence of the phototactic behaviour of the Δ*cph2/cph2(5-6)* mutant, which resembles the WT phenotype. Thus, the C-terminal module of Cph2 suffices to complement the Δ*cph2* phenotype under blue light illumination. However, the Cph2(5-6) module is not competent to replace intact full-length Cph2 under daylight conditions. In contrast to the *cph2*-expressing WT that exhibits phototaxis under white light, the Δ*cph2/cph2(5-6)* mutant is rendered immobile possibly because of the blue light contribution of the light source (Fig. 2A). The wavelength dependency observed for the mutant expressing *cph2(5-6)* is abolished, when a mutation is introduced into the CBCR domain at the second covalent attachment site for its chromophore (C994A). Substitution of this cysteine that reversibly forms a thioether linkage to the chromophore in CBCRs leads to a photochemically inactive protein that is arrested in a P_r-like state (Fig. 3C). This protein shows constitutive DGC activity *in vitro* (Fig. 3B) and inhibits phototaxis also under green light *in vivo* (Fig. 2A). Analogously, an alteration of the GGEEF motif (E1182A/E1183A) in Cph2(5-6), which is crucial for activity, abolished inhibition of phototaxis under white and blue light irradiation caused by the Cph2(5-6) module (Fig. 2A). Taken together, these data clearly indicate that expression of the Cph2(5-6) (CBCR-GGDEF2) module of Cph2 produces c-di-GMP mainly under blue light irradiation, thus leading to inhibition of phototaxis.

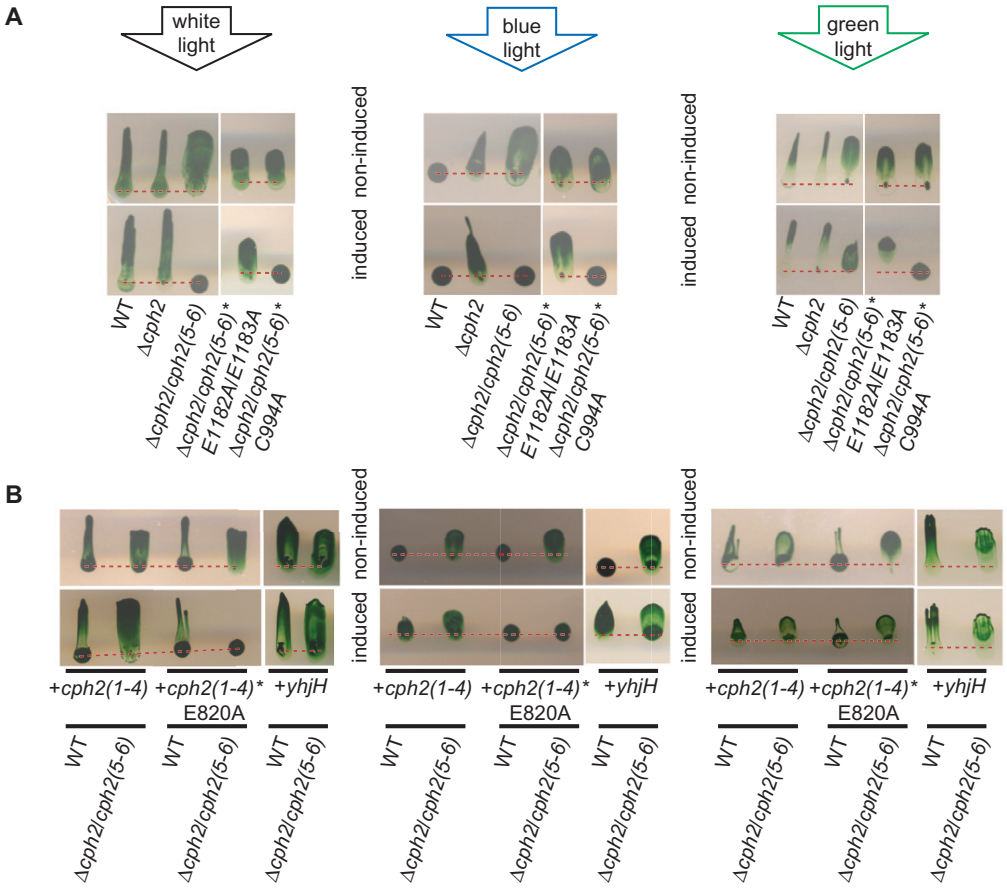

Fig. 2. The Cph2(5-6) module regulates phototaxis in *Synechocystis* 6803 cells.
A. Phototaxis assays under white, blue or green light illumination with different *Synechocystis* 6803 strains. The arrows indicate the direction of illumination. Cells of the Δ*cph2/cph2(5-6)* mutant along with the WT and Δ*cph2* mutant were analysed under inducing (0 μM $CuSO_4$) and non-inducing (2.5 μM $CuSO_4$) conditions. Δ*cph2/cph2(5-6)**C994A, mutant expressing photoinactive Cph2(5-6) in Δ*cph2* background; Δ*cph2/cph2(5-6)**E1182A/E1183A, mutant expressing catalytically inactive Cph2(5-6) in Δ*cph2* background. Dotted lines show the initial position of spotted cells before illumination.
B. Complementation analysis under white, blue or green light illumination with mutants expressing EAL domain proteins. The arrows indicate the direction of illumination. For degradation of c-di-GMP produced by the Cph2(5-6) module, a Δ*cph2/cph2(5-6)* mutant strain was engineered to express the EAL domain protein YhjH from *E. coli* (Δ*cph2/cph2(5-6)/+yhjH*) or the Cph2(1-4) protein (Δ*cph2/cph2(5-6)/+cph2(1-4)*). Δ*cph2/cph2(5-6)/+cph2(1-4)**E820A, mutant expressing the catalytically inactive EAL domain of the Cph2(1-4) module. Slight, but repeatedly observed differences in the shape of moving *Synechocystis* 6803 colonies were not considered to be relevant, because altered c-di-GMP concentrations may have additional effects on the phenotype like exopolysaccharide secretion influencing the motility on surfaces (Burriesci and Bhaya, 2008).

Our experiments suggest that c-di-GMP is produced in a light-dependent manner by the C-terminal GGDEF2 domain and that large amounts of c-di-GMP inhibit motility in *Synechocystis* 6803. In order to test this hypothesis, we expressed the stand-alone EAL domain YhjH from *E. coli* (Simm *et al.*, 2004; Ryjenkov *et al.*, 2006) in *Synechocystis* 6803 Δ*cph2/cph2(5-6)* mutant cells under control of the *petJ* promoter on a self-replicating plasmid. YhjH is expected to hydrolyse the c-di-GMP produced by Cph2(5-6), thus suppressing the non-motile phenotype of *cph2(5-6)*-expressing cells under blue light. Indeed, expression of *yhjH* in the Δ*cph2/cph2(5-6)* genetic background (Δ*cph2/cph2(5-6)/+yhjH*) led to complementation of the blue light-dependent non-motile phenotype under copper limitation where both proteins, Cph2(5-6) and YhjH, are produced (Fig. 2B). Likewise, expression of *yhjH* in WT background (WT/+*yhjH*) also led to phototaxis towards blue light, suggesting that the EAL domain protein YhjH overrides the function of the entire Cph2 photoreceptor present in WT cells (Fig. 2B).

Next, we analysed whether coproduction of the N-terminal Cph2(1-4) module (GAF1-GAF2-GGDEF1-EAL, harbouring the P_r/P_{fr} photosensory module, the putatively inactive GGDEF1 domain and a putatively active

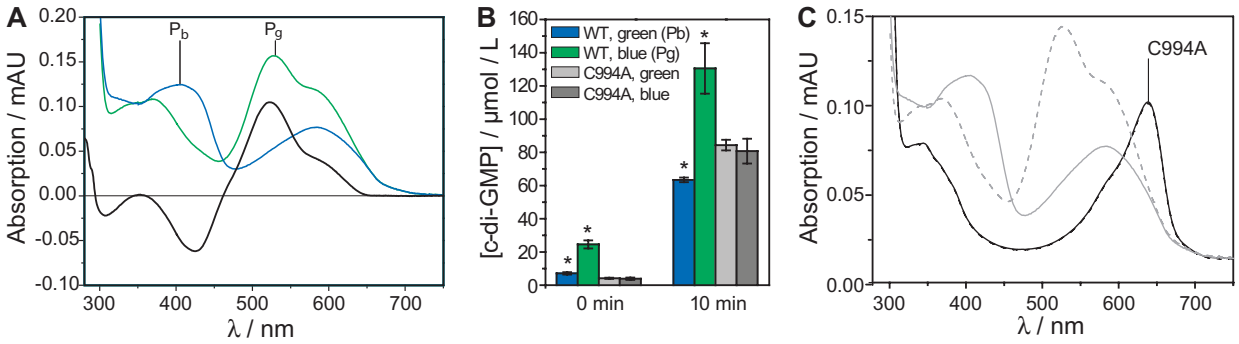

Fig. 3. The recombinantly produced Cph2(5-6) module is a CBCR-type blue/green light photoreceptor.
A. Absorption spectra of the P_b state (blue), the P_g state (green) and difference spectrum (black, P_g minus P_b) for the Cph2(5-6) module produced in PCB-synthesizing *E. coli*.
B. Enzymatic synthesis of c-di-GMP by the recombinant proteins Cph2(5-6) and its mutated photochemically inactive variant Cph2(5-6) C994A under continuous irradiation with green and blue light respectively. Aliquots were taken of the reaction mixture at 0 and 10 min and monitored by HPLC/UV. P_b (blue bar; after green irradiation), P_g (green bar, after blue irradiation), C994A irradiated with green (light gray) and blue (dark gray) light. Values are means of three independent assay experiments measured each twice. Error bars shown are standard deviations. Asterisks denote differences between P_b and P_g states with a statistical significance set at $P < 0.05$ (*t*-test). Residual activity recorded at zero time is caused by the time delay (*c.* 15 s) required for stopping the reaction. No c-di-GMP was produced in the absence of Cph2(5-6) (Fig. S3).
C. Absorption spectrum of the photochemically inactive C994A mutant protein. Spectra are shown following incubation in the dark (solid) and after irradiation with red light (dashed). For comparison the absorption spectra of the WT are shown in gray (P_b solid, P_g dashed).

EAL domain; Fig. 1A) is able to complement the lack of motility in the Δ*cph2/cph2(5-6)* genetic background under white light and to restore the WT phenotype. Indeed, the Cph2(1-4) module counteracts the inhibitory activity of the Cph2(5-6) module by allowing phototaxis towards white light (Fig. 2B). Under blue light, compensation of the non-motile phenotypes of both strains Δ*cph2/cph2(5-6)* and WT by coproduction of the Cph2(1-4) module is also observed (Fig. 2B). The action of the Cph2(1-4) module is mediated by its c-di-GMP degrading EAL domain. This is shown by analysing a strain harbouring a catalytically inactive EAL domain (E820A) that causes loss of the previously observed function for the Cph2(1-4) module (Fig. 2B). In summary, hydrolysis of accumulated c-di-GMP by either the *E. coli* PDE YhjH or the EAL domain of Cph2(1-4) obviously compensates the loss of motility in the WT as well as mutant cells. As it is yet impossible to monitor the c-di-GMP content of *Synechocystis* 6803 cells, we performed *in vitro* studies of the recombinant Cph2(5-6) module.

In vitro *studies of photoconversion of the Cph2(5-6) module*

We characterized the recombinant Cph2(5-6) module with respect to spectroscopic and catalytic properties in order to address the mechanism responsible for wavelength-dependent motility control in *Synechocystis* 6803. Contrary to earlier findings (Wu and Lagarias, 2000) recombinant Cph2(5-6) showed reversible photoconversion between a blue light-absorbing P_b state and a green light-absorbing P_g state (Fig. 3A). Formation of c-di-GMP from GTP in presence of Cph2(5-6) proved that the GGDEF2 domain is catalytically active (Fig. 3B). Moreover, when Cph2(5-6) was irradiated with either blue or green light, its catalytic turnover for c-di-GMP formation varied up to a factor of 2 (10.6 vs. 5.6 min^{-1}). The higher activity was observed when the sample was irradiated with blue light, indicating that the catalytic activity of the P_g state surpasses that of the P_b state (Fig. 3B), so that P_b represents the resting state, whereas P_g is the signalling state.

The absorption spectra of the Cph2(5-6) module (P_b and P_g form, Fig. 3A) indicate that a significant part of the recombinant photoreceptor is photochemically inactive (shoulder at about 600 nm) and assumes a P_r-like state. To test whether the high background enzymatic activity of the P_b state of Cph2(5-6) originates from this dormant P_r-like state, we mutated the second cysteine (C994), known to be crucial for CBCR function, to alanine. As anticipated, the C994A mutant protein shows neither photoconversion of its bilin chromophore (Fig. 3C) nor a light-dependent c-di-GMP enzymatic production (Fig. 3B). Furthermore, the GGDEF domain is constitutively active with a turnover of about 8.0 min^{-1}, with the activity of the C994A mutant of the Cph2(5-6) module thus being 25% higher than the P_b form. Given these findings, one has to conclude that the P_b/P_g conversion of the Cph2(5-6) module that is expressed in *Synechocystis* 6803 most probably causes a significantly larger change of the specific activity than observed *in vitro*.

Compared to other DGCs the Cph2(5-6) module exerts a high specific activity. For example, the DGC YdeH has a turnover of 1.6 μM c-di-GMP min^{-1} μM $protein^{-1}$ (Zähringer *et al*., 2011). Under our conditions, YdeH showed a turnover of 1.3 μM c-di-GMP min^{-1} μM $protein^{-1}$ (data not shown), which is one-tenth of the activity measured for the P_g state of Cph2(5-6) (Fig. 3B). This implies that once activated the GGDEF2 domain of Cph2 becomes highly active and may be capable of dominating the cytosolic c-di-GMP metabolism of *Synechocystis* 6803.

Blue light perception in CBCRs has been suggested to be based on reversible disruption of the chromophore π-system caused by a second thioether linkage from a cysteine moiety located in the conserved Asp-Xaa-Cys-Phe (DXCF) motif of the apoprotein (Ishizuka *et al*., 2006; Rockwell and Lagarias, 2010). This has recently been corroborated by Fourier transform infrared spectroscopy (Ishizuka *et al*., 2011). Indeed, substitution of the candidate cysteine (C994) yielded an absorption spectrum similar to that of the P_r state of canonical phytochromes with concomitant loss of photoconversion in Cph2(5-6) (Fig. 3C) and in other CBCRs (Ulijasz *et al*., 2009; Rockwell *et al*., 2008).

Mass spectrometry analysis of tryptic digests of Cph2(5-6) (P_b and P_g) revealed that its chromophore, PCB or the isomer phycoviolobilin (PVB), is covalently bound to C1022 (Fig. 4A and B). In addition, a fragment matching the m/z ratio of a chromophore linked to C1022 and C994 was detected in both the P_b and the P_g states (Fig. 4C–E). This chromophore shows a mass difference of –2 relative to PCB/PVB and is most likely derived from dihydrobiliverdin, an intermediate in the biosynthesis of PCB. One may hence conclude that only this doubly linked chromophore species is sufficiently stable to be detected by mass spectrometry analysis.

As mass spectrometry cannot distinguish between PCB and PVB species, denaturation analyses were performed for both states of Cph2(5-6). These studies revealed a mixture of PCB and PVB (Fig. S2), which is consistent with the notions that blue/green-absorbing GAF domains belonging to the CBCR family isomerize their chromophore *in situ* (Ishizuka *et al*., 2007; 2011) and photoconversion of the P_b to the P_g state is accompanied by a $Z \rightarrow E$ isomerization of the double bond between C15 and C16. Presence of both PCB and PVB within Cph2(5-6) is also evident from near-UV/Vis CD spectra. At wavelengths shorter than 550 nm the CD spectrum of the P_g state of Cph2(5-6) bears similarity to the spectrum of α-phycoerythrocyanin with the PVB chromophore in a *ZZE* conformation (Fig. 5 and Wiegand *et al*., 2002).

Overall, the recombinant CBCR domain binds at least three different tetrapyrrole species when produced in *E. coli*, which is in line with the promiscuity of CBCRs described by Ishizuka *et al*. (2007). The high background activity observed for the P_b state has hence to be attributed to the fact that samples of recombinant Cph2(5-6) module contained a high portion of the non-switching P_r-like contamination.

Discussion

Recent data reveal that c-di-GMP inhibits motility in several bacteria (Wolfe and Visick, 2008) including *E. coli* (Ryjenkov *et al*., 2006; Boehm *et al*., 2010). Here, the swimming speed of *E. coli* cells is tightly regulated by the c-di-GMP binding protein YcgR, which interacts directly with flagellar motor components (Boehm *et al*., 2010; Paul *et al*., 2010). Upon binding of c-di-GMP YcgR gradually inhibits flagellar motor function, possibly to adapt swimming speed to nutrient availability.

While the existence of GGDEF and EAL encoding genes in *Synechocystis* 6803 already suggests that c-di-GMP plays a major role in this cyanobacterium, this is the first study identifying c-di-GMP as a functional second messenger in *Synechocystis* 6803 and Cph2 as its primary, light-regulated modulator. Just like in other prokaryotes, where c-di-GMP was shown to control both pili- and flagella-based motility (Kazmierczak *et al*., 2006; Boehm *et al*., 2010), c-di-GMP is involved in the regulation of cyanobacterial motility. Interestingly, *Synechocystis* 6803, but not all other cyanobacteria, lacks established c-di-GMP receptor domains, such as the PilZ domain (Amikam and Galperin, 2006), which mediates binding of c-di-GMP in YcgR (Ryjenkov *et al*., 2006). However, it has been shown that catalytically inactive GGDEF or EAL domains can alternatively act as sensing parts of effectors (Christen *et al*., 2005; Lee *et al*., 2007; Duerig *et al*., 2009; Newell *et al*., 2009). Even completely unrelated c-di-GMP binding proteins such as FleQ from *Pseudomonas aeruginosa* (Hickman and Harwood, 2008) or a CRP-like transcription factor from *Xanthomonas axonopodis* pv. *citri* (Leduc and Roberts, 2009) were found to take over c-di-GMP sensing function. Thus, the identity of the c-di-GMP receptor protein interacting with either type IV pili or regulating motility by other means remains currently elusive in *Synechocystis* 6803.

Our data show that the Δ*cph2* mutant phenotype cannot only be complemented by expression of full-length *cph2* (Fiedler *et al*., 2005), but also by its C-terminal CBCR-GGDEF module. This module is sufficient to inhibit motility of *Synechocystis* 6803 under blue light conditions. Relieve of phototactic behaviour by white light requires the additional presence of the four N-terminal domains of Cph2, apparently reducing cytosolic c-di-GMP levels in *Synechocystis* 6803 much like the EAL domain protein YhjH from *E. coli*, which we used as a control. This indicates that not only the GGDEF2 domain, but also the EAL domain of Cph2, is catalytically active. Because of a

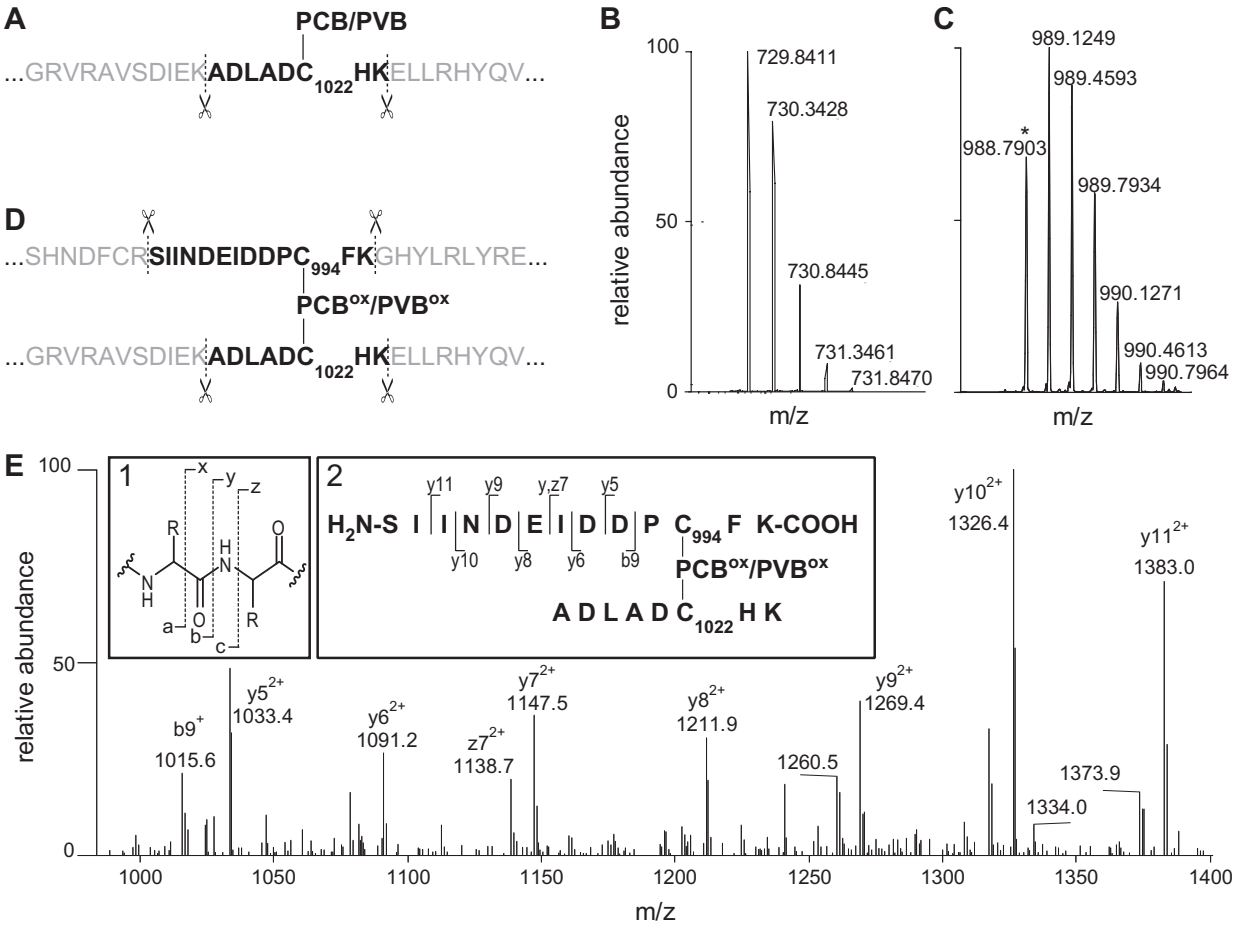

Fig. 4. The second covalent protein–chromophore linkage within the CBCR domain.
A. Tryptic digestion of the polypeptide chain. The chromophore of recombinant Cph2(5-6), either PCB or PVB, is attached to C1022. Trypsin recognition sites are depicted as scissors.
B. FT-ICR-MS spectrum of the ion depicted in A. The difference between the individual peaks ($\Delta m/z \approx 0.5$) indicates that the charge of the ion is +2.
C. FT-ICR-MS spectrum of the chromophore attached to the CBCR domain of Cph2 via C1022 and C994. The peak indicated with an asterisk corresponds to the lightest isotope. The difference between the individual peaks ($\Delta m/z \approx 0.3$) indicates that the charge of the ion is +3.
D. Schematic representation of the ion corresponding to the peak in C.
E. MS/MS spectrum of the ion with m/z = 989.1249. Inlay 1 depicts the nomenclature used to describe fragmentations of peptide bonds. The a, b and c fragments are numbered from the N-terminus, x, y and z fragments from the C-terminus. Inlay 2 points to fragments shown in the spectrum. Charges are indicated in the MS/MS spectrum.

degenerated GGDEF motif, the GGDEF1 domain is incapable of catalysing c-di-GMP formation. However, its RxxD motif, which constitutes an allosteric, regulatory binding site in functional GGDEF domains (Christen *et al*., 2006), is present here as well as in the catalytically active GGDEF2 domain. In the case of Cph2 the counteracting activities of both its EAL and GGDEF2 domains raise the question, how these output domains are regulated such, that one defined photostate allows either synthesis or degradation of c-di-GMP. The molecular architecture of Cph2 from *Synechocystis* 6803 indicates that this photoreceptor is a hybrid of a Cph2-type phytochrome and a blue/green light-absorbing CBCR. As red and far-red light photons are absorbed by photosystems and partly by the phycobilisome antenna pigments, *Synechocystis* 6803 cells should indeed benefit from an override of blue light-mediated inhibition of phototaxis. Accordingly, long wavelength contribution from white light that is absorbed by the N-terminal GAF1/2 module abolishes the blue light-induced inhibition of motility. Furthermore, cells move towards a red or far-red light source even if irradiated by blue light from the opposite side, although this effect is dependent on light intensity as shown by Wilde *et al*. (2002). The dominant role of the CBCR-GGDEF module

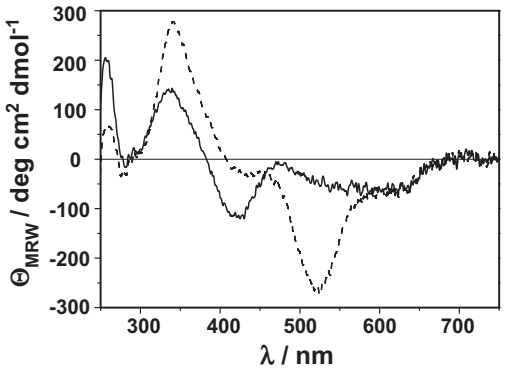

Fig. 5. Near-UV/Vis CD spectra of the recombinant Cph2(5-6) module. CD spectra of the P_b state (solid) and the P_g state (dashed) are shown.

in controlling cyanobacterial behaviour is reflected by the relatively widespread occurrence of this module among cyanobacteria. At least 17 gene products encoding a functional CBCR-GGDEF module are found in cyanobacterial genomes (Fig. 6). The CBCR-GGDEF module is part of different multi-domain proteins, where it is always located at the C-terminus. Interestingly, a hybrid photosensor like Cph2 from *Synechocystis* 6803 is only found in three other cyanobacterial species, *Cyanothece* sp. PCC 7424 and 7822 as well as in *Lyngbya* sp. PCC 8106. At least in two cyanobacteria, *Microcoleus vaginatus* FGP-2 and *Oscillatoria* sp. PCC 6506, the two functional modules of Cph2 are found in two separate gene products. Overall, the co-occurrence of many cyanobacterial signalling proteins consisting of only a subset and/or various combinations of phytochrome, GGDEF and EAL domains indicates that fusion as well as separation of signalling and effector modules is a common strategy of cyanobacteria to adapt to changing environmental factors, especially light quality. The different domain contexts, in which the CBCR-GGDEF module is found (Fig. 6), indicate that other environmental signals than red/far-red light can modulate the sessility-inducing effect of this c-di-GMP producing module.

In conclusion, Cph2 is a photoreceptor that can sense a very broad spectral range stretching from the near UV to the far-red region and translates this information into changes of c-di-GMP levels. Until recently the CBCR domain of Cph2 was thought to only bind PCB yielding a

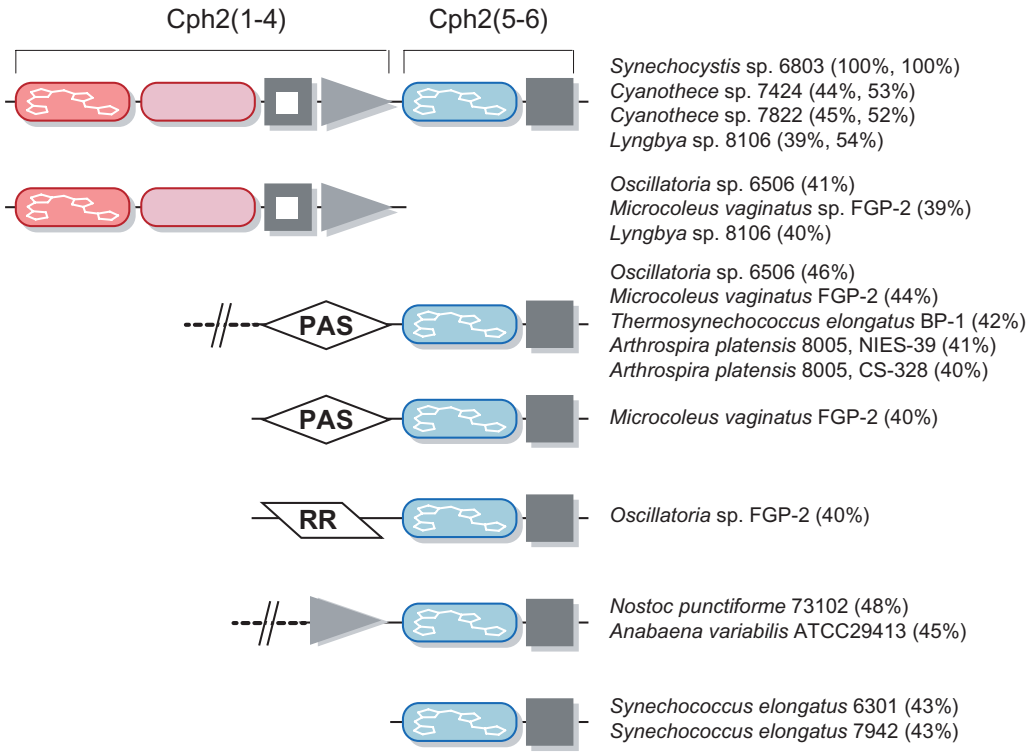

Fig. 6. CBCR-GGDEF modules within the cyanobacterial branch. BLAST searches with the Cph2(5-6) module of *Synechocystis* 6803 revealed 17 hits in the non-redundant GenBank (05/12) that harbour the two cysteines of the CBCR domain crucial for photochemistry, C994 and C1022. All 17 hits are found in cyanobacterial genomes. For comparison, the Cph2(1-4) module is present in only seven cyanobacterial gene products, four of them with the *Synechocystis* 6803 architecture of Cph2, three as a stand-alone module. Values in parentheses give the pair-wise sequence identities of the Cph2(1-4) and CBCR-GGDEF modules respectively.

photochemically inactive species. Here, we show that it undergoes photoconversion between blue- and green-absorbing photostates like other CBCRs, e.g. TePixJ (Ishizuka *et al.*, 2006; 2007; 2011; Ulijasz *et al.*, 2009) and Tlr0924 (Rockwell *et al.*, 2008), and hereby utilizes the same photochemistry including the double tethering of the bilin chromophore by two cysteines, C994 and C1022. The detection of a doubly tethered tetrapyrrole species in the CBCR domain of Cph2 in our mass spectrometry studies gives the final direct proof of such a complex protein–chromophore linkage.

Experimental procedures

Growth conditions

Escherichia coli BL21 gold (DE3) cells were grown in Terrific Broth medium at 37°C supplemented with 50 μg ml^{-1} streptomycin and 100 μg ml^{-1} ampicillin. The *E. coli* strain DH5α was grown in Lysogeny Broth medium with 100 μg ml^{-1} ampicillin or 25 μg ml^{-1} chloramphenicol at 37°C. *Synechocystis* 6803 strains were grown photoautotrophically in liquid BG-11 medium (Rippka *et al.*, 1979) supplemented with 10 mM TES at 30°C and at 50 μmol photons m^{-2} s^{-1} white light (Philips TLD Super 80/840). If needed, antibiotics were added at concentrations of 40 μg ml^{-1} for kanamycin, 14 μg ml^{-1} for chloramphenicol and 10 μg ml^{-1} streptomycin.

The gene was placed under the control of the *petJ* promoter from *Synechocystis* 6803 which is repressed by Cu^{2+}. Transcription is induced in BG-11 medium lacking copper in the trace metal mix. For full repression 2.5 μM $CuSO_4$ was used in the medium.

Vector construction and mutagenesis

All oligonucleotides used in this study are listed in Table S1. To reintegrate the C-terminal GGDEF domain of Cph2 into the genome of *Synechocystis* 6803, a DNA fragment containing the nucleotides 2763–3828 of the *sll0821* locus from *Synechocystis* 6803 was amplified by PCR from genomic DNA with primers p1 and p2 incorporating the restriction sites NdeI and XhoI. The PCR fragment was cloned into the pJET1.2/blunt cloning vector (Fermentas) and verified by sequencing. It was then ligated into the appropriately cut pSK9 vector. For the termination of transcription the *oop* terminator sequence from phage Lambda was introduced at a BglII site of the pSK9 vector via two oligonucleotides O1 and O2, which included BglII and BamHI restriction sites, yielding the plasmid pSDC01. The correct orientation of the insert was verified by sequencing. The pSK9 vector allows chromosomal integration of the target gene under the control of the *petJ* promoter in the intergenic region between the two genes *parA* (*slr1597*) and *hspA* (*sll1514*). A kanamycin-resistant Δ*cph2* insertion mutant (Wilde *et al.*, 2002) was transformed with the plasmid pSDC01 and transformants were selected on BG-11 agar plates containing 14 μg ml^{-1} chloramphenicol and 40 μg ml^{-1} kanamycin. The plasmid pSDC01 was used for replacing the WT *cph2(5-6)* DNA fragment by the mutated versions *cph2(5-6)* C994A and E1182A/E1183A. DNA fragments containing the site-directed mutation were amplified from plasmids pPS02 and pPS03 (see below), respectively with primers p1 and p12 and ligated into pSDC01 using the introduced restriction sites NdeI and BamHI.

For *in vitro* production of Cph2(5-6) plasmid pPS01 was generated by PCR amplification of the same region (nucleotides 2763–3828) with primer pair p3 and p4 (adding a serine after the start methionine and incorporating EcoRI and SalI restriction sites), Phusion DNA polymerase (Finnzymes) and subsequent ligation into the pCDF Duet-1 vector (Novagen) using restriction enzymes EcoRI and SalI. The recombinant Cph2(5-6) module possesses an N-terminal His_6-tag for detection and affinity purification. The plasmid pPS02 containing the *cph2(5-6)* C994A mutant gene was generated utilizing a two-step approach. In two separate reactions pPS01 was amplified with the primer pair p3/C994A *as* and p4/C994A *s*. The resulting oligonucleotides were then fused using primers p3 and p4. After digestion with EcoRI and SalI the PCR fragment was ligated into the pCDF Duet vector. The plasmid pPS03 harbouring the *cph2(5-6)* E1182A/E1183A mutant gene was generated with the two-step approach utilized for the construction of pPS02, using primer pair p3/GGAAF *as* and p4/GGAAF *s*. The identity of the insert was confirmed by restriction digestion and sequencing.

For construction of the *yhjH* and *cph2(1-4)*-expressing strains the DNA fragments from *E. coli* and *Synechocystis* 6803 were amplified using the primer pairs p8/p9 and p13/p14 respectively (Table S1). The promoter region of *petJ* together with a FLAG-tag (for detection of the recombinant protein) from vector pskFLAG (Peter *et al.*, 2009) was amplified using primer pair p10/p11 (Table S1), ligated into a modified pVZ321 vector (Zinchenko *et al.*, 1999) (chloramphenicol resistance cassette was exchanged by the *aadA* gene conferring streptomycin resistance) using KpnI and EcoRI restriction sites, followed by ligation of *yhjH* or *cph2(1-4)* genes immediately downstream of the FLAG-tag sequence via EcoRI and BamHI restriction sites. Using primer pair O3 and O4 the *oop* terminator sequence was added after the stop codon to the 3′-end using BglII and PstI restriction sites. This self-replicating plasmid was transferred using triparental conjugation (Zinchenko *et al.*, 1999) into the Δ*cph2/cph2(5-6)* strain and WT cells as a control. Confirmation of mutants was performed by PCR analysis. Site-directed mutagenesis of the EAL domain of Cph2(1-4) was performed using the QuikChange II site-directed mutagenesis kit (Stratagene) using primers p15 and p16 (Table S1). Expression of WT and mutated versions of Cph2 modules was confirmed by Western blot analysis using anti-Cph2(5-6) or anti-FLAG (Fig. S1A).

Western blot analysis

Synechocystis 6803 cells were grown in BG-11 medium to an OD_{750nm} of 1.0 with the copper concentrations indicated. The sample preparation and SDS-PAGE was carried out as described in Dühring *et al.* (2006). For primary detection an anti-Cph2(5-6) or anti-FLAG (Sigma) antibody was used. The polyclonal antibody was produced using the Cph2(5-6) module recombinantly overproduced in *E. coli* (Pineda AB-Service, Berlin, Germany).

Phototaxis experiments

Phototactic movement was examined on BG-11 0.5% (w/v) agar plates (Bacto agar; Difco) supplemented with 10 mM TES and 50 mM glucose. These plates were incubated in boxes that were open on one side. White light was produced as mentioned above. LEDs (blue: Luxeon K2/PR14, λ_{max} 450 nm; green: Luxeon K2/PM14, λ_{max} 540 nm) were used for blue and green light illumination respectively. Phototaxis plates were incubated for up to 2 weeks at 30°C.

Production of the recombinant Cph2(5-6) wild-type or C994A mutant protein

Escherichia coli BL21 Gold (DE3) cells were cotransformed with plasmids pPS01 or pPS02 and p45.2 as described by Landgraf *et al*. (2001). p45.2 harbours the *Synechocystis* 6803 genes *ho1* and *pcyA*, whose gene products (haem oxygenase 1 and PCB:ferredoxin oxidoreductase) catalyse the synthesis of the PCB chromophore from haem. Cells were grown for 24 h at 37°C for PS01 or 48 h at 30°C for PS02 and harvested at 2800 *g* for 15 min. Pellets were resuspended in lysis buffer (50 mM K_2HPO_4, 300 mM NaCl, 10 mM imidazole, 10% glycerol, pH 7.5, 10 ml l^{-1} cell culture) and flash frozen or used immediately. Cells were treated with 30 μg ml^{-1} lysozyme (Serva), 1 mM phenylmethylsulfonyl fluoride and passed through a precooled French press (900 psig, Thermo Fisher Scientific). Cell debris was pelleted at 40 000 *g* for 60 min; the supernatant was purified using Ni-NTA affinity chromatography (Qiagen) and subsequent size exclusion chromatography (Superdex 200, GE Healthcare) in SEC buffer (50 mM K_2HPO_4, 300 mM NaCl, 10% glycerol, pH 7.5). The eluate was concentrated using an Amicon-Ultra concentrator (30 kDa cut-off). Covalent binding of the cofactor was verified by Zn^{2+}-induced fluorescence (2 mM final concentration) after SDS-PAGE (Berkelman and Lagarias, 1986).

Spectroscopic analyses

Absorption spectra were measured with a UV/Vis spectrophotometer (Jasco V660) at 20°C and a protein concentration of 2 mg ml^{-1} (1.0 nm bandwidth, 400 nm min^{-1} scan speed, 10 mm cell length). Prior to the measurement the sample was irradiated with blue or green light until no further photoconversion could be observed (1–2 min). Spectra are shown as the smoothed average of three measurements. CD spectra were recorded with a spectropolarimeter (Jasco J-810) at 20°C with a cell length of 2 mm at protein concentrations of 4 mg ml^{-1}.

In vitro *activity assays*

Diguanylate cyclase activity was measured in triplicates under continuous irradiation with green or blue LEDs. Assays were performed in Tris/HCl buffer (50 mM Tris/HCl, 50 mM NaCl, 10 mM $MgCl_2$, 0.5 mM EDTA, pH 7.5) at 25°C with 1 μM Cph2(5-6). Samples were preincubated at 25°C with blue or green light for 3 min. The reaction was started by addition of GTP at a final concentration of 1 mM and stopped by heating the samples to 98°C for 3 min. The samples were then centrifuged (~20 000 *g*, 15 min); the supernatant was filtered with an 0.22 μm Ultrafree-MC filter (Millipore) and analysed by HPLC/UV [Nucleodur C18 Pyramid 3 μm (Macherey-Nagel), HPLC system 1100 series with a VWD UV detector (Agilent)] using an ammonium acetate gradient (buffer A: 18 mM ammonium acetate, 1 mM acetic acid, pH 5.9; buffer B: methanol) (Ryjenkov *et al*., 2005) starting with 0% B at t = 0 min, followed by 20% B (t = 10 min), 95% B (t = 15 min), 95% B (t = 18 min), 0% B (t = 20 min) for additional 25 min. Column temperature was 40°C with a flow rate of 0.2 ml min^{-1}. UV absorption was measured at 254 nm (λ_{max} of c-di-GMP). Integrals of UV absorption were correlated to c-di-GMP concentration via a calibration plot obtained by measuring defined c-di-GMP concentrations of commercially obtained c-di-GMP (BioLog) in buffer. To verify the identity of c-di-GMP, MS spectra were performed. The reaction mixture of enzymatic assays was analysed by an Agilent HPLC system coupled to a LTQ-FT-Ultra mass analyser (Thermo Scientific) using same column, eluents and gradient as for obtaining the chromatograms of enzymatic assay analysis.

Mass spectrometry analysis of tryptic protein digests

For tryptic digestion 10 μg of trypsin (Promega) was added to Cph2(5-6) (11 μM, 100 μg of total protein) in SEC buffer under blue or green light. The sample was incubated in the dark for 16 h at 37°C. The corresponding peptide mixtures were analysed with an Agilent 1100 HPLC system coupled to a LTQ-FT-Ultra mass analyser (Thermo Scientific) using a Phenomenex 150/3 Kinetex C18 column (2.6 μm particle size, 100 Å pore diameter) at 40°C and a flow rate of 0.2 ml min^{-1}. The gradient applied was as follows [solvent A: 0.1% TFA in water (trifluoroacetic acid); solvent B: 0.1% TFA in acetonitrile]: holding 5% B for 10 min, then linear increase of the concentration of B within 150 min to 60% B, followed by an increase to 90% B within 5 min and holding 90% B for additional 15 min. Exact mass spectra of the eluting peptides were generated within the FT-ICR mass analyser at an m/z resolution of 100 000. Additionally, data-dependent fragmentation was performed within the LTQ mass analyser.

Acknowledgements

The vectors pSK9 and p45.2 were kind gifts of S. Zinchenko and J. Hughes respectively. Purified YdeH was a kind gift of F. Zähringer. The authors want to thank U. Linne, J. Bamberger and N. Fritzler for MS analysis and support for HPLC/UV measurements and S. Kiontke for the spectroscopic set-up. This work was supported by DFG grant ES152/7 (L.-O. E.) and the LOEWE centre for Synthetic Microbiology.

References

Amikam, D., and Galperin, M.Y. (2006) PilZ domain is part of the bacterial c-di-GMP binding protein. *Bioinformatics* **22:** 3–6.

Anders, K., von Stetten, D., Mailliet, J., Kiontke, S., Sineshchekov, V.A., Hildebrandt, P., *et al*. (2011) Spectroscopic

and photochemical characterization of the red-light sensitive photosensory module of Cph2 from *Synechocystis* PCC 6803. *Photochem Photobiol* **87:** 160–173.

Barends, T.R., Hartmann, E., Griese, J.J., Beitlich, T., Kirienko, N.V., Ryjenkov, D.A., *et al*. (2009) Structure and mechanism of a bacterial light-regulated cyclic nucleotide phosphodiesterase. *Nature* **459:** 1015–1018.

Berkelman, T.R., and Lagarias, J.C. (1986) Visualization of bilin-linked peptides and proteins in polyacrylamide gels. *Anal Biochem* **156:** 194–201.

Bhaya, D. (2004) Light matters: phototaxis and signal transduction in unicellular cyanobacteria. *Mol Microbiol* **53:** 745–754.

Bhaya, D., Bianco, N.R., Bryant, D., and Grossman, A.R. (2000) Type IV pilus biogenesis and motility in the cyanobacterium *Synechocystis* sp. PCC6803. *Mol Microbiol* **37:** 941–951.

Bhaya, D., Nakasugi, K., Fazeli, F., and Burriesci, M.S. (2006) Phototaxis and impaired motility in adenylyl cyclase and cyclase receptor protein mutants of *Synechocystis* sp. strain PCC 6803. *J Bacteriol* **188:** 7306–7310.

Boehm, A., Kaiser, M., Li, H., Spangler, C., Kasper, C.A., Ackermann, M., *et al*. (2010) Second messenger-mediated adjustment of bacterial swimming velocity. *Cell* **141:** 107–116.

Burriesci, M., and Bhaya, D. (2008) Tracking phototactic responses and modeling motility of *Synechocystis* sp. strain PCC6803. *J Photochem Photobiol B* **91:** 77–86.

Cao, Z., Livoti, E., Losi, A., and Gärtner, W. (2010) A blue light-inducible phosphodiesterase activity in the cyanobacterium *Synechococcus elongatus*. *Photochem Photobiol* **86:** 606–611.

Christen, B., Christen, M., Paul, R., Schmid, F., Folcher, M., Jenoe, P., *et al*. (2006) Allosteric control of cyclic di-GMP signaling. *J Biol Chem* **281:** 32015–32024.

Christen, M., Christen, B., Folcher, M., Schauerte, A., and Jenal, U. (2005) Identification and characterization of a cyclic di-GMP-specific phosphodiesterase and its allosteric control by GTP. *J Biol Chem* **280:** 30829–30837.

Dienst, D., Dühring, U., Mollenkopf, H.J., Vogel, J., Golecki, J., Hess, W.R., and Wilde, A. (2008) The cyanobacterial homologue of the RNA chaperone Hfq is essential for motility in *Synechocystis* sp. PCC 6803. *Microbiology* **154:** 3134–3143.

Duerig, A., Abel, S., Folcher, M., Nicollier, M., Schwede, T., Amiot, N., *et al*. (2009) Second messenger-mediated spatiotemporal control of protein degradation regulates bacterial cell cycle progression. *Genes Dev* **23:** 93–104.

Dühring, U., Irrgang, K.D., Lünser, K., Kehr, J., and Wilde, A. (2006) Analysis of photosynthetic complexes from a cyanobacterial *ycf37* mutant. *Biochim Biophys Acta* **1757:** 3–11.

Fiedler, B., Börner, T., and Wilde, A. (2005) Phototaxis in the cyanobacterium *Synechocystis* sp. PCC 6803: role of different photoreceptors. *Photochem Photobiol* **81:** 1481–1488.

Hickman, J.W., and Harwood, C.S. (2008) Identification of FleQ from *Pseudomonas aeruginosa* as a c-di-GMP responsive transcription factor. *Mol Microbiol* **69:** 376–389.

Hirose, Y., Shimada, T., Narikawa, R., Katayama, M., and Ikeuchi, M. (2008) Cyanobacteriochrome CcaS is the green light receptor that induces the expression of phycobilisome linker protein. *Proc Natl Acad Sci USA* **105:** 9528–9533.

Hirose, Y., Narikawa, R., Katayama, M., and Ikeuchi, M. (2010) Cyanobacteriochrome CcaS regulates phycoerythrin accumulation in *Nostoc punctiforme*, a group II chromatic adapter. *Proc Natl Acad Sci USA* **107:** 8854–8859.

Hitomi, K., Okamoto, K., Daiyasu, H., Miyashita, H., Iwai, S., Toh, H., *et al*. (2000) Bacterial cryptochrome and photolyase: characterization of two photolyase-like genes of *Synechocystis* sp. PCC6803. *Nucleic Acids Res* **28:** 2353–2362.

Hughes, J., Lamparter, T., Mittmann, F., Hartmann, E., Gärtner, W., Wilde, A., and Börner, T. (1997) A prokaryotic phytochrome. *Nature* **386:** 663.

Ikeuchi, M., and Ishizuka, T. (2008) Cyanobacteriochromes: a new superfamily of tetrapyrrole-binding photoreceptors in cyanobacteria. *Photochem Photobiol Sci* **7:** 1159–1167.

Ishizuka, T., Shimada, T., Okajima, K., Yoshihara, S., Ochiai, Y., Katayama, M., and Ikeuchi, M. (2006) Characterization of cyanobacteriochrome TePixJ from a thermophilic cyanobacterium *Thermosynechococcus elongatus* strain BP-1. *Plant Cell Physiol* **47:** 1251–1261.

Ishizuka, T., Narikawa, R., Kohchi, T., Katayama, M., and Ikeuchi, M. (2007) Cyanobacteriochrome TePixJ of *Thermosynechococcus elongatus* harbors phycoviolobilin as a chromophore. *Plant Cell Physiol* **48:** 1385–1390.

Ishizuka, T., Kamlya, A., Suzuki, H., Narikawa, R., Noguchi, T., Inomata, K., and Ikeuchi, M. (2011) The cyanobacteriochrome, TePixJ, isomerizes its own chromophore by converting phycocyanobilin to phycoviolobilin. *Biochemistry* **50:** 953–961.

Jenal, U., and Malone, J. (2006) Mechanisms of cyclic-di-GMP signaling in bacteria. *Annu Rev Genet* **40:** 385–407.

Jung, K.H., Trivedi, V.D., and Spudich, J.L. (2003) Demonstration of a sensory rhodopsin in eubacteria. *Mol Microbiol* **47:** 1513–1522.

Kazmierczak, B.I., Lebron, M.B., and Murray, T.S. (2006) Analysis of FimX, a phosphodiesterase that governs twitching motility in *Pseudomonas aeruginosa*. *Mol Microbiol* **60:** 1026–1043.

Kehoe, D.M., and Grossman, A.R. (1996) Similarity of a chromatic adaptation sensor to phytochrome and ethylene receptors. *Science* **273:** 1409–1412.

Landgraf, F.T., Forreiter, C., Pico, A.H., Lamparter, T., and Hughes, J. (2001) Recombinant phytochrome in *Escherichia coli*. *FEBS Lett* **508:** 459–462.

Leduc, J.L., and Roberts, G.P. (2009) Cyclic di-GMP allosterically inhibits the CRP-like protein (Clp) of *Xanthomonas axonopodis* pv. *citri*. *J Bacteriol* **191:** 7121–7122.

Lee, V.T., Matewish, J.M., Kessler, J.L., Hyodo, M., Hayakawa, Y., and Lory, S. (2007) A cyclic-di-GMP receptor required for bacterial exopolysaccharide production. *Mol Microbiol* **65:** 1474–1484.

Montgomery, B.L., and Lagarias, J.C. (2002) Phytochrome ancestry: sensors of bilins and light. *Trends Plant Sci* **7:** 357–366.

Moon, Y.J., Kim, S.Y., Jung, K.H., Choi, J.S., Park, Y.M., and Chung, Y.H. (2011) Cyanobacterial phytochrome Cph2 is a negative regulator in phototaxis towards UV-A. *FEBS Lett* **585:** 335–340.

Narikawa, R., Zihara, K., Okajima, K., Ochiai, Y., Katayama, M., Schichida, Y., *et al.* (2006) Three putative photosensory light, oxygen or voltage (LOV) domains with distinct biochemical properties from the filamentous cyanobacterium *Anabaena* sp. PCC 7120. *Photochem Photobiol* **82:** 1627–1633.

Narikawa, R., Fukushima, Y., Ishizuka, T., Itoh, S., and Ikeuchi, M. (2008) A novel photoactive GAF domain of cyanobacteriochrome AnPixJ shows reversible green/red photoconversion. *J Mol Biol* **380:** 844–855.

Newell, P.D., Monds, R.D., and O'Toole, G.A. (2009) LapD is a bis-(3′,5′)-cyclic dimeric GMP-binding protein that regulates surface attachment by *Pseudomonas fluorescens* Pf0-1. *Proc Natl Acad Sci USA* **106:** 3461–3466.

Okajima, K., Fukushima, Y., Suzuki, H., Kita, A., Ochiai, Y., Katayama, M., *et al.* (2006) Fate determination of the flavin photoreceptions in the cyanobacterial blue light receptor TePixD (Tll0078). *J Mol Biol* **363:** 10–18.

Park, C.M., Kim, J.I., Yang, S.S., Kang, J.G., Kang, J.H., Shim, J.Y., *et al.* (2000) A second photochromic bacteriophytochrome from *Synechocystis* sp. PCC 6803: spectral analysis and downregulation by light. *Biochemistry* **39:** 10840–10847.

Paul, K., Nieto, V., Carlquist, W.C., Blair, D.F., and Harshey, R.M. (2010) The c-di-GMP binding protein YcgR controls flagellar motor direction and speed to affect chemotaxis by a 'backstop brake' mechanism. *Mol Cell* **38:** 128–139.

Paul, R., Weiser, S., Amiot, N.C., Chan, C., Schirmer, T., Giese, B., and Jenal, U. (2004) Cell cycle-dependent dynamic localization of a bacterial response regulator with a novel di-guanylate cyclase output domain. *Genes Dev* **18:** 715–727.

Peter, E., Salinas, A., Wallner, T., Jeske, D., Dienst, D., Wilde, A., and Grimm, B. (2009) Differential requirement of two homologous proteins encoded by *sll1214* and *sll1874* for the reaction of Mg protoporphyrin monomethylester oxidative cyclase under aerobic and micro-oxic growth conditions. *Biochim Biophys Acta* **1787:** 1458–1467.

Rippka, R., Deruelles, J., Waterbury, J.B., Herdman, M., and Stanier, R.Y. (1979) Generic assignments, strain histories and properties of pure cultures of cyanobacteria. *J Gen Microbiol* **111:** 1–61.

Rockwell, N.C., and Lagarias, J.C. (2010) A brief history of phytochromes. *Chemphyschem* **11:** 1172–1180.

Rockwell, N.C., Njuguna, S.L., Roberts, L., Castillo, E., Parson, V.L., Dwojak, S., *et al.* (2008) A second conserved GAF-domain cysteine is required for the blue/green photoreversibility of cyanobacteriochrome Tlr0924 from *Thermosynechococcus elongatus*. *Biochemistry* **47:** 7304–7316.

Rockwell, N.C., Martin, S.S., Feoktistova, K., and Lagarias, J.C. (2011) Diverse two-cysteine photocycles in phytochromes and cyanobacteriochromes. *Proc Natl Acad Sci USA* **108:** 11854–11859.

Römling, U., and Amikam, D. (2006) Cyclic di-GMP as a second messenger. *Curr Opin Microbiol* **9:** 218–228.

Ryjenkov, D.A., Tarutina, M., Moskvin, O.V., and Gomelsky, M. (2005) Cyclic diguanylate is a ubiquitous signaling molecule in bacteria: insights into biochemistry of the GGDEF protein domain. *J Bacteriol* **187:** 1792–1798.

Ryjenkov, D.A., Simm, R., Römling, U., and Gomelsky, M. (2006) The PilZ domain is a receptor for the second messenger c-di-GMP: the PilZ domain protein YcgR controls motility in enterobacteria. *J Biol Chem* **281:** 30310–30314.

Schmidt, A.J., Ryjenkov, D.A., and Gomelsky, M. (2005) The ubiquitous protein domain EAL is a cyclic diguanylate-specific phosphodiesterase: enzymatically active and inactive EAL domains. *J Bacteriol* **187:** 4774–4781.

Simm, R., Morr, M., Kader, A., Nimtz, M., and Römling, U. (2004) GGDEF and EAL domains inversely regulate cyclic di-GMP levels and transition from sessility to motility. *Mol Microbiol* **53:** 1123–1134.

Song, J.Y., Cho, H.S., Cho, J.I., Jeon, J.S., Lagarias, J.C., and Park, Y.I. (2011) Near-UV cyanobacteriochrome signaling system elicits negative phototaxis in the cyanobacterium *Synechocystis* sp. PCC 6803. *Proc Natl Acad Sci USA* **108:** 10780–10785.

Tarutina, M., Ryjenkov, D.A., and Gomelsky, M. (2006) An unorthodox phytochrome from *Rhodobacter sphaeroides* involved in turnover of the second messenger c-di-GMP. *J Biol Chem* **281:** 34751–34758.

Terauchi, K., Montgomery, B.L., Grossman, A.R., Lagarias, J.C., and Kehoe, D.M. (2004) RcaE is a complementary chromatic adaptation photoreceptor required for green and red light responsiveness. *Mol Microbiol* **51:** 567–577.

Tous, C., Vega-Palas, M.A., and Vioque, A. (2001) Conditional expression of RNase P in the cyanobacterium *Synechocystis* sp. PCC6803 allows detection of precursor RNAs. Insight in the in vivo maturation pathway of transfer and other stable RNAs. *J Biol Chem* **276:** 29059–29066.

Ulijasz, A.T., Cornilescu, G., Stetten, D.V., Cornilescu, C., Escobar, F.V., Zhang, J., *et al.* (2009) Cyanochromes are blue/green light photoreversible photoreceptors defined by a stable double cysteine linkage to a phycoviolobilin-type chromophore. *J Biol Chem* **284:** 29757–29772.

Wiegand, G., Parbel, A., Seifert, M.H., Holak, T.A., and Reuter, W. (2002) Purification, crystallization, NMR spectroscopy and biochemical analyses of alpha-phycoerythrocyanin peptides. *Eur J Biochem* **269:** 5046–5055.

Wilde, A., Fiedler, B., and Börner, T. (2002) The cyanobacterial phytochrome Cph2 inhibits phototaxis towards blue light. *Mol Microbiol* **44:** 981–988.

Wolfe, A.J., and Visick, K.L. (2008) Get the message out: cyclic-di-GMP regulates multiple levels of flagellum-based motility. *J Bacteriol* **190:** 463–475.

Wu, S.H., and Lagarias, J.C. (2000) Defining the bilin lyase domain: lessons from the extended phytochrome superfamily. *Biochemistry* **39:** 13487–13495.

Yeh, K.C., Wu, S.H., Murphy, J.T., and Lagarias, J.C. (1997) A cyanobacterial phytochrome two-component light sensory system. *Science* **277:** 1505–10508.

Yoshihara, S., Suzuki, F., Fujita, H., Geng, X.X., and Ikeuchi, M. (2000) Novel putative photoreceptor and regulatory genes required for the positive phototactic movement of the unicellular motile cyanobacterium *Synechocystis* sp. PCC 6803. *Plant Cell Physiol* **41:** 1299–1304.

Yoshihara, S., Katayama, M., Geng, X., and Ikeuchi, M. (2004) Cyanobacterial phytochrome-like PixJ1 holoprotein shows novel reversible photoconversion between blue-

and green-absorbing forms. *Plant Cell Physiol* **45:** 1729–1737.

Zähringer, F., Massa, C., and Schirmer, T. (2011) Efficient enzymatic production of the bacterial second messenger c-di-GMP by the diguanylate cyclase YdeH from *E. coli*. *Appl Biochem Biotechnol* **163:** 71–79.

Zinchenko, V.V., Piven, I., Melnik, V., and Shestakov, S. (1999) Vectors for the complementation analysis of cyanobacterial mutants. *Genetika* **35:** 291–296.

Supporting information

Additional supporting information may be found in the online version of this article.

Please note: Wiley-Blackwell are not responsible for the content or functionality of any supporting materials supplied by the authors. Any queries (other than missing material) should be directed to the corresponding author for the article.

Supporting information

Table S1. Oligonucleotides used in this study. Recognition sites for restriction endonucleases are underlined.

Oligonucleotide	
p1	CATATGGTCAAGGAAAAATTAGTGTTGAAAATTGC
p2	CTCGAGAACTTCCCCATCAACATGGG
O1	GATCTAACGCTCGGTTGCCGCCGGGCGTTTTTTATTG
O2	GATCCAATAAAAAACGCCCGGCGGCAACCGAGCGTTA
p3	GCGGCGAATTCAGTCAAGGAAAAATTAGTGTTG
p4	CATGTTGATGGGGAAGTTTAGGTCGACAATTC
C994A s	CAATTATTAACGATGAAATTGACGATCCCGCATTCAAGGGCCATTATCTGCG GCTGTATCGAG
C994A as	CTCGATACAGCCGCAGATAATGGCCCTTGAATGCGGGATCGTCAATTTCAT CGTTAATAATTG
p6	TTTGTCATCCTCGACTGTGC
p7	GGTGAAAGTTCAGCTTTCCT
p8	CAGAATTCATAAGGCAGGTTATCCAGCGA
p9	ACGGATCCTTATAGCGCCAGAACCGC
O3	GATCCAACGCTCGGTTGCCGCCGGGCGTTTTTTATTCTGCA
O4	GAATAAAAAACGCCCGGCGGCAACCGAGCGTTG
p10	GTCGACTACGCCCGGTAGTGATC
p11	GAATTCTTTATCATCATCATCAAATAT
p12	GTGGATCCTCATTAAACTTCCCCATCAAC
p13	GAATTCAACCCTAATCGATCCTTAGAA
p14	GTGGATCCTCATTAATCAAGAATCTGTGGATAG
p15	CTGGAAACTGTGGCCGCAGGGATCGAATCGGAAGCC
p16	GGCTTCCGATTCGATCCCTGCGGCCACAGTTTCCAG

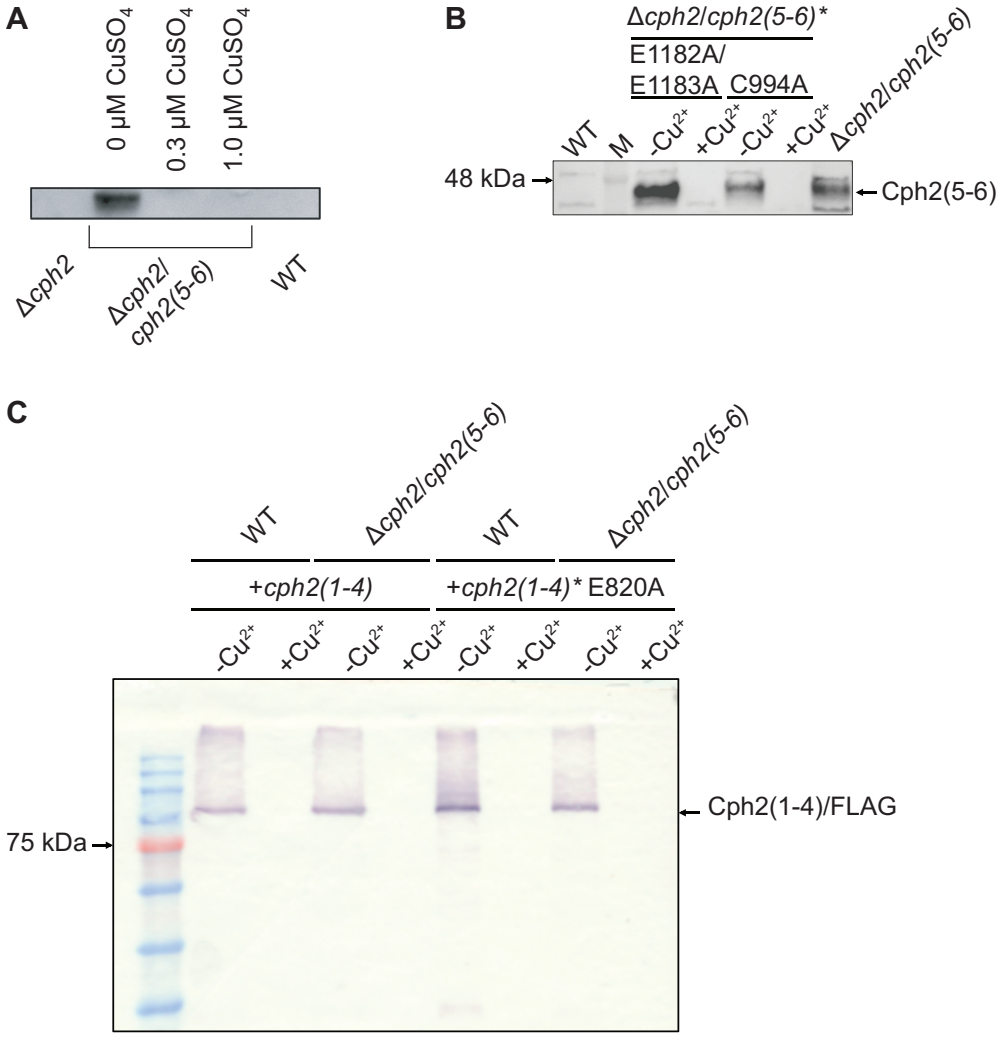

Fig. S1. Expression of Cph2(5-6) and Cph2(1-4) in *Synechocystis* 6803 mutants.

A. Western Blot analysis of cell lysates from the Δ*cph2/cph2(5-6)* mutant (clone 1) grown in BG-11 with different concentrations of copper, the WT and the Δ*cph2* mutant, both grown in copper free medium. An α-Cph2(5-6) antibody was used for detection.

B. Western Blot analysis of cell lysates from the Δ*cph2/cph2(5-6)* mutant strains under inducing (-Cu^{2+}) and non-inducing (+Cu^{2+}) conditions using anti-Cph2(5-6) antiserum. Expression was confirmed also for Δ*cph2/cph2(5-6)** mutant strains harboring amino acid residue changes in the chromophore binding domain (C994A) and in the catalytic domain (E1182A/E1183A). An α-Cph2(5-6) antiserum was used for detection.

C. Western Blot analysis of cell lysates from the wild type and Δ*cph2/cph2(5-6)* mutant strains expressing the 3xFLAG tagged Cph2(1-4) truncated protein and its mutated version Cph2(1-4)* of the EAL domain (E820A) under inducing (-Cu^{2+}) and non-inducing (+Cu^{2+}) conditions. An α-FLAG antibody coupled to alkaline phosphatase was used for detection.

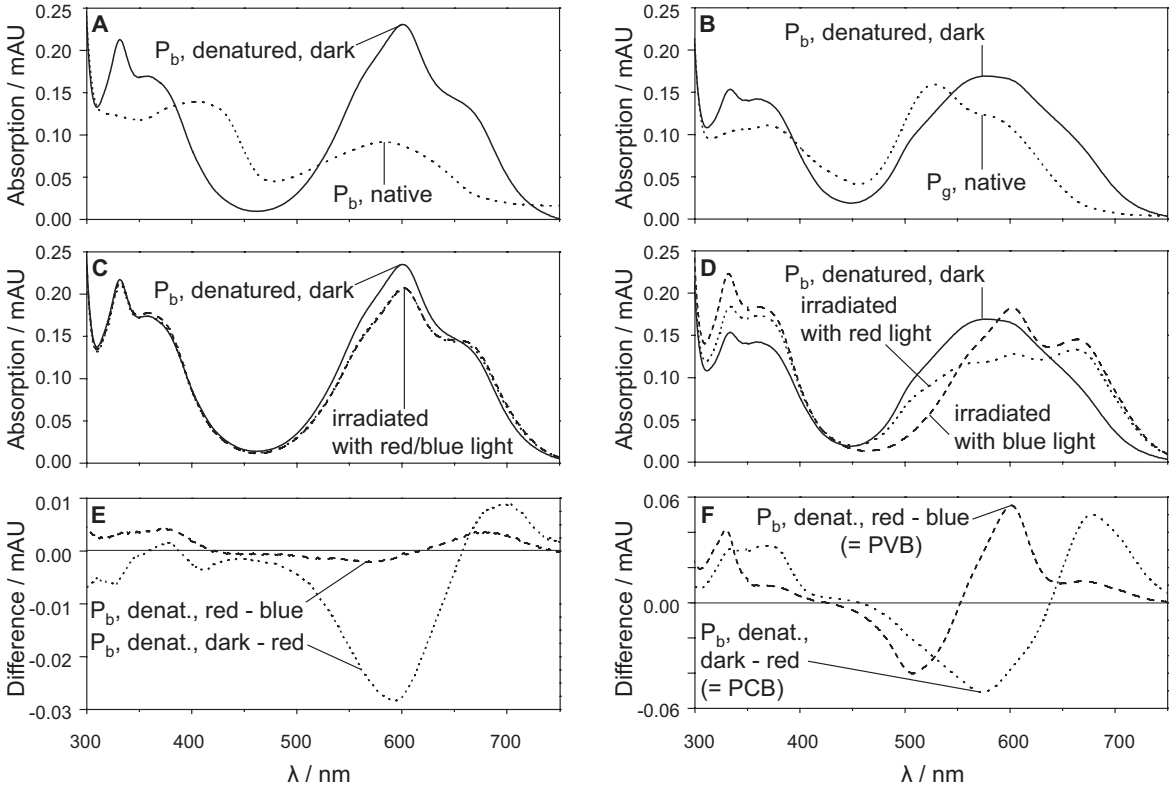

Fig. S2. Denaturation analysis of Cph2(5-6) reveals a mixture of PCB and PVB.

The photochemically accessible forms of Cph2(5-6) were denatured in the absence of light and absorption spectra were taken. The samples were then irradiated with red and blue light. After each irradiation absorption spectra were recorded.

A. Absorption spectrum of Cph2(5-6) P_b denatured in the dark (solid). The spectrum of the native protein is shown for comparison (dotted).

B. Absorption spectrum of Cph2(5-6) P_g denatured in the dark (solid). The spectrum of the native protein is shown for comparison (dotted).

C. Absorption spectrum of dark denatured Cph2(5-6) P_b after irradiation with first red light (dotted line) and then blue light (dashed line). The dark denatured state is shown as a solid line for reference.

D. Absorption spectrum of dark denatured Cph2(5-6) P_g after irradiation with first red light (dotted line) and then blue light (dashed line). The dark denatured state is shown as a solid line for reference.

E. To highlight changes in the spectra, difference spectra were calculated from C as (dark denatured) - (dark denatured after red light) (dotted line) and (dark denatured after red light) - (dark denatured after blue light) (dashed line).

F. To highlight changes in the spectra, difference spectra were calculated from D as (dark denatured) - (dark denatured after red light) (dotted line) and (dark denatured after red light) - (dark denatured after blue light) (dashed line).

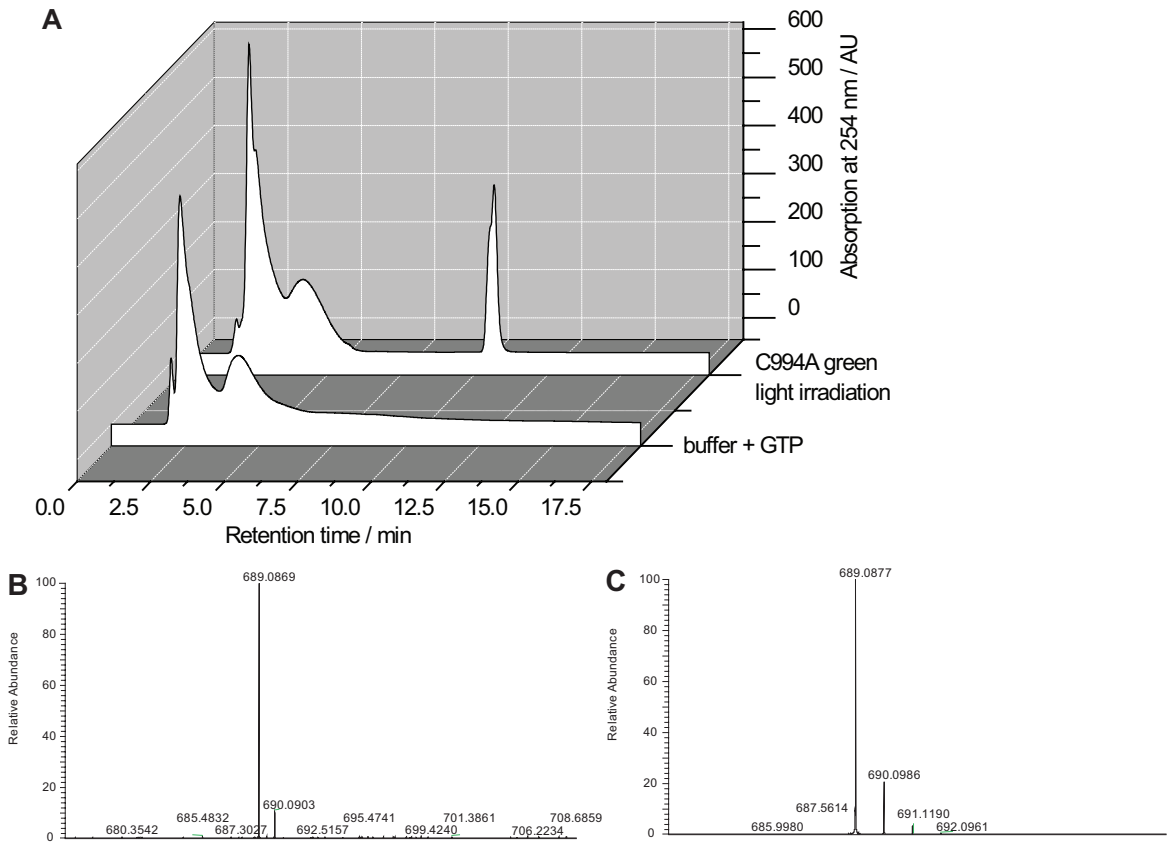

Fig. S3. HPLC/UV/MS analytics of c-di-GMP

A. HPLC/UV analysis of the no-protein control (buffer + GTP) and reaction solution of the enzymatic production of c-di-GMP by Cph2(5-6) C994A under green light irradiation at reaction time 10 min. Retention times: c-di-GMP, 10 min; GTP, 4 min; buffer, 2 min.

B. MS of enzymatically synthesized c-di-GMP.

C. MS of chemically synthesized c-di-GMP.

5.3 Structural characterization of *Syn*Cph2(1-2)

This research was originally published in The Journal of Biological Chemistry. *Katrin Anders, Grazia Daminelli-Widany, Maria Andrea Mroginski, David von Stetten and Lars-Oliver Essen.* **Structure of the cyanobacterial phytochrome 2 photosensor implies a tryptophan switch for phytochrome signaling.** The Journal of Biological Chemistry. 2013; 288:35714-35725.

Summary

We solved the crystal structure of the N-terminal photosensory module from *Syn*Cph2 in the P_r conformation at a resolution of 2.6 Å. The conformation of crystalline *Syn*Cph2(1-2) seems to resemble the native conformation as UV/vis and RR spectra of crystalline and dissolved *Syn*Cph2(1-2) are similar. The protein crystallized as antiparallel dimer in the bilobal shape of a tandem-GAF module. In *Pa*BPhP a parallel arrangement of the monomers in the crystal is observed, which is believed to be crucial for the signal transduction in phytochromes[11], especially when being fused to downstream HK-like domains. Due to the different output domains in *Syn*Cph2(1-2) the antiparallel arrangement could be functionally relevant and not just an crystallization artifact as in *Syn*Cph1. The two GAF domains of *Syn*Cph2(1-2) are connected *via* a long α-helix and mimic the overall organization of canonical GAF-PHY modules including the tongue-like protrusion of the GAF2 domain. The figure-of-eight knot, an attribute of Group I phytochromes, is missing in *Syn*Cph2(1-2) caused by the lack of the PAS domain. The N-terminal, in *Syn*Cph1 knot-building, helix is in *Syn*Cph2(1-2) part of a six-helix bundle in the dimer interface. The PCB chromophore in the *ZZZssa* conformation is well defined by the electron density map. It is covalently attached to Cys-129; its new chiral center $C3^1$ has *R* configuration. The chromophore is non-planar and exhibits a tilt between rings B-C and C-D that is the largest among known phytochrome and PCB-binding phycobilisomes. We addressed the question if these high tilts are caused by X-ray radiation damage. Single crystal UV/vis and RR measurements showed that upon X-ray irradiation the spectral signatures of *Syn*Cph2(1-2) change but this effect can be reversed by cryo-annealing. The RR spectra indicate that the alterations occur near the ring B and C nitrogens and may be caused by the pyrrole water. These changes are marginal and the main conformation of the PCB chromophore is undistorted. We further optimized the structure of the PCB binding site using a QM/MM approach. In all calculations the large twist that is observed between rings B and C is maintained and the protein environment remains conserved. This proves that the tilt is enforced by the protein matrix and not by radiation damage.

The local environment of the chromophore's D-ring is conserved between *Syn*Cph2(1-2)

and *Syn*Cph1. In the chromophore propionate surroundings the loop, which in *Syn*Cph1 is part of the knot region, interacts in *Syn*Cph2(1-2) differently with the B-ring propionate. Here, the propionate builds a salt bridge to Lys-104 which is on an additional β-strand. In *Syn*Cph1 the B-ring propionate interacts with Arg-254 from the loop region and partner swaps upon photoconversion to Arg-222[137]. Both arginines and a possible interaction partner in P_{fr} are missing in *Syn*Cph2(1-2). Interestingly, sequence alignments of Group II phytochromes show that the propionate interactions seem to vary according to the type of effector domains. The B-ring interactions itself are not crucial for P_r to P_{fr} conversion as *e.g.* an alanine variant of Lys-104 exhibits wild type photochemistry.

The tip of the tongue region that covers the PCB binding site of GAF1 is highly conserved among Group I and II phytochromes. The stem region of the tongue is built of β-strands; in the P_{fr} structure of *Pa*BPhP an α-helical conformation is adopted. In *Syn*Cph2(1-2) and *Syn*Cph1 the overall position of the conserved $W^G/_A G$, PRxSF and WxE motifs is well conserved. In the P_{fr} structure of *Pa*BphP the motifs differ significantly and are displaced in comparison to *Syn*Cph2(1-2). Alanine variants of the tryptophans from the $W^G/_A G$ and WxE motifs are arrested in an intermediate state upon red light illumination whereas phenylalanine variants show P_{fr} formation. This indicates that the bulky side chains of these tryptophans are needed as anchors to stabilize the P_r and a different tongue formation in the P_{fr} state. In the P_r and P_{fr} structures one tryptophan is located on similar positions in the tongue-GAF1 interface, but belong either to the $W^G/_A G$ motif or the WGG motif, hinting to a major tongue reorganization during photoconversion. This is further supported by the PRxSF motif that in both structures adopts an inverted orientation including the residues involved in forming the salt bridge to the aspartate of GAF1's DIP motif. We suggest a model for structural changes upon photoconversion, which involves a conformational switching of the tongue region *via* a swap of the tryptophans. The Asp-Arg salt bridge, stabilizing the tongue-GAF1 interface, is broken and the alterations of the tongue's tip involve the disordering of the β-hairpin stem region and the formation of a new Asp-Ser salt bridge. This large conformational change is supported by an increased α-helical content in P_{fr} that was observed before by CD spectroscopy[138].

Contributions

K. Anders designed experiments, cloned the plasmids, produced and purified the proteins, performed absorbance and CD spectroscopical measurements as well as protein crystallization, analyzed the data, solved and refined the structure and wrote the manuscript, G. Daminelli-Widany performed QM/MM calculations, M. A. Mroginski analyzed QM/MM data and wrote this part of the manuscript, D. von Stetten performed and analyzed RR experiments as well as single crystal UV/vis spectroscopy, L.-O. Essen designed experiments, solved the structure, wrote and revised the manuscript.

THE JOURNAL OF BIOLOGICAL CHEMISTRY VOL. 288, NO. 50, pp. 35714–35725, December 13, 2013

Structure of the Cyanobacterial Phytochrome 2 Photosensor Implies a Tryptophan Switch for Phytochrome Signaling*[S]

Received for publication, August 16, 2013, and in revised form, October 22, 2013 Published, JBC Papers in Press, October 30, 2013, DOI 10.1074/jbc.M113.510461

Katrin Anders[‡], **Grazia Daminelli-Widany**[§], **Maria Andrea Mroginski**[§], **David von Stetten**[¶], **and Lars-Oliver Essen**[‡1]

From the [‡]*Department of Chemistry, Biomedical Research Centre, Philipps-Universität, D-35032 Marburg, Germany, the* [§]*Department of Chemistry, Technische Universität Berlin, D-10623 Berlin, Germany, and the* [¶]*European Synchrotron Radiation Facility, F-38043 Grenoble Cedex, France*

Background: Phytochromes are red/far-red photoreceptors using a bilin chromophore.
Results: Compared with Cph1, the Cph2 bilin-binding site differs around the propionates, but utilizes an otherwise conserved tongue for sealing the chromophore from solvent.
Conclusion: The tongue signals via a tryptophan switch within the tongue-GAF domain interface.
Significance: The first structure of a Cph2-type phytochrome indicates a common mechanism for photoswitching in all canonical phytochromes.

Phytochromes are highly versatile photoreceptors, which occur ubiquitously in plants as well as in many light-responsive microorganisms. Here, photosynthetic cyanobacteria utilize up to three different phytochrome architectures, where only the plant-like and the single-domain cyanobacteriochromes are structurally characterized so far. Cph2 represents a third group in *Synechocystis* species and affects their capability of phototaxis by controlling c-di-GMP synthesis and degradation. The 2.6-Å crystal structure of its red/far-red responsive photosensory module in the P_r state reveals a tandem-GAF bidomain that lacks the figure-of-eight knot of the plant/cph1 subfamily. Its covalently attached phycocyanobilin chromophore adopts a highly tilted *ZZZssa* conformation with a novel set of interactions between its propionates and the GAF1 domain. The tongue-like protrusion from the GAF2 domain interacts with the GAF1-bound chromophore via its conserved PR*X*SF, W*X*E, and W(G/A)G motifs. Mutagenesis showed that the integrity of the tongue is indispensable for $P_r \rightarrow P_{fr}$ photoconversion and involves a swap of the motifs' tryptophans within the tongue-GAF1 interface. This "Trp switch" is supposed to be a crucial element for the photochromicity of all multidomain phytochromes.

Phytochromes are red/far-red light absorbing photoreceptors first discovered in plants (1), and later in many photosynthetic and non-photosynthetic bacteria (2) as well as in several fungi (3). A hallmark of these photochromic light sensors is their bilin chromophore covalently bound to a cGMP phosphodiesterase/adenylyl cyclase/FhlA (GAF)[2] domain. Upon red light illumination of its P_r state, this chromophore undergoes a $Z \rightarrow E$ isomerization around the C14–C15 double bond of the C-D ring methine bridge. In the *ZZEssa* conformation of the newly formed far-red-sensitive P_{fr} state the D-ring is flipped and the protein environment is altered to accommodate this rotation. These alterations ultimately control signal transfer either to effector proteins (inter-molecular (4)) or effector domains like histidine kinase domains (intra-molecular (5)). How these allosteric effects are triggered by D-ring rotation at the molecular level is still unknown thus prompting alternative scenarios for downstream signaling by phytochromes including an additional A-ring rotation upon $P_r \rightarrow P_{fr}$ photoconversion (6).

Phytochromes can be classified into subfamilies according to the domain architecture of their photosensory module. Group I includes canonical plant and eubacterial phytochromes such as Cph1 from the cyanobacterium *Synechocystis* sp. PCC 6803 (*Syn*Cph1 (7)) as well as fungal and eubacterial bacteriophytochromes. These phytochromes use a three-domain PAS-GAF-PHY (PAS, period/ARNT/single-minded; PHY, phytochrome) photosensory module, where an unusual figure-of-eight knot is formed by the N terminus of the PAS domain and a loop protruding from the chromophore-binding GAF domain (Fig. 1*A*). The succeeding PHY domain belongs also to the GAF superfamily and stabilizes the chromophore, by sealing it from solvent access, through its tongue-like extension (8, 9). Together, the GAF domain, N terminus, and tongue region form a complex, tripartite pocket enclosing the bilin chromophore. The Cph2 subfamily (Group II) lacks the PAS domain and utilizes instead only a tandem-GAF module as exemplified by the N-terminal photosensory module in Cph2 from *Synechocystis* sp. (*Syn*Cph2) (10) and several other cyanobacterial phytochromes (11). Finally, the cyanobacteriochromes (CBCRs,

* This work was supported by Deutsche Forschungsgemeinschaft Grants ES152/9-1 and MR81/3-1 and the LOEWE Center for Synthetic Microbiology (to L.-O. E.).
[S] This article contains supplemental Figs. S1 and S2 and Tables S1 and S2.
The atomic coordinates and structure factors (code 4BWI) have been deposited in the Protein Data Bank (http://wwpdb.org/).
[1] To whom correspondence should be addressed: Biomedical Research Centre/FB15, Philipps-Universität Marburg, Hans-Meerwein-Str., D-35032 Marburg, Germany. Tel.: 4964212822032; Fax: 4964212822191; E-mail: essen@chemie.uni-marburg.de.

[2] The abbreviations used are: GAF, cGMP phosphodiesterase/adenylyl cyclase/FhlA; PCB, phycocyanobilin; PAS, period/ARNT/single-minded; PHY, phytochrome; CBCR, cyanobacteriochrome; r.m.s. deviation, root mean square deviation; QM-MM, quantum mechanical/molecular mechanical; PDB, Protein Data Bank.

Group III) utilize a single, bilin-binding GAF domain (11, 12). CBCRs cover a broad range of the visible/near UV spectrum but are restricted to cyanobacteria. Whereas, the photosensory modules of several prokaryotic phytochromes from Groups I (8, 9) and III (13, 14) have been characterized structurally, little is known about Cph2 homologues in Group II.

Interestingly, the founding member of the Cph2 subfamily, *Syn*Cph2, is a bimodular photoreceptor (15, 16) (molecular mass 144.7 kDa) that functions as a light-dependent master regulator for cyanobacterial motility by controlling cytosolic levels of the eubacterial second messenger c-di-GMP (17). c-di-GMP is known to be a universal regulator for pili-based motility in eubacteria (18) with domains of the GGDEF and EAL type being responsible for its synthesis and degradation (19). *Syn*Cph2 inhibits phototaxis, when cyanobacterial cells are exposed to blue but not to white or red light (20, 21). Accordingly, the complex architecture of *Syn*Cph2 (Fig. 1*A*) harbors not only at its N terminus the red/far-red sensitive tandem-GAF module (*Syn*Cph2(1–2) (10)) that precedes a GGDEF*-EAL effector module, but also CBCR and catalytically active GGDEF domains. This C-terminal CBCR-GGDEF module is capable of switching between blue and green light sensitive states and controls the catalytic activity of the GGDEF domain, thereby inhibiting motility by increasing c-di-GMP levels (17). The GGDEF*-EAL module likely acts as c-di-GMP degrading phosphodiesterase, as its EAL domain is catalytically active, whereas the apparently inactive GGDEF* domain is predicted to act as an allosteric, c-di-GMP-dependent regulator.

Here, we report the crystal structure of the photosensory module *Syn*Cph2(1–2) in its P_r conformation. An antiparallel dimer is formed in which both the N-terminal PAS domain and the associated knot structures are missing. Other significant differences relative to known phytochrome structures are apparent in the phycocyanobilin (PCB) binding pocket. On the other hand, the interactions between the tongue region of GAF2 and the bilin-binding site of GAF1 are conserved, implying a universal route for signal transduction in Group I and II phytochromes that involves a toggling of conserved Trp motifs within the tongue/GAF1 interface.

EXPERIMENTAL PROCEDURES

Crystallization and Data Collection—Recombinant *Syn*Cph2(1–2) was produced as a histidine-tagged fusion with phycocyanobilin co-assembled *in vivo*. The expression and purification of *Syn*Cph2(1–2) was performed as previously described (10). Crystals for the native datasets were grown using the hanging-drop vapor-diffusion method. The drops contained 1 μl of 20 mg/ml of *Syn*Cph2(1–2)/P_r-state in crystallization buffer (10 mM HEPES, 100 mM NaCl, pH 8.0) and 1 μl of reservoir solution (0.1 M HEPES, pH 7.0, 1.0 M NH_4COOH, 0.1% (w/v) lysine, 0.16% (w/v) arginine, 0.05% (w/v) glutamate). Crystals were streak-seeded with a solution of crushed *Syn*Cph2(1–2) crystals. After pipetting the pre-irradiated (far-red light, λ_{max} = 735 nm) protein solution under blue-safe light (λ_{max} = 482 nm) conditions the plate was irradiated with far-red light to ensure 100% occupancy of the P_r state. The crystals grew at 18 °C in the dark, were visualized under blue light, and frozen in reservoir buffer supplemented with 20% (v/v) glycerol. Selenomethionine-labeled *Syn*Cph2(1–2) crystals appeared with streak seeding using a reservoir solution of 0.1 M HEPES, pH 6.5, 0.5 M NH_4COOH and an initial protein concentration of 10 mg/ml.

Native datasets were recorded at beamline ID14–1 (European Synchrotron Radiation Facility (ESRF), Grenoble, France) and at beamline 14.1 (Berliner Elektronenspeicherring-Gesellschaft für Synchrotronstrahlung (BESSY-II), Berlin, Germany). The 3.9-Å SAD dataset from the selenomethionine-labeled crystal was recorded at ID 14-4 (ESRF, Grenoble, France).

Initial SAD phasing was performed with PHENIX (22) using the native 3.20-Å dataset. Subsequent structural refinement with a 2.60-Å dataset was executed with PHENIX and COOT (23). Stereochemical restraints were configured for the PCB chromophore and its covalent attachment. Figures were created by using PYMOL 0.99 (24).

Single-crystal Resonance Raman Spectroscopy—Resonance Raman (RR) spectra were recorded offline at the Cryobench (European Synchrotron Radiation Facility (ESRF), Grenoble (France)) with a 785 nm near-IR laser using an inVia (Renishaw) Raman spectrometer (4 cm^{-1} spectral resolution) (25). Resonance Raman spectra of the crystal (1 M $MgOAc_2$ as cryo-protectant) were collected under cryo-conditions (100 K) in the 200–2000 cm^{-1} range using the SynchroScan method with a laser power of 300 milliwatts (50 milliwatts at the sample position) and 20-s exposure time. 30–50 spectra were accumulated and baseline corrected to remove contributions from fluorescence and normalized to the 1642 cm^{-1} peak. Resonance Raman spectra were recorded before x-ray exposure, and then the crystal was irradiated like during data collection (ID 14–1, 100% transmission, 4 s exposure time per image, 350 images, 0.5° oscillation range; flux: $\sim 4.8 \times 10^{10}$ photons/s; the crystal size was ~30% of beam size so that a dose of $\sim 1.4 \times 10^{10}$ photons/s reached the crystal). The crystal was characterized spectroscopically and then annealed by short thawing for 4 s in the dark, whereupon another Raman spectrum was taken. The crystal remained under cryo-conditions during the whole data collection/spectra recording process.

Single-crystal UV-visible Absorption Spectroscopy—UV-visible spectra of the crystal were measured online at 100 K with a HR2000 spectrometer (OceanOptics) and a DH-2000-BAL light source (Mikropack) at beamline ID 14-1 (ESRF, Grenoble (26)). Spectra were taken before x-ray irradiation, immediately after irradiation (60 s exposure; 100% transmission; flux: $\sim 4.2 \times 10^{10}$ photons/s; crystal size ~30% of x-ray beam diameter), after a 3-s cryo-annealing and subsequent freezing, and after a 60-s incubation under cryo-conditions following x-ray irradiation. Initial two exposure pictures were taken following a 3-s exposure per image with a 1.0° oscillation.

Quantum Mechanical/Molecular Mechanical (QM/MM) Calculations—The initial structural models were set up by adding missing hydrogen atoms and solvent water to the experimental x-ray structure. Two models were considered in this work: (*a*) the crystal structure of *Syn*Cph2(1–2) itself and (*b*) a modified structure of *Syn*Cph2(1–2) with a planar PCB chromophore as found in the structure of the *Syn*Cph1 photosensory module (8).

Structure of the Cph2 Photosensor

The insertion of hydrogen atoms was done with the HBUILD routine of CHARMM (31). All titratable amino acids were protonated according to pH 7. In the case of the histidines, the protonation states were chosen upon visual inspection of their environment. In particular, His^{130} and His^{160}, lying in the vicinity of the chromophore, were modeled with a hydrogen atom at the ϵ-nitrogen and δ-nitrogen, respectively. In addition, based on spectroscopic evidence (27, 28) the PCB chromophore is nitrogen-protonated, whereas the propionic side chains are deprotonated yielding a total charge of $-1e$.

The geometry optimization of the PCB chromophore and binding site of Cph2 and Cph1 phytochromes, comprising all atoms within a 22-Å radius from the chromophore, were performed at the QM/MM level (29). Although the QM fragment, consisting of the PCB chromophore, the Cys^{129} side chain, and the pyrrole water that is bound to rings A, B, and C nitrogens, were described with the B3LYP density functional (30), the remaining protein atoms as well as solvation waters with the CHARMM22 force field (31). The coupling between the QM and MM regions was described with the electrostatic embedding model combined with a charge shifted scheme (32), as implemented in the ChemShell software. The covalent bond cut at the QM/MM border on the Cys^{129} was saturated with a hydrogen link atom. The optimization was performed using a limited memory quasi-Newton L-BFGS algorithm working with hybrid delocalized internal coordinates (33).

Production and Spectral Characterization of SynCph2(1–2) Variants—*Syn*Cph2(1–2) mutants were produced by QuikChange site-directed mutagenesis (Stratagene) of the pCDFDuet-1/*Syn*Cph2(1–2). They were co-transformed into BL21 Gold (DE3) (Novagen) together with the p171 vector that includes genes for PCB production (34). The recombinant overproduction and purification of the proteins were performed as previously described (10).

Orthologous swapping variants of *Syn*Cph2(1–2) in the tongue and propionate region were produced by adding additional restriction sites into pCDFDuet-1/*Syn*Cph2(1–2). Thus the stretches Trp^{369}-Glu^{391} in the tongue variants and Val^{97}-Val^{126} in the propionate variants, respectively, were replaced by regions of Cph2-like phytochromes from *Nostoc punctiforme* PCC 73102 (YP_001868577.1), *Oscillatoria* sp. PCC 6506 (WP_007353933.1), and *Cyanothece* sp. PCC 7822 (YP_003886347.1) using synthetic gene fragments cloned into pCDFDuet-1/*Syn*Cph2(1–2).

UV-visible absorbance spectra were measured with a Jasco V-660 spectrometer at 1-nm resolution at room temperature. In a cell of 1-cm path length the sample was irradiated for 30 s with red or far-red LED sources (B5–436-30D, λ_{max} 664 nm and SMC735, λ_{max} 735 nm; Roithner, Vienna). Difference spectra were calculated via $A(P_r) - A(P_{Photoequilibrium})$. Determined pure P_{fr} spectra of the wild type are discussed in Ref. 10.

Near UV-visible circular dichroism (CD) spectra were measured following irradiation of the sample with a J-810 spectropolarimeter (Jasco) at room temperature in a 1-mm path length cell. P_r spectra were averaged over three scans. Short-lived intermediate or P_{fr} states were averaged over six scans where the sample was irradiated in between.

TABLE I
Data collection and refinement statistics
Values in parentheses denote the highest resolution shell.

	*Syn*Cph2 - Native 1	*Syn*Cph2 – SeMet (peak)	*Syn*Cph2 - Native 2 (4BWI)
Data collection			
Wavelength [Å]	0.93340	0.97950	0.91841
Space group		$P2_1$	
Cell dimensions	*a*=77.0 Å, *b*=88.2 Å, *c*=84.4 Å, *β*=109.6°	*a*=77.1 Å, *b*=87.9 Å, *c*=84.9 Å, *β*=109.6°	*a*=77.4 Å, *b*=88.5 Å, *c*=84.9 Å, *β*=109.9°
Resolution [Å]	39.7-3.40 (3.58-3.40)	46.5-3.90 (4.11-3.90)	46.5-2.60 (2.76-2.60)
Measured & unique reflections	53277, 14761 (7434, 2135)	66235, 9745 (8114, 1383)	140618, 32838 (20574, 4784)
R_{merge}	0.116 (0.469)	0.113 (0.404)	0.055 (0.538)
$I/\sigma(I)$	11.4 (2.9)	15.1 (5.4)	21.0 (3.4)
Wilson *B* factor (Å^2)	70.2	62.2	63.7
Mosaicity [°]	0.194	1.067	0.289
Completeness [%]	99.8 (99.8)	99.0 (99.0)	98.7 (98.7)
Solvent content [%]	55.1	54.8	55.2
Multiplicity	3.6 (3.5)	6.8 (5.9)	4.3 (4.3)
Refinement			
Resolution [Å]			29.6 – 2.6
R_{work}, R_{free}			0.196, 0.253
Reflections (work, test)			31155, 1624
Residues			760
Water molecules			181
r.m.s.d. bonds [Å]			0.003
r.m.s.d. angles [°]			0.711
defined in mol. A			N4-S114, G121-A281, N309-G374, N379-Q421
defined in mol. B			N4-I113, G121-Q278, C310-I418

RESULTS AND DISCUSSION

Overall Structure of the SynCph2 Photosensor—The N-terminal photosensory module of *Syn*Cph2 (M1-T424, (10)) in its P_r state crystallizes as an antiparallel dimer whose structure was solved at 2.6-Å resolution by a combination of molecular replacement and single-wavelength anomalous diffraction (SAD)-phasing (final R_{factor}/R_{free}, 19.6/25.3%, see Table 1).

The *Syn*Cph2(1–2) photosensor shows the characteristic bilobal shape of a tandem-GAF module with the N-terminal, PCB-binding GAF domain (Thr^{23}-Thr^{187}; GAF1) being linked to the second GAF domain (Lys^{197}-Gln^{420}; GAF2) via a 71-Å long α-helix (Thr^{168}-Tyr^{215}). The GAF domains of *Syn*Cph2(1–2) hence mimic the overall organization of canonical photosensory GAF-PHY-modules of phytochromes, including the tongue-like protrusion (Glu^{362}-Asn^{400}) that juts of the GAF2 domain and contacts the chromophore-binding pocket of the GAF1 domain (Fig. 1*B*).

The GAF1 domain with its buried PCB chromophore resembles the bilin-binding domains of canonical phytochromes such as *Syn*Cph1 and *Rp*BphP3 (root mean square deviation (r.m.s.) deviations of 0.98 and 1.02 Å for 175 and 164 C_α atoms, respectively). In contrast, the core of the GAF2 domain diverges significantly from known PHY domains yet remains more closely related to PHY domains from biliverdin-dependent bathy phytochromes such as *Rp*BphP3 or *Pa*BPhP (2.26 and 2.82 Å for 117 and 135 C_α atoms, respectively) than to PCB-dependent phytochromes like Cph1 (3.40 Å for 150 C_α atoms). Structural

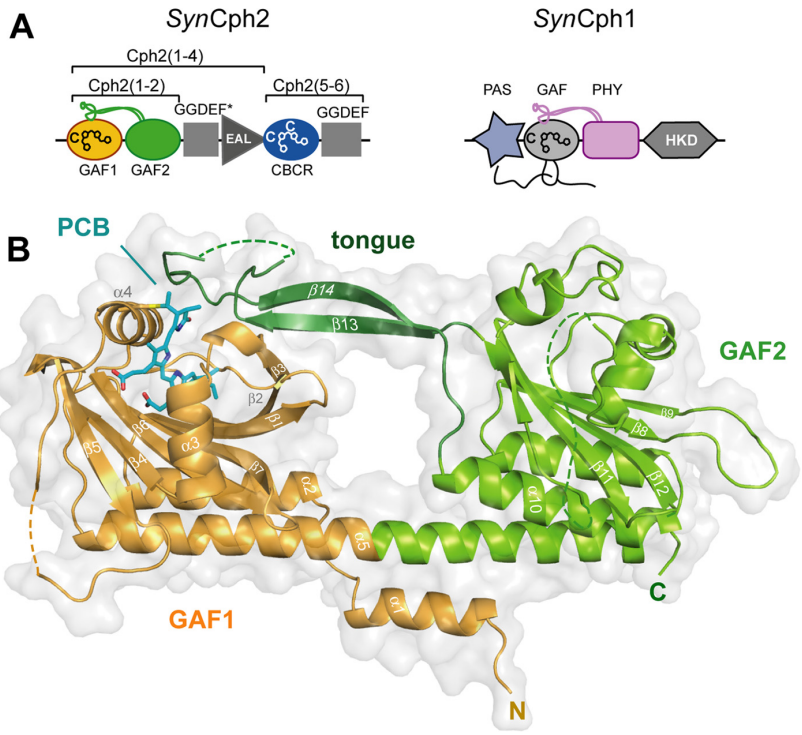

FIGURE 1. **Structure of the *Syn*Cph2(1–2) photosensor.** *A,* domain organization of *Syn*Cph1 and *Syn*Cph2. The tongue-like regions protruding from the GAF2 and PHY domains are shown in *green* and *purple*, respectively; the knot in *Syn*Cph1 as *black lines*. *Syn*Cph1 and *Syn*Cph2 differ in their effector domains: a histidine kinase domain (*HKD*) and c-di-GMP turnover (*GGDEF* and *EAL*) and regulatory (*GGDEF**) domains. *B,* crystal structure of the *Syn*Cph2(1–2) module. GAF2 (*green*) contains a tongue-like region (*dark green*) for sealing the PCB (*cyan*)-binding pocket. The GAF1 domain is in *orange*.

differences are mostly around the five-pleaded central β-sheet, including the elongated loops connecting β-strands 8–9 and 11–12 as well as the α-helices covering the β-sheet opposite the α-helix linking GAF1 and GAF2 (Fig. 1*B*). Furthermore, in both dimer subunits an additional stretch of 27 amino acids (Ala^{282}-Thr^{308}) is structurally disordered as indicated by missing electron density. Interestingly, this stretch is unique for Cph2 as it is absent from PHY domains of Group I phytochromes.

Crystals of *Syn*Cph2 are cyan-colored due to the incorporated PCB cofactor and give the same UV-visible and resonance Raman spectra as in solution. Accordingly, this proves that *Syn*Cph2(1–2) adopts a native-like conformation for its bilin chromophore in the crystalline state (Fig. 2) (35).

Despite its monomeric state in solution (10) *Syn*Cph2(1–2) forms an antiparallel dimer in crystals similar to the photosensory module of *Syn*Cph1 (Fig. 3). Its interface area is predicted by the PISA server to be ~1904 $Å^2$ and thus considerably smaller than that of *Syn*Cph1 (2545 $Å^2$) (8) due to the missing PAS domain. Its staggered and antiparallel orientation differs from other known phytochrome structures such as *Pa*BPhP, in which a parallel association is observed over the whole length of the GAF-PHY linker helices. The latter mode of association is thought to be crucial for signal transduction to histidine kinase domains (9, 36) and illustrated by the cryoEM structure of full-length bacteriophytochrome *Dr*BphP, where the photosensory module provides the largest dimerization interface. Like in parallel dimers of the photosensory phytochrome modules, the antiparallel arrangement of *Syn*Cph2(1–2) is mainly stabilized by association of its linker α_5-helices between GAF1 and GAF2 (Figs. 1*B* and 3*A*). Interestingly, the α_5-helices resemble those of the Y263F *Syn*Cph1 mutant (37), whereas in the wild type *Syn*Cph1 (Fig. 3*B*) and *Pa*BphP structures these helices are significantly kinked. Some structural plasticity between the GAF and PHY domains as observed for *Pa*BphP and *Syn*Cph1 (8, 9, 37) may be involved in long-distance signal transmission. Accordingly, the GAF2 domains of the two copies of *Syn*Cph2(1–2) in the crystal structure are off-rotated by 6.4° relative to each other, whereas the tongue regions are almost invariantly associated with the GAF1 domains.

Another striking feature of *Syn*Cph2(1–2) is its missing figure-of-eight knot, a hallmark of Group I phytochromes. In *Syn*Cph1 the N-terminal helix threads through the loop region connecting β_9 with α_8 and is part of the PCB binding pocket. The Group II *Syn*Cph2(1–2) phytochrome lacks this knot along with the associated PAS domain, so that the binding pocket is partly solvent-exposed at the A- and B-rings of the PCB chromophore (Fig. 3*B*). Instead, the N-terminal α_1-helix of *Syn*Cph2(1–2) is part of a six-helix bundle comprising α_1, α_5, α_6, and α_{10} of one monomer and α_2 and α_5 of the other monomer (Fig. 3*A*). In this interface, the amphiphilic α_1-helix makes first several polar interactions via its residues Arg^5, Lys^{17}, and His^{19} with Glu^{34} and Glu^{181} from α_2 and α_5, respectively. Second, for hydrophobic interactions the α_1-helix packs its residues Leu^7, Phe^{10}, Leu^{11}, Val^{14}, and Phe^{18} against a surface patch generated by Val^{30}, Ile^{31}, Phe^{38}, Leu^{177}, and Leu^{178} of α_2 and α_5. Accordingly, one may hence postulate that the dimerization of

Structure of the Cph2 Photosensor

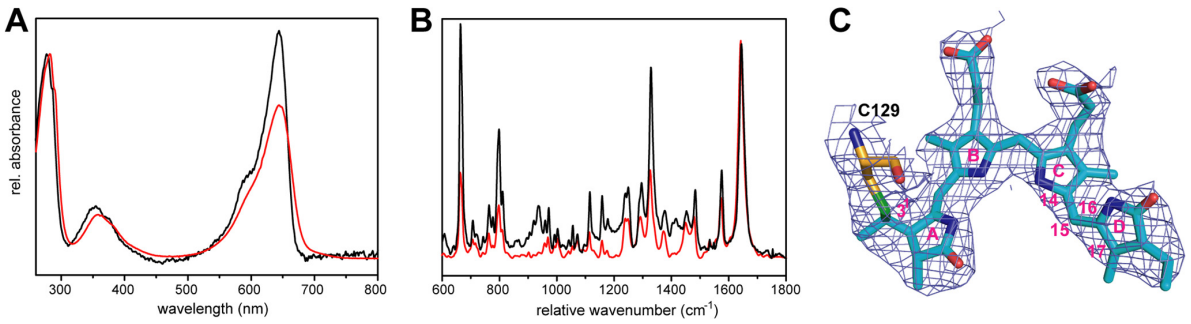

FIGURE 2. **Spectral characteristics of *Syn*Cph2(1–2) in soluble and crystallized forms.** *A,* UV-visible absorbance spectra of *Syn*Cph2(1–2) in solution at room temperature (*red curve*) and a crystal (*black*) at 100 K in the P_r conformation. *B,* Raman spectra of the protein in frozen solution (*red curve*) at 100 K and in crystalline form (*black*) at 100 K. *C,* omit electron density of the PCB chromophore and its covalent attachment to Cys^{129} (contouring level 1.0 σ).

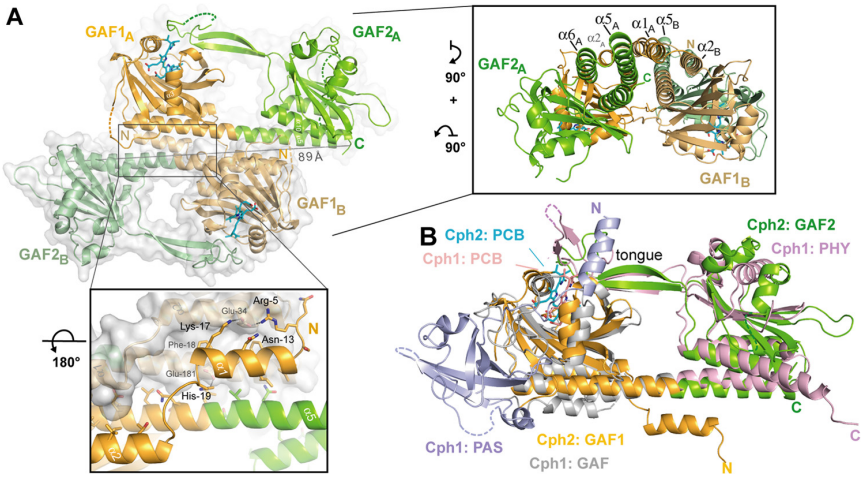

FIGURE 3. **Quaternary structure of the knotless *Syn*Cph2(1–2) photosensor and comparison to *Syn*Cph1.** *A,* the antiparallel dimer of *Syn*Cph2(1–2). The distance between C-terminal residues His^{421} (molecule A) and Ile^{418} (molecule B) is 89 Å; *lower inlet*, the N-terminal helix forms part of the dimer interface; *inlet on the right side*, perpendicular view on the *Syn*Cph2(1–2) dimer. The interface between the monomers is built of a helix bundle composed of the linker α-helix and shorter helices, especially the N-terminal helix. *B,* structural superposition of *Syn*Cph2 and *Syn*Cph1 (r.m.s. deviation 2.64 Å for 249 C_α atoms); the PAS, GAF, and PHY domains of *Syn*Cph1 are depicted in *blue*, *gray,* and *pale red*, respectively.

PAS-less phytochromes like *Syn*Cph2(1–2) depends on their N-terminal helix.

The different output domains, especially the GGDEF*–EAL module downstream of the *Syn*Cph2(1–2) sensor, imply that the antiparallel association of the photosensory domains could be functionally relevant in *Syn*Cph2 and not just a crystallization artifact as found for *Syn*Cph1 (8). For example, FimX from *Pseudomonas aeruginosa*, a twitching motility regulator, also carries GGDEF-EAL domains. Here, the overall quaternary organization corresponds to an elongated antiparallel dimer, where the GGDEF-EAL modules are not involved in dimerization (38). Such an arrangement of the photosensory *Syn*Cph2(1–2) module may be of physiological relevance for signaling toward the GGDEF*–EAL module. This contrasts to eubacterial phytochromes such as *Syn*Cph1, which are part of two-component signaling systems. Only these phytochromes have to form parallel homodimers (36) similar to the structurally characterized sensor histidine kinases YF1 and VicK (39, 40) to allow proper dimerization and thereby catalytic activity of their histidine kinase domain-like regions.

The PCB-binding Site of SynCph2(1–2)—Overall, the bilin chromophore is well defined in the GAF1 domain including its thioether linkage to Cys^{129} (Fig. 2*C*). Despite structural differences in the protein environment relative to other Group I phytochromes, mainly around pyrrole rings A and B, the conformation of the chromophore resembles *Syn*Cph1. First, the new chiral center at $C3^1$, as formed by covalent attachment to Cys^{129}, has an *R* configuration. This may not be a general feature for bilin chromophores covalently tethered to GAF domains; for example, in the structure of the Y263F mutant of *Syn*Cph1 both stereochemical configurations have been found for the $C3^1$–Cys thioether linkage (37). Second, and as expected, for the *Syn*Cph2(1–2) P_r state, the chromophore adopts the *ZZZssa* conformation (Fig. 2*C*, supplemental Table S1), but in a strongly non-planar conformation, when compared with other phytochrome structures harboring bilin chromophores.

Despite the latter, the local environment of the D-ring is well conserved between *Syn*Cph2 and *Syn*Cph1 as exemplified by the residues Tyr^{47}, Val^{57}, Asp^{79}, Tyr^{133}, Leu^{134}, Met^{137}, and His^{160}. Differences here are mainly found for Lys^{45} or Leu^{70}, but appear to only play a minor role in the $P_r \rightarrow P_{fr}$ conversion, as the *Syn*Cph2 K45M mutant shows only a ~3 nm hypsochromic shift in its P_{fr} state. Other residues of the C- and D-ring binding

site like Tyr[133] are functionally similar to their structural counterparts in *Syn*Cph1 (Tyr[263]) as indicated by the similar photochemistry of their mutants, for example, Y133F or H160A (supplemental Fig. S1 and Table S2) (37).

The loop connecting β_5 and α_4 in *Syn*Cph2, which is otherwise part of the knot region of Group I phytochromes, is partly disordered due to a lack of further interactions. Furthermore, the *Syn*Cph2 loop appears to interact with the B-ring propionate differently than in *Syn*Cph1. *Syn*Cph2 forms an additional β-strand (β_5, Arg[102]-Glu[108]), of which Lys[104] makes a surface-exposed salt bridge with the B-ring propionate (Fig. 4*A*). In *Syn*Cph1 as well as other Group I phytochromes this propionate interacts with Arg[254] (loop region) in P_r, but probably swaps partners upon photoconversion to interact with Arg[222], part of β-strand 9 (41) (Fig. 4*B*). Both of these arginines are missing in *Syn*Cph2. Here, Lys[104] apparently substitutes for Arg[254] in *Syn*Cph1. However, an equivalent interaction partner for the B-ring propionate in the P_{fr} state seems to be missing. Thus the propionate signaling route envisaged for Group I phytochromes (8) is unlikely for *Syn*Cph2. Multiple sequence alignments of Group II phytochromes (Fig. 5) show that Lys[104] is conserved in other cyanobacterial phytochromes with the same complex domain architecture of *Syn*Cph2. In Group II phytochromes with different architectures, for example, GAF-GAF-GGDEF*-EAL (17) or GAF-GAF-histidine kinase domain, this residue is replaced by polar or isoleucine residues. Interestingly, Cph2 orthologues with downstream histidine kinase effector domains harbor both *Syn*Cph1 arginines (Arg[222] and Arg[254]). It seems, therefore, that the propionate interactions may vary according to the route required for signal transmission to the effector domains.

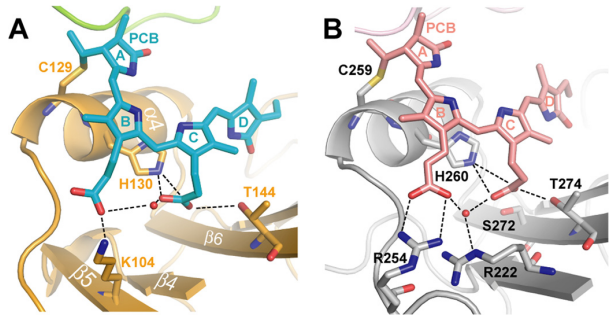

FIGURE 4. **Close-up view of the chromophore binding sites of the *Syn*Cph2(1–2) (*A*) and *Syn*Cph1 (*B*) photosensor.** The PCB chromophore within *Syn*Cph2(1–2) is structurally distorted compared with the almost planar A-, B-, and C-rings of *Syn*Cph1. The hydrogen bond network of the B- and C-ring propionates is indicated with *dashed lines*.

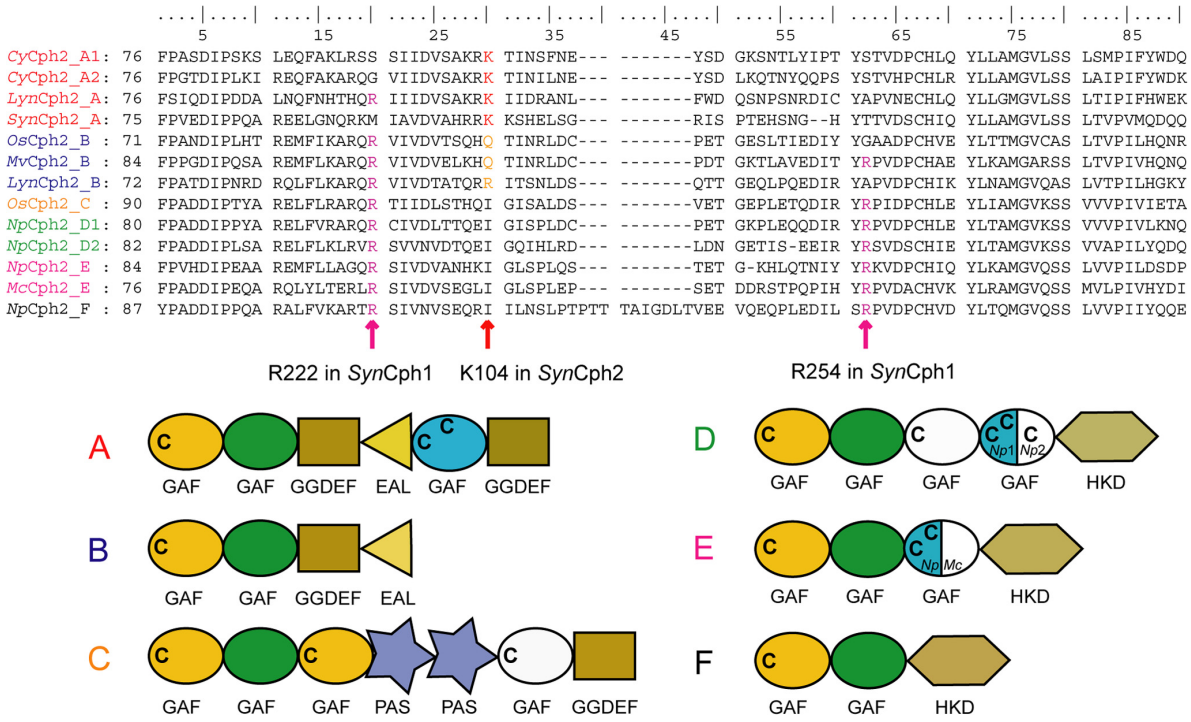

FIGURE 5. **Multiple sequence alignment of Cph2-like Group II phytochromes.** GAF1 sequences forming the knot/propionate binding site region. Abbreviations: *Syn*Cph2_A (organism: *Synechocystis* sp. PCC 6803; GenBank entry NP_442466.1; sequence identity: 100%), *Cy*Cph2_A1 (*Cyanothece* sp. PCC 7424; YP_002378924.1; 38%), *Cy*Cph2_A2 (*Cyanothece* sp. PCC 7822; YP_003886347.1; 39%), *Lyn*Cph2_A (*Lyngbya* sp. PCC 8106; WP_009783799.1; 33%), *Os*Cph2_B (*Oscillatoria* sp. PCC 6506; WP_007353933.1; 36%), *Mv*Cph2_B (*Microcoleus vaginatus* FGP-2; WP_006623727.1; 34%), *Lyn*Cph2_B (*Lyngbya* sp. PCC 8106; WP_009783371.1; 33%), *Os*Cph2_C (*Oscillatoria* sp. PCC 6506; WP_007357482.1; 30%), *Np*Cph2_D1 (*N. punctiforme* PCC 73102; YP_001870049.1; 31%), *Np*Cph2_D2 (*N. punctiforme* PCC 73102; YP_001868068.1; 33%), *Np*Cph2_E (*N. punctiforme* PCC 73102; YP_001868577.1; 34%), *Mc*Cph2_E (*Microcoleus chthonoplastes* PCC 7420; WP_006100748.1; 31%), *Np*Cph2_F (*N. punctiforme* PCC 73102; YP_001865364.1; 31%). Pairwise sequence homologies to *Syn*Cph2(1–2) were performed with the BLOSUM62 exchange matrix. *Letters at the end of the abbreviation* describe the domain architecture of the proteins described below: *C* indicates conserved cysteines; *green*, GAF domain of the "PHY"-type; *blue*, GAF domain of the "CBCR"-type; *white*, GAF domain with sequence similarities with "CBCR"-type but with one or no conserved cysteine. *Mixed colors*, gene-dependent domain organization as indicated by the organism abbreviation.

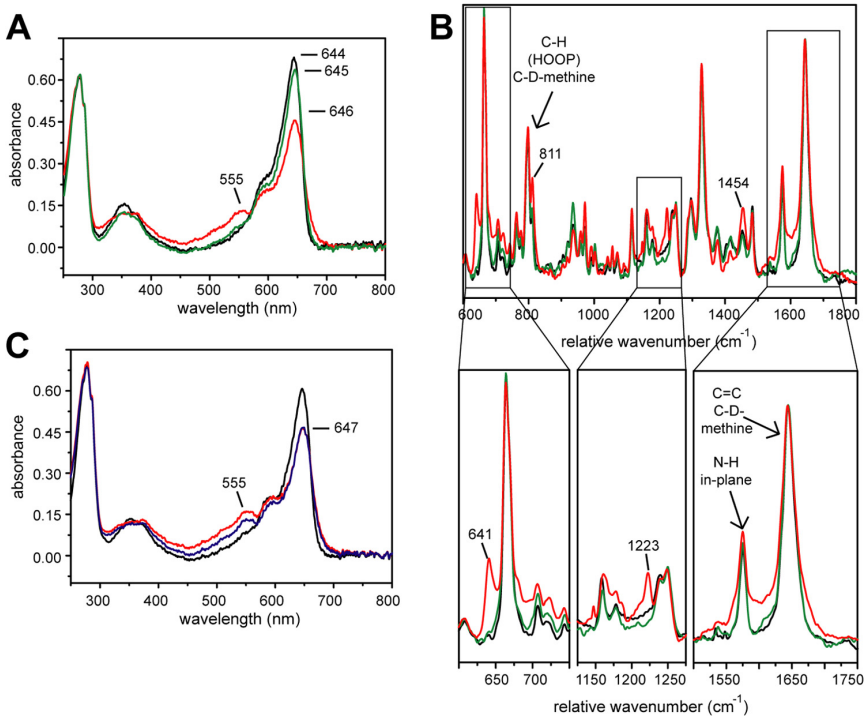

FIGURE 6. **Temporary radiation effect on *Syn*Cph2(1–2).** *Black*, no x-ray; *red*, after x-ray; *green*, after annealing; *blue*, 60 s after exposure. *A,* UV-visible absorbance spectra of a crystal before x-ray, after 60 s exposure (ID 14-1 (ESRF, Grenoble), 100% transmission; flux: ~4.2 × 10^{10} photons/s (approximately ~1.4 × 10^{10} photons/s reached the crystal)), and after 3 s of annealing in the dark (annealing process was not complete). *B,* Raman spectra of a crystal before x-ray, after 30 min x-ray irradiation (ID 14 –1 (ESRF, Grenoble), 100% transmission, 4-s exposure time per image, 350 images, 0.5° oscillation range; flux: ~4.8 × 10^{10} photons/s) and after 4 s of annealing in the dark; *below*: partial scale-up of the Raman spectra. *C,* UV-visible absorbance spectra of a crystal before x-ray, after exposition for 60 s, and 60 s after exposure.

The unusual interactions of the B- and C-ring propionates are not crucial for $P_r \rightarrow P_{fr}$ photoconversion, however. Alanine mutants of Lys^{104} and the neighboring amino acids Arg^{103} and Lys^{105} show wild type $P_r \rightarrow P_{fr}$ photoconversion. Only a ~3 nm hypsochromic shift is observed for the P_r and P_{fr} states of K104A. Even swapping variants of *Syn*Cph2(1–2), where the whole region around the B-ring propionate (Val^{97}-Val^{126}) is exchanged with regions of other phytochromes of the Cph2 subfamily, show almost normal P_{fr} (supplemental Fig. 1 and Table S2).

A study of the B- and C-ring propionate amide adducts in *Syn*Cph1 reveals that a free B-ring propionate is essential for wild type P_r and that full photoconversion to P_{fr} requires a conformational switch at the C-ring propionate (42). Apart from the missing arginines in *Syn*Cph2 B-ring propionate interactions, the C-ring propionate interactions are similar in *Syn*Cph1 and *Syn*Cph2 and involve residues Thr^{144} and His^{130}, as well as a water molecule.

SynCph2(1–2) Induces the Tilted PCB Conformation—An unusual feature of the PCB chromophore compared with other phytochrome and even phycobilisome-PCB structures is the strong tilt between its constituent rings (see supplemental Table S1). The chromophore shows tilts of 19.2°, 32.5°, and 59.8° between rings A-B, B-C, and C-D, respectively (in comparison *Syn*Cph1: 9.8°, 1.5°, and 26.3°). The tilt between rings B-C and C-D is hence the largest among known phytochromes and PCB-binding phycobilisomes. Only non-conjugated chromophores in phycobiliproteins showed so far similar or higher tilts (see supplemental Table S1). Given earlier suggestions that the phytochrome chromophore conformation might generally be damaged by x-ray radiation (6), we validated the observed PCB conformation by a combination of single crystal UV-visible and resonance Raman spectroscopy with QM/MM geometry calculations based on structural models of *Syn*Cph2(1–2).

Upon x-ray irradiation of crystals the spectral signatures of the P_r state of *Syn*Cph2(1–2) are changed. First, in the UV-visible spectrum an additional shoulder at 555 nm appears, whereas the signal at 644 nm decreases and the maximum shifts to 646 nm (Fig. 6*A*) accompanied by a broadening of the 646 nm peak. Second, in single-crystal Raman spectra (Fig. 6*B*) x-ray exposure of *Syn*Cph2(1–2) crystals cause additional Raman signals at 641 cm^{-1} and 1223 cm^{-1}, a signal increase at 811 cm^{-1} and 1454 cm^{-1}, and a slight peak broadening between 1550 and 1700 cm^{-1}. Only cryo-annealing restores the pre-x-ray UV-visible and resonance Raman spectra. Under cryogenic conditions, after x-ray exposure, a slow relaxation process takes place within minutes (Fig. 6*C*), where the shoulder at 555 nm in the UV-visible spectrum decreases but the signal at ~644 nm remains unchanged. Again cryo-annealing allows complete reversal to the P_r state before x-ray irradiation.

These data are in line with previous observations on the photosensory module of *Syn*Cph1, where long x-ray radiation induced additional absorbance peaks in the UV-visible spectra (43). In *Syn*Cph2(1–2) the x-ray-induced species relaxes in at

least two steps. At 100 K it decays to a further species without recovery of the P_r maximum (Fig. 6*C*). Apparently, the activation energy needed for conversion into native-like P_r cannot be overcome and the chromophore of *Syn*Cph2(1–2) remains hence arrested in an intermediate state. Further relaxation to P_r, which means recovery of the spectral characteristics of *Syn*Cph2(1–2) crystals, proceeds only at higher temperature.

The resonance Raman spectra indicate that alterations occur near the ring B and C nitrogens and could be caused by the pyrrole water that is hydrogen bonded to the pyrrole nitrogens. However, because the absolute positions of the Raman bands, in particular those in the fingerprint region between 1500 and 1700 cm^{-1} (Fig. 6*B*), are virtually identical in irradiated- and non-irradiated samples, one may infer that the main conformation of the tetrapyrrole chromophore is undistorted upon irradiation. Thus, x-ray damage is not *per se* responsible for the very large tilts observed between rings B and C.

TABLE 2

Ring tilts of PCB from x-ray crystallography and QM/MM calculations

Cph2 refers to the crystal structure of *Syn*Cph2(1–2). The planar geometries relate to a modified *Syn*Cph2(1–2) structure, where the chromophore was substituted by the PCB chromophore from the *Syn*Cph1 structure (PDB 2VEA).

	Tilt A-B	Tilt B-C	Tilt C-D
X-ray *Syn*Cph2 (PDB 4BWI)	19.2°	32.5°	59.8°
X-ray *Syn*Cph1 (PDB 2VEA)	9.8°	1.5°	26.3°
X-ray *Syn*Cph2 QM/MM optimized	17.8°	23.1°	40.9°
*Syn*Cph2-planar QM/MM optimized	19.5°	17.5°	41.6°

To assess the significance of the tilt between rings B and C, for example, excluding that the tilts are caused by the nature of the parameters used during crystallographic refinement, we optimized the structure of the PCB binding site of *Syn*Cph2(1–2) using a QM/MM approach as described under "Experimental Procedures." The geometry of PCB converges to a conformation, which is only slightly different than in the crystal structure, as indicated by a r.m.s. deviation of only 0.4 Å. In particular, the large twist observed at the B-C methine bridge (Table 2) is maintained (23°) and exceeds those observed for any other phytochrome. In the optimized structure, the protein environment around the chromophore remains largely conserved. Analogous results are obtained for a *Syn*Cph2 planar model, where the chromophore of *Syn*Cph2 is substituted by the nearly planar PCB chromophore from the *Syn*Cph1 structure. QM/MM calculations based on this model again provide a non-planar PCB chromophore that is strongly twisted at the B-C methine bridge (18°). These calculations indicate that the large tilt between the B- and C-rings is indeed enforced by the *Syn*Cph2 protein matrix rather than by radiation damage.

Interactions of the Tongue Region with the PCB-binding Pocket—The hairpin-like tip of the GAF2 tongue region, which contacts the GAF1 domain, is highly conserved among Group I and II phytochromes. However, the stem regions of the tongue connect differently to the GAF and/or PHY domains in different homologs (Fig. 7*A*). These differences are exemplified by

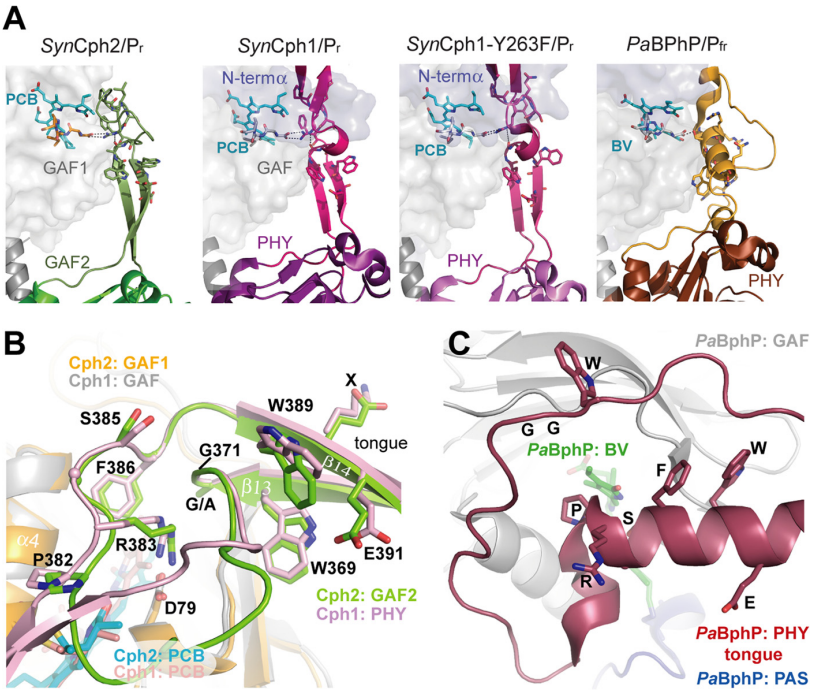

FIGURE 7. **The tongue-like region of *Syn*Cph2(1–2).** *A*, structure and interactions between the tongues and the chromophore-bearing GAF domains of phytochromes. *B*, comparison of the tongue regions of *Syn*Cph2 and *Syn*Cph1, superimposition of the GAF domains (r.m.s. deviation = 1.095 Å for 125 C_α); GAF1 and GAF2 of *Syn*Cph2 are displayed in *orange* and *green*; PAS, GAF, and PHY of *Syn*Cph1 in *blue*, *gray*, and *pale red*, respectively. The chromophores are shown in *cyan* (Cph2) and *red* (Cph1). The positions of the PR*X*SF, W(G/A)G, and W*X*E motifs in the tongue regions are conserved between *Syn*Cph1 and *Syn*Cph2, the residues are numbered along the *Syn*Cph2 count. *C*, tongue region of *Pa*BphP (PDB code 3NHQ), the PAS (*blue*), GAF (*gray*) and PHY (*red*) domains and biliverdin in *green*. In contrast to *Syn*Cph2 and *Syn*Cph1 the tongue region consists of an extended loop region and α-helical elements. The spatial positions of the conserved motifs differ in *Pa*BphP. The orientation of the tongue region correlates to that of *Syn*Cph2.

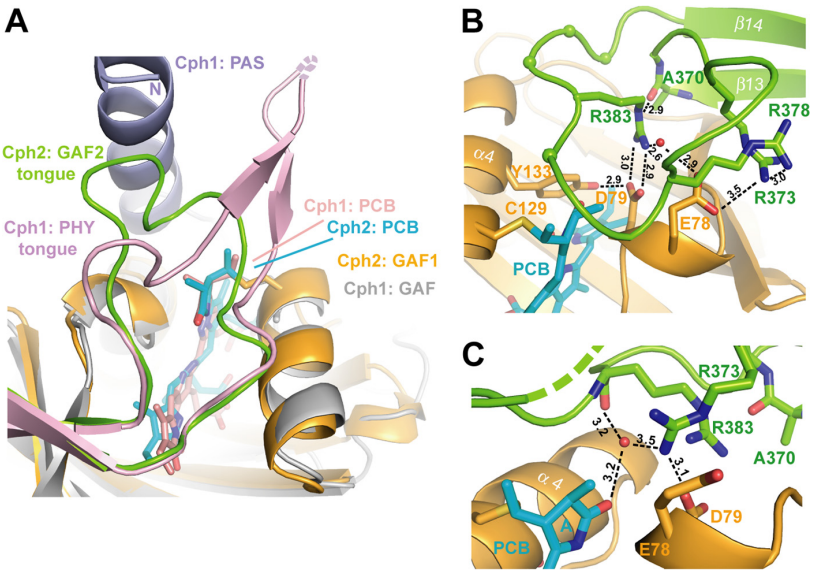

FIGURE 8. **The tip of the tongue region of *Syn*Cph2.** *A,* comparison of the photosensory modules of *Syn*Cph2 and *Syn*Cph1 at the tongue-GAF1 interface, color-coding corresponds to Fig. 7. *B,* the tongue region seals the PCB-binding pocket. In molecule B the whole tongue is defined by electron density. Only Arg^{383} of the PR*X*SF motif (*spheres*) is depicted as stick representation. Hydrogen bond distances are given in Å. *C,* chain A shows that the tip of the tongue is rather motile as several residues are missing and Arg^{373} adopts a different conformation.

the structure of *Pa*BphP in the P_{fr} state (Fig. 7*C*), where a mostly α-helical conformation is adopted.

Although in *Syn*Cph2 the β-strands (β_{13}, β_{14}) forming the stem of the tongue are longer than in *Syn*Cph1 (the GAF2 domain is tilted further away from GAF1 than the PHY domain in *Syn*Cph1), the overall positions of the conserved W(G/A)G, PR*X*SF, and W*X*E motifs relative to the GAF1 domain are well conserved between the two (Fig. 7*B*). Only in the P_{fr} state of *Pa*BphP do these motifs differ significantly (Fig. 7*C*), allowing only the α-helical part of the tongue to cover the PCB binding pocket and displacing the W(G/A)G and W*X*E motifs by 11–15 Å relative to their counterparts in *Syn*Cph2 and *Syn*Cph1.

In *Syn*Cph2 the W(G/A)G motif (Trp^{369}-Gly^{371}) extends from β_{13} into the hairpin tip region of the tongue. This region is distal from the GAF1 domain by being located on an elongated loop region in *Pa*BphP/P_{fr} (Fig. 7*C*). In the *Syn*Cph2/P_r structure, Trp^{369} of the W(G/A)G motif forms an H-bond via the indole nitrogen with Glu^{391} from the W*X*E motif on β_{14}. The role of the former anchor-like WGG motif is underlined by the finding that the W369A mutant remains arrested in an intermediate state upon red light illumination. The same is observed for the W389A mutation within the second anchor of the tongue, the W*X*E motif, but not for the E391A mutant, a fact suggesting that the interaction of the latter with Trp^{369} is not crucial for photoconversion. Given the large distance of 9–14 Å to the PCB binding pocket in the P_r state of *Syn*Cph1 and *Syn*Cph2, the involvement of the Trp motifs in P_{fr} formation conversion is elusive. As mutant Group I phytochromes in which the PHY domain has been deleted, are known to be unable to form *bona fide* P_{fr}, one may conclude that the bulky side chains of these tryptophans are required to stabilize not only the P_r state, but also an alternative conformation of the tongue when switched to the P_{fr} state. Indeed, mutations of Trp^{369} or Trp^{389} to phenylalanine in *Syn*Cph2 allow P_{fr} formation (Fig. 9), albeit with compromised efficiency for the W369F mutant (supplemental Fig. S2). This underlines the importance of the general bulky aromatic character of these tryptophans for the structural reorganization of the tongue during $P_r \rightarrow P_{fr}$ photoconversion. When comparing the *Syn*Cph2 and *Syn*Cph1 P_r structures with the *Pa*BphP/P_{fr} structure, it can be observed that in both states a tryptophan is sandwiched at almost the same position in the tongue-GAF1 interface. However, in P_r the indole moiety comes from the W(G/A)G, but in P_{fr} from the W*X*E motif. In this way, the swap of the bulky tryptophan side chains in the tongue-GAF1 interface may support the bistability and hence photochromicity of Group I and II phytochromes.

The third conserved motif within the tip of the tongue, the PR*X*SF motif, shields the entrance to the PCB binding pocket by adopting an elongated conformation above it and allowing for Arg^{383} to project into the GAF1 domain where it forms a salt bridge with Asp^{79} of the DIP motif. The conformation of the PR*X*SF motif, including the outward orientation of the serine residue and the backbone conformation until the W*X*E motif, is absolutely conserved between *Syn*Cph2 and *Syn*Cph1 (Figs. 7*B* and 8*A*). Mutants of the salt bridge involving the PR*X*SF motif like R383D or D79R remain hence either arrested in an intermediate state (10), or are photochemically impotent (supplemental Fig. S1).

Pro^{382} from the PR*X*SF motif is directly placed above the thioether bridge between Cys^{129} and ring A of the PCB chromophore. Together with Pro^{81} of the DIP motif, Pro^{382} forms a clamp hindering large conformational changes of the A-ring. Interestingly, earlier NMR studies on the P_{fr}-like state of an isolated GAF domain of another Group II phytochrome postulated A-ring rotation as part of the photocycle (6). Given that this ubiquitous structural restraint in Group I and II phyto-

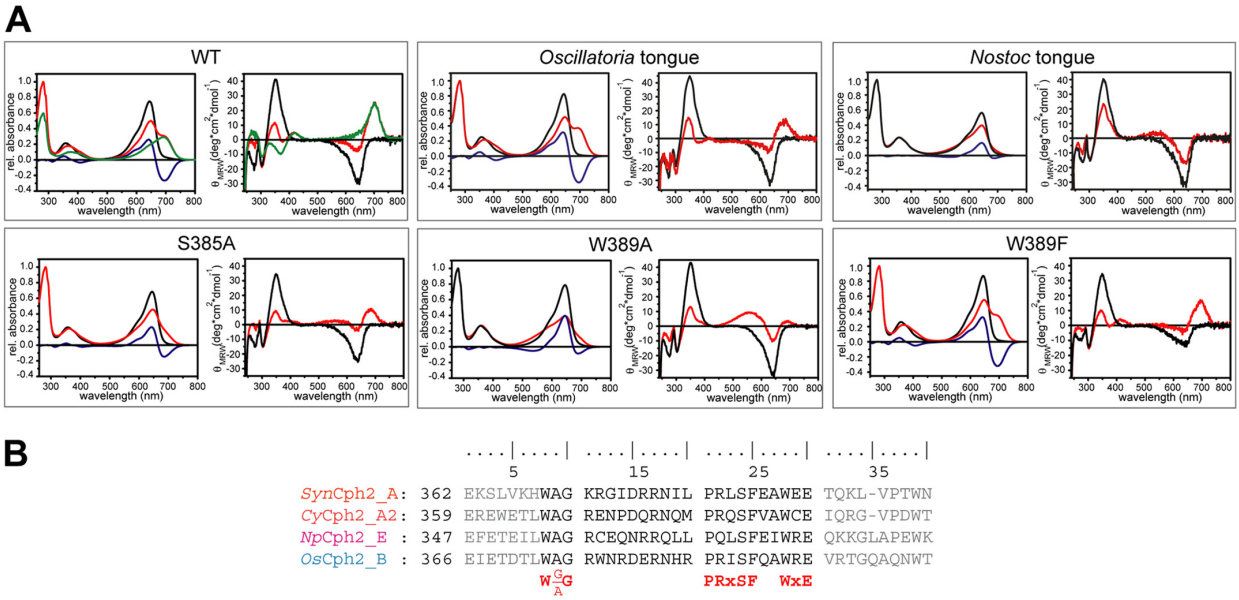

FIGURE 9. **Mutants and hybrids of the *Syn*Cph2 tongue region.** *A,* UV-visible absorbance (*left*) and CD spectra (*right*) of *Syn*Cph2(1–2) wild type and mutants after far-red (P_r-state, *black line*) and red light illumination (*red*). Difference spectra ($A_{Pr} - A_{Photoequilibrium}$) are shown in *blue*. *Green curves* in the wild type spectra are calculated for pure P_{fr} (10). The partial lack of a wild type-like P_{fr} CD spectrum of *Oscillatoria* tongue is due to its instability. *B,* multiple sequence alignment of Group II phytochromes for GAF2 sequence stretches defining the tongue region. Tongue regions swapped between hybrid variants are depicted in *black*, conserved motifs are highlighted in *red*. Abbreviations: *Syn*Cph2_A (organism: *Synechocystis* sp. PCC 6803; GenBank entry: NP_442466.1; sequence identity: 100%), *Cy*Cph2_A2 (*Cyanothece* sp. PCC 7822; YP_003886347.1; 39%), *Os*Cph2_B (*Oscillatoria* sp. PCC 6506; WP_007353933.1; 36%), *Np*Cph2_E (*N. punctiforme* PCC 73102; YP_001868577.1; 34%).

chromes is missing in that case, it is feasible that the tongue-GAF interaction serves to exclude alternative isomerization pathways for bound bilin chromophores. Clearly, a disturbance of the A-ring clamp as given by the *Syn*Cph2 P382G mutant causes a lack of photoconversion to P_{fr} (supplemental Fig. S2) and again suggests that a rigid element is needed here to allow conformational $P_r \rightarrow P_{fr}$ switching. Interestingly, a threonine mutant of Pro^{382} photoconverts to P_{fr} like the wild type but exhibits a faster dark reversion (supplemental Fig. S2). Accordingly, this backbone version requires only partial restriction of its conformational space to maintain the function of the tongue motif.

Finally, the S385A and F386A mutants, like most of the other mutants of the tongue motifs, fail to form P_{fr} upon red light illumination. Phe^{386} is buried in the tongue-GAF1 interface close to the hydrophobic environment of ring D and thus stabilizes at least the P_r state. In contrast, the surface-exposed Ser^{386} makes no interactions to any other residue in the *Syn*Cph2 structure. When comparing the P_r state structures of *Syn*Cph2 and *Syn*Cph1 with the P_{fr} state of *Pa*BphP, it is apparent that the PR*X*SF motif adopts an inverted orientation in the latter; the serine instead of the arginine points into the binding pocket to build a hydrogen bond to the aspartate of the DIP motif. The role of this serine is further underlined by the fact that a mutation to alanine destabilizes the P_{fr} state of *Pa*BphP (9). Together with the role of the tryptophan motifs one can suggest that during conversion into P_{fr} the salt bridge is released and the tip of the tongue undergoes huge conformational changes (Fig. 10). According to this model these residues are crucial for conformational stabilization of the P_{fr} state and thus for complete photoconversion. Interestingly, in the case of the *Syn*Cph2(1–2) module, such a large conformational change is indicated by an increased α-helical content and hydrodynamic diameter upon P_{fr} formation (10).

Apart from the conserved motifs mentioned above for the tongue tip there is some length variation of different phytochromes, which is illustrated by the 5-amino acid larger tongue tip for *Syn*Cph1 than for *Syn*Cph2. The tip of the loop in *Syn*Cph2 adopts alternative conformational states within the crystal. In chain A of *Syn*Cph2 the Asp^{79}-Arg^{383} salt bridge is part of a hydrogen-bonding network consisting of Tyr^{133}, together with a second arginine from the tip of the tongue (Arg^{373}) as well as a water molecule. The latter stabilizes the tongue-GAF1 interaction by coordinating the amide nitrogen of Arg^{383} and the ring A carbonyl group (Fig. 8*C*). In chain B Arg^{373} flips out and interacts with Arg^{378} and Glu^{78}. This interaction stabilizes the loop region, which can be clearly defined by electron density (Fig. 8*B*). However, in both molecules, Arg^{383} H-bonds to the backbone carbonyl of Ala^{370} of the W(G/A)G motif. The tongue-GAF1 interaction is further stabilized by an interaction absent in *Syn*Cph1. Lys^{367}, located in β_{13} of the tongue contacts the edge of the GAF1 domain via an extended hydrogen bond network between His^{74} and Ser^{54}.

The Tongue Region as a Functional Module within Phytochromes—Given the strict dependence of the P_{fr} conformation on conserved motifs within the tongue region, we wondered whether the tongue extension presents on its own a functional module that is interchangeable between different phytochromes of the Cph2 family. We generated swapping variants of *Syn*Cph2(1–2) in the tongue region by replacing the

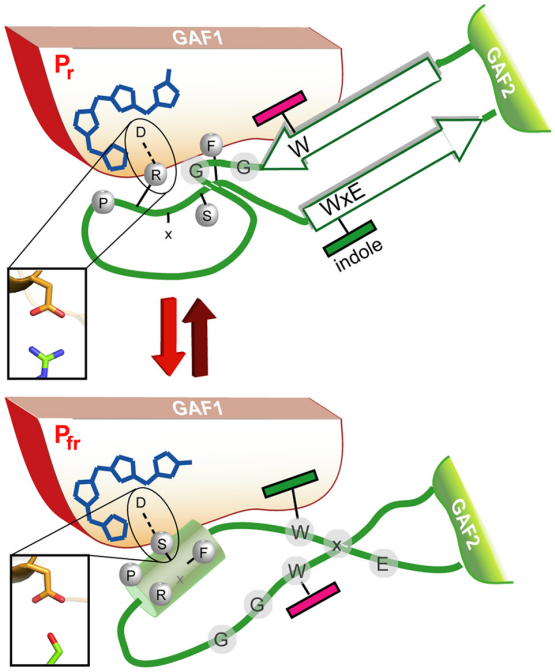

FIGURE 10. **A model for the Trp motif switch within phytochromes.** Upon red-light triggered formation of the P_{fr} state and breakage of the tongue/GAF1 Asp-Arg salt bridge (inlet) the tip of the tongue refolds with concomitant disordering of the stalk-like β-hairpin and formation of an Asp-Ser salt bridge (inlet).

stretch between the W(G/A)G motif and the W*X*E motif (Trp^{369}-Glu^{391}) with regions of orthologous Group II phytochromes from *N. punctiforme*, *Oscillatoria* sp. and *Cyanothece* sp. (see Fig. 9 and supplemental Fig. S2). The *Oscillatoria* sp. and *Cyanothece* sp. tongue-containing variants exhibit normal photoconversion, whereas the *Cyanothece* sp. tongue-containing variant showed only partial P_{fr} formation after red light illumination. Interestingly, the variant with the *N. punctiforme* tongue displayed incomplete photoconversion. This tongue harbors a degenerated PR*X*SF motif due to an arginine to glutamine substitution. Nevertheless, a R383Q mutant in *Syn*Cph2(1–2) showed normal P_r/P_{fr} photoconversion indicating that in the P_r state glutamine can form analogous H-bonds with Asp^{79} as the arginine and that in the P_{fr} state other residues are at least equally crucial for the proper association of the tongue with the GAF1-bilin binding site.

The Tongue, a Subdomain for P_{fr} Stabilization and/or Signaling?—So far, the light-triggered $Z \rightarrow E$ isomerization around the C15-C16 double bond is insufficient to rationalize the strong bathochromic shift of the P_{fr} state of Group I and II phytochromes by about 100–130 nm when compared with simple bilin-chromopeptides. Clearly, the complex bilin-binding site of phytochromes stabilizes these P_{fr} photo states by an unresolved mechanism, *e.g.* by electrostatic interaction, steric control of bilin conformation, or even formation of enol-like tautomers (44). Our structural and mutagenesis data on *Syn*Cph2 indicate that the conserved PR*X*SF, W(G/A)G, and W*X*E motifs of the tongue region are crucial for P_{fr} formation. Other structural elements, which contribute to the bilin-binding site of a canonical phytochrome such as *Syn*Cph1 (8, 9), are either missing (N terminus) or replaced like the subsite for ring B and C propionates. The W(G/A)G and W*X*E motifs are shared by Group I and II phytochromes and affect $P_r \rightarrow P_{fr}$ photoconversion due to their distance and link to the bilin binding pocket via a conserved H-bonding network. Together with structural data on the P_{fr} state of bathy phytochromes (9) we suggest conformational switching of the tongue region via swap of the tryptophans in the tongue-GAF1 interface during $P_r \rightarrow P_{fr}$ conversion (Fig. 10). This folding event on the local protein level is predicted to be part of the slow, light-independent lumi-R $\rightarrow P_{fr}$ conversion that occurs in the millisecond range. Accordingly, bathy phytochromes may prefer P_{fr} as the paternal state to P_r due to different energetics of the interaction between their chromophore/GAF1-adduct and the tongue region. Slow protein conformational changes such as the suggested Trp switch are instrumental for further signal transfer either to the C-terminal effector domains as in bacterial phytochromes or for modulating protein-protein interactions as in plant phytochromes. Interestingly, the tongue region of known phytochrome structures passes into a helix that directly connects the PHY/GAF2 domains with downstream effector modules and thus provides a short route for intra-molecular signaling. This may suggest that different effector domains such as histidine kinases, diguanylate cyclases, and c-di-GMP-specific phosphodiesterases share a common mechanism for intramolecular signal transduction.

Acknowledgments—We thank the beamline staff of the ESRF, Grenoble, and BESSY-II, Berlin, for support, Holger Steuber for data collection, Yann Geisselbrecht, Holger Steuber, and Maik Veelders for support in structure solution and refinement, Petra Gnau and Ralf Pöschke for technical support, and Georgios Psakis for discussions.

REFERENCES

1. Butler, W. L., Norris, K. H., Siegelman, H. W., and Hendricks, S. B. (1959) Detection, assay, and preliminary purification of the pigment controlling photoresponsive development of plants. *Proc. Natl. Acad. Sci. U.S.A.* **45,** 1703–1708
2. Hughes, J., Lamparter, T., Mittmann, F., Hartmann, E., Gärtner, W., Wilde, A., and Börner, T. (1997) A prokaryotic phytochrome. *Nature* **386,** 663
3. Rodriguez-Romero, J., Hedtke, M., Kastner, C., Müller, S., and Fischer, R. (2010) Fungi, hidden in soil or up in the air. Light makes a difference. *Annu. Rev. Microbiol.* **64,** 585–610
4. Nagatani, A. (2010) Phytochrome. Structural basis for its functions. *Curr. Opin. Plant Biol.* **13,** 565–570
5. Vierstra, R. D., and Zhang, J. (2011) Phytochrome signaling. Solving the Gordian knot with microbial relatives. *Trends Plant Sci.* **16,** 417–426
6. Ulijasz, A. T., Cornilescu, G., Cornilescu, C. C., Zhang, J., Rivera, M., Markley, J. L., and Vierstra, R. D. (2010) Structural basis for the photoconversion of a phytochrome to the activated Pfr form. *Nature* **463,** 250–254
7. Rockwell, N. C., Su, Y. S., and Lagarias, J. C. (2006) Phytochrome structure and signaling mechanisms. *Annu. Rev. Plant Biol.* **57,** 837–858
8. Essen, L. O., Mailliet, J., and Hughes, J. (2008) The structure of a complete phytochrome sensory module in the Pr ground state. *Proc. Natl. Acad. Sci. U.S.A.* **105,** 14709–14714
9. Yang, X., Kuk, J., and Moffat, K. (2008) Crystal structure of *Pseudomonas aeruginosa* bacteriophytochrome. Photoconversion and signal transduction. *Proc. Natl. Acad. Sci. U.S.A.* **105,** 14715–14720
10. Anders, K., von Stetten, D., Mailliet, J., Kiontke, S., Sineshchekov, V. A.,

Hildebrandt, P., Hughes, J., and Essen, L. O. (2011) Spectroscopic and photochemical characterization of the red-light sensitive photosensory module of Cph2 from *Synechocystis* PCC 6803. *Photochem. Photobiol.* **87,** 160–173
11. Montgomery, B. L., and Lagarias, J. C. (2002) Phytochrome ancestry. Sensors of bilins and light. *Trends Plant Sci.* **7,** 357–366
12. Rockwell, N. C., and Lagarias, J. C. (2010) A brief history of phytochromes. *ChemPhysChem* **11,** 1172–1180
13. Narikawa, R., Ishizuka, T., Muraki, N., Shiba, T., Kurisu, G., and Ikeuchi, M. (2013) Structures of cyanobacteriochromes from phototaxis regulators AnPixJ and TePixJ reveal general and specific photoconversion mechanism. *Proc. Natl. Acad. Sci. U.S.A.* **110,** 918–923
14. Burgie, E. S., Walker, J. M., Phillips, G. N., Jr., and Vierstra, R. D. (2013) A photo-labile thioether linkage to phycoviolobilin provides the foundation for the blue/green photocycles in DXCF-cyanobacteriochromes. *Structure* **21,** 88–97
15. Park, C.-M., Shim, J.-Y., Yang, S.-S., Kang, J.-G., Kim, J.-I., Luka, Z., and Song, P.-S. (2000) Chromophore-apoprotein interactions in *Synechocystis* sp. PCC6803 phytochrome Cph1. *Biochemistry* **39,** 6349–6356
16. Wu, S. H., and Lagarias, J. C. (2000) Defining the bilin lyase domain. Lessons from the extended phytochrome superfamily. *Biochemistry* **39,** 13487–13495
17. Savakis, P., De Causmaecker, S., Angerer, V., Ruppert, U., Anders, K., Essen, L. O., and Wilde, A. (2012) Light-induced alteration of c-di-GMP level controls motility of *Synechocystis* sp. PCC 6803. *Mol. Microbiol.* **85,** 239–251
18. Jain, R., Behrens, A.-J., Kaever, V., and Kazmierczak, B. I. (2012) Type IV pilus assembly in *Pseudomonas aeruginosa* over a broad range of cyclic di-GMP concentrations. *J. Bacteriol.* **194,** 4285–4294
19. Simm, R., Morr, M., Kader, A., Nimtz, M., and Römling, U. (2004) GGDEF and EAL domains inversely regulate cyclic di-GMP levels and transition from sessility to motility. *Mol. Microbiol.* **53,** 1123–1134
20. Fiedler, B., Börner, T., and Wilde, A. (2005) Phototaxis in the cyanobacterium *Synechocystis* sp. PCC 6803. Role of different photoreceptors. *Photochem. Photobiol.* **81,** 1481–1488
21. Wilde, A., Fiedler, B., and Börner, T. (2002) The cyanobacterial phytochrome Cph2 inhibits phototaxis towards blue light. *Mol. Microbiol.* **44,** 981–988
22. Adams, P. D., Afonine, P. V., Bunkóczi, G., Chen, V. B., Davis, I. W., Echols, N., Headd, J. J., Hung, L.-W., Kapral, G. J., Grosse-Kunstleve, R. W., McCoy, A. J., Moriarty, N. W., Oeffner, R., Read, R. J., Richardson, D. C., Richardson, J. S., Terwilliger, T. C., and Zwart, P. H. (2010) PHENIX. A comprehensive Python-based system for macromolecular structure solution. *Acta Crystallogr. D* **66,** 213–221
23. Emsley, P., and Cowtan, K. (2004) Coot. Model-building tools for molecular graphics. *Acta Crystallogr. D* **60,** 2126–2132
24. DeLano, W. L. (2002) *The PyMOL Molecular Graphics System*, DeLano Scientific, San Carlos, CA
25. Carpentier, P., Royant, A., Ohana, J., and Bourgeois, D. (2007) Advances in spectroscopic methods for biological crystals. 2. Raman spectroscopy. *J. Appl. Crystallogr.* **40,** 1113–1122
26. McGeehan, J., Ravelli, R. B., Murray, J. W., Owen, R. L., Cipriani, F., McSweeney, S., Weik, M., and Garman, E. F. (2009) Colouring cryo-cooled crystals. Online microspectrophotometry. *J. Synchrotron Radiat.* **16,** 163–172
27. Kneip, C., Hildebrandt, P., Schlamann, W., Braslavsky, S. E., Mark, F., and Schaffner, K. (1999) Protonation state and structural changes of the tetrapyrrole chromophore during the Pr → Pfr phototransformation of phytochrome. A resonance raman spectroscopic study. *Biochemistry* **38,** 15185–15192
28. Strauss, H. M., Hughes, J., and Schmieder, P. (2005) Heteronuclear solution-state NMR studies of the chromophore in cyanobacterial phytochrome Cph1. *Biochemistry* **44,** 8244–8250
29. Senn, H. M., and Thiel, W. (2007) QM/MM studies of enzymes. *Curr. Opin. Chem. Biol.* **11,** 182–187
30. Becke, A. D. (1993) Density-functional thermochemistry. III. The role of exact exchange. *J. Chem. Phys.* **98,** 5648–5652
31. MacKerell, A. D., Bashford, D., Bellott, Dunbrack, R. L., Evanseck, J. D., Field, M. J., Fischer, S., Gao, J., Guo, H., Ha, S., Joseph-McCarthy, D., Kuchnir, L., Kuczera, K., Lau, F. T. K., Mattos, C., Michnick, S., Ngo, T., Nguyen, D. T., Prodhom, B., Reiher, W. E., Roux, B., Schlenkrich, M., Smith, J. C., Stote, R., Straub, J., Watanabe, M., Wiórkiewicz-Kuczera, J., Yin, D., and Karplus, M. (1998) All-atom empirical potential for molecular modeling and dynamics studies of proteins. *J. Phys. Chem. B* **102,** 3586–3616
32. Bakowies, D., and Thiel, W. (1996) Hybrid models for combined quantum mechanical and molecular mechanical approaches. *J. Phys. Chem.* **100,** 10580–10594
33. Billeter, S. R., Turner, A. J., and Thiel, W. (2000) Linear scaling geometry optimisation and transition state search in hybrid delocalised internal coordinates. *Phys. Chem. Chem. Phys.* **2,** 2177–2186
34. Landgraf, F. T., Forreiter, C., Hurtado Picó, A., Lamparter, T., and Hughes, J. (2001) Recombinant holophytochrome in *Escherichia coli*. *FEBS Lett.* **508,** 459–462
35. von Stetten, D., Günther, M., Scheerer, P., Murgida, D. H., Mroginski, M. A., Krauss, N., Lamparter, T., Zhang, J., Anstrom, D. M., Vierstra, R. D., Forest, K. T., and Hildebrandt, P. (2008) Chromophore heterogeneity and photoconversion in phytochrome crystals and solution studied by resonance Raman spectroscopy. *Angew. Chem. Int. Ed. Engl.* **47,** 4753–4755
36. Li, H., Zhang, J., Vierstra, R. D., and Li, H. (2010) Quaternary organization of a phytochrome dimer as revealed by cryoelectron microscopy. *Proc. Natl. Acad. Sci. U.S.A.* **107,** 10872–10877
37. Mailliet, J., Psakis, G., Feilke, K., Sineshchekov, V., Essen, L. O., and Hughes, J. (2011) Spectroscopy and a high-resolution crystal structure of Tyr-263 mutants of cyanobacterial phytochrome Cph1. *J. Mol. Biol.* **413,** 115–127
38. Navarro, M. V., De, N., Bae, N., Wang, Q., and Sondermann, H. (2009) Structural analysis of the GGDEF-EAL domain-containing c-di-GMP receptor FimX. *Structure* **17,** 1104–1116
39. Diensthuber, R. P., Bommer, M., Gleichmann, T., and Möglich, A. (2013) Full-length structure of a sensor histidine kinase pinpoints coaxial coiled coils as signal transducers and modulators. *Structure* **21,** 1127–1136
40. Wang, C., Sang, J., Wang, J., Su, M., Downey, J. S., Wu, Q., Wang, S., Cai, Y., Xu, X., Wu, J., Senadheera, D. B., Cvitkovitch, D. G., Chen, L., Goodman, S. D., and Han, A. (2013) Mechanistic insights revealed by the crystal structure of a histidine kinase with signal transducer and sensor domains. *Plos Biol.* **11,** e1001493
41. Song, C., Psakis, G., Lang, C., Mailliet, J., Gärtner, W., Hughes, J., and Matysik, J. (2011) Two ground state isoforms and a chromophore D-ring photoflip triggering extensive intramolecular changes in a canonical phytochrome. *Proc. Natl. Acad. Sci. U.S.A.* **108,** 3842–3847
42. Shang, L., Rockwell, N. C., Martin, S. S., and Lagarias, J. C. (2010) Biliverdin amides reveal roles for propionate side chains in bilin reductase recognition and in holophytochrome assembly and photoconversion. *Biochemistry* **49,** 6070–6082
43. Mailliet, J., Psakis, G., Schroeder, C., Kaltofen, S., Dürrwang, U., Hughes, J., and Essen, L. O. (2009) Dwelling in the dark: procedures for the crystallography of phytochromes and other photochromic proteins. *Acta Crystallogr. D* **65,** 1232–1235
44. Lagarias, J. C., and Rapoport, H. (1980) Chromopeptides from phytochromes. The structure and linkage of the P_r form of the phytochrome chromophore. *J. Am. Chem. Soc.* **102,** 4821–4828

Supplementary Information

Structure of the cyanobacterial phytochrome 2 photosensor implies a tryptophan switch for phytochrome signaling

Katrin Anders[1], Grazia Daminelli-Widany[2], Maria Andrea Mroginski[2], David von Stetten[3], Lars-Oliver Essen[1,*]

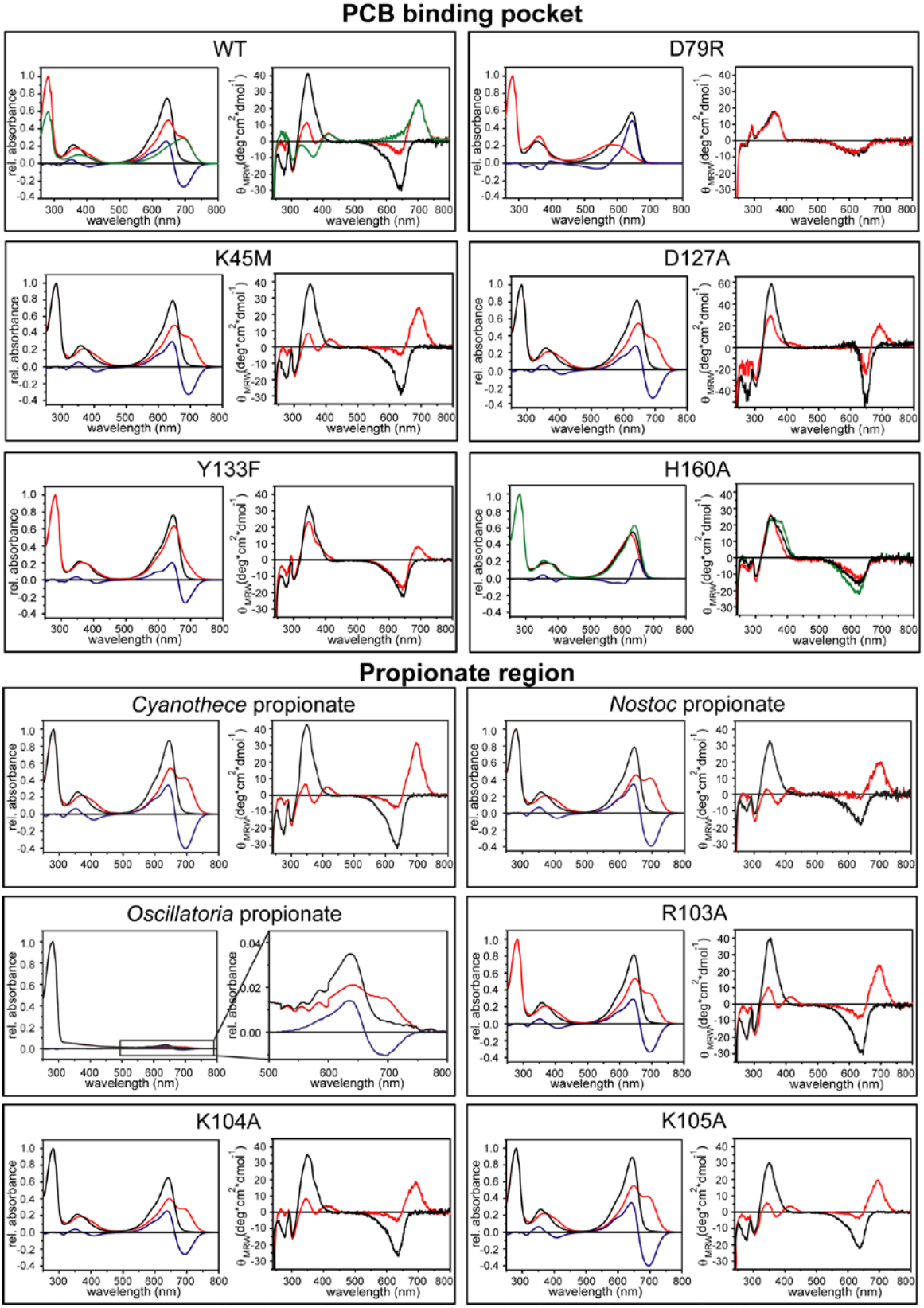

Supplementary Fig. 1: UV/vis absorbance (left) and CD spectra (right) of *Syn*Cph2(1-2) wild type and variants of the binding pocket and of the propionate region after far-red (black line) and red light (red line). Difference spectra ($A_{Pr} - A_{Photoequilibrium}$) are shown in blue. The green line in the wild type spectrum is a calculated pure P_{fr} spectrum (1). The spectra of H160A after a dark reversion of 2 h are also in green. In the *Oscillatoria* variant of the propionate region only a small amount of chromophore is attached, the red region of the UV/vis absorbance spectrum is enlarged. At these low intensities device-specific effects occur in the range of 520 – 600 nm. The CD spectra were omitted because the chromophore was not detectable.

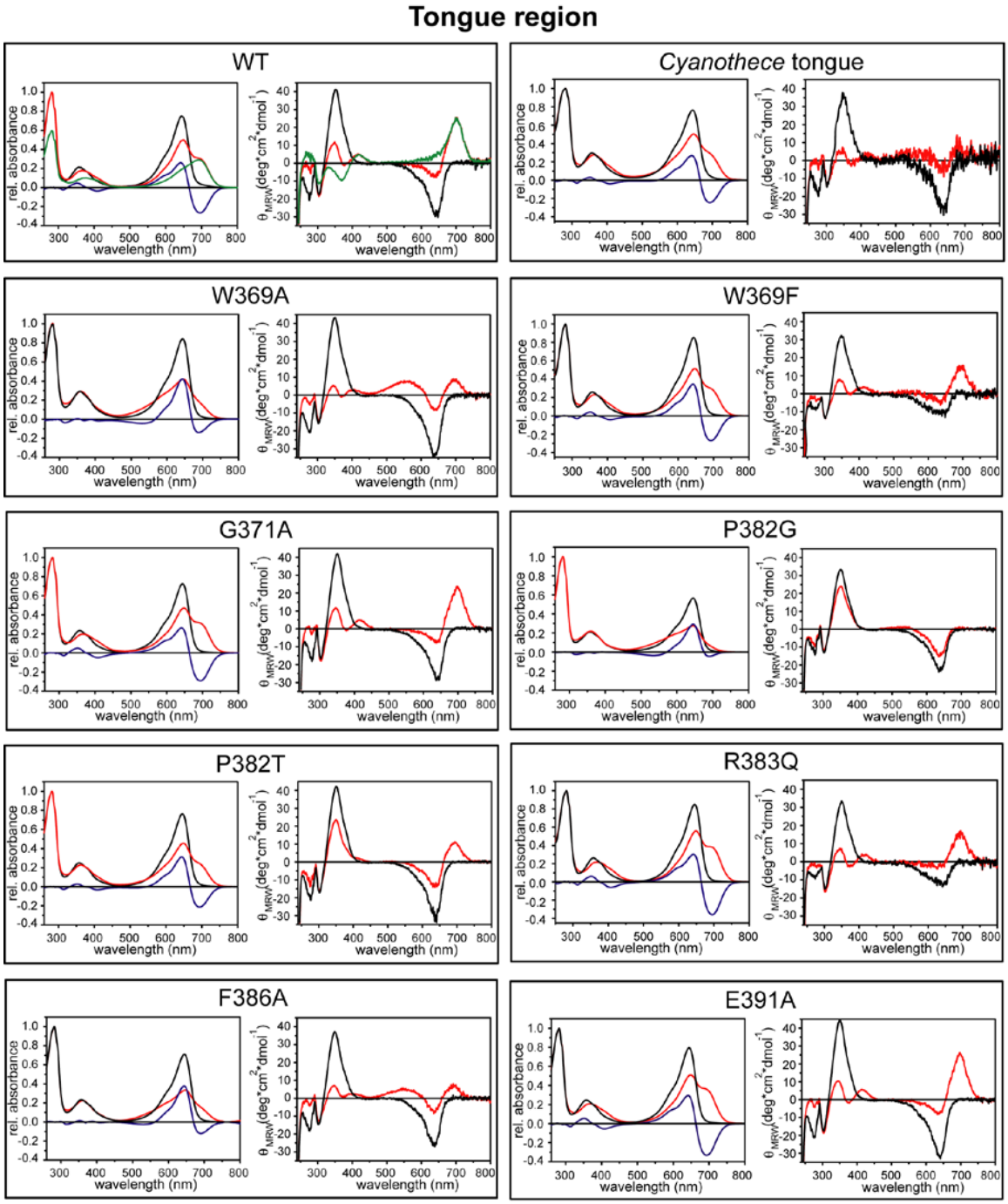

Supplementary Fig. 2: UV/vis absorbance (left) and CD spectra (right) of *Syn*Cph2(1-2) wild type and mutants in tongue region after far-red and red light irradiation. Spectra after far-red light illumination are displayed in black. Spectra following red light irradiation are in red. Difference spectra (A_{Pr} - $A_{Photoequilibrium}$) are shown in blue. Calculated wild type P_{fr} spectra are in green (1).

Supplementary Table I. Analysis of bilin conformations in phytochromes and phycocyanins.

Protein	PDB-Code	Reso-lution (Å)	Tilt A-B (°)	Tilt B-C (°)	Tilt C-D (°)	Chromo-phore	Confor-mation	Chirality C3[1]
*Syn*Cph2 (B)	4BWI	2.6	**19.2**	**32.5**	**59.8**	PCB	*ZZZssa*	R
*Syn*Cph1	2VEA	2.5	**9.8**	**1.5**	**26.3**	PCB	*ZZZssa*	R
*Syn*Cph1/Y263F	3ZQ5	2.0	**16.2**	**5.8**	**37.3**	PCB	*ZZZssa*	S, R
*Dr*CBD	2O9C	1.5	**15.2**	**1.3**	**50.8**	BV	*ZZZssa*	-
*Dr*CBD	2O9B	2.2	**17.3**	**0.3**	**54.8**	BV	*ZZZssa*	-
*Rp*BphP3 (A+B)	2OOL	2.2	**19.5**	**5.8**	**42.0**	BV	*ZZZssa*	-
*Pa*BphP (A)	3NHQ	2.6	**30.1**	**18.2**	**55.7**	BV	*ZZEssa*	-
Allophycocyanin (A)	1ALL	2.3	24.5	8.7	1.9	PCB	*ZZZasa*	R
Allophycocyanin (B)	1ALL	2.3	28.9	15.7	46.3	PCB	*ZZZasa*	R
C-Phyococyanin (A)	1CPC	1.7	21.5	12.7	37.6	PCB	*ZZZasa*	R
R-Phycoerythrin (A)	1EYX	2.2	7.7	18.2	56.4	PCB	*ZZZasa*	S
C-Phycocyanin (A)	1GH0	2.2	63.4	7.5	36.9	PCB	*ZZZasa*	R
C-Phycocyanin (A)	1HA7	2.2	18.5	16.5	36.6	PCB	*ZZZasa*	R
Allophycocyanin	1KN1	2.2	32.6	17.5	25.3	PCB	*ZZZasa*	S
R-Phycoerythrin (A)	1LIA	2.8	37.2	8.6	34.9	PCB	*ZZZasa*	S
C-Phycocyanin (A)	1ON7	2.7	12.2	14.7	33.1	PCB	*ZZZasa*	R
C-Phycocyanin (A)	1PHN	1.7	21.8	14.5	34.1	PCB	*ZZZasa*	R
α-Phycoerythrocyanin (A)	2J96	2.2	26.5	11.7	87.9	PVB	*ZEsa*	R
Phycoerythrin (A)	2VJH	2.2	25.6	11.9	37.3	PEB	*ZZas*	R

Letters in brackets indicate the analyzed chain, when several chains are available per asymmetric unit.

Supplementary Table II. Spectroscopical features of *Syn*Cph2(1-2) wild type and mutants.

	conformations	dark reversion	characteristics	P_r Max. (nm)	Max. after red light (nm)	SAR
wild type	P_r, P_{fr}	yes		644	695	0.8
K45M	P_r, P_{fr}	yes	wt-like	645	~692	0.79
D79R	P_r, bleached state	no	irreversible	644	580, 605	0.58
R103A	P_r, P_{fr}	yes	wt-like	644	~691	0.81
K104A	P_r, P_{fr}	yes		641	~691	0.65
K105A	P_r, P_{fr}	yes	wt-like	644	693	0.89
D127A	P_r, P_{fr}	yes		643	~693	0.81
Y133F	P_r, P_{fr}	yes	only little P_{fr}	646	~692	0.76
H160A	P_r, P_{nr}	yes	reversible, P_{nr} after red light, complete P_r only achieved by dark reversion	640	628	0.63
W369A	P_r, Intermediate	yes		644	645	0.85
W369F	P_r, P_{fr}, Intermediate	yes		644	~691	0.85
G371A	P_r, P_{fr}	yes	wt-like	644	695	0.73
P382G	P_r, Intermediate	yes		645	645	0.56
P382T	P_r, P_{fr}, Intermediate	yes		646	695	0.76
R383Q	P_r, P_{fr}	yes		645	691	0.85
S385A	P_r, Intermediate	yes		646	647	0.54
F386A	P_r, Intermediate	yes		646	646	0.39
W389A	P_r, Intermediate	yes		644	645	0.79
W389F	P_r, P_{fr}	yes		644	~691	0.87
E391A	P_r, P_{fr}	yes	wt-like	644	~691	0.79
***Cyanothece* tongue**	P_r, P_{fr}, Intermediate,	yes	unstable	644	~696	0.76
***Nostoc* tongue**	P_r, Intermediate	yes		644	644	0.56
***Oscillatoria* tongue**	P_r, P_{fr}	yes	unstable	644	693	0.82
***Cyanothece* propionate**	P_r, P_{fr}	yes	wt-like	644	693	0.87
***Nostoc* propionate**	P_r, P_{fr}	yes	wt-like, but higher P_{fr} content; unstable	645	694	0.78
***Oscillatoria* propionate**	P_r, P_{fr}	?	only little chromophore attachment	637	695	0.035

The absorbance maxima in the red region of the spectrum as well as the 644 nm/280 nm specific absorbance ratio (SAR) are listed. P_{nr} of H160A denotes a near-red absorbing state.

References

1. Anders, K., von Stetten, D., Mailliet, J., Kiontke, S., Sineshchekov, V. A., Hildebrandt, P., Hughes, J., and Essen, L.-O. (2011) Spectroscopic and photochemical characterization of the red-light sensitive photosensory module of Cph2 from *Synechocystis* PCC 6803. *Photochem. Photobiol.* **87**, 160-173

5.4 Kinetical characterization of *Syn*Cph2(1-2)

This research was submitted to The Journal of Biological Chemistry on 03.03.2014. *Katrin Anders, Alexander Gutt, Wolfgang Gärtner and Lars-Oliver Essen.* **Phototransformation of the red-light sensor Cph2 from *Synechocystis* sp. depends on its tongue motifs.** The Journal of Biological Chemistry. 2014; 289:pp-pp.

Summary

In the first kinetic study of a Group II phytochrome we characterized *Syn*Cph2(1-2) *via* time-resolved spectroscopy in the $P_r \rightarrow P_{fr}$ photoconversion and the $P_{fr} \rightarrow P_r$ back reaction. The influence of the conserved PRxSF and WxE motifs was illuminated by investigating the chronology of intermediate formation during phototransformation of the S385A, W389A and W389F mutants.

The $P_r \rightarrow P_{fr}$ photoconversion of *Syn*Cph2(1-2) is completed within 80 ms and involves four intermediates, a Lumi-R-like intermediate (Lumi-R_L), R1, R2 and R3 with lifetimes of 1.3 µs, 299 µs, 2.56 ms and 17.1 ms, respectively. The formation of Lumi-R_L occurs in the picosecond time range and is too fast to be resolved in this study; its decay represents the first observable process. Lumi-R_L displays an increased absorbance at ~670 nm. The next intermediate R1 shows an absorbance rise at 690 nm but also a decrease at 620 nm. In the third R2 intermediate the absorbance at lower wavelengths is further decreased as it reveals an absorbance decay at 660 nm. The last intermediate R3 comprises an increase of absorbance close to the P_{fr} maximum, so it is the dominant component of P_{fr} state formation. In the $P_{fr} \rightarrow P_r$ photoconversion *Syn*Cph2(1-2) displays three intermediates, Lumi-F, F1 an F2 with lifetimes of 0.9 µs, 798 µs and 6.20 ms that all show the major characteristics of the P_r state. This reverse phototransformation is three-times faster than the $P_r \rightarrow P_{fr}$ reaction. The intermediates show only modest absorption changes and the last intermediate F2 exhibits the absorbance rise at ~640 nm, thus leading to the P_r state.

The Ser-385 within the conserved PRxSF motif is located in the tongue region of the GAF2 domain. In the P_r crystal structure of *Syn*Cph2(1-2) it points away from the chromophore binding pocket and does not interact with the GAF1 domain[139]. In bathyphytochromes it hydrogen-bonds to the aspartate of the conserved DIP motif thus stabilizing the GAF-PHY interactions. A S385A variant of *Syn*Cph2(1-2) exhibits a steady state spectrum after red light illumination that differs from the wild type's as it comprises a broadened peak between 500 nm and 620 nm, as well as a bleaching at 646 nm. Time-resolved spectroscopy reveals four intermediates, whereby the first three intermediates are similar to *Syn*Cph2(1-2) but with up to threefold shorter lifetimes. The last intermediate R3' differs as it shows a broader

increase above 590 nm with maximal changes at 660 nm instead of an absorbance increase at 700 nm as in *Syn*Cph2(1-2). In the $P_{fr} \rightarrow P_r$ photoconversion three intermediates can be observed. The first intermediate, Lumi-F' differs from *Syn*Cph2(1-2) as it displays an absorbance rise also at wavelengths above ~640 nm. The intermediates F1 and F2 are similar to *Syn*Cph2(1-2), only F2 decays nearly two-times faster.

The WxE motif in the tongue region is about 15 Å distant from the bilin binding pocket and is suggested to be part of a tryptophan-switch during photoconversion [139]. A W389A mutant of *Syn*Cph2(1-2) exhibits a degenerated spectrum after red light illumination with a highly broadened, bleached peak including an unusual absorbance rise between 450 - 600 nm. W389A comprises three instead of four intermediates upon photoconversion. The first two intermediates resemble *Syn*Cph2(1-2) but the intermediate R2' does not only show an absorbance decrease in the range of R2 (λ_{max} ~660 nm) but also at longer wavelengths. In addition, it comprises a pronounced rise of absorbance below 580 nm and decays to a degenerated red light adapted state named P_{deg}. In the $P_{deg} \rightarrow P_r$ back conversion three intermediates can be observed that are all distinct from *Syn*Cph2(1-2), although they already show P_r-like features. A phenylalanine mutation of Trp-389 can restore wild type-like behavior in the $P_r \rightarrow P_{fr}$ as well as in the $P_{fr} \rightarrow P_r$ photoconversion. Only intermediate R3 comprises a lifetime that is two-times longer than in *Syn*Cph2(1-2).

In this study we could demonstrate that the W389A mutation causes major implications on the photocycle in comparison to S385A. Assuming that the structural changes during photoconversion imply rearrangements in the tongue region one can postulate a "miss-docked" and a well-docked" tongue in W389A and S385A, respectively. The results for the W389F variant imply that the bulky and/or aromatic character of the tryptophan is important for the function as switch. All these findings show that in the intermediates Lumi-R_L and R1 of the $P_r \rightarrow P_{fr}$ photoconversion only the chromophore and its nearest surroundings are altered whereas in R2 changes in the tongue region occur that depend on the WxE motif. The difference between phenylalanine and tryptophan in this position affects intermediate R3. This intermediate is also impaired by the S385A mutation which suggests that the movement of the serine residue and the formation of the hydrogen bond network occur during R3 formation.

Contributions

K. Anders designed the experiments, produced and purified the proteins, performed steady state absorbance spectroscopy, analyzed the data and wrote the manuscript, A. Gutt performed flash photolysis measurements and analyzed the data, W. Gärtner analyzed the data and revised the manuscript, L.-O. Essen designed experiments as well as wrote and revised the manuscript.

Phototransformation of the red-light sensor Cph2 from *Synechocystis* sp. depends on its tongue motifs

Katrin Anders[a1], Alexander Gutt[b1], Wolfgang Gärtner[b,2], Lars-Oliver Essen[a,2]

[1]These authors contributed equally to this work

[a]Biomedical Research Center/Department of Chemistry, Philipps-University, D-35032 Marburg, Germany;

[b]Max-Planck-Institute for Chemical Energy Conversion, D-45470 Mülheim a. d. Ruhr, Germany

[2]To whom correspondence should be addressed:

Lars-Oliver Essen, Department of Chemistry/Biomedical Research Center, Philipps-University Marburg, Hans-Meerwein-Str. 4, D-35032 Marburg, Germany, phone: +4964212822032, fax: +4964212822191, mail: essen@chemie.uni-marburg.de

Wolfgang Gärtner, Max-Planck-Institute for Chemical Energy Conversion, Stiftstraße 34-36, D-45470 Mülheim a. d. Ruhr, Germany, phone: +492083063693, mail: wolfgang.gaertner@cec.mpg.de

Running title: Photocycle of cyanobacterial phytochrome *Syn*Cph2(1-2)

Key words: Tryptophan switch, bilin chromophore, cyanobacterial phytochrome, photo intermediates, time-resolved spectroscopy

Background: Phytochromes are bilin-dependent red/far red photoreceptors.

Results: Late processes of the $P_r \rightarrow P_{fr}$ photoconversion involve large-scale conformational changes within the tongue region.

Conclusion: Early intermediates lumi-R and R1 affect only the chromophore and its nearest surroundings, whereas late R2 formation recruits the Trp-motifs in the peripheral tongue.

Significance: The conserved motifs of the tongue region are important for photoconversion and presumably for signaling.

Abstract

Phytochromes are photoreceptors using a bilin tetrapyrrole as chromophore, which switch in canonical phytochromes between red (P_r) and far red light (P_{fr}) absorbing states. Cph2 from *Synechocystis* sp., a non-canonical phytochrome, harbors besides a cyanobacteriochrome domain a second photosensory module, a P_r/P_{fr}-interconverting GAF-GAF bidomain (*Syn*Cph2(1-2)). Like in canonical phytochromes, a unique motif of the second GAF domain, the tongue region, seals the bilin binding site in the GAF1 domain from solvent access. Time-resolved spectroscopy of the *Syn*Cph2(1-2) module shows four intermediates during $P_r \rightarrow P_{fr}$ phototransformation and three intermediates during $P_{fr} \rightarrow P_r$ back-conversion. A mutation in the tongue's conserved PRxSF motif, S385A, affects the formation of late intermediate R3 and of a P_{fr}-like state, but not the back-conversion to P_{fr} *via* a lumi-F-like state. In contrast, a mutation in the likewise conserved WxE motif, W389A, changes the photocycle at intermediate R2 and causes a degenerated red-light adapted state. Here, back-conversion to P_r proceeds *via* intermediates differing from *Syn*Cph2(1-2). Replacement of this tryptophan that is ~15 Å distant from the chromophore by another aromate, W389F, restores native $P_r \rightarrow P_{fr}$ phototransformation. These results indicate large-scale conformational changes within the tongue region of GAF2 during the final processes of phototransformation. We propose that in early intermediates only the chromophore and its nearest surroundings are altered, whereas late changes during R2 formation depend on the distant WxE motifs of the tongue region. Ser-385 within the PRxSF motif affects only late intermediate R3, when refolding of the tongue and docking to the GAF1 domain are almost completed.

Introduction

Within the broad range of photoreceptors existing in photosynthetic and non-photosynthetic bacteria, bilin-binding GAF domain-containing proteins like phytochromes and cyanobacteriochromes (CBCRs) cover the whole light spectrum. Despite different spectral characteristics between the red / far red-light absorbing phytochromes and CBCRs, which switch between all kinds of colors, they both harbor the same kind of chromophore: a covalently attached linear tetrapyrrole. Classical phytochromes photoconvert between two conformations: the red and far red light absorbing P_r and P_{fr} state. Upon red-light illumination of P_r

the excited state P_r^* is formed that decays and converts into the primary red-shifted photoproduct lumi-R (also called I_{700}) within picoseconds (1). This step involves the Z → E isomerization of the C15, C16 double bond of the bilin chromophore. The further steps are light independent and proceed thermally driven in longer time scales. Accordingly, phytochrome photoconversion starts within picoseconds and can last up to seconds (2,3). The light-triggered reaction from P_{fr} → P_r undergoes different intermediates (4,5).

Full-length oat PhyA shows pairs of intermediates in the P_r → P_{fr} phototransformation with similar spectroscopic signatures but different lifetimes (2). This is caused by at least two distinct P_r conformations each leading to one set of subsequent intermediates (6). Cph1 from *Synechocystis* sp., a bacterial phytochrome with a plant-like sensory module architecture, exhibits a multistep photoconversion reminiscent of the PhyA P_r → P_{fr} reaction. However, *Syn*Cph1 displays a different kinetics (5,7) with an intermediate that has no counter-part in any other phytochrome.

In contrast to canonical phytochromes from plants or bacteria the domain architecture of the second phytochrome from *Synechocystis* sp., *Syn*Cph2, exhibits some remarkable differences. First of all, *Syn*Cph2 is a bimodule photoreceptor (MW ~145 kDa) with a complex domain architecture, GAF1-GAF2-GGDEF1*-EAL-GAF3-GGDEF2 (8,9). The common PAS-GAF-PHY sensor module (PAS: Period/ARNT/Single-minded, GAF: cGMP phosphodiesterase/adenylyl cyclase/FhlA, PHY: Phytochrome), that defines canonical Group I phytochromes (10), is here altered to a GAF-GAF bidomain (Group II phytochromes) as the N-terminal photosensory module. Despite the lack of a PAS domain this *Syn*Cph2(1-2) module exhibits P_r/P_{fr} photochromicity known from Group I phytochromes (9). *Syn*Cph2 covalently attaches phycocyanobilin (PCB) *via* thioether linkage that is partly solvent-exposed due to the missing PAS domain (8). Similar to plant phytochrome B, but unlike *Syn*Cph1 and PhyA, the P_{fr}-state of this photosensory module undergoes dark reversion to its P_r-state (9). Besides the UV/Vis spectra, Resonance Raman spectra of *Syn*Cph2(1-2), which are highly sensitive to structural changes at the chromophore binding site, resemble closely the spectral features of *Syn*Cph1 in both states, P_r and P_{fr}. Accordingly, one may consider the *Syn*Cph2(1-2) module as a minimal model of P_r/P_{fr} photoconversion in canonical phytochromes. Besides the red / far red-light sensitive GAF-GAF bidomain, *Syn*Cph2 harbors a CBCR-like GAF3 domain as its second photosensory module with a blue/green photochemistry. This photochromic switch controls light regulated c-di-GMP levels (11) by tuning the catalytic activity of the GGDEF2 domain. GGDEF and EAL domains (named after their conserved motifs) produce and degrade c-di-GMP, an eubacterial second messenger, respectively (12). A GGDEF1*- EAL module with an inactive GGDEF domain is found in *Syn*Cph2 following the N-terminal GAF-bidomain sensor module (Fig. 1A).

The crystal structure (8) of the red/far red phytochrome region confirmed that the GAF2 domain is directly related to the PHY domains of canonical phytochromes. Like the latter, it comprises a tongue-like extension that covers the bilin binding site of the GAF1 domain and may be hence involved in intramolecular signal transduction. Despite significant sequence divergence between the core GAF2 and PHY domains, three motifs within the tongue region, $W^G/_AG$, PRxSF and WxE, are almost invariant in Group I and II phytochromes and were hence suggested to be crucial for phototransformation and stability of the resulting P_{fr} state. The significance of the bulky aromatic character of the tryptophan residues in the $W^G/_AG$ and WxE motifs for P_{fr} formation was derived from site-directed mutagenesis and structural comparison to the tongue conformation of bathyphytochromes in their P_{fr} ground state. The resulting model of a "tryptophan switch" during photoconversion implies that the tongue undergoes a red-light triggered conformational change thus altering the conformation and/or orientation of the conserved PRxSF motif and thereby its interactions with the chromophore binding site. In this context, the tryptophans of the $W^G/_AG$ and WxE motifs are supposed to swap their positions and play an important role in the stabilization of a P_{fr}-specific conformation of the tongue region (8).

Here, we characterize *Syn*Cph2(1-2) and three of its tongue mutants by time-resolved absorption spectroscopy to track slow conformational changes, which are mostly indicative of structural changes within the protein moiety. Whereas the native *Syn*Cph2(1-2) module and its W389F mutant exhibit both a cognate spectral behavior under steady-state conditions, the W389A and S385A mutants were found to fail in the formation of a P_{fr}-like state upon red light illumination (Fig. 1B). We analyzed the light-induced $P_r \rightarrow P_{fr}$ and $P_{fr} \rightarrow P_r$ photoconversions in the micro- to millisecond time range by laser flash photolysis and time-resolved absorption spectroscopy. The data were used in global fit analysis to obtain lifetime associated difference spectra (LADS) of the intermediates.

Materials and Methods

*Syn*Cph2(1-2) and mutants were produced and purified as described (9); the measurements with the PCB assembled proteins were performed in Tris buffer (50 mM Tris, 300 mM NaCl, 5 mM EDTA, pH 8.0). For flash photolysis the protein sample was diluted to an absorbance of 0.5 at the P_r maximum. Absorption spectra were recorded before and after the measurements (spectrophotometer UV-2401 P, Shimadzu) to exclude denaturation of the protein. The sample in a quartz cuvette with 1 cm path length was kept at 288 K (15°C). Photoconvertion of the proteins to 100% P_r or the highest P_{fr} occupancy the cuvette was accomplished by irradiation with a 720 nm and a 625 nm LED light source (High power LED, Roithner; 720 nm: 350 mA; 1.8 V; 625 nm: 350 mA, 2.2 V), respectively. An OPO, coupled to a Spitlight 300 Ne-YAG laser (Versascon HB, GWU-Lasertechnik) was used for excitation (pulse

length: 9 ns; energy output 640 nm: 70 µJ; 700 nm: 45 µJ) with λ_{ex} = 640 nm for the $P_r \rightarrow P_{fr}$ conversion and λ_{ex} = 700 nm for the reverse reaction. The resulting absorption change was detected at various wavelengths between 520 nm and 720 nm. For *Syn*Cph2(1-2), the S385A and W389A mutant, the entire spectral range was recorded in 10 nm steps. The variant W389F was measured with 6-7 wavelengths (590 nm, 640 nm, 660 nm, 665 nm, 690 nm, 700 nm, 720 nm) that display the highest absorbance changes throughout the intermediate spectra, allowing the prediction of the photocycle according to the previously recorded spectra and lifetimes. Absorbance changes were detected *via* a cw xenon lamp (Amko) and two matched monochromators (A 1020) placed before and behind the sample. Absorbance changes were recorded by a photomultiplier mounted to the second monochromator, from which the signals were read into a computer for further data handling and fitting. The detection range covered times between few µs up to 100 ms. The resolution is limited to ~0.1 µs at the lower and ~1 µs at the higher time limit. Beyond 80 ms the photoconversion was complete for *Syn*Cph2(1-2) as well as for its mutants. For each wavelength and single time traces 10 measurements were averaged to improve the signal to noise ratio. Between individual measurements the sample was irradiated with the LED light sources for 8 s and 5 s, respectively, to revert photochemically generated products and to achieve maximal P_r or P_{fr} state occupancy.

For data analysis the single time traces were baseline corrected if necessary and assembled (usually three time windows with different scaling were measured separately and later combined into a single wavelength recording trace). Global fit analysis was performed by fitting the curves with a sum of exponential functions (13-15) (MATLAB), yielding lifetimes for the individual transitions between intermediates and the lifetime associated difference spectra (LADS). Care was taken to minimize laser or scattering light artefacts during the short time windows that might impair detection of early intermediates.

Results

We hereby report the first kinetic study of the late intermediates of the $P_r \rightarrow P_{fr}$ phototransformation and the $P_{fr} \rightarrow P_r$ back reaction of a Cph2-type phytochrome module. We also address the influence of the highly conserved PRxSF and WxE motifs within the tongue on photoconversion. For that purpose, the S385A, W389A and W389F mutants (Fig. 1A) were generated and their chronology of intermediate formation during photoconversion was studied by time-resolved spectroscopy. In *Syn*Cph2(1-2) as well as in the mutants phototransformation was complete within 80 ms, later intermediates could not be observed.

Photokinetics of the SynCph2(1-2) module

The $P_r \rightarrow P_{fr}$ transition was triggered by a 9 ns laser pulse of red light (λ = 640 nm) that was tuned close to the λ_{max} of the P_r state of *Syn*Cph2(1-2)

(λ_{max} = 644 nm). During photoconversion *Syn*Cph2(1-2) forms distinct intermediates that can all be followed in single time traces at 665 nm (Fig. 2). The formation of the first intermediate, lumi-R, occurs in phytochromes in the picosecond time range (1) and is hence too fast to be resolved in this study. Accordingly, the decay of a lumi-R like state (lumi-R_L) represents the first observable process. For *Syn*Cph2(1-2) four intermediates, lumi-R_L, R1, R2 and R3 were found for the $P_r \rightarrow P_{fr}$ conversion with lifetimes of 1.3 µs, 299 µs, 2.56 ms and 17.1 ms (Table 1). Their spectral features are reflected by their LADS shown in Figure 3. Notably, these LADS are defined as difference spectra, where positive amplitudes indicate a decaying species, *i.e.* the absorbance at the specific wavelength decreases between the preceding state and the considered one, whereas negative LADS amplitudes specify an absorbance rise.

During $P_r \rightarrow P_{fr}$ phototransformation of *Syn*Cph2(1-2) the first intermediate corresponds to the lumi-R-like state with an increase in absorbance at about 670 nm and a calculated lifetime of 1.3 µs. The bathochromic shift of the lumi-R_L absorbance as compared to the initial P_r state is continued by the next intermediate, R1 (lifetime 299 µs), due to a further rise of absorbance at 690 nm. The LADS of the R1 intermediate is bimodal as it shows also a shallow decrease of absorbance at 620 nm. Furthermore, its absorbance changes related to this lifetime show relatively small positive and negative amplitudes. The third intermediate, R2 (lifetime of 2.56 ms), reveals an absorbance decay at 660 nm thus further lowering the absorbance at shorter wavelengths. The last intermediate R3, (lifetime of 17.1 ms), displays an absorbance rise already close to the P_{fr} maximum and thus is indicative for the dominant component of the final P_{fr} state formation. The resulting 'constant difference spectrum' from the time-resolved data, reflecting final – initial state (Fig. 3, green curves), is very close to the observed steady-state difference spectrum (Fig. 1B) and proofs hence the applicability of the method.

For the $P_{fr} \rightarrow P_r$ transition (excitation at 700 nm) the global analysis revealed three intermediates (lumi-F, F1, F2) with lifetimes of 0.9 µs, 798 µs and 6.20 ms. This makes the reverse photoconversion about three-times faster than the $P_r \rightarrow P_{fr}$ phototransformation. Like other phytochromes, *Syn*Cph2(1-2) undergoes hereby different intermediates than during the 'forward' $P_r \rightarrow P_{fr}$ conversion. The absorbance changes between the intermediates are not as pronounced as in the $P_r \rightarrow P_{fr}$ phototransformation (Fig. 4) which is reflected in the LADS by displaying only small changes for the associated amplitudes (Fig. 3). Already the early lumi-F intermediate formed in the $P_{fr} \rightarrow P_r$ phototransformation resembles the P_r state and the further F1 and F2 intermediates show only modest absorption changes. The last intermediate, F2, with a lifetime of 6.20 ms displays an absorbance rise at about 640 nm and leads finally to the P_r state.

Light-induced kinetics of SynCph2(1-2) tongue mutants

Ser-385 is located in the conserved PRxSF motif that is situated in the common tongue region of Group I and II phytochromes. In the *Syn*Cph2(1-2) P_r crystal structure (8) this polar residue shows no interaction with the GAF1 domain and its embedded PCB chromophore and points away from the chromophore binding pocket, whereas in bathyphytochromes this residue was found to form a hydrogen bond with the aspartate of the conserved DIP motif within the chromophore binding site. Accordingly, the S385A mutant of *Syn*Cph2(1-2) exhibits a P_{fr} steady state absorbance spectrum that deviates significantly from that of the native *Syn*Cph2(1-2) module (Fig. 1B). After red light illumination of the P_r state the P_{fr} spectrum shows a broadened peak in the red region between 500 nm to 620 nm. At the photodynamic equilibrium the resulting spectrum exhibits a bleaching at 646 nm and an isosbestic point at 556 nm relative to the P_r-state with its λ_{max} at 644 nm. At wavelengths shorter than the isosbestic point the mutant shows increased absorbance upon photoconversion unlike native *Syn*Cph2(1-2).

The global analysis of the time-resolved data from the S385A mutant reveals as in the native *Syn*Cph2(1-2) four intermediates (lumi-R_L, R1, R2, R3') with lifetimes of 1.3 µs, 112 µs, 1.57 ms and 8.10 ms for the forward reaction, *i.e.* $P_r \rightarrow P_{fr}$. The first three intermediates are similar to *Syn*Cph2(1-2) but with up to threefold shorter lifetimes. Accordingly, the overall photoconversion is about two-times faster than in native *Syn*Cph2(1-2) and leads to a final state with a difference spectrum akin that of native *Syn*Cph2(1-2), but with a 2.6 fold reduced overall amplitude. Likewise, the late R2 and R3 intermediates exhibit similarly lowered overall amplitudes, whereas the lumi-R_L and R1 intermediates are almost unaffected. Like in *Syn*Cph2(1-2), the lumi-R_L-like intermediate decays with a lifetime of 1.3 µs and exhibits an increase in absorbance in the long wavelength range at about 690 nm. This effect is continued in the second intermediate (R1, lifetime of 112 µs) that also displays a reduced absorbance at 620 nm. The highest impact on the absorbance change takes place during the formation of the R2 intermediate with a lifetime of 1.57 ms, also nearly two-times faster than in native *Syn*Cph2(1-2). Here, a pronounced absorbance decrease around 655 nm takes place. The last intermediate, R3', with a lifetime of 8.10 ms is distinct from the R3 intermediate of native *Syn*Cph2(1-2). Instead of an absorbance increase at 700 nm as detected for the native photosensor, the R3' intermediate of the S385A mutant displays a broader increase above 590 nm with maximal changes at 660 nm. This spectral signature reflects the broad absorbance band of the P_{fr} form, as was seen before in steady state difference spectra.

The signals in the S385A measurements are threefold diminished compared to the native *Syn*Cph2(1-2) module not only during the $P_r \rightarrow P_{fr}$ but also the $P_{fr} \rightarrow P_r$ photoconversion. Like *Syn*Cph2(1-2), S385A shows three intermediates

for the $P_{fr} \rightarrow P_r$ conversion, lumi-F', F1, F2 with lifetimes of 1.3 µs, 619 µs and 3.53 ms, which all exhibit the spectral signatures of a state close to P_r. The lumi-F' intermediate is the only one that differs from lumi-F of intact *Syn*Cph2(1-2), because it displays an absorbance rise also at wavelengths above ~640 nm. The greatest absorbance changes occur during the formation of intermediate F2 with an absorbance rise at 640 nm. The lumi-F' and F1 intermediates decay similarly as their *Syn*Cph2(1-2) counterparts; only the F2 intermediate decays nearly two-times faster.

The *Syn*Cph2(1-2) mutant W389A addresses the role of the conserved WxE motif in the tongue region. This motif is about 15 Å distant from the bilin chromophore and is suggested of being part of a tryptophan-switch during photoconversion (8). Like the S385A mutant the W389A mutant shows a degenerated spectrum after red light illumination by lacking the signatures of the P_{fr} state (Fig 1B). The steady state spectrum is highly broadened with an unusual absorbance rise in the 450 – 600 nm region that surpasses the one of S385A. The P_r peak at 644 nm is bleached, the isosbestic point at 573 nm is red-shifted compared to S385A because of the broader absorbance. Global analysis of the time-resolved data reveals three instead of four intermediates (lumi-R_L, R1, R2') with lifetimes of 1.4 µs, 414 µs and 2.28 ms (Fig. 3). Interestingly, these intermediates resemble the native intermediates not only in their lifetimes but also in the global features of their difference spectra. The first lumi-R-like intermediate with a lifetime of 1.4 µs shows an absorbance rise at 700 nm that is continued by the intermediate R1. The 2.28 ms R2' intermediate exhibits an absorbance decrease not only in the range of *Syn*Cph2(1-2) (λ_{max} ~660 nm) but also at longer wavelengths, where intermediate R1 already shows signatures of the P_{fr} state. Unlike the wild type and the S385A mutant this tongue mutant shows a pronounced rise of absorbance below 580 nm for the R2‘ intermediate. A fourth intermediate R3 like in *Syn*Cph2(1-2) and S385A indicative of late conformational changes of the photoreceptor module is missing. The signal intensities of the late R2' intermediate and the final state of the W389A variant are again three- to four-times smaller than in *Syn*Cph2(1-2) and hence in accordance with the S385A variant.

The $P_{fr} \rightarrow P_r$ back conversion of W389A reveals three intermediates (lumi-F'', F1', F2') with lifetimes of 1.2 µs, 2.21 ms and 19.5 ms. Although the intermediates show already the known P_r-like features, their LADS differ from native *Syn*Cph2(1-2) and its S385A mutant. Furthermore, the back reaction takes three-times longer and the constant difference spectrum (Fig. 3) corresponding to the final P_r conformation shows a comparatively broadened peak.

For the variant W389F with native *Syn*Cph2(1-2)-like steady state spectra, only a few wavelengths were measured to allow the prediction of the intermediates and their lifetimes. W389F behaves like *Syn*Cph2(1-2) in all observed wavelengths (Fig. 5) and reveals four observable intermediates in the forward reaction. The intermediates'

lifetimes calculated from the single time traces and not by global analysis are 1.5 µs, 380 µs, 2.0 ms and 33.3 ms. The lifetimes of lumi-R_L, R1 and R2 are in good agreement with those of the native *Syn*Cph2(1-2) photosensor. Only the intermediate R3 differs in its lifetime that is two times longer than in *Syn*Cph2(1-2). In the reverse reaction only the lifetime of intermediate F2 could be assigned *via* fit of the single time traces. Without global analysis, the absorbance changes between the intermediates are too small to allow reliable fitting of the curves. The lifetime of intermediate F2 (3.1 ms) is two-times faster than that of *Syn*Cph2(1-2).

Discussion

Photoconversion of SynCph2(1-2), a PAS-less phytochrome

Cyanobacterial phytochromes of Group I (*e.g.* Cph1, CphA) are well characterized with respect to their photochemical activity (5,7,16-18). In contrast, photoreceptors such as the here studied *Syn*Cph2(1-2), composed of only two GAF domains in a tandem array and lacking the N-terminal PAS domain, have not been investigated before by time-resolved spectroscopy. Despite the deviant domain arrangement, the tandem-GAF Cph2 photoreceptor highly resembles canonical phytochromes by undergoing a photochromic switch between a red- and a far red-absorbing state. Here, the photocycles of recombinant *Syn*Cph2(1-2) and three mutants within the PRxSF and WxE motif of the tongue region were characterized in the micro- to-millisecond timescale. For native *Syn*Cph2(1-2), three intermediates, R1 - R3, could be observed after lumi-R_L formation. Whereas the decay time of 2.56 ms, assigned to intermediate R2, identifies the decay of short-wavelength intermediates, the dominant contribution to P_{fr} formation is found for R3 with an observed lifetime of 17.1 ms.

In the canonical phytochromes from plants the $P_r \rightarrow P_{fr}$ phototransformation was found to be extremely complex with up to six intermediates (16), which can comprise a further series of P_{fr}-like states prior to the final formation of P_{fr}. For *Syn*Cph2(1-2) similar slow reactions cannot *per se* be excluded, because the reported late spectral changes were too red-shifted (> 700 nm) to be in the range of this study. However, the absorbance properties of *Syn*Cph2(1-2) are blue-shifted compared to these canonical phytochromes (9).

It is intriguing to compare the here detected absorbance changes for *Syn*Cph2(1-2) with those from Group I phytochromes, especially in the short time range. The excitation/detection set-up as employed here yields a step function in the wavelength range of the first intermediate (around 700 nm), as 'lumi-R', or I_{700}, is formed within ps (1) and remains constant far into the µs time range. The decay of this intermediate is described for Group I phytochromes with a lifetime of ca. 80-100 µs (7,17). In Group I phytochromes the following intermediates (meta-R or I_{bleach}) show reduced oscillator strength ('I_{bleach}'), the decay of the first intermediate follows monoexponential kinetics. In Cph2, however, the absorbance around 700 nm, after being formed as a step function,

remains positive over the entire time range of detection. Accordingly, one may assume that *Syn*Cph2(1-2) intermediates following the lumi-R-like state show a larger oscillator strength and thus do not cause a transient bleaching. For the reverse $P_{fr} \rightarrow P_r$ reaction three intermediates, lumi-F, F1 and F2, are detected that all show the signatures of the P_r state and undergo only minor changes. These findings, especially the spectral similarity of all intermediates with the final photoproduct, P_r, are in accordance to the behavior of Group I phytochromes. For comparison, laser flash photolysis studies of *Syn*Cph1 revealed five intermediates with time constants of at 4.5 µs, 270 µs, 3.8 ms, 30 ms and 280 ms at pH 8.0 during the $P_r \rightarrow P_{fr}$ phototransformation (19). The fifth intermediate with a comparable long lifetime hence cannot be found in *Syn*Cph2(1-2). Initial *Z* → *E* isomerization in *Syn*Cph1 occurs in the electronically excited P_r* state with a time constant of 30 ps according to an infrared spectroscopy analysis (20). A complementary Raman spectroscopy study could show that 85% of the molecules relax back from the excited P_r* state to the P_r ground state explaining the low quantum yield of phytochrome phototransformation. After isomerization the residual 15% reach a product-like electronically excited Lumi-R* state that decays to the Lumi-R ground state which is formed within 30 ps (21). Kinetic data of *Syn*Cph1 (5,7,19,20,22) combined with structural NMR data (23,24) allow the assignment of structural changes to the several intermediates. Unfortunately, only the nearest chromophore environment in the chromophore binding site was addressed which excludes most of the tongue region, which is very similar in *Syn*Cph1 and *Syn*Cph2 (8).

Another cyanobacterial phytochrome of Group I, the *Syn*Cph1 orthologue CphA from *Calothrix* sp. PCC7601 (also known as *Fremyella diplosiphon* or *Tolypothrix* sp.) revealed four intermediates with lifetimes of 8 µs, 330 µs, 3.2 ms and 23 ms for the P_r to P_{fr} conversion and four intermediates with lifetimes of 1.5 µs, 1.5 ms, 6 ms and 50 ms for the backward reaction (18). These results are again in good agreement with the *Syn*Cph2(1-2) lifetimes apart from the fourth intermediate of CphA in the $P_{fr} \rightarrow P_r$ photoconversion. Cryotrapping experiments of CphA in combination with UV/Vis and Fourier transform infrared difference spectroscopy revealed the presence of three intermediates in the forward and two intermediates in the backward reaction that show remarkable similarities with the intermediates of *Syn*Cph1 (25).

The assignment of intermediates to structural changes can be achieved for at least two intermediates in the P_r to P_{fr} conversion (23). The lumi-R state is initially formed by double-bond Z → E isomerization between C15 and C16 (21,26). In the meta-R state the chromophore is transiently deprotonated at the D-ring nitrogen that is then reprotonated upon P_{fr} formation (19).

In *Syn*Cph2(1-2), the lumi-R state can be assigned to the first intermediate of this study. Because of its fast formation below the resolution limit of the measurements, only its decay can be followed.

The remaining intermediates reflect structural changes in the protein as well as adaptions of the chromophore. The assignment of the transient protonation to the intermediates is not possible at the current state. Model compounds exhibit a red-shift upon protonation (27-29). For *Syn*Cph1 the transient proton release and a kinetic isotope effect were assigned to an intermediate with 320 µs lifetime (7). Interestingly, its difference spectrum and lifetime resembles intermediate R1 of *Syn*Cph2(1-2); both exhibit a red-shifted absorbance.

The $P_{fr} \rightarrow P_r$ conversion starts like the forward reaction with the double bond isomerization between C15 and C16 leading to the lumi-F intermediate. Subsequent conformational changes in the range of rings C and D with an accompanying break of the D-ring nitrogen – aspartate hydrogen bond results in the formation of the intermediate meta-F. The meta-F $\rightarrow P_r$ transition is accompanied by the generation of a new hydrogen bond between the D-ring nitrogen and a water molecule (24).

The tongue variants and their impact on the photocycle.

The tongue region of the GAF2 domain seals the chromophore binding pocket in GAF1 and is supposed to be involved in signal transduction (8,30). This arrangement is comparable to the Group I phytochromes where the tongue protrudes from the PHY domain, which is actually a degenerated GAF domain. Ser-385 is located in the PRxSF motif within a loop region of the tongue (Fig. 1A). The preceding residue Arg-383 of this motif is involved in the arginine to aspartate salt bridge, thereby generating a tight interaction between the GAF1 and GAF2 domain. Ser-385 points out of the binding pocket in the crystal structure of the P_r conformation, whereas Trp-389 is part of the conserved WxE motif in the stem region of the tongue consisting of two β-strands (Fig. 1A). Although Ser-385 and Trp-389 are ~13 Å and ~16 Å, respectively, apart from the D-ring of the chromophore in the P_r state, they affect formation of the P_{fr} state. Steady-state absorbance spectra of their alanine variants reveal that they fail to form a P_{fr} state-like native *Syn*Cph2(1-2) (Fig. 1B).

In this study we could show that S385A exhibits four intermediates in the $P_r \rightarrow P_{fr}$ reaction like native *Syn*Cph2(1-2). Both share the first three intermediates lumi-R_L, R1 and R2 of the $P_r \rightarrow P_{fr}$ reaction. The fourth intermediate R3' differs in S385A (Fig. 4), but nevertheless decays to a P_{fr}-like state (Fig. 6). The $P_{fr} \rightarrow P_r$ conversion is very similar to *Syn*Cph2(1-2), suggesting that the red light adapted state of S385A decays into a comparable intermediate like the P_{fr} state of *Syn*Cph2(1-2) and that the P_{fr} and P_{fr}-like states correspond to each other. From this first intermediate lumi-F' the protein decays *via* the common intermediates F1 and F2 of the *Syn*Cph2(1-2) $P_{fr} \rightarrow P_r$ photoconversion.

In contrast, the photocycle of W389A mutant at first glance differs from native *Syn*Cph2(1-2). This tongue mutant apparently misses the last intermediate R3 and does not generate a P_{fr}-like

state (Fig. 3, panel bottom, left), although a meta-R-like decay with a lifetime of ca. 2.3 ms (akin those of the wild type and the S385A mutant) can clearly be identified. The inspection of the steady state P_r/P_{fr} difference spectrum of this mutant (Fig. 1B, bottom, left) clarifies this confusion, as it shows a P_{fr} form with a very broad absorbance band and an apparently small oscillator strength that cannot be detected in the lifetime-associated-difference-spectrum. Interestingly, any conversion processes of intermediates of the entire detection range are covered from the contributions of the very broad absorbance of the P_{fr} form.

Unlike S385A, W389A does not display red light driven conversion into a P_{fr}-like state. The forward $P_r \rightarrow P_{fr}$ reaction proceeds through the first two *Syn*Cph2(1-2)-like intermediates lumi-R_L and R1. The third intermediate R2' differs and decays without a fourth intermediate like in *Syn*Cph2(1-2) to the red light adapted state which is though degenerated and therefore named here P_{deg}. It shows a broadened steady-state spectrum, also including an absorbance rise around 550 nm. The difference between the red light adapted states of S385A and W389A is also reflected by their circular dichroism (CD) spectra. Here, W389A shows increased ellipticity at 550 nm, whereas S385A exhibits only a smaller effect and corresponds to *Syn*Cph2(1-2) (8). The steady state absorbance difference spectrum of W389A resembles that of a 45 kDa fragment (aa 1-425) of PhyA from *Avena sativa.* This recombinant protein was originally designed to study the properties of the proteolytic 39-kDa fragment of phyA of *A. sativa*, however, trypsin digestion of the native protein also causes loss of the N-terminal 65 amino acids. It absorbance at 550 nm in its red light adapted state (31). This fragment lacks most of the PHY domain which leads upon irradiation to the formation of a very broad absorbance band with only moderate thermal stability, thus phenomenologically indicating the importance of the PHY domain (and the tongue region). The spectral similarity between these two proteins, *i.e.*, the 45-kDa fragment and the W389A mutant of *Syn*Cph2(1-2) now clearly identifies the relevance of the tryptophan in the WxE motif during tongue-rearrangement for the stability of the P_{fr} form. Accordingly, W389A undergoes three intermediates in the back reaction to P_r that differ clearly from the intermediates of *Syn*Cph2(1-2) (Fig. 6), and the overall time elapsed to arrive at the P_r state is three-times longer than for *Syn*Cph2(1-2) (19.5 vs. 6.20 ms, *cf*. Table 1).

From these findings one can conclude that though the Ser-385 residue contributes to a native-like P_{fr} formation, it is not essential for the formation of the first three intermediates of the $P_r \rightarrow P_{fr}$ reaction and intermediate two and three of the $P_{fr} \rightarrow P_r$ photoconversion. Only formation of the final $P_r \rightarrow P_{fr}$ intermediate R3 and of lumi-F is affected by the serine. So this variant shows likely only conformational changes at the protein and not at the chromophore level during photoconversion, just the last rearrangement to P_{fr} is affected. Interestingly, Ser-385 apparently stabilizes the intermediates because its alanine mutation exhibits about fivefold faster photoconversions.

The alanine mutation of Trp-389 on the other hand shows major implications on the photocycle; it only shares the first two intermediates with *Syn*Cph2(1-2). This suggests that this amino acid plays a key role in the structural rearrangements during the late photoconversion. Interestingly, the phenylalanine mutation suffices to restore the native *Syn*Cph2(1-2) behavior.

Mutagenesis studies in the photosensory module of oat phytochrome A (32) with amino acids in close proximity of the chromophore in the GAF domain revealed different effects on the decay of I_{700} (lumi-R). Some mutants displayed faster decays and accelerated P_{fr} formation, whereas a proline to alanine mutation resulted in a slower P_{fr} formation due to a more rigid conformation in the mutant. The acceleration was assigned to an increase in polarity or a weakened interaction between two protein domains enabling faster conformational changes (32). In *Syn*Cph2(1-2) the S385A mutation accelerated the formation of the red light adapted state, where the decrease of polarity inhibits interactions that stabilize the intermediates. W389F shows a slower P_{fr} formation due to the less bulky amino acid substitute that is crucial to allow formation of the new tongue conformation.

Lessons from the photocycle: a tryptophan switch for signaling.

We previously suggested a conformational change during photoconversion that involves a tryptophan-switch of residues in the tongue region (8). We suggested the tryptophan residues of the $W^{G}/_{A}G$ and WxE motif to act as anchors within the structure for stabilizing either the P_r or the P_{fr} state. It can be concluded that bulky aromatic residues like phenylalanine can substitute the function of tryptophan and preserve the *Syn*Cph2(1-2) behavior, whereas small residues as alanine fail to do so.

In this study we demonstrate that the W389A variant has indeed major implications on the photocycle in comparison to S385A. On their way to the red-light adapted state the alanine mutation of the former prevents structural changes important for P_{fr} formation. Assuming that these structural changes imply rearrangements of the tongue, one can postulate that W389A forms a “miss-docked” and S385A a “well docked” tongue after red-light illumination. The fact that S385A has a smaller effect on the photocycle and does not further affect P_{fr} formation demonstrates that only tryptophans provide contributions crucial to the photoconversion. The *Syn*Cph2(1-2) like behavior of W389F shows that a bulky and/or aromatic character is important for the function of the switch. Interestingly, only the lifetime of the final intermediate R3 in the W389F photocycle differs from *Syn*Cph2(1-2). Its lifetime is two-fold longer than its wild type counterpart, apparently caused by the smaller amino acid and the higher intrinsic flexibility. The alanine mutation affects already intermediate R2. This suggests that the intermediates lumi-R_L and R1 reflect only changes in the chromophore and its nearest environment whereas in the intermediate R2 large-scale changes in the tongue region occur, where a big

aromatic amino acid in the Trp-389 position is needed to complete this process. The difference between phenylalanine and tryptophan in this position affects only the last intermediate R3. The S385A variant shows that the involvement of the serine in the interactions occurs later than that of the tryptophan residue in intermediate R3. In bathyphytochrome structures, which correspond to their P_{fr} ground state, this serine points towards the chromophore in contrast to P_r structures and is there involved in an extended hydrogen bond network including also the pyrrole nitrogen of ring D. Our results suggest that a movement of the serine residue of the PRxSF motif and hence the formation of the hydrogen bond network occurs during the formation of intermediate R3.

During $P_{fr} \rightarrow P_r$ photoconversion the S385A mutation only affects lumi-F whereas photoconversion of W389A proceeds *via* a different set of intermediates. The implications of the mutations on the back reaction are not as big as in the forward reaction, because already in lumi-F the protein shows P_r–like characteristics and the following intermediates reflect only minor changes. This finding again demonstrates the paramount importance of the tryptophan residues in the Trp-switch for the P_{fr} formation of phytochromes.

References

1. Andel, F., Hasson, K. C., Gai, F., Anfinrud, P. A., and Mathies, R. A. (1997) Femtosecond time-resolved spectroscopy of the primary photochemistry of phytochrome. *Biospectroscopy* **3**, 421-433
2. Jorissen, H. J., Quest, B., Remberg, A., Coursin, T., Braslavsky, S. E., Schaffner, K., de Marsac, N. T., and Gartner, W. (2002) Two independent, light-sensing two-component systems in a filamentous cyanobacterium. *Eur. J. Biochem.* **269**, 2662-2671
3. Müller, M. G., Lindner, I., Martin, I., Gärtner, W., and Holzwarth, A. R. (2008) Femtosecond kinetics of photoconversion of the higher plant photoreceptor phytochrome carrying native and modified chromophores. *Biophys. J.* **94**, 4370-4382
4. Bischoff, M., Hermann, G., Rentsch, S., and Strehlow, D. (2001) First steps in the phytochrome phototransformation: a comparative femtosecond study on the forward (Pr → Pfr) and back reaction (Pfr → Pr). *Biochemistry* **40**, 181-186
5. Heyne, K., Herbst, J., Stehlik, D., Esteban, B., Lamparter, T., Hughes, J., and Diller, R. (2002) Ultrafast dynamics of phytochrome from the cyanobacterium *Synechocystis*, reconstituted with phycocyanobilin and phycoerythrobilin. *Biophys. J.* **82**, 1004-1016
6. Michler, I., and Braslavsky, S. E. (2001) Time-resolved thermodynamic analysis of the oat phytochrome A phototransformation. A photothermal beam deflection study. *Photochem. Photobiol.* **74**, 624-635
7. Remberg, A., Lindner, I., Lamparter, T., Hughes, J., Kneip, C., Hildebrandt, P., Braslavsky, S. E., Gartner, W., and Schaffner, K. (1997) Raman spectroscopic and light-induced kinetic characterization of a recombinant phytochrome of the cyanobacterium *Synechocystis*. *Biochemistry* **36**, 13389-13395
8. Anders, K., Daminelli-Widany, G., Mroginski, M. A., von Stetten, D., and Essen, L.-O. (2013) Structure of the cyanobacterial phytochrome 2 photosensor implies a tryptophan switch for phytochrome signaling. *J. Biol. Chem.* **288**, 35714-35725

9. Anders, K., von Stetten, D., Mailliet, J., Kiontke, S., Sineshchekov, V. A., Hildebrandt, P., Hughes, J., and Essen, L.-O. (2011) Spectroscopic and photochemical characterization of the red-light sensitive photosensory module of Cph2 from *Synechocystis* PCC 6803. *Photochem. Photobiol.* **87**, 160-173
10. Rockwell, N. C., and Lagarias, J. C. (2010) A brief history of phytochromes. *ChemPhysChem* **11**, 1172-1180
11. Savakis, P., De Causmaecker, S., Angerer, V., Ruppert, U., Anders, K., Essen, L.-O., and Wilde, A. (2012) Light-induced alteration of c-di-GMP level controls motility of Synechocystis sp. PCC 6803. *Mol. Microbiol.* **85**, 239-251
12. Simm, R., Morr, M., Kader, A., Nimtz, M., and Romling, U. (2004) GGDEF and EAL domains inversely regulate cyclic di-GMP levels and transition from sessility to motility. *Mol. Microbiol.* **53**, 1123-1134
13. Chizhov, I., Chernavskii, D. S., Engelhard, M., Mueller, K. H., Zubov, B. V., and Hess, B. (1996) Spectrally silent transitions in the bacteriorhodopsin photocycle. *Biophys. J.* **71**, 2329-2345
14. Chizhov, I., and Engelhard, M. (2001) Temperature and halide dependence of the photocycle of halorhodopsin from *Natronobacterium pharaonis*. *Biophys. J.* **81**, 1600-1612
15. Chizhov, I., Schmies, G., Seidel, R., Sydor, J. R., Lüttenberg, B., and Engelhard, M. (1998) The photophobic receptor from *Natronobacterium pharaonis*: temperature and pH dependencies of the photocycle of sensory rhodopsin. *Biophys. J.* **75**, 999-1009
16. Schmidt, P., Gertsch, T., Remberg, A., Gärtner, W., Braslavsky, S. E., and Schaffner, K. (1998) The complexity of the Pr to Pfr phototransformation kinetics is an intrinsic property of native phytochrome. *Photochem. Photobiol.* **68**, 754-761
17. Remberg, A., Ruddat, A., Braslavsky, S. E., Gärtner, W., and Schaffner, K. (1998) Chromophore incorporation, Pr to Pfr kinetics, and Pfr thermal reversion of recombinant N-terminal fragments of phytochrome A and B chromoproteins. *Biochemistry* **37**, 9983-9990
18. Chizhov, I., Zorn, B., Manstein, Dietmar J., and Gärtner, W. (2013) Kinetic and thermodynamic analysis of the light-induced processes in plant and cyanobacterial phytochromes. *Biophys. J.* **105**, 2210-2220
19. van Thor, J. J., Borucki, B., Crielaard, W., Otto, H., Lamparter, T., Hughes, J., Hellingwerf, K. J., and Heyn, M. P. (2001) Light-induced proton release and proton uptake reactions in the cyanobacterial phytochrome Cph1. *Biochemistry* **40**, 11460-11471
20. Yang, Y., Linke, M., von Haimberger, T., Hahn, J., Matute, R., González, L., Schmieder, P., and Heyne, K. (2012) Real-time tracking of phytochrome's orientational changes during Pr photoisomerization. *J. Am. Chem. Soc.* **134**, 1408-1411
21. Dasgupta, J., Frontiera, R. R., Taylor, K. C., Lagarias, J. C., and Mathies, R. A. (2009) Ultrafast excited-state isomerization in phytochrome revealed by femtosecond stimulated Raman spectroscopy. *Proc. Natl. Acad. Sci. U.S.A.* **106**, 1784-1789
22. Heyes, D. J., Khara, B., Sakuma, M., Hardman, S. J., O'Cualain, R., Rigby, S. E., and Scrutton, N. S. (2012) Ultrafast red light activation of Synechocystis phytochrome Cph1 triggers major structural change to form the Pfr signalling-competent state. *PloS one* **7**, e52418
23. Song, C., Rohmer, T., Tiersch, M., Zaanen, J., Hughes, J., and Matysik, J. (2013) Solid-state NMR spectroscopy to probe photoactivation in canonical phytochromes. *Photochem. Photobiol.* **89**, 259-273
24. Rohmer, T., Lang, C., Bongards, C., Gupta, K. B. S. S., Neugebauer, J., Hughes, J., Gärtner, W., and Matysik, J. (2010) Phytochrome as molecular machine: revealing chromophore action during the Pfr → Pr photoconversion by magic-angle spinning NMR spectroscopy. *J. Am. Chem. Soc.* **132**, 4431-4437
25. Schwinté, P., Gärtner, W., Sharda, S., Mroginski, M.-A., Hildebrandt, P., and Siebert, F. (2009) The photoreactions of recombinant phytochrome CphA from the cyanobacterium Calothrix PCC7601: a low-temperature UV–Vis and FTIR study. *Photochem. Photobiol.* **85**, 239-249
26. Andel, F., Lagarias, J. C., and Mathies, R. A. (1996) Resonance raman analysis of chromophore

structure in the Lumi-R photoproduct of phytochrome. *Biochemistry* **35**, 15997-16008
27. Borucki, B. (2006) Proton transfer in the photoreceptors phytochrome and photoactive yellow protein. *Photochem. Photobiol. Sci.* **5**, 553-566
28. Margulies, L., and Stockburger, M. (1979) Spectroscopic studies on model compounds of the phytochrome chromophore. Protonation and deprotonation of biliverdin dimethyl ester. *J. Am. Chem. Soc.* **101**, 743-744
29. Stanek, M., and Grubmayr, K. (1998) Protonated 2,3-dihydrobilindiones—models for the chromophores of phycocyanin and the red-absorbing form of phytochrome. *Chem. Eur. J.* **4**, 1653-1659
30. Essen, L. O., Mailliet, J., and Hughes, J. (2008) The structure of a complete phytochrome sensory module in the Pr ground state. *Proc. Natl. Acad. Sci. U.S.A.* **105**, 14709-14714
31. Gärtner, W., Hill, C., Worm, K., Braslavsky, S. E., and Schaffner, K. (1996) Influence of expression system on chromophore binding and preservation of spectral properties in recombinant phytochrome A. *Eur. J. Biochem.* **236**, 978-983
32. Remberg, A., Schmidt, P., Braslavsky, S. E., Gärtner, W., and Schaffner, K. (1999) Differential effects of mutations in the chromophore pocket of recombinant phytochrome on chromoprotein assembly and Pr-to-Pfr photoconversion. *Eur. J. Biochem.* **266**, 201-208

Acknowledgements

The authors like to thank Norbert Dickmann and Petra Gnau for technical assistance. This work was supported by grants of the Deutsche Forschungsgemeinschaft (ES152/9, ES152/10). A.G. and W.G. thank the Max-Planck-Society for generous support.

Abbreviations

The abbreviations used are: GAF, cGMP phosphodiesterase/adenylyl cyclase/FhlA; PCB, phycocyanobilin; PAS, period/ARNT/single-minded; PHY, phytochrome; CBCR, cyanobacteriochrome; LADS, lifetime-associated difference spectra

Figure legends

Fig. 1: Structure of *Syn*Cph2(1-2) (PDB code: 4BWI) including the positions of the mutations in the tongue region and absorbance UV/Vis spectra of the variants. (*A*) Structure of *Syn*Cph2(1-2) with a detailed view of the chromophore binding pocket (inlay). The GAF1 domain is displayed in orange, the GAF2 domain with the tongue region in green, respectively. The PCB chromophore is shown in cyan. Amino acid positions Ser-385 and Trp-389 as well as the cofactor binding Cys-129 are displayed in sticks presentation. The residues of the conserved PRxSF motif are depicted as spheres. (*B*) Steady state UV/Vis absorbance spectra of *Syn*Cph2(1-2) and the variants S385A, W389A and W389F as shown in (8) after far red (P_r state, black line) and red light illumination (red line). Difference spectra are calculated with $A_{Pr} - A_{Photoequilibrium}$ and shown in blue. A calculated pure P_{fr} spectrum for *Syn*Cph2(1-2) is presented in green (9).

Fig. 2: Single time traces of the *Syn*Cph2(1-2) $P_r \rightarrow P_{fr}$ transition measured at 665 nm. Here, the intermediates show alternately lower or higher absorbance than the P_r reference state and can be observed without further data analysis. (*A*-*D*) shows the time traces with increasing time scales; the approximate appearance of intermediates is indicated by arrows. The intermediate lifetimes are also presented. The final intermediate R3 exhibits similar absorption than the P_{fr} conformation (*D*). The initial ten percent of the time traces prior to the laser pulse are recorded to determine the baseline level; at t = 0 the laser flash triggered the photoconversion. (*E*) The individual time traces (*A*) to (*D*) were assembled. Here, the fit of the resulting data is shown in green as well as the residuals (below).

Fig. 3: Lifetime-associated difference spectra (LADS) of *Syn*Cph2(1-2) (top panel) and its S385A (middle) and W389A variant (bottom) in the respective $P_r \rightarrow P_{fr}$ (left) or $P_{fr} \rightarrow P_r$ (right) transition. The lifetimes of the intermediates are shown in the inlays. The constant difference spectrum (green) reflects the subtraction of the starting state absorbance spectrum from the final state that should correspond to the difference between P_r and P_{fr} ($P_r \rightarrow P_{fr}$ transition: $\Delta Abs = A(P_{fr}) - A(P_r)$). The other LADS show the subtraction of the intermediate spectrum from the previous intermediate spectrum ($P_r \rightarrow P_{fr}$ transition: ΔAbs = A(Intermediate1) – A(Intermediate2)). A positive absorbance difference in the LADS reflects an absorbance decay from the last to the considered intermediate, a negative signal an absorbance increase.

Fig. 4: Single time traces of the *Syn*Cph2(1-2) $P_{fr} \rightarrow P_r$ transition measured at 640 nm. The absorbance difference between the intermediates is not as high as in the forward reaction. In (*A*-*D*) the single time traces with increasing time scales are shown as well as the assignment of the absorbance differences to the intermediates and their lifetimes. As in the forward reaction, the formation of the first intermediate Lumi-F is too fast for the resolution of these measurements. (*E*) Fit of the assembled data from (*A*) to (*D*) (green) and its residuals.

Fig. 5: Single time traces of the *Syn*Cph2(1-2) W389F $P_r \rightarrow P_{fr}$ transition measured at 665 nm. (*A*-*D*) shows the single time traces with increasing time scales that are similar to *Syn*Cph2(1-2). The intermediates with their lifetimes are indicated by the arrows. The lifetimes were calculated *via* fitting of the single time traces and are averaged over the different observed wavelengths.

Fig. 6: *A:* Photocycle of the Group II phytochrome *Syn*Cph2(1-2) (black lines) and its S385A (green) and W389A (red) mutants. Rounded rectangles highlight the ground state P_r and the P_{fr}- or P_{fr}-like states. Circles indicate the intermediates of the *Syn*Cph2(1-2) photocycle. The lifetimes of the wild type

intermediates are shown next to them in blue. Arrows indicate deviations from the native photocycle as caused by mutations within the tongue region. The corresponding intermediates are depicted with stars. *B:* Photocycles of Group I phytochromes. Only a minimal model is shown for the photocycle of plant phytochromes (top). The photocycle of CphA, another Group I phytochrome, from the cyanobacterium *Calothrix* sp. PCC7601 (18) includes the lifetimes of the observed intermediates (blue) as obtained by a procedure comparable to *Syn*Cph2(1-2).

TABLES

Table 1: Intermediate lifetimes of *Syn*Cph2(1-2), S385A, W389A, and W389F photocycles. The lifetimes of *Syn*Cph2(1-2), S385A and W389A are calculated *via* global fit analysis. The lifetimes of W389F are averages from fits of single time traces. The lifetimes of the first two intermediates of the $P_{fr} \rightarrow P_r$ photoconversion of W389F could not be derived (n.a.: not available) due to the low absorbance changes between its early intermediates.

Table 1:

		Wild type	**S385A**	**W389A**	**W389F**
P_r to P_{fr}	**Lumi-R:**	1.3 µs	1.3 µs	1.4 µs	1.5 µs
	R1:	299 µs	112 µs	414 µs	380 µs
	R2:	2.56 ms	1.57 ms	2.28 ms	2.0 ms
	R3:	17.1 ms	8.10 ms		33.3 ms
P_{fr} to P_r	**Lumi-F:**	0.9 µs	1.3 µs	1.2 µs	n.a.
	F1:	798 µs	619 µs	2.21 ms	n.a.
	F2:	6.20 ms	3.53 ms	19.5 ms	3.1 ms

Photocycle of cyanobacterial phytochrome *Syn*Cph2(1-2)

Figures

Fig. 1

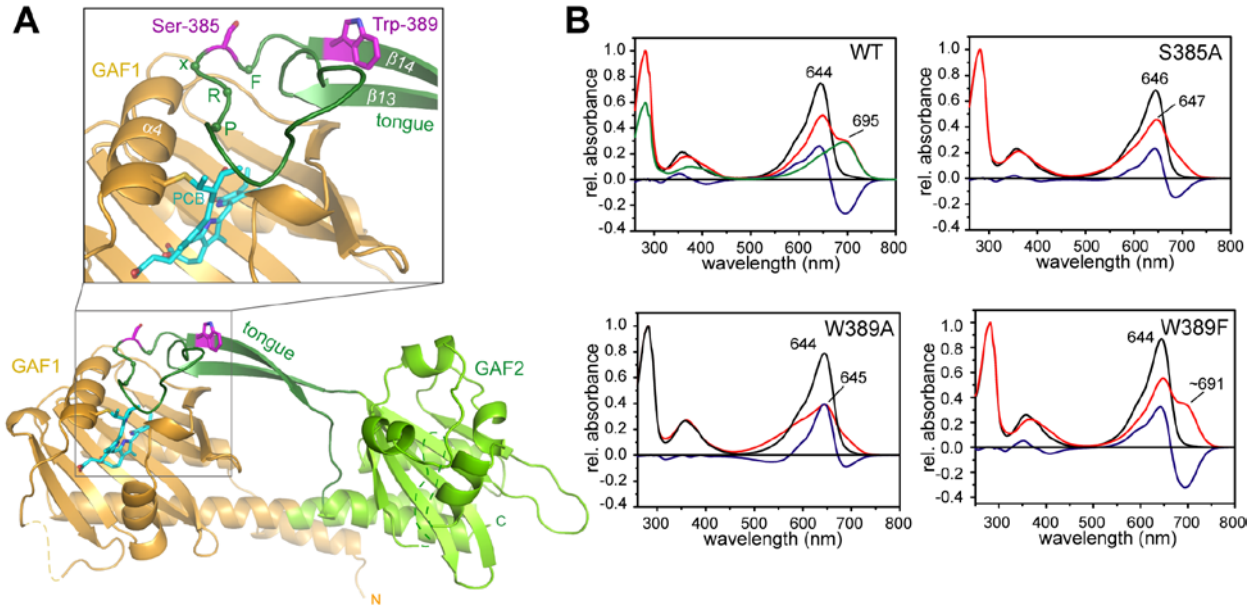

Fig. 2:

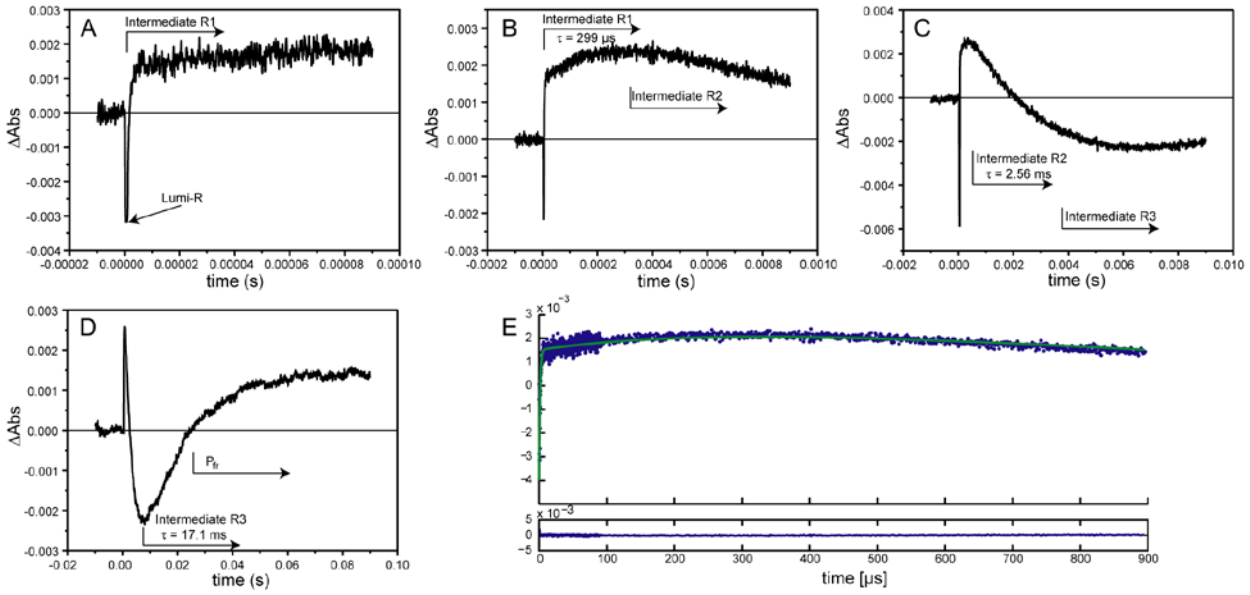

Fig. 3

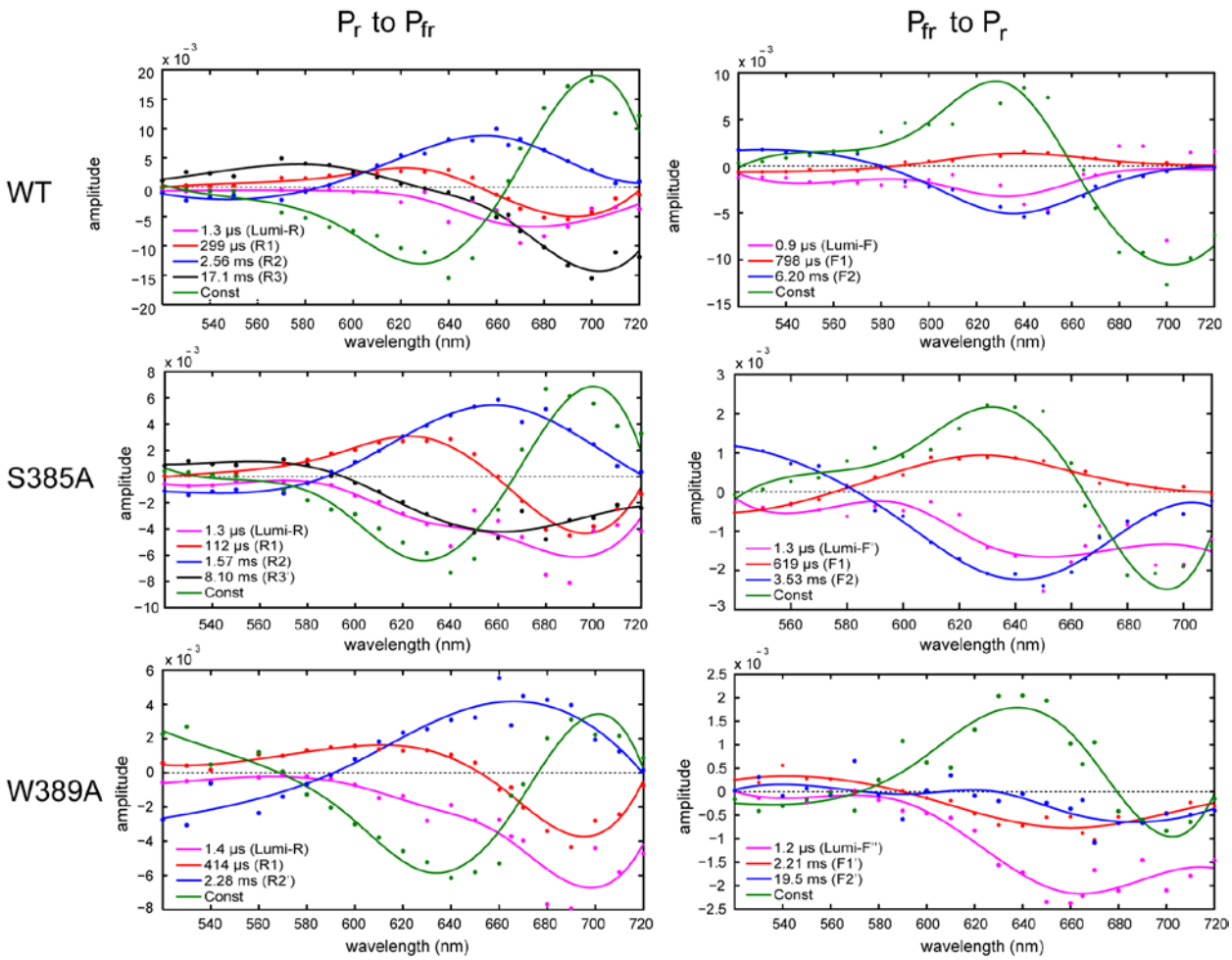
Pr to Pfr
Pfr to Pr
WT
S385A
W389A
amplitude
wavelength (nm)
1.3 µs (Lumi-R)
299 µs (R1)
2.56 ms (R2)
17.1 ms (R3)
Const
0.9 µs (Lumi-F)
798 µs (F1)
6.20 ms (F2)
112 µs (R1)
1.57 ms (R2)
8.10 ms (R3')
1.3 µs (Lumi-F')
619 µs (F1)
3.53 ms (F2)
414 µs (R1)
2.28 ms (R2')
1.4 µs (Lumi-R)
1.2 µs (Lumi-F'')
2.21 ms (F1')
19.5 ms (F2')

Fig. 4:

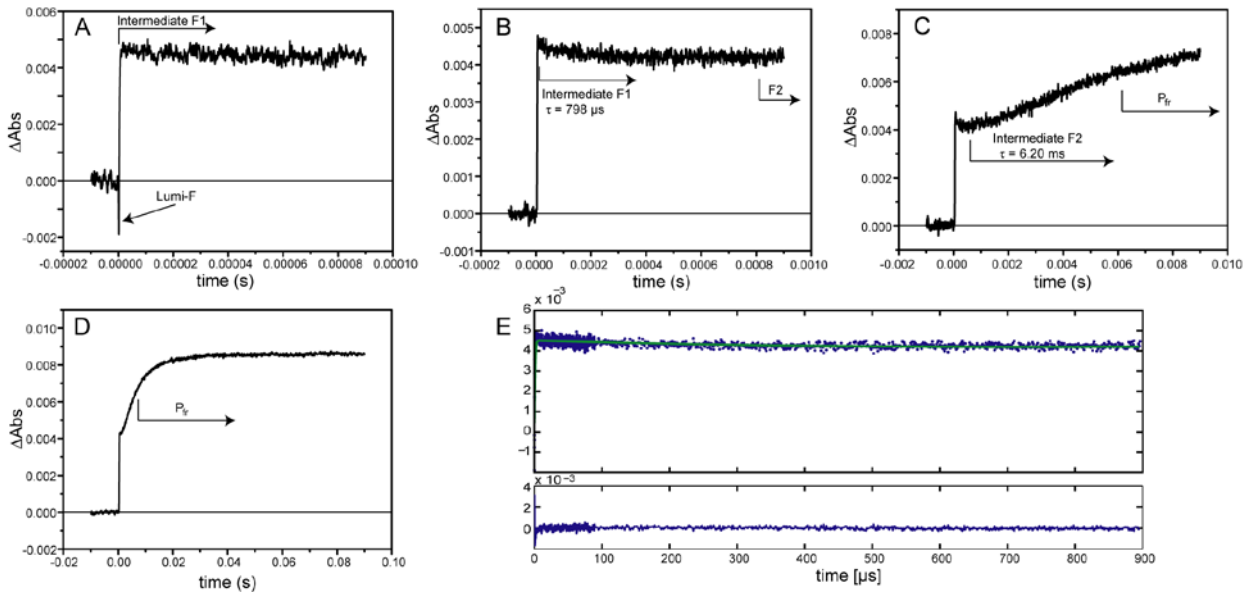
A
Intermediate F1
Lumi-F
B
Intermediate F1
τ = 798 µs
F2
C
Intermediate F2
τ = 6.20 ms
Pfr
D
Pfr
E
ΔAbs
time (s)
time [µs]

Photocycle of cyanobacterial phytochrome *Syn*Cph2(1-2)

Fig. 5:

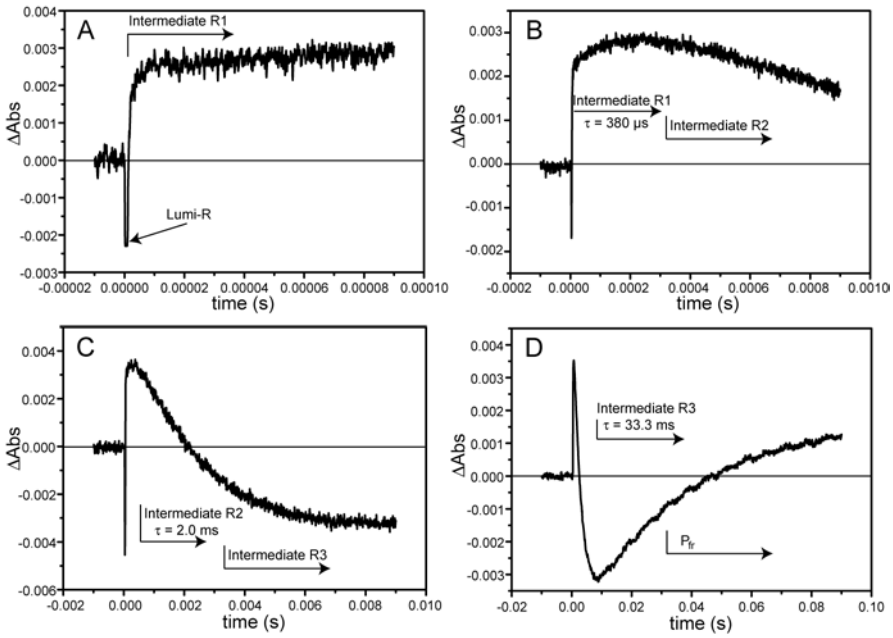

Fig. 6

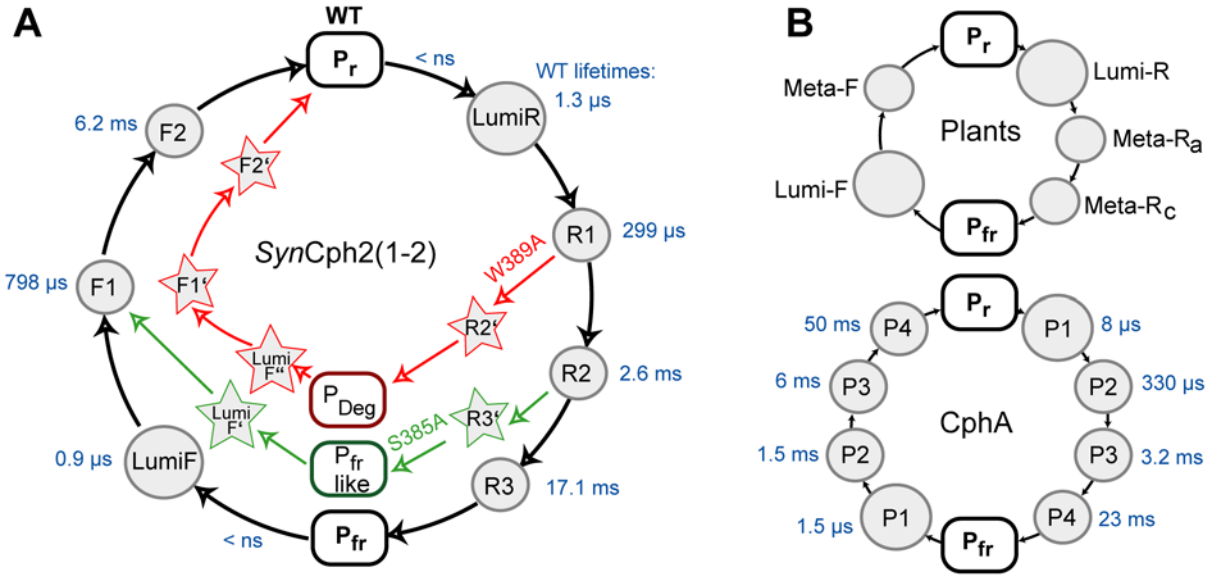

6 Discussion

6.1 Biliproteins - spectral diversity with one chromophore

The bilin chromophore enables GAF-containing photoreceptors like phytochromes and CBCRs to cover most ranges of the visible light spectrum. Just retinal-dependent rhodopsin photoreceptors of animals and especially of shrimps exhibit a comparable wide absorbance range[140] [141] in contrast to other photoreceptor chromophores (see Fig. 3.1). Fig. 6.1 shows an analysis of the spectral characteristics from biochemically characterized phytochromes and CBCRs. BV-binding phytochromes can be found (with one exception, see below) in the 750 nm range of the *15E*-state and are thus the most red-shifted GAF-containing photoreceptors. This is caused by the additional double bond in the π-system of BV in comparison to other phytochrome chromophores (see Fig. 3.2). Interestingly, all known bathyphytochromes (bathy-BphPs), that form P_{fr} as ground state, belong to the group of BV-binding phytochromes. Accordingly, an involvement of BV in the change of the ground state cannot be ruled out. Relative to these phytochromes PΦB binding plant phytochromes are blue shifted in their *15Z*- and *15E*-states. This effect is further enhanced in PCB-binding phytochromes of Group I. Group II phytochromes also bind PCB and display the most far-ranging blue shift in the absorbance maxima, especially in the P_r state[88,138]. The N-terminal photosensory module *Syn*Cph2(1-2) is a Group II phytochrome that is the name-giving representative of this group[8]. As other Cph2-phytochromes[88] it exhibits a blue-shifted absorbance[138].

Two unusual phytochromes of Group I demonstrate that a versatile spectral characteristics has not to be limited to CBCRs. The exceptional, *via* lateral gene transfer acquired, bacteriophytochrome *Br*BphP3 of the aerobic photosynthetic bacterium *Bradyrhizobium* sp. proves that phytochromes can exert other photochemistry than exhibit red / far red photoconversion. This phytochrome photoconverts between a *15Z* P_o and a *15E* P_r conformation and thus exhibits despite PAS-GAF-PHY architecture and the binding of a PCB chromophore an extremely blue-shifted absorbance[67]. This outstanding behavior is caused by an unusual high entropy of the P_o state. The authors suggest that the binding site of *Br*BphP3 sets reduced constraints to the chromophore. This could be the reason why the P_o absorbance spectrum resembles that of free PCB although the chromophore is covalently attached. The *15E*-state resembles the P_r conformation of BphPs but is in con-

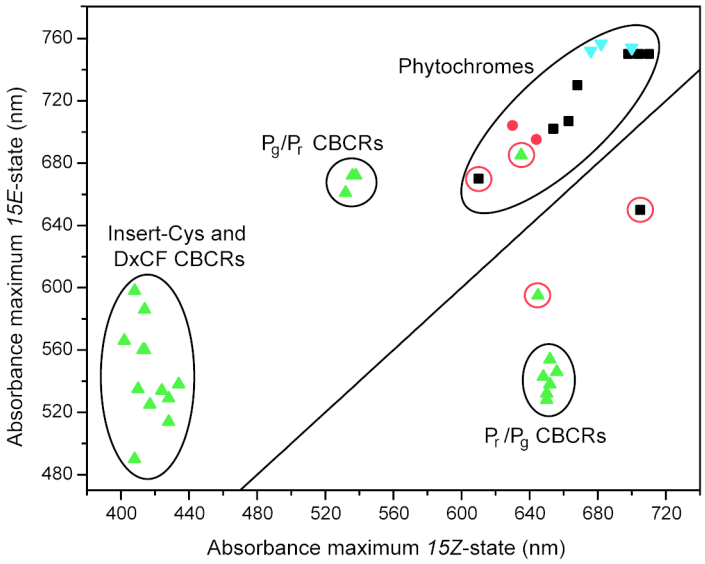

Figure 6.1: Absorbance maxima of the *15Z*- and *15E*-states from spectroscopically characterized photosensory modules from GAF-containing photoreceptors of Group I - III. Black squares represent Group I phytochromes that have a PAS-GAF-PHY photosensory architecture; cyan colored triangles show bathy-BphPs with a P_{fr} ground state that also belong to this group. Red dots indicate members of Group II, Cph2-like phytochromes; and green triangles represent members of Group III, the CBCRs. The black line is a diagonal in the wavelength scale (x = y). Black frames show the assignment of the proteins to families, red circles indicate unusual CBCRs or phytochromes. Further information about the proteins, their organisms, the group assignments, the chromophores and the designation as well as absorbance maxima of their *15Z*- and *15E*-states are shown in Section 9.1, Table 9.1.

trast to classical P_r states[142] non-fluorescent[67].

The second unusual phytochrome is *Rp*BphP3 from *Rhodopseudomonas palustris* that binds BV and photoconverts between a *15Z* P_r and a *15E* P_{nr} state (Fig. 6.1). The latter is blue-shifted by 55 nm compared to P_r, which demonstrates, that the *15E*-state in phytochromes is not necessarily the long-wavelength state. The authors suggest that this may be caused by a shortened π-system induced by a D-ring distortion[143]. A *15Z* long-wavelength state is also achieved in P_r/P_g CBCRs, a similar photoconversion mechanism of *Rp*BphP3 as in this family is possible.

The distribution of CBCRs with different absorbance properties is shown in Fig. 6.1. P_g/P_r and P_r/P_g CBCRs are located in small areas of *15Z* / *15E* absorbances; insert-Cys and DxCF CBCRs are distributed in a *15Z*-absorbance range of 400 - 440 nm, but exert a more varied absorbance of the *15E*-state in the 480-600 nm range. There are also some unusual proteins in the CBCR family like AphC(GAF1) from *Nostoc* sp. PCC 7120 which exhibits a phytochrome-like P_r/P_{fr} photochemistry but is eventually part of a Group II module and AphC(GAF3) of the same protein that shows P_r/P_o photoconversion with a

long-wavelength *15Z*-state[116].

The GAF3 domain of *Syn*Cph2 is a blue/green absorbing CBCR. Its spectral characteristics suggest that it belongs to the dual-Cys CBCRs[126] that use two cysteine residues for the chromophore binding. As *Syn*Cph2(5-6) contains a DxCF motif[144] and can isomerize the chromophore PCB to PVB[145] it can be clearly assigned to the group of DxCF CBCRs within the dual-Cys family[115]. A possible photocycle for this family was proposed[127] (Fig. 3.16) that involves the second covalent attachment of the chromophore between *C10* and a cysteine residue in the *15Z*-state and a phytochrome-like *Z/E* isomerization.

The absorbance properties of GAF-containing photoreceptors depend on the chromophore and its protein environment. Besides double bond isomerization, its protonation state has an effect on the spectral characteristics of the bilin chromophore. Studies on PCB in chloroform show that protonation red-shifts the visible absorption peak by 57 nm[146] which can be observed in other model compounds as well[147][148]. In addition, conformational changes of the chromophore have an effect on its absorbance characteristics. *Syn-anti* rotations in bilins, like from closed (*sss*) to open (*e.g. asa*) conformations, lead to a blue-shift of the absorbance. This is caused by the pyrrole rings that are twisted out-of-plane because of steric reasons and force the π-system to remain strictly localized[149]. Also slight conformational changes of the chromophore are important as planarity induces a red-shift because the π-electron system becomes maximally delocalized. Besides protonation and conformational changes, different chromophores with shorter or longer π-systems like PCB *vs.* BV, have an impact on absorbance properties. Also the surrounding amino acids influence the spectral characteristics[139] (Section 6.3).

In CBCRs spectral tuning is accomplished by protonation[150] and the formation of a second thioether linkage to the chromophore that results in a shortening of the π-system[127]. Furthermore, an isomerization of the chromophore can change the absorbance properties as PVB can be formed from PCB[111].

*Syn*Cph2(1-2) shows a blue-shifted absorbance spectrum in comparison to Group I phytochromes. This does not result from a different protonation state since we could demonstrate that all four pyrrole rings are protonated in the P_r as well as in the P_{fr} state[138] which is observed for other PCB-binding phytochromes, too[38]. The blue-shift in *Syn*Cph2(1-2) might be caused by the missing PAS domain in comparison to Group I phytochromes. Fig. 6.2 shows the protein surfaces of *Syn*Cph2(1-2) and *Syn*Cph1 (PDB codes of all phytochrome and CBCR structures: Section 9.2, Table 9.2). In the latter, the chromophore is nearly completely covered by the N-terminal helix of the PAS domain, the GAF and by the tongue region of the PHY domain, whereas in *Syn*Cph2(1-2) the PCB chromophore is solvent-exposed at rings A and B due to the missing PAS domain[139]. Apart from possible absorbance changes due to the differences between protein surrounding and partial solvatization of PCB in both proteins, the missing PAS domain leads to a higher flexibility

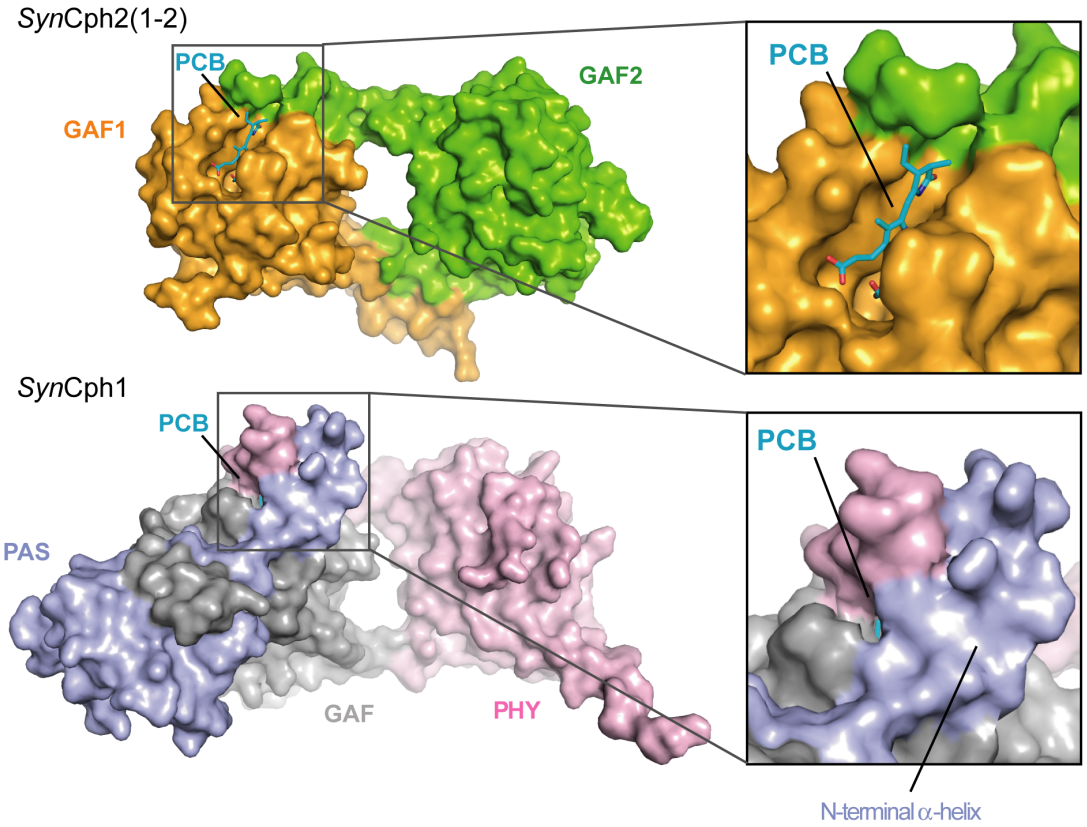

Figure 6.2: Differences in the solvent exposure of the chromophores in *Syn*Cph2(1-2) (above) and *Syn*Cph1 (below) (PDB codes: Section 9.2, Table 9.2). The GAF1 and GAF2 domains of *Syn*Cph2(1-2) are displayed in orange and green, respectively. PAS, GAF and PHY of *Syn*Cph1 are shown in blue, gray and purple. The PCB chromophore of both proteins is presented in cyan. The inlets show a magnification of the PCB binding site. In the inlet of *Syn*Cph1, the N-terminal α-helix of the PAS domain is highlighted.

within the chromophore due to less sterical restrictions. Like in the *Br*BphP3 protein[67] this could lead to a significant blue-shift as the higher flexibility may result in a shortened π-system.

Another reason for the blue-shifted absorbance of *Syn*Cph2(1-2) could be that one or two pyrrole rings are twisted out-of-plane so that the π-electrons are not delocalized over the whole chromophore any more. In the crystal structure of *Syn*Cph2(1-2) the PCB chromophore exhibits large tilts between rings B and C as well as between rings C and D (A-B: 19.2°, B-C: 32.5°, C-D: 59.8°). The tilt between the B- and C-ring is the largest observed for phytochromes and PCB-binding phycobiliproteins. We were able to demonstrate that the large twist is not caused by X-ray radiation damage but is enforced by the protein matrix[139]. As *Syn*Cph2(1-2) crystals exhibit solution-like UV/vis absorbance and RR spectra, it can be assumed that this chromophore conformation is also the native one in solution. A comparable tilt between rings B and C can be observed in an NMR (**N**uclear **M**agnetic **R**esonance) structure of *Sy*B-Cph1(GAF) that shows a comparable

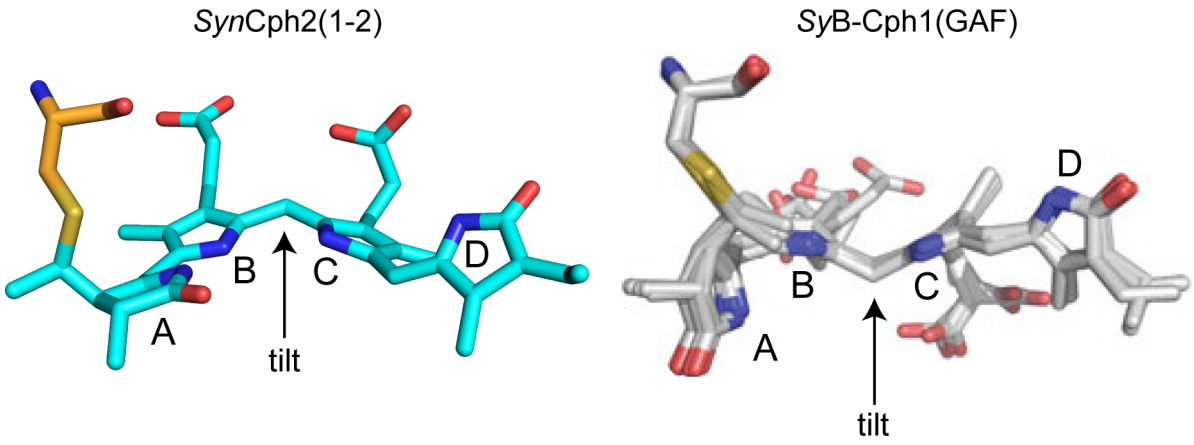

Figure 6.3: Tilted PCB chromophores covalently attached to the cysteine in the P_r conformation of the *Syn*Cph2(1-2) structure (left) and the five lowest energy NMR conformers of *Sy*B-Cph1(GAF) (PDB code: 2KOI)[91]. The large tilt between rings B and C is indicated by an arrow.

blue-shifted absorbance (Fig. 6.3)[91]. The GAF1 domain of this Cph2-type GAF-PHY domain protein shows photoconversion to a P_{fr}-like state that is blue-shifted by 15 nm compared to the GAF-PHY domain protein[88]. Interestingly, in the RR spectra of the GAF1 protein but not in the GAF-PHY protein the predominant feature for the P_{fr} state, the C-H out-of-plane (HOOP) mode of the C-D methine bridge, is missing thus implying a non-native chromophore in the GAF-only protein[138]. A preliminary NMR study of *Sy*B-Cph1(GAF) (PDB code: 2K2N) revealed nearly coplanar B and C rings, a 20° rotation of ring A and a 80° rotation of ring D relative to the rings B and C[90]. In the subsequent NMR study of the same protein (PDB code: 2KOI (P_r), 2KLI (P_{fr})) the tilted structure was observed[91]. Apart from the twist between rings B and C an unusual A-ring conformation occurred; the A-ring is nearly perpendicular to the B and C rings (Fig. 6.3). The authors suggest that during photoconversion ring A rotates instead of ring D[91]. These results were recently refuted in another NMR study[151] which proves that ring A does not photoflip although major changes at the covalent linkage to the cysteine can be observed. The D-ring rotates upon photoconversion but is strongly tilted in both states. Due to the missing PHY domain the authors suggest that the P_{fr} formation cannot be reached and the protein remains in a bleached Meta-R-like state upon red-light illumination[151]. A structural study of the complete photosensory module from *Sy*B-Cph1 would reveal the native-like P_r conformation of PCB in this protein. This could answer the question if the highly tilted chromophore is a general feature of Cph2-type phytochromes and hence responsible for their blue-shifted absorbance.

6.2 The knotless structure of *Syn*Cph2(1-2)-a comparison

We were able to solve the structure of *Syn*Cph2(1-2) in the P_r conformation at a resolution of 2.6 Å[139]. A detailed analysis of the structure and a comparison to *Syn*Cph1 is included in Ref.[139]. The GAF-GAF bidomain module of *Syn*Cph2(1-2) crystallizes as an antiparallel dimer and shares characteristics with the GAF-PHY domain module of Group I phytochromes. For example, the GAF1 domain, where the chromophore is covalently attached, is linked *via* a long α-helical linker to the GAF2 domain. The latter mimics

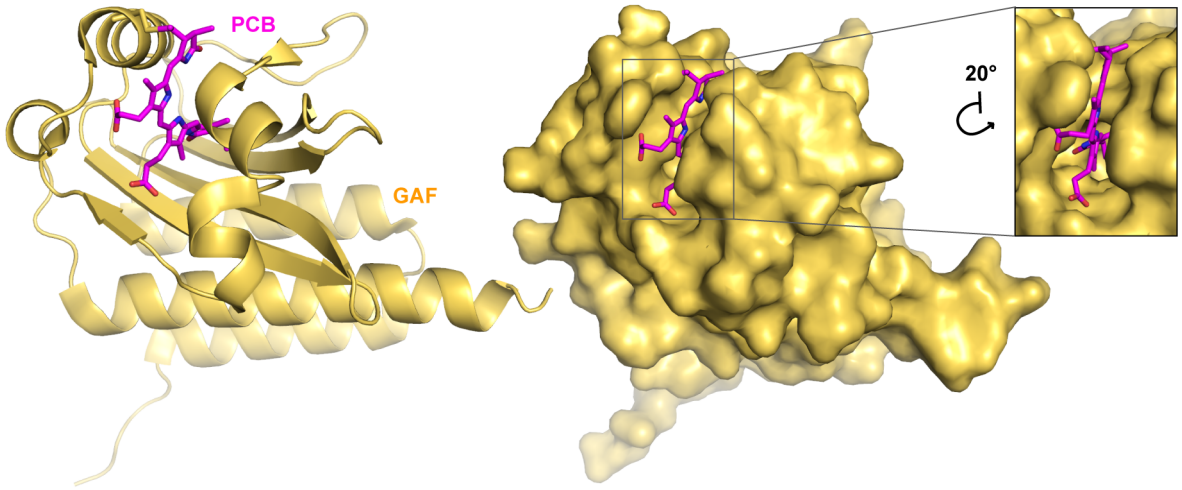

Figure 6.4: Structure of the second GAF domain from *An*PixJ reveals a solvent-exposes chromophore (PDB code: 3W2Z). **Left:** the GAF domain and the PCB chromophore are displayed in yellow and magenta, respectively. **Right:** Protein surface of *An*PixJ. The magnification illustrates the solvent exposure of the chromophore.

canonical PHY domains by protruding a tongue-like extension that reaches to the GAF1 domain and contacts the PCB-binding pocket. Regarding the known Group I structures (Fig. 3.9) of *Syn*Cph1[10,84], *Pa*BphP[11,86], *Rp*BphP1[69], *Rp*BphP3[83] and *Dr*BphP[13,152] (see also PDB code: 4IJG) as well as the Group II structure of *Syn*Cph2(1-2)[139] these structural features seem to be mandatory for the two groups. CBCR photosensory modules on the other hand lack these characteristics as here one single GAF domain suffices to gain a functional photochemistry[8]. Due to the missing PAS and PHY domains the chromophore is even more solvent-exposed than in *Syn*Cph2(1-2) as shown for *An*PixJ-GAF2[122] (Fig. 6.4, in contrast to Fig. 6.2). A comparison of the GAF domains from Group I - III (Fig. 6.5) shows that all GAF domains of Group I exhibit nearly the same architecture, including also the bathy-BphP structures. Even the loop lengths and orientations do not differ very much. In Group III the GAF domains of *An*PixJ-GAF2 and *Te*PixJ (*15Z*) show a high similarity, whereas the structure of *Te*PixJ (*15E*) (Fig. 6.5 C, salmon pink) differs. A superimposition of representatives of Groups I - III (Fig. 6.5 D) demonstrates the differences in the GAF domains. For example, the helix orientations diverge, especially of the α-helix binding the

chromophore in non-BphPs that is distinctly oriented in Group I, II and III photoreceptors (Fig. 6.5 D, upper inlet). In addition, loop regions at the end of the β-sheet and above the chromophore binding site differ. The latter is shown in the upper inlet of Fig. 6.5 D. Here, Group I-II phytochromes build a short helix that includes the conserved DIP motif (Sub-

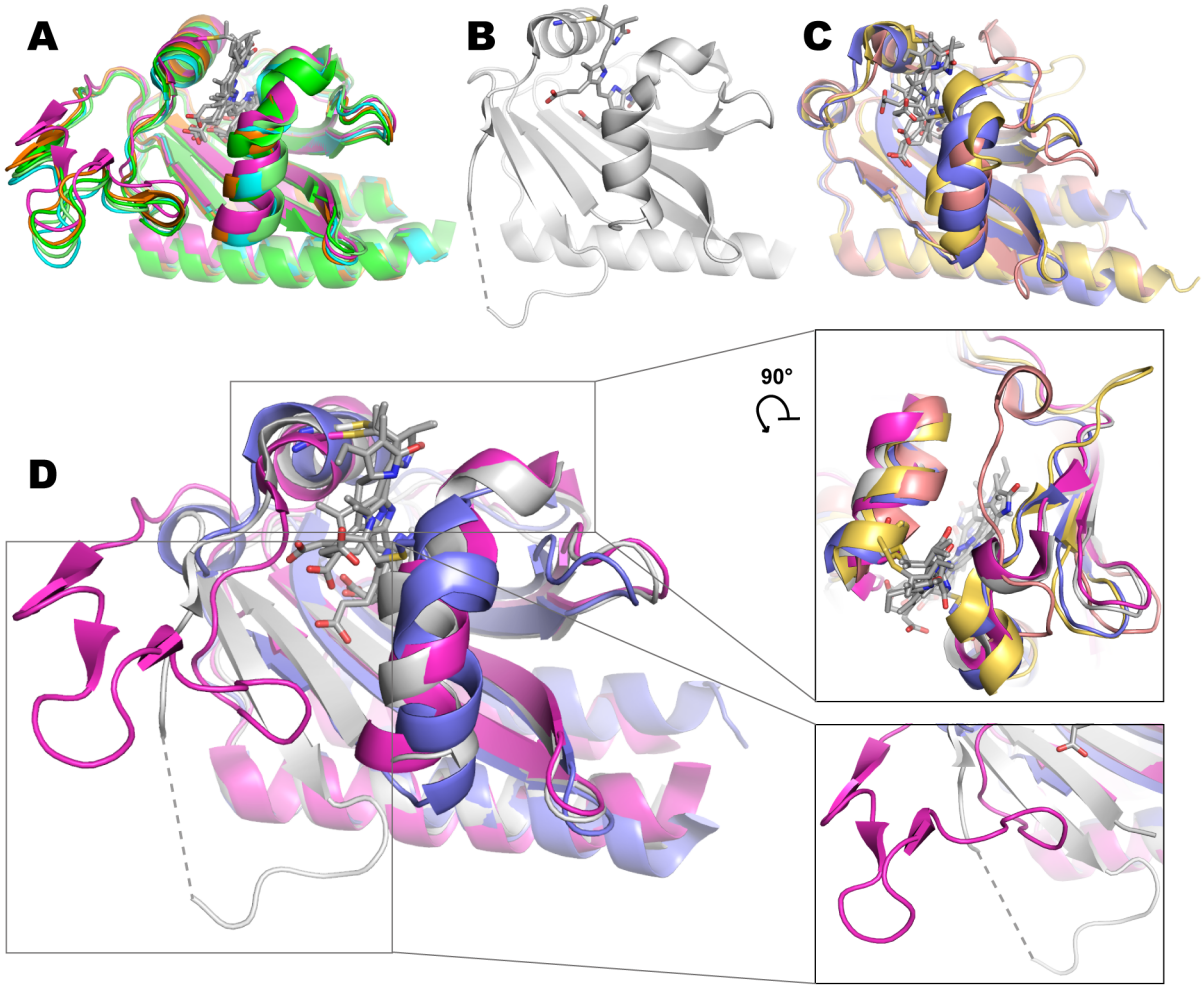

Figure 6.5: Comparison of the GAF domains from Group I, II and III photoreceptors. The Group I phytochromes *Syn*Cph1 (2VEA), *Pa*BphP (3NHQ), *Rp*BphP1 (4GW9) and *Dr*BphP (2O9C and 4IJG) are displayed in magenta, dark green, orange, cyan and light green, respectively. The Group II phytochrome *Syn*Cph2(1-2) (4BWI) is gray and the Group III CBCRs *Te*PixJ (*15Z*, 4GLQ), *Te*PixJ (*15E*, 3VV4) and *An*PixJ (3W2Z) are shown in blue, salmon pink and yellow. The chromophores are displayed in gray. **A:** Superimposition of GAF domains from the Group I phytochromes. **B:** GAF1 domain of *Syn*Cph2(1-2) that is a Group II phytochrome. **C:** Overlay of Group III GAF domains. **D:** Superimposition of *Syn*Cph1 (Group I), *Syn*Cph2(1-2) (Group II) and *Te*PixJ (*15Z*) (Group III); the inlets illustrate differences between the GAF domains. The upper inlet displays a magnification of the chromophore binding site regarded from the top. In addition also *An*PixJ and *Te*PixJ (*15E*) are shown in this inlet. The lower inlet shows the knot-forming loop region in Group I phytochromes at the end of the β-sheet in the GAF domain.

section 6.3.3). The aspartate of this motif is part of a salt bridge in Group I and II phytochromes that connects the tongue region of the PHY (GAF2) domain with the GAF (GAF1) domain, the course of the following loop/β-strand region is similar in both groups. In CBCRs the DIP motif helix is missing, the subsequent loop regions are more shifted towards the PCB-binding α-helix thus narrowing the cleft that leads to the bilin binding site which is otherwise blocked by the missing PHY domain. In *Te*PixJ (*15E*)[123] (Fig. 6.5 C, salmon pink) this loop region is so shifted that it nearly closes the cleft. The other striking difference in Group I - III GAF domains is the knot-forming loop at the end of the β-sheet (Fig. 6.5 D, lower inlet). As in Group I phytochromes the N-terminal helix of the PAS domain threads through this loop, it shows an elongated architecture in this group. *Syn*Cph2(1-2), a Group II phytochrome and therefore PAS-less, possesses a shortened loop region that contains in comparison to Group I and III an additional β-strand elongating the β-sheet. In CBCR GAF domains this region is maximally shortened as it directly leads to the chromophore-binding α-helix.

The tongue region of Group I and Group II phytochromes differs in the known four structures of *Syn*Cph1, *Syn*Cph2(1-2), *Pa*BphP and *Rp*BphP1 that include the PHY or GAF2 domain, respectively. Here, bathy- and non-bathy phytochromes comprise different tongue architectures including also the secondary structure elements. *Syn*Cph2(1-2) and *Syn*Cph1 share the β-strand stem region that spans between the GAF2 (PHY) and GAF1 domain. The positions as well as the amino acid orientation of the $W^G/_AG$, PRxSF and WxE motifs are conserved between the two phytochromes although *Syn*Cph2(1-2) does not

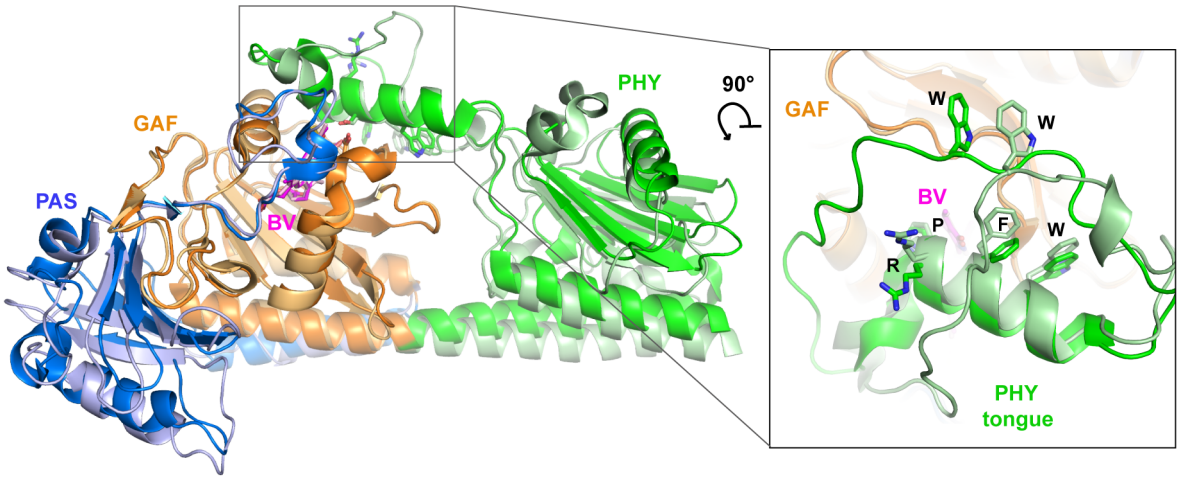

Figure 6.6: In the bathy-BphPs *Pa*BphP (PDB code: 3NHQ) and *Rp*BphP1 (PDB code: 4GW9) the secondary structures of the tongue region are conserved; a superimpositions of the GAF domains (r.m.s. deviation = 0.740 Å for 156 C_α) is shown. PAS, GAF and PHY domains are displayed in blue, orange and green, respectively. The BV chromophore is colored in violet. Pale and rich colors belong to *Rp*BphP1 and *Pa*BphP, respectively. Conserved amino acids are highlighted. The inlet shows a magnification of the tongue region from above.

contain a PHY but an additional GAF domain (see Ref.[139]: Fig. 7B). Interestingly, in both bathy-BphP structures the stem region is built of an α-helix and a loop region. The positions of the $W^{G}/_{A}G$ and PRxSF motifs in the α-helix are conserved in bathy-BphPs but the pointing direction of the amino acids differs from the *Synechocystis* phytochromes (Fig. 6.6). The serine - aspartate salt bridge that stabilizes the GAF - tongue interface is conserved in the two proteins. The position of the tongue's loop region is altered in *Pa*BphP and *Rp*BphP1 but the WxE motif is nearly in the same place.

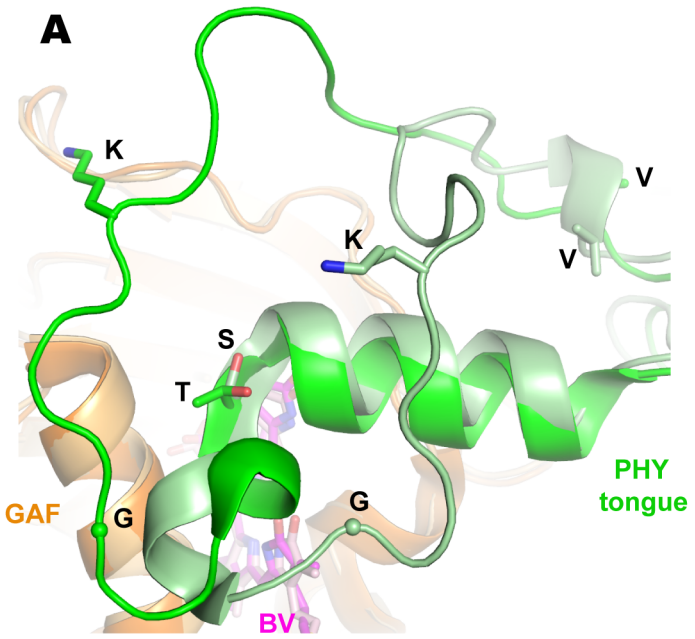

B

```
RpBphP1    458 PERVHTVTWGGDPKKPFTMG--DTPADLSPRRSFAKWHQVVEGTSDPWTA
BrBphP     442 PEQVRTVTWGGDPLKAVIIG--DDPSDLSPRRSFAQWHQLVEGKSEPWSP
AtBphP2    432 KEIVQNLNWAGNPEKSYETG--PMGDRLTPRKSFAIWKETVRLQAQPWSE
PaBphP     429 HEEVHRIRWGGKPEKLLTIG--PSGPRLTPRGSFEAWEEVVRGHSTPWSE
SynCph1    442 PEVLQTVNWGGDPNHAYEATQEDGKIELHPRQSFDLWKEIVRLQSLPWQS
SynCph2    361 KEKSLVKHWAGKR--------GIDRRNILPRLSFEAWEET-QKLVPTWNR
```

Figure 6.7: Additionally conserved amino acids in the bathy-BphP tongue region in comparison to *Syn*Cph2 and *Syn*Cph1. **A:** Tongue region of *Pa*BphP (rich colors) and *Rp*BphP1 (pale colors), BV as well as the GAF domain and the tongue region of the PHY domain are displayed in violet, orange and green, respectively. Additionally conserved amino acids are shown in stick representation; glycines are highlighted by spheres. **B:** Alignment in the tongue region of *Syn*Cph1 (YP_005652297.1) and *Syn*Cph2 (BAA10536.1) as well as the bathy-BphPs *At*BphP2 (NP_355125), *Br*BphP (YP_001203744.1), *Rp*BphP1 (YP_001990729.1) and *Pa*BphP (NP_252806.1). The secondary structures were predicted by the PsiPred server[153]. Orange and red letters refer to the predicted secondary structures β-strand and α-helix, respectively. Orange and red boxes show observed strands or helices in the crystal structures of *Pa*BphP, *Rp*BphP1, *Syn*Cph1 and *Syn*Cph2. Black boxes highlight amino acids that are conserved in bathy-BphPs but not in *Syn*Cph1 and *Syn*Cph2.

A phylogenetic analysis of phytochromes based on their GAF domains reveals five bathy-BphPs that are located on different branches of the tree[68] (Fig. 3.17 B). Their different positions indicate that the primary structure requirements to establish a P_{fr} ground state are not solely located in the GAF domain although mutations in the latter can cause the alteration of the ground state from P_{fr} to P_r (Section 6.3). Instead of the GAF domain rather the PHY domain and especially the tongue region could be held responsible for the P_{fr} ground state formation. The PHY domain was found to stabilize the P_{fr} conformation[22] [23] and provides functional photochemistry[68]. In the bathy-BphP *At*BphP2 from *Agrobacterium tumefaciens* (also: Agp2) a truncation of the PHY domain leads to a non-photochromic protein that fails to form a dark-adapted P_{fr} state but generates a bleached P_r-like state[68,154]. In *Pa*BphP alanine substitutions of Ser-459 and Arg-453 in the tongue region, that are involved in a hydrogen bond network with the aspartate of the DIP motif in the GAF domain, destabilize the P_{fr} state and establish P_r as ground state[11]. As the P_{fr} stabilization of PHY or more precisely of the tongue region was shown for bathy- and non-bathy phytochromes, there must be different interactions in both families that stabilize the respective ground state. On the one hand all known bathy-BphPs harbor BV as chromophore which seems to be a mandatory requirement. BV comprises an additional double bond in the A-ring and thus an elongated π-system. Also the thioether linkage is built to $C3^2$ and not to $C3^1$ as in PΦB and PCB (Fig. 3.2). Nevertheless, no further stabilizing interactions to the A-ring can be observed that would explain this chromophore selectivity in bathy-BphPs. On the other hand, the tongue region of the latter comprises more conserved amino acids than in other phytochromes (Fig. 6.7). The sequence alignment of four bathy-BphPs reveals that the tongue's tip, *i.e.* the loop region of the tongue (region between $W^G/_A G$ and PRxSF motif) has exactly the same length in the observed bathy-BphPs in contrast to other phytochromes where is shows more variation[10]. Secondary structure predictions indicate that the α-helical arrangement of the PRxSF and WxE motif is conserved among bathy-BphPs (Fig. 6.7 B). However, also for *Syn*Cph1 an α-helix in this region was predicted that forms instead a β-strand at the WxE motif in the crystal structure[10]. Interestingly, four amino acids, valine, lysine, glycine, and serine/threonine are conserved in the bathy-BphP tongue region that are absent in other phytochromes (Fig. 6.7). These residues have no further interactions in the P_{fr} state and besides the glycine, that is located in a bended region, the function of these amino acids remains elusive. In the crystal structures of *Pa*BphP and *Rp*BphP1 the kink regions do not overlay but the positions of the conserved amino acids hint towards a possible flapping of the kink region. Due to the conserved lysine and glycine residues this might reflect a mechanism that could be involved in photoconversion.

6.3 *Syn*Cph2(1-2) - chromophore surroundings, as usual?

In this section the binding of the chromophore from *Syn*Cph2(1-2) as well as an extended mutagenesis study of conserved amino acids are addressed to shed light on their function in photoconversion.

6.3.1 PCB, the chromophore of *Syn*Cph2(1-2)?

*Syn*Cph2(1-2) was produced heterologously with PCB co-assembled *in vivo*[138], while a direct proof that this chromophore is actually the native one has not been given, yet. *Synechocystis* sp. PCC 6803 contains two HOs that both catalyze the cleavage of heme to BV[155]. Like all cyanobacteria it also contains PcyA for the biosynthesis of PCB from the precursor BV[28]. *Synechocystis* sp. PCC 6803 lacks phycoerythrin[28] and crude cell extracts provide no evidence for the production of PEB[156]. Also the PΦB-synthase is absent as it can be only found in land plants and is missing in cyanobacteria[155]. Therefore, only BV, PCB and their potential isomerization products are present in *Synechocystis* cells to coassemble with the apo-phytochrome. As BV in BphPs is attached to the N-terminal helix of the PAS and not in the GAF domain it is very unlikely that it is the native *Syn*Cph2(1-2) chromophore. Although it is available during production of *Syn*Cph2(1-2), it does not attach to the apoprotein, as only PCB could be identified by mass spectrometry analysis[138]. Interestingly, in the BV-binding bacteriophytochrome *Dr*BphP mutagenesis studies were performed concerning the covalent attachment of PCB and BV. The wild type protein binds BV with a four-times higher efficiency than the PCB chromophore. In the double mutant C24A/M259C, that removes the N-terminal cysteine and adds a cysteine residue in the GAF domain corresponding to Cys-259 in *Syn*Cph1, PCB comprises a four-fold higher binding affinity than BV. So the preference of PCB is 16-fold increased by switching the chromophore binding site from the N-terminus to the GAF domain. In a mutant where both binding sites are available, BV and PCB attach to the apoprotein with nearly equal efficiency[13]. Due to the affinity of PCB to cysteine binding sites in the GAF domain, it is hence very likely that PCB is the natural chromophore of the PAS-less *Syn*Cph2(1-2). Its covalent attachment results in a stable protein with reasonable spectral characteristics. The isomerization of PCB to PVB is only observed in DxCF CBCRs like *Syn*Cph2(5)[145] and not in other phytochromes so it can be ruled out that PVB is a cognate chromophore of *Syn*Cph2(1-2).

In addition to the conserved cysteine residue, the chromophore surroundings are more or less conserved in phytochromes and CBCRs. We performed an extended mutagenesis study in *Syn*Cph2(1-2) to illuminate the role of conserved residues in the chromophore vicinity[138,139]. Fig. 6.8 displays the positions of the respective amino acids and the implication of their

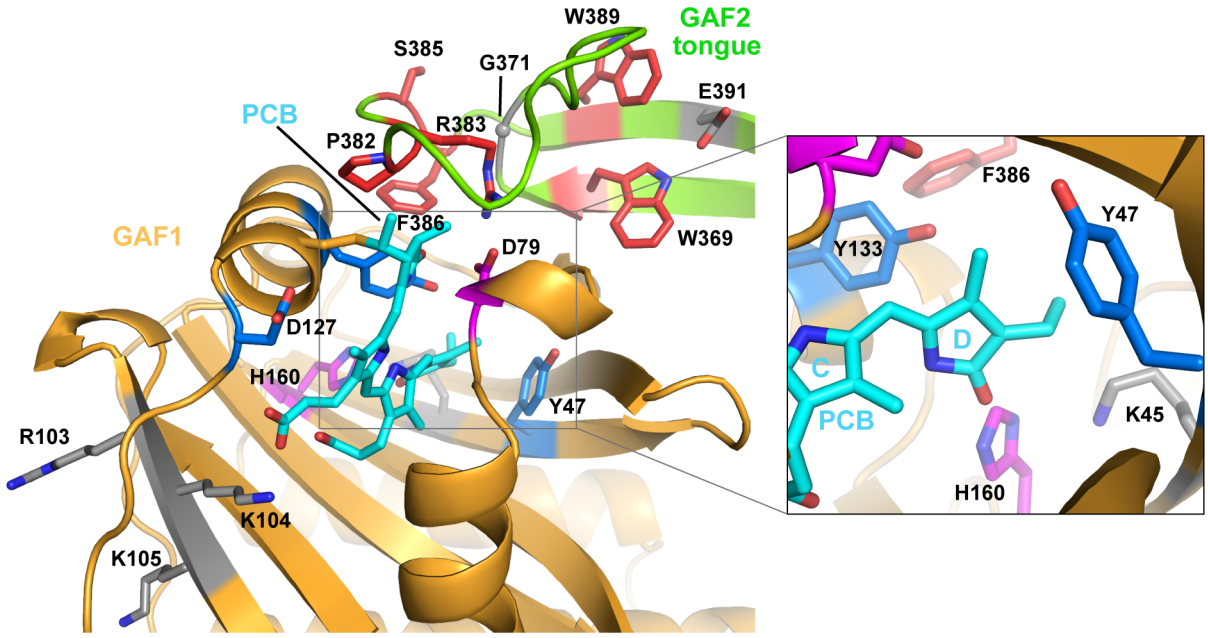

Figure 6.8: Chromophore binding pocket in the *Syn*Cph2(1-2) chain B structure. The magnification shows the D-ring environment. The GAF1 and GAF2 domains are displayed in orange and green, respectively. The PCB chromophore is colored in cyan. The highlighted amino acids show positions where in other variants of *Syn*Cph2(1-2) single amino acid substitutions were performed. The UV/vis absorbance and CD spectroscopical behavior of these variants is indicated by the coloring of the residues. Gray residues display wild type-like behavior in the respective mutants (see Ref.[138,139] for the exact nature of the substitutions), blue and red corresponds to reduced P_{fr} formation and a degenerated P_{fr} state, respectively. Magenta colored residues indicate deviant spectroscopical behavior. A D79R mutant was not able to reversibly photoconvert and H160A showed P_r / P_{nr} photoconversion.

substitutions for the photochemistry of *Syn*Cph2(1-2) which are discussed in the following subsection.

6.3.2 Substitution of a tyrosine residue = easy way of discrimination?

Tyr-47 is in close proximity of the D-ring from the chromophore in *Syn*Cph2(1-2) (Fig. 6.8, inlet) and is conserved in all GAF-containing photoreceptors[122]. A histidine substitution of this tyrosine residue is believed to distinguish between two types of D-ring rotation in phytochromes[136].

According to *Rockwell et al.*[136], phytochromes can be divided into at least two classes with different photocycles, comprising BV and phytobilin-binding phytochromes, respectively, that possess similar P_r states but differ in their P_{fr} formation. Phytobilin-, in contrast to BV-binding phytochromes, show a sign inversion of the CD signal upon formation of the P_{fr} state and require a free C-ring propionate chain for $P_r \rightarrow P_{fr}$ photoconversion[136]. A

negative CD signal in the long wavelength transition was assigned to an α-facial position of the D-ring compared to rings B and C (Fig. 6.9) and a positive CD signal to a β-facial conformation [112,136]. Accordingly, the authors suggest a β-facial and an α-facial D-ring conformation of phytobilin and BV-binding phytochromes in the P_{fr} states, respectively. This is caused by a counter-clockwise D-ring rotation in phytobilin phytochromes and a clockwise rotation in BV phytochromes [136] (Fig. 6.9, inlet).

Rockwell et al. suppose that the side chain conformation of a conserved tyrosine residue (Tyr-47 in *Syn*Cph2) diverges in the two phytochrome photocycle classes as the interaction between the tyrosine and the C-ring propionate in the P_{fr} structure of *Pa*BphP and *Rp*BphP1 would be sterically disfavored in a β-facial D-ring position in phytobilin phytochromes. The authors suggest a histidine substitution of that tyrosine residue can distinguish between the two classes as in phytobilin phytochromes this results in loss of photochemistry and in an intense red fluorescence whereas in BV-binding phytochromes

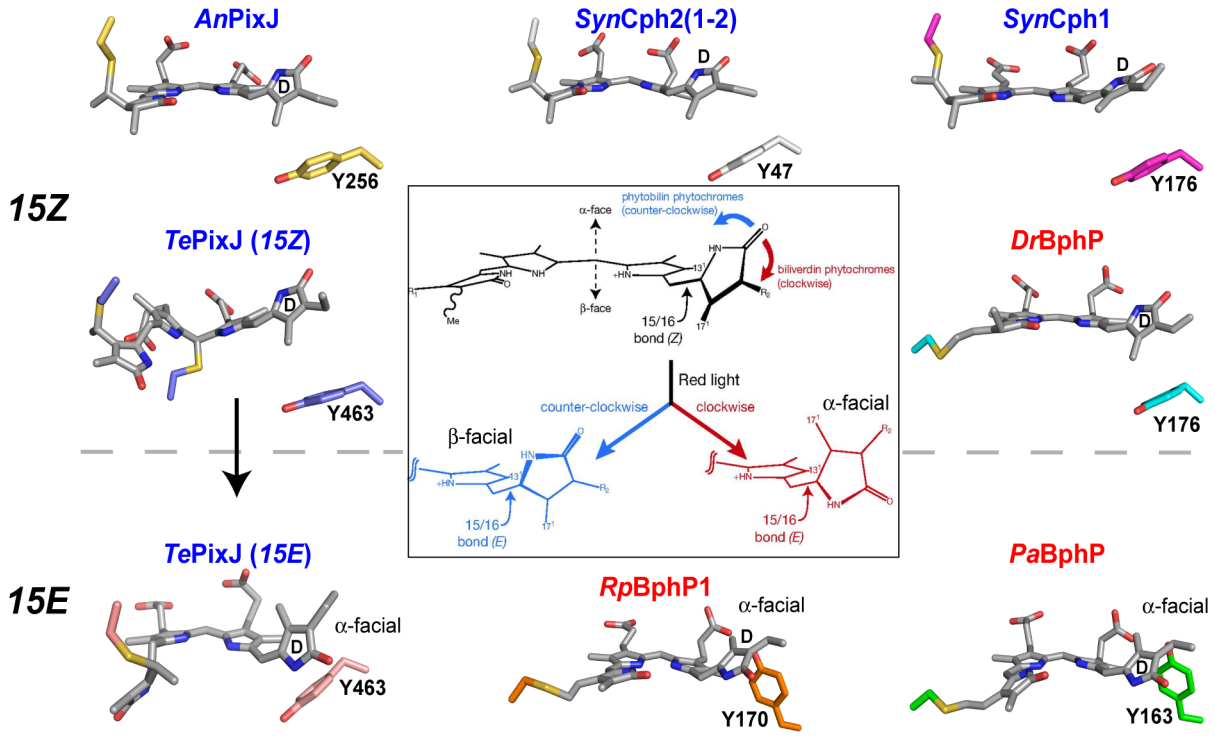

Figure 6.9: Conformation of the D-ring in PCB and BV phytochrome and CBCR structures. The inlet in the middle according to Ref. [136] illustrates the hypothesis of clockwise and counter-clockwise D-ring rotation in BV- and phytobilin-binding phytochromes during photoconversion into P_{fr}, respectively. The supposed α- and β-facial conformation of the D-ring in P_{fr} is shown in the lower part of the inlet. The latter is surrounded by the phytochrome and CBCR chromophore structures with the conserved tyrosine residue whose histidine substitution is supposed to be able to distinguish between two classes of photoconversion [136]. The protein designations are shown in blue and red if the protein binds a phytobilin or a BV chromophore, respectively.

this mutation retains P_r / P_{fr} photoconversion and wild type-like fluorescence. It is supposed that histidine in phytobilin phytochromes adopts the side chain rotamer of the tyrosine in the *Pa*BphP structure thus inhibiting the β-facial D-ring position in P_{fr} [136].

Interestingly, in NMR experiments with the PCB-binding *Syn*Cph1 the β-facial D-ring conformation in the P_{fr} state could be observed as predicted by *Rockwell et al.* [137]. Also the structure of the bathy-BphP *Rp*BphP1 confirms an α-facial position of the D-ring in BV-binding phytochromes and the side chain rotamer of Tyr-170, which points, like in *Pa*BphP, to the α-face of the chromophore and interacts with the C-ring propionate (Fig. 6.9). The CBCR *15E*-structure of *Te*PixJ contradicts this hypothesis as the D-ring, although it is part of the phytobilin PCB chromophore, exhibits an α-facial conformation like in the bathy-BphP structures. The conserved tyrosine residue points towards the β-face of the chromophore as in all other Group I-III structures including the proposed P_r structure of a Q188L *Pa*BphP mutant [85] (PDB code: 3G6O) but except from the bathy-BphP P_{fr} structures. However, CBCR chromophores undergo different changes during photoconversion than in phytochromes, like covalent attachment of a second cysteine [126], and might not be covered by this hypothesis.

According to the predicted behavior of tyrosine to histidine substitutions in BV-binding phytochromes, the Y163H mutant in *Pa*BphP retains wild type-like $P_r \rightarrow P_{fr}$ photoconversion without an enhancement of fluorescence [85]. Furthermore, the equivalent Y176H variant of *Syn*Cph1 confirms the hypothesis of *Rockwell et al.* [136] as it comprises an intense fluorescence and is nearly photoinactive as predicted for phytobilin phytochromes [157]. In addition, the same mutation in *Arabidopsis thaliana* PhyB, assembled with PCB, or in the PCB- as well as in the PΦB-binding PhyA exhibits these spectral properties [158]. Interestingly, the Y276H mutation of PhyB *in vivo* showed light-independent activity as it behaves constitutively like P_{fr} [159,160]. In contrast to the predicted behavior of BV-binding phytochromes, in Y176H of *Dr*BphP no proper photoconversion into P_{fr} can be observed while the fluorescence is not enhanced [161]. For phytobilin-binding phytochromes, the Group II members *Syn*Cph2(1-2) and *Sy*B also contradict this notion as their tyrosine to histidine mutants comprise P_r / P_{fr} photoconversion, however, with a decreased P_{fr} content at the photoequilibrium and only moderate fluorescence [88,91,138].

The conserved Tyr-47 residue is important for photoconversion as it stabilizes the P_{fr} state [138]. All observed mutations affect either the occurrence or the extent of photoconversion. In *Syn*Cph1 no other amino acid substitution of the tyrosine residue can retain wild type spectroscopical behavior [158] thus reflecting the strict requirements for this position. Contradicting to *Rockwell et al.* [136] a histidine mutation cannot distinguish between two possible photoconversion classes in phytochromes. Whether the β-facial orientation of the D-ring in phytobilin-binding phytochromes is adopted in contrast to the CBCR *Te*PixJ *15E*-structure must be shown in further experiments.

6.3.3 The DIP motif

The DIP motif is conserved in all Group I and II phytochromes[81] but not in CBCRs[122]. It is located near the A-ring of the chromophore at the periphery of the GAF domain. The aspartate is involved in a salt bridge to an arginine residue of the tongue from the GAF2 (or PHY) domain in P_r and is therefore essential for the tongue-GAF interactions. In the bathy-BphP P_{fr} structures it participates in a hydrogen bond network involving the serine residue of the tongue's PRxSF motif and the D-ring nitrogen (Fig. 6.10 C-D). In the P_r phytochrome structures of *Syn*Cph2(1-2) and *Syn*Cph1 (Fig. 6.10 A, B) the carboxylate group of the aspartate from the DIP motif points towards the tongue and just the amide oxygen interacts with the pyrrole nitrogens and the pyrrole water, a water molecule that is hydrogen bonded to the latter. In the P_{fr} structures of *Pa*BphP and *Rp*BphP1 the amide oxygen remains hydrogen bonded to the pyrrole water and pyrrole nitrogens but the carboxylate group of the aspartate side chain interacts, though still oriented towards the tongue, with the D-ring pyrrole nitrogen (Fig. 6.10 C, D). In the crystal structure of *Rp*BphP1 no pyrrole water can be observed[69].

In *Syn*Cph2(1-2) a D79R mutation (Fig. 6.8) comprises a wild type-like P_r state but upon

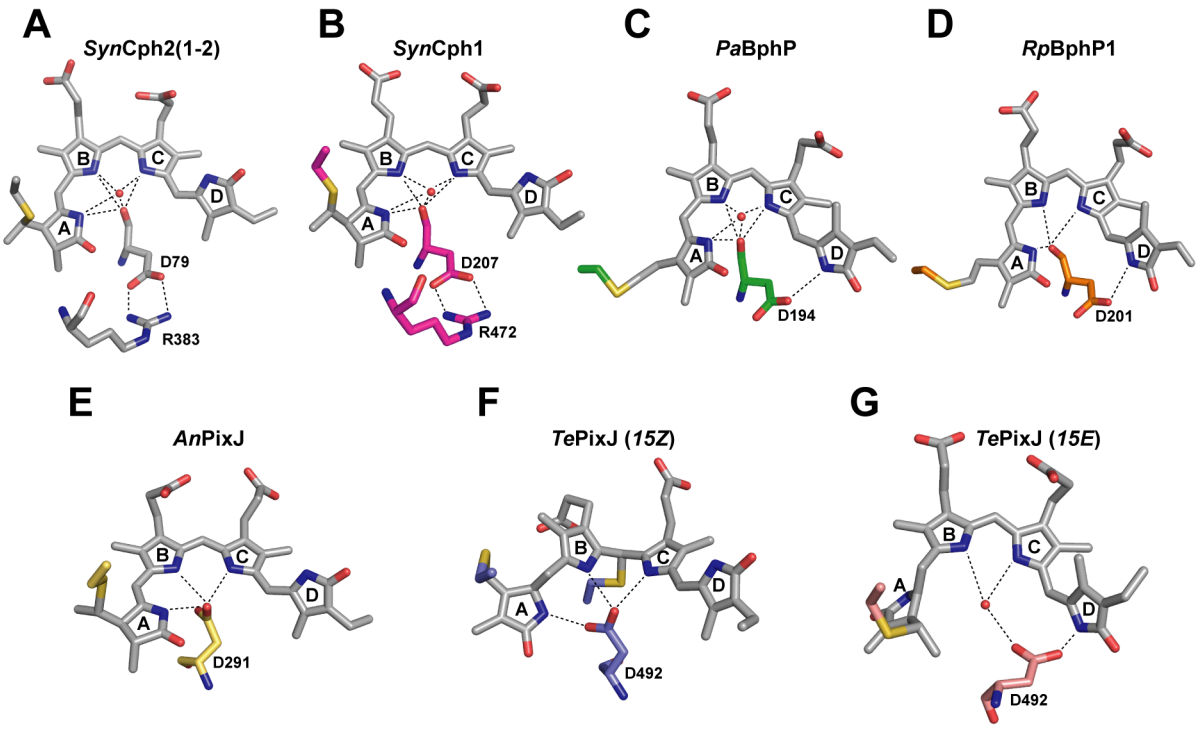

Figure 6.10: A conserved aspartate residue interacts with the chromophore in phytochromes (**A-D**: *Syn*Cph2(1-2), *Syn*Cph1, *Pa*BphP and *Rp*BphP1) and CBCRs (**E-G**: *An*PixJ, *Te*PixJ (*15Z*), *Te*PixJ (*15E*)). Pyrrole waters, as present in the structure, are shown; the hydrogen bond network is indicated by dashed lines. In *Syn*Cph2(1-2) and *Syn*Cph1 also the salt bridge to the tongue-arginine residue is presented.

red light illumination a bleached blue-shifted photoproduct is built that is photochemically impotent[139]. The same characteristics are observed in the D86H GAF-PHY protein of the Group II phytochrome *Sy*B[88,91]. In *Arabidopsis thaliana* PhyB the D307A variant also fails to photoconvert into P_{fr} but reversibly builds a bleached red-light absorbing state upon red light illumination. *In vivo* this mutation results in a greatly reduced phenotypic activity[162]. The importance of this aspartate residue for P_{fr} formation can also be observed in *Syn*Cph1 D207A[81] and in variants of Asp-207 in *Dr*BphP[161], where the mutants get arrested in a P_r-state without P_{fr} formation. In bathy-BphPs equal photochemical characteristics can be observed, because in *Pa*BphP the D194A mutation results in a destabilization of the P_{fr} ground state as the mutant remains photochemically inactive in P_r[11]. Interestingly, asparagine and glutamate substitutions of D207 in *Dr*BphP result in photochemically active proteins comprising a bleached state with absorbance in the far red region after red light illumination[161].

Besides the stabilization of the tongue-GAF1 interaction by the salt bridge in P_r and a P_{fr} stabilization *via* a hydrogen bond network, an involvement of the aspartate in the protonation cycle of the $P_r \rightarrow P_{fr}$ photoconversion could be shown as demonstrated for *Syn*Cph1[81], *Dr*BphP[161] and for *At*BphP1. In the latter, the aspartate is supposed to be the proton release group during the transient de- and reprotonation of the chromophore in the $P_r \rightarrow P_{fr}$ photoconversion[163]. Substitutions of the aspartate residue in the DIP motif result in intensely fluorescent proteins[88,161]. Interestingly, a mutation of this residue was used in structure-guided engineering in the PAS-GAF protein of *Dr*BphP where the reduced photoconversion in the D207H mutant resulted in an infrared fluorescent protein[152].

In CBCRs the aspartate of the DIP motif is also conserved[122]. Relieved from forming the salt bridge to the tongue-aspartate as in Group I and Group II phytochromes, the carboxylate side chain of the aspartate is rotated in CBCRs towards the chromophore and directly hydrogen bonds to the ring A, B and C nitrogens in the *15Z*-states of *An*PixJ and *Te*PixJ[122,123]. In the *15E*-state of *Te*PixJ it directly interacts with the D-ring nitrogen and the pyrrole water[122], the side chain still pointing towards the chromophore (Fig. 6.10 E, F, G). In *Te*PixJ the D492L mutation of this aspartate yields a chromophore-bound, photoinactive species that comprises poor absorption in the visible light whereas a D492S variant displays nearly wild type-like photoconversion[123]. This shows that in CBCRs the requirements to the aspartate residue are less restrictive than in phytochromes presumably because the tongue region is missing.

The second residue in the DIP motif, isoleucine, was also subject of mutagenesis studies. A hydrophobic substitution of isoleucine, I208A, in *Dr*BphP retained the P_r / P_{fr} photoconversion, thus with a reduced P_{fr} content at the photoequilibrium[161].

The proline residue was shown to be essential for chromophore ligation as a P309L mutation in the DIP motif of *Arabidopsis thaliana* PhyB leads *in vitro* to a reduced chromophore

incorporation and an abnormal bleached difference spectrum in the far red region. *In vivo* this results in a complete loss of photosensory activity[164]. In contrast, the *Dr*BphP P209G mutant binds BV, leading to a holoprotein with wild type-like photochemical properties, except for a blue shift of the P_r and P_{fr} absorption maxima[161]. These results indicate that the substitution with glycine can preserve the kink produced by the proline residue that seems to be important for the photochemical and folding properties of the phytochrome whereas leucine might not.

Interestingly, in the tongue region of *Syn*Cph2(1-2) the opposite effect can be observed as a glycine substitution of the proline in the PRxSF motif results in too much conformational flexibility, which inhibits wild type-like photochemical behavior[139]. This behavior is not observed for the *Dr*BphP P209G mutant, thus indicating that the sterical restrains around the DIP motif seem sufficient to overcome this effect.

6.3.4 The interactions of the chromophore's propionates

In *Syn*Cph2(1-2) the B-ring propionate forms a salt bridge to a lysine residue, Lys-104 (Fig. 6.8, 6.11 A). Compared to other GAF domains of phytochromes and CBCRs (Section 6.2) this residue lies on an additional β-strand at the end of the β-sheet. The lysine is conserved in cyanobacterial phytochromes with the same domain architecture as *Syn*Cph2. In other GGDEF domain containing phytochromes it is replaced by a polar residue whereas in HK domain containing phytochromes the unpolar residue isoleucine can be found, in addition to two conserved arginine residues[139]. This implicates that the way of B-ring propionate interaction depends on the effector domains in the protein. We produced swapping variants of *Syn*Cph2(1-2), where the whole region around the B-ring propionate (Val-97 - Val-126) is replaced by regions of phytochromes from the afore-mentioned three types of B-ring propionate interaction partner-conservation. Interestingly, they show P_{fr} formation almost like the wild type[139] thus suggesting that in *Syn*Cph2(1-2) the propionate surrounding is not essential for P_{fr} formation. In the most phytochromes two arginine residues are conserved that interact with the B-ring propionate. In *Syn*Cph1 the latter builds a salt bridge to Arg-254 in P_r and is supposed to swap partners during photoconversion to P_{fr} by interacting with Arg-222[137] (Fig. 6.11 B). In the bathy-BphP P_{fr} structures of *Pa*BphP and *Rp*BphP1 indeed the analogue amino acid to Arg-222: Arg-209 and Arg-216, respectively, form a salt bridge to the B-ring propionate (Fig. 6.11 C, D). An appropriate interaction partner in P_{fr} for the *Syn*Cph2(1-2) B-ring propionate is missing. Lys-104 and the nearby Arg-103 and Lys-105 residues in *Syn*Cph2(1-2) are though not essential in the $P_r \rightarrow P_{fr}$ photoconversion as the alanine mutants show wild type-like behavior except of a ~3 nm blue-shift in the K104A P_r and P_{fr} absorption maxima.

In contrast, in the phytochromes with conserved arginine residues amino acid substitutions

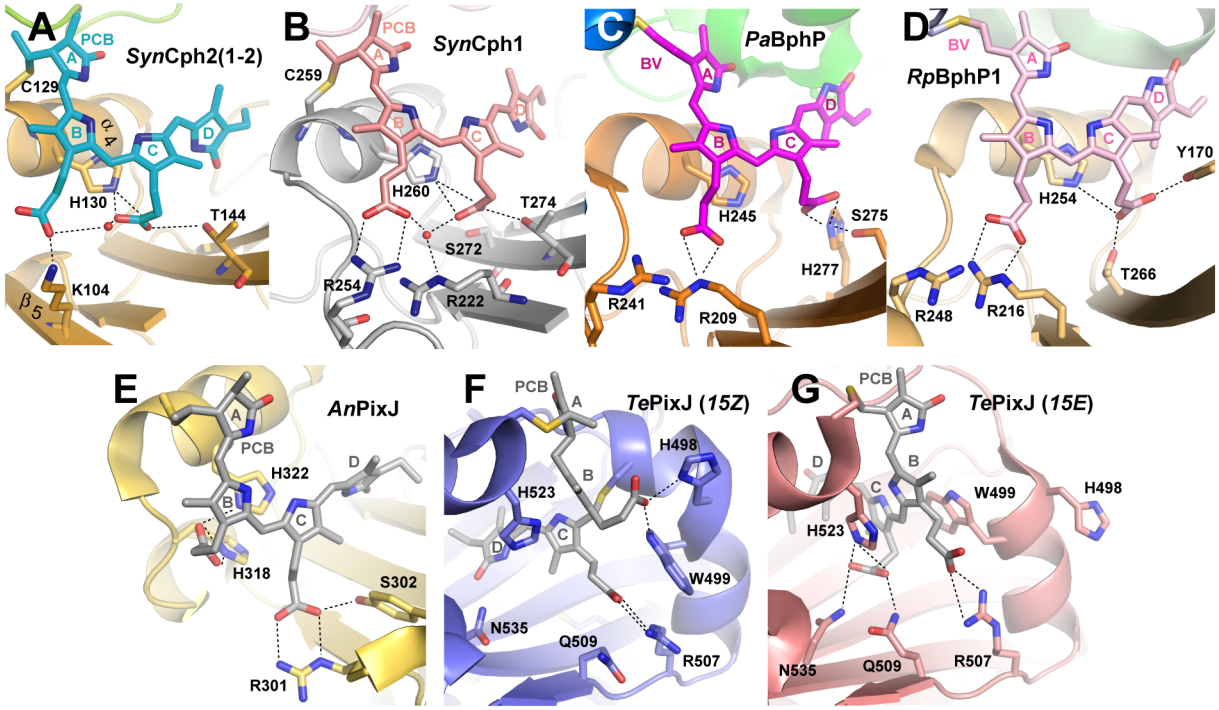

Figure 6.11: Propionate surroundings of phytochromes with a P_r ground state (**A, B**), bathy-BphPs in P_{fr} (**C, D**) and CBCR structures in the *15Z*- (**E, F**) and *15E*-state (**G**). The hydrogen bond network is indicated by dashed lines. **A** and **B** were already published in Ref.[139].

have an impact on photochemistry. In the Group II phytochrome *Sy*B it could be shown that the two arginine residues have opposing roles. Arg-101, according to the partner swapping hypothesis the interaction partner in P_{fr}, was shown to stabilize the latter as a R101A variant shows despite wild type-like spectral behavior a faster dark reversion into P_r. A substitution with lysine on the other hand does not result in an accelerated dark reversion, so the salt bridge is critical for P_{fr} stability[90]. Also in Group I phytochromes the equivalent arginine residue stabilizes the P_{fr} conformation. In PhyB of *Arabidopsis thaliana* a R322A mutation exhibits wild type-like photochemistry but a 6 nm shift of the P_{fr} absorption maximum. This variant as well as R322Q comprise very fast dark reversion[162,164]. Also in *Pa*BphP the R209A mutation leads to a destabilization of P_{fr}. Here, a mixed P_r / P_{fr} state can be observed even after incubation in the dark[85].

On the other hand, Arg-133 of the Group II phytochrome *Sy*B, that should be the interaction partner of the B-ring propionate in P_r, was shown to destabilize the P_{fr} state as the R133A variant exhibits less P_{fr} content at the photoequilibrium but a slower dark reversion than the wild type[90]. In Group I phytochromes the destabilizing effect is even enhanced upon substitution of the arginine. The analogue mutation in *Dr*BphP R254A shows an altered P_r spectrum and an increased P_{fr} stability along with no dark reversion back to P_r[161]. This implicates that the arginine not only destabilizes P_{fr} but is essential

for P_r stabilization. Also in *Arabidopsis thaliana* PhyB the R352A mutation stabilizes P_{fr} against thermal reversion[162]. On the other hand it could be shown for the R352K variant that it comprises a reduced biological activity[164]. In *Syn*Cph1 the R254A mutant shows a wild type-like P_{fr} spectrum but a 10 nm blue-shift in the P_r absorption maximum as well as slight folding differences compared to the wild type protein[81]. Interestingly, a R254Q mutation in *Dr*BphP inhibits the attachment of the chromophore[161]. In the bathy-BphP *Pa*BphP the R241A mutation also effects the P_r state, the dark reversion to P_{fr} is accelerated.

In all of the analyzed proteins that contain the conserved arginines the latter show a stabilizing or destabilizing effect. It might be surprising that just a little sub-group of Group II phytochromes diverge from the otherwise conserved B-ring propionate interactions[139]. A correlation with the effector domains in the protein is obvious but must be proved.

Interestingly, apart from *Syn*Cph2-like phytochromes also CBCRs deviate from the conserved propionate surrounding. Other residues are used to fix the propionate's position here. What is conserved in all phytochrome and CBCR structures is that one propionate chain of the chromophore is bent whereas the other one is stretched[122]. The bent conformation is fixed by an interaction of the propionate to His-130 in *Syn*Cph2(1-2), as well as in *Syn*Cph1, *Rp*BphP1, *An*PixJ and *Te*PixJ (*15E*). This histidine residue is highly conserved in phytochromes and most CBCR subfamilies[122] (Subsection 6.3.6). In the deviating structures of *Pa*BphP and *Te*PixJ (*15Z*) another histidine residue stabilizes the bent propionate (Fig. 6.11). In the *15Z*-state of *An*PixJ and *Te*PixJ the B-ring propionate and not the C-ring propionate like in the other structures exhibits a bent conformation.

Unlike in canonical phytochromes, the position of the two arginine residues is not conserved in CBCRs. Nevertheless, an arginine residue, though not situated within the β-sheet, is involved in a salt bridge to the stretched propionate chain, too. This arginine is conserved in the respective subclass and is specific to it[122]. In the *15Z*-state of *An*PixJ the stretched C-ring propionate interacts with Arg-301 and Ser-302 (Fig. 6.11 E); in the same state of *Te*PixJ the stretched C-ring propionate interacts with Arg-507. Interestingly, the B-ring propionate is not bent towards the conserved histidine residue His-523 (His-130 in *Syn*Cph2) like in all other structures but in the other direction, where it is involved in a hydrogen bond network with His-498 and Trp-499. These residues are not conserved in this subgroup[122], but the substituting amino acids maintain the ability to interact with the propionate. As for *Te*PixJ apart from the *15Z*-structure also the *15E*-structure is available; the propionate interactions after photoconversion can be easily analyzed. Interestingly, in contrast to *Syn*Cph1[137], both propionate chains are involved in a partner swap. They also toggle between the bent and stretched conformation, respectively. Upon *15E* $\rightarrow$ *15Z* photoconversion and the covalent attachment of the second cysteine Cys-494 to C10 of the chromophore, the α-helix of His-498 and Trp-499 is structurally affected and

these two residues are rotated. Also Asn-535, Gln-509, His-523 and Arg-507 change their conformation and turn towards the chromophore (Fig. 6.11 F, G). The C-ring propionate interacts with Asn-535, Gln-509 and His-523 (His-130 in *Syn*Cph2) in the *15Z*-state; the now stretched B-ring propionate with Arg-507.

Whether these rotations of both propionate chains are just a consequence of the binding from the second cysteine to the chromophore or are a feature for all GAF-containing photoreceptors is elusive at present. But in the P_r and P_{fr} structures of phytochromes the C-ring propionate is rotated, respectively, although in NMR experiments of *Syn*Cph1 only a small rotation of the C-ring propionate carboxylate group is detected that does not have major impact on the propionate interactions[137]. On the other hand it was shown that the PCB-binding *Syn*Cph1 requires a free C-ring propionate for the P_{fr} formation whereas the BV-binding *Dr*BphP does not[136,165] suggesting a difference in C-ring propionate movement for the latter. Regarding this, a C-ring propionate partner swap instead of the B-ring propionate in *Syn*Cph2(1-2) cannot be ruled out.

6.3.5 The tongue region

We could show that the tongue region in phytochromes is important for formation and stabilization of the P_{fr} state as mutations in the $W^G/_A G$, PRxSF and WxE motifs lead to proteins that arrest in an intermediate state upon photoconversion or show a reduced P_{fr} content at the photoequilibrium[138,139]. Only the G371A and E391A mutations in the first and last mentioned motifs comprise wild type-like behavior (Fig. 6.8). In the bathy-BphP *Pa*BphP a S459A mutation in the PRxSF motif destabilizes P_{fr} in a way that the ground state is changed to P_r with a limited photoconversion to P_{fr}[11]. Accordingly, in *Syn*Cph2 the S385A mutant remains in an intermediate state upon photoconversion[139,166]. In *Arabidopsis thaliana* PhyA the S584F mutation results in an abnormal difference spectrum with a shallower, blue-shifted minimum in the far red region and a very fast dark reversion to P_r[164], suggesting reduced or compromised P_{fr}. This mutant comprises decreased responsiveness to lower light intensities[164]. On the other hand, in the same protein a R582A mutation in the PRxSF motif shows $P_r \rightarrow P_{fr}$ photoconversion with a ten-fold slower dark reversion. Interestingly, also the P_r state is affected as it shows a 9 nm blue-shift in its absorbance maximum. The R582A mutant exhibits wild type-like signaling but is slightly hyperactive *in vivo*[162]. In contrast to *Syn*Cph2(1-2) where the R383D mutant remains in an intermediate bleached state after red light illumination, the conserved arginine residue in PhyA is not required for photochemistry and destabilizes the P_{fr} state. In the bathy-BphP *Pa*BphP an alanine substitution of Arg-453 that is involved in a hydrogen bond network with the D-ring nitrogen, the DIP-aspartate and Ser-459 from the PRxSF motif and is also conserved in in *At*BphP2 but not in other phytochromes (Fig. 6.7) comprises P_r instead of a P_{fr} dark adapted state and exhibits limited photoconversion[11].

In conclusion, the arginine and serine residue of the PRxSF motif and an additional arginine residue in *Pa*BphP stabilize the P_{fr} state, only in PhyA the PRxSF-arginine shows reversed characteristics. We produced variants of *Syn*Cph2(1-2) with tongue regions of other Group II members to prove the stabilizing effect on the P_{fr} state. We could show that the tongue region is a functional module that can be exchanged between different phytochromes without loosing wild type-like spectral behavior[139].

6.3.6 A histidine residue - key to spectral tuning?

His-130 is situated on an α-helix next to the chromophore-binding cysteine in phytobilin phytochromes and is conserved in all phytochromes[81] as well as in most CBCR subfamilies[122]. In the phytochrome and CBCR structures it is involved in a hydrogen bond network to the ring C propionate (*Syn*Cph2(1-2), *Syn*Cph1, *Rp*BphP1, *Te*PixJ (*15E*), Fig. 6.11 A, B, D, G) and in the *An*PixJ (*15Z*) structure to the B-ring propionate (Fig. 6.11 E) whereby the histidine stabilizes the bent conformation of the propionate side chain (Subsection 6.3.4). Only in the *Pa*BphP (and *Te*PixJ (*15Z*)) structure it comprises no interactions with the chromophore (Fig. 6.11 C, F). In the unusual Group I phytochrome TP1 from *Nostoc punctiforme* this histidine residue is replaced by a cysteine residue[126]. According to dual-cysteine CBCRs this cysteine is supposed to be involved in a second thioether linkage to C10 of the chromophore in TP1. In the PAS-GAF-PHY construct the second cysteine results in a trichromatic photocycle with a violet absorbing ground state. Upon violet illumination an orange-absorbing photoproduct is built that thermally converts to a red-absorbing state that comprises a *15E*-PCB chromophore. Mutagenesis experiments with a histidine substitution of this second cysteine result in a photoinactive red-absorbing protein. Interestingly, the converse H260C mutant in *Syn*Cph1 also exhibits a violet-absorbing state and a small amount of orange-absorbing species after illumination with violet light[126]. Although this mutant does not thermally convert to a red-absorbing state, because also other residues are required for TP1-like spectral behavior, these experiments show that the position of the conserved histidine residue is very sensitive to spectral engineering. An equivalent H130C mutation in *Syn*Cph2(1-2) on the other hand resulted in insolubility of the protein. In the CBCR *Te*PixJ a H523L mutation results, like in TP1, in a tripartite photocycle as upon illumination a blue-absorbing species is formed that decays into an orange-absorbing state. The latter is metastable and thermally reverts to the original blue-absorbing conformation[123]. The red-shifted state was similar to that of *Nostoc punctiforme* F1000 that also comprises a leucine residue in this position[123,128]. The less basic asparagine and glutamine substitutions in the same protein cannot substitute the histidine residue as the resulting proteins are instable or show only poor photoconversion[123].

The conserved histidine residue His-130 in *Syn*Cph2(1-2) is essential for photoconversion

as it is supposed to be involved in the transient deprotonation in the Meta-R_c state during the $P_r \rightarrow P_{fr}$ transition[163]. A H139A mutant in *Sy*B is photoinactive with a degenerated P_r state[91]. The same mutation, H250A, in *At*BphP1 results in a bleached photoproduct in which the chromophore is deprotonated. The reprotonation of Meta-R_c, leading to the formation of P_{fr}, cannot be observed for H250A[163] as well as for the H260A mutant of *Dr*BphP[161]. Also in *Syn*Cph1 this residue is critical for chromophore protonation[81].

6.3.7 The D-ring surroundings

The D-ring cavity is built of hydrophobic residues whereas the ring D nitrogen and the carbonyl group are stabilized by hydrogen bond interactions to hydrophilic residues; this is conserved in Group I-III GAF-containing photoreceptors. Residues in the D-ring surroundings of *Syn*Cph2(1-2) that were analyzed *via* mutagenesis studies are Lys-45, His-160 and Tyr-133 (Fig. 6.8, inlet). The lysine residue is conserved in *Sy*B and several other Group II phytochromes whereas in the most phytochromes aliphatic side chains like leucine, isoleucine or methionine are preferred[83,90]. A methionine substitution of lysine in *Syn*Cph2(1-2)[139], *Sy*B[90] and *Rp*BphP3[83] does not affect the binding of the chromophore and exhibits wild type-like spectroscopical characteristics. The K45M mutant in *Syn*Cph2(1-2) even comprises an enhanced P_{fr} content at the photoequilibrium[139]. Although this residue hydrogen-bonds to the D-ring carbonyl in *Rp*BphP3 and to His-160 in the *Syn*Cph2(1-2) structure its substitution to unpolar residues does not affect P_{fr} formation.

In the P_r phytochrome and *Te*PixJ (*15Z*) structures His-160 hydrogen bonds to the D-ring carbonyl. In *An*PixJ the histidine is substituted by a tyrosine residue that also hydrogen-bonds to the D-ring and is conserved only in this CBCR subgroup[122]. In the bathy-BphP structures the histidine interacts with the bent C-ring propionate side chain (Fig. 6.11). An equivalent interaction of the histidine in *Syn*Cph1 after photoconversion to P_{fr} cannot be detected; like in the *Te*PixJ (*15E*) structure no interaction to the chromophore occurs in the P_{fr} state[137].

In *Syn*Cph2(1-2) the histidine residue His-160 is essential for P_{fr} stabilization. A H160A mutant in *Syn*Cph2(1-2) comprised a blue-shifted P_r-like P_{nr} state after red light illumination[139]. In the bathy-BphP *Pa*BphP the alanine substitution of the histidine results in a protein with a P_r instead of a P_{fr} dark state that comprises only limited efficiency of photoconversion into P_{fr}[85].

Tyr-133 is conserved in phytochromes[162] but not in CBCRs[122]. In the P_r phytochrome structures it is part of a hydrogen bond network that stabilizes the side chain conformation of Asp-79 which forms the salt bridge to the tongue-arginine. In the bathy-BphP structures of *Pa*BphP and *Rp*BphP it participates in a hydrogen bond network with

the D-ring carbonyl group. A phenylalanine substitution in *Pa*BphP yields a protein that is photochemically active but comprises a mixed P_r / P_{fr} ground state[11]. Also in *Syn*Cph2(1-2)[139] and *Sy*B[91] the P_{fr} state is destabilized by this mutation as the P_{fr} content at the photoequilibrium is decreased. A histidine substitution in *Dr*BphP inhibits P_{fr} formation, supposedly because the position of the aspartate residue (Asp-79 in *Syn*Cph2(1-2)) is altered by the histidine[161]. As highly fluorescent, the mutation Y263F in the PAS-GAF construct of *Dr*BphP is used in engineering a fluorescent protein[152].

For *Syn*Cph1 it could be shown that the aromatic character and not the hydroxyl group of the tyrosine residue is mandatory for P_{fr} formation as the phenylalanine substitution resulted in wild type-like photoconversion though with a blue-shift of the P_{fr} absorbance maximum[84]. The same photochemical characteristics are observed for the Y361F mutant of *Arabidopsis thaliana* PhyB. Nevertheless, the photoconversion rates in PhyB are slightly reduced and the dark reversion is four-fold slower suggesting a P_{fr} stabilization by phenylalanine. *In vivo* this mutation results in greatly enhanced light sensitivity so that this mutant was supposed for agricultural applications as it dramatically increases the sensitivity of hypocotyls to red light and enhances the germination response of seeds in white light[162].

In the crystal structure of the analogue mutant Y263F from *Syn*Cph1 (PDB code: 3ZQ5) the relative position of the PHY domain compared to the wild type is altered[84] suggesting an important role of this residue in the positioning of the domains relative to each other.

In *Te*PixJ Tyr-133 is replaced by a glutamine residue that is conserved within this CBCR subgroup[122]. This glutamine interacts with the pyrrole water-replacing Asp-492 residue in the *15Z*-structure (Fig. 6.10 F) whereas in the *15E*-state it directly hydrogen bonds to the B and C-ring nitrogens.

6.4 A tongue-twister for signal transduction?

For phytochromes different possibilities of intra- and intermolecular signal transduction are proposed. In this chapter the diverse strategies are discussed for *Syn*Cph2.

6.4.1 Signaling *via* interaction partners

Plant phytochrome signaling is very complex and involves the binding of interaction partners in the cytoplasm as well as in the nucleus (Subsection 3.4.1). For prokaryotic phytochromes signaling *via* interaction partners has not been shown yet but cannot be ruled out.

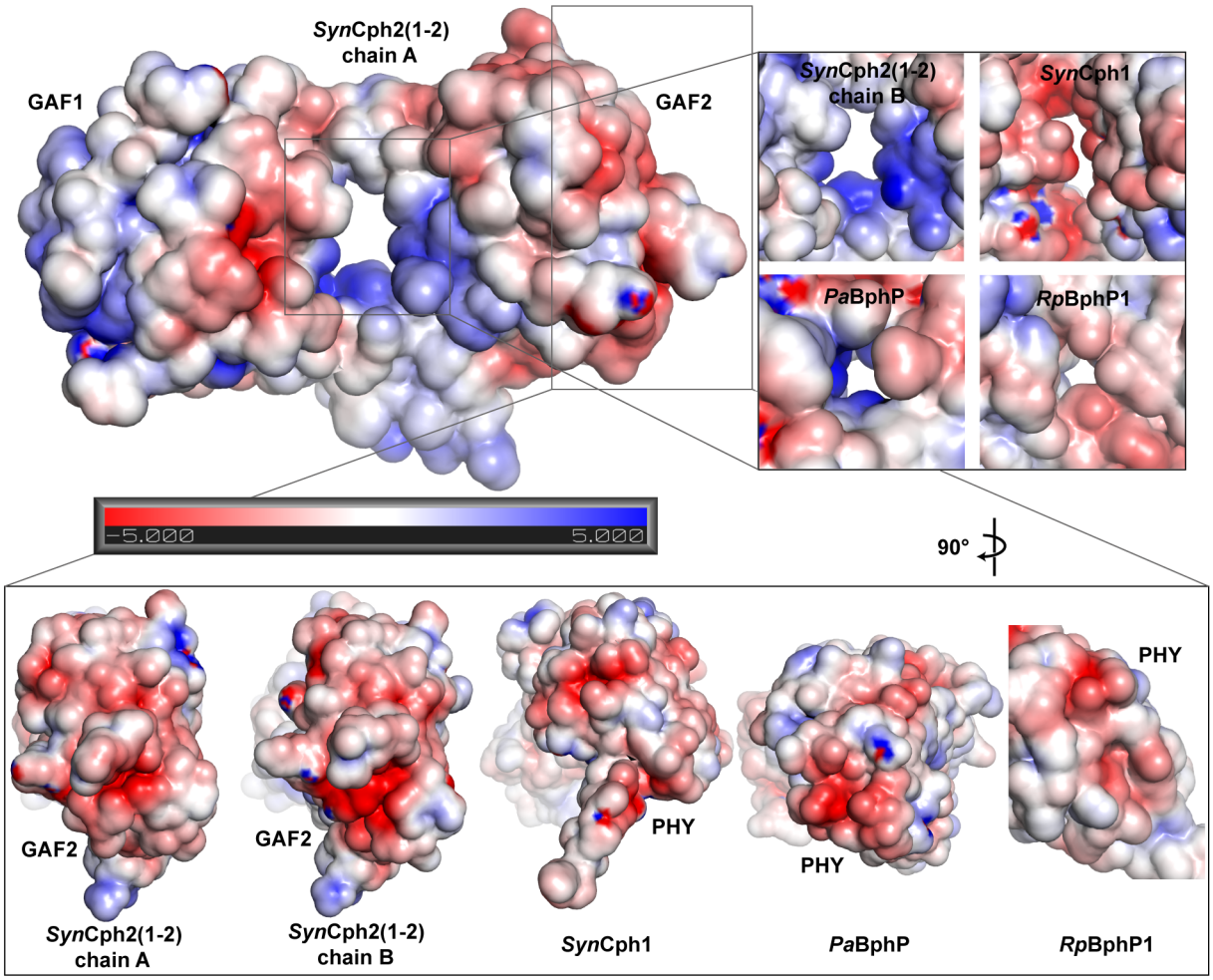

Figure 6.12: Electrostatic surface potential of *Syn*Cph2(1-2) (±5 kT/e) generated by APBS[167] (ion strength (+1/-1): 0.15, (+2/-2): 0; ion radius (+1): 2.0, (-1): 1.8, (+2/-2): 2.0; grid size: x=y=z= -1; 10 grid points/Å^2). PQR files were generated using the PDB2PQR server[168]. The color code indicates a negative (red) or positive (blue) potential on the surface, respectively. The inlet on the right displays a magnification of the region between GAF1/GAF2 of the *Syn*Cph2(1-2) chain B, *Syn*Cph1, *Pa*BphP and *Rp*BphP1. Below, the side view of GAF2 is shown.

The electrostatic surface potential of a protein might give a hint on possible binding sites or interaction interfaces. The surface potential of *Syn*Cph2(1-2) is displayed in Fig. 6.12 and reveals a positive region consisting of the amino acids that surrounds the hole in the protein structure built by the GAF1 domain, the domain-connecting long α-helix, the GAF2 domain and the tongue region of GAF2 (Fig. 6.12 inlet on the right). The positive potential at this position is not conserved in other phytochromes; *Syn*Cph1 for example comprises residues with a negative potential there. Also the size of the hole varies, as in the bathy-BphP structures of *Pa*BphP and *Rp*BphP1 it is rather small compared to *Syn*Cph2(1-2) or *Syn*Cph1. This is caused by the loop region following the tongue that proceeds into the C-terminal α-helix. In bathy-BphPs this loop region is shifted towards

the GAF domain (Ref.[139]: Fig. 7A) thus reducing the size of the hole. In the structure of the *Syn*Cph1 Y263F mutant a 17° shift of the PHY domain compared to the native *Syn*Cph1 structure is observed as the domain-linking α-helix can adopt various distinct conformations mediated by a hinge region within. Notwithstanding the major shift of the PHY domain the tongue still contacts the GAF domain. The authors suggest that the hinged linking α-helix might be functionally significant[84]. A change of the domain positions and subsequent reduction of the size of the hole during photoconversion therefore might be possible. A relevance of the hole region as interaction interface to potential binding partners seems unlikely given the size of the hole and the conservation of the charge distribution.

The electrostatic surface potential of *Syn*Cph2(1-2) shows a negative patch at the GAF1-averted face of the GAF2 domain (Fig. 6.12, lower inlet). The number of residues with a negative potential at this face is the highest in *Syn*Cph2 but also in the bathy-BphP and *Syn*Cph1 structures negative residues can be found. Given the position of this region, whose exposition must be hindered by the C-terminal effector domains, it is unlikely that another protein interacts at this position unless a conformational change would enhance the accessibility. Regarding the surface potential of *Syn*Cph2(1-2) it seems unlikely that it binds interaction partners though it cannot be ruled out.

6.4.2 Signaling *via* the chromophore's propionates

The chromophore propionate residues provide a possible route of intramolecular signal transduction[137]. Upon photoconversion a propionate-arginine partner swap occurs[85,137] in *Syn*Cph1 (for further details: Subsection 6.3.4) that can be also found in the signaling system of FixL, an oxygen sensor where the heme propionate partner swaps between two arginine residues in the different redox states[169]. For *Syn*Cph1 it was supposed that D-ring rotation after red-light illumination affects the positions of rings B and C and therefore the salt bridges which could have influence on the PAS / GAF interface[10]. In *Syn*Cph2(1-2) and other Group II phytochromes the propionate residues and the partner swap upon photoconversion are not conserved. It seems that the conservation of the arginine residues depends on the effector domains in the protein as lysine or polar residues instead of arginines are conserved in GGDEF domain-containing proteins[139]. Also in CBCRs these kinds of interaction are not observed (Fig. 6.11).

It is very unlikely for *Syn*Cph2(1-2) that the propionate surroundings are involved in signal transduction because they are very distant from the effector domains, the arginine residues are not conserved and an alanine substitution of Lys-104 does not affect the P_{fr} formation. Nevertheless, in HK domain-containing proteins the conserved arginine residues are very important for P_{fr} stabilization and therefore they participate at least indirectly on signal

transduction by stabilizing a chromophore conformation that can trigger the structural changes within the protein. It is also possible that the propionate partner swap induces changes in the α-helix bundle of the dimerization interface thus enhancing a signaling effect (Subsection 6.4.3).

On the other hand, a signal transduction pathway *via* the PAS domain is unlikely given the conservation of the arginines in Group I and PAS-less phytochromes . A direct proof against the propionate signaling path is difficult as the arginine conservation is given.

6.4.3 Parallel *vs.* antiparallel monomer orientation in the dimer

*Syn*Cph2(1-2) crystallizes as antiparallel dimer[139] though it is monomeric in solution[138]. *Syn*Cph1 also comprises an antiparallel arrangement[10] which is supposed to be a crystallization artifact as HKes like *Syn*Cph1 need a parallel association to allow trans-phosphorylation in the dimer[61,170,171]. It is supposed that the dimerization interface of HK-phytochromes is not just limited to the HK domain but proceeds also along the photosensory module[11,87]. In *Pa*BphP the monomers crystallize in parallel dimers where the interface extends over the whole length of the GAF-PHY linking helices[11]. In *Syn*Cph2(1-2) due to the missing PAS domain an additional N-terminal helix can contribute to the helical bundle and thus to the dimerization interface[139]. As crystal structures of phytochromes show tertiary and quaternary plasticity in the helical bundles of the interface[10,11,84,85] (Fig. 6.13) and even in the *Pa*BphP structure two distinct tertiary structures of the linking α-helix occur, the

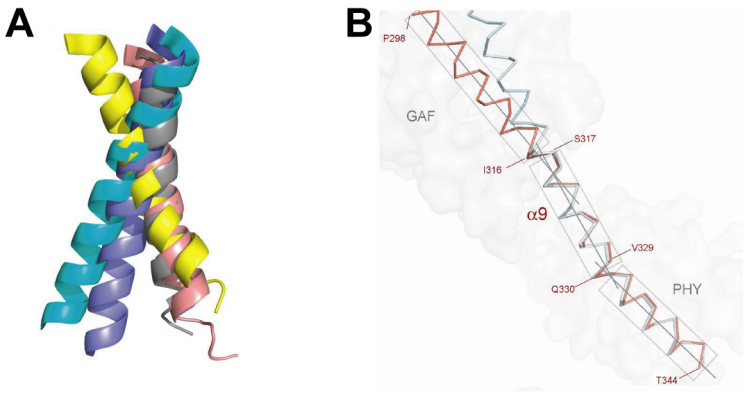

Figure 6.13: The GAF-PHY domain connecting α-helices differ in their quaternary structure. **A:** orientation of the α-helices in the dimers of *Dr*BphP (1ZTU: pink, 2O9C: gray), *Rp*BphP3 (2OOL, yellow), *Pa*BphP (3C2W, cyan) and *Pa*BphP-Q188L (3G6O, blue). The monomers of the dimer structures were aligned according to the PAS and GAF domains, the wide variation of the helix orientation in the other monomer is shown (figure from Ref.[11]). **B:** Conformational differences in the long α-helical linker of *Syn*Cph1 (cyan) and its Y263F mutant (red) . The amino acids in the hinge region are numbered (figure from Ref.[84]).

authors suggest that this plasticity plays an important role in signal transmission over long distances[11]. A cryo-EM structure of full-length *Dr*BphP, a PAS-GAF-PHY-HK BphP in the P_r state, shows a parallel dimer with a twisted structure including a central hole (Fig. 6.14 A)[87]. Available crystal structures were docked into the observed structure. Thereby,

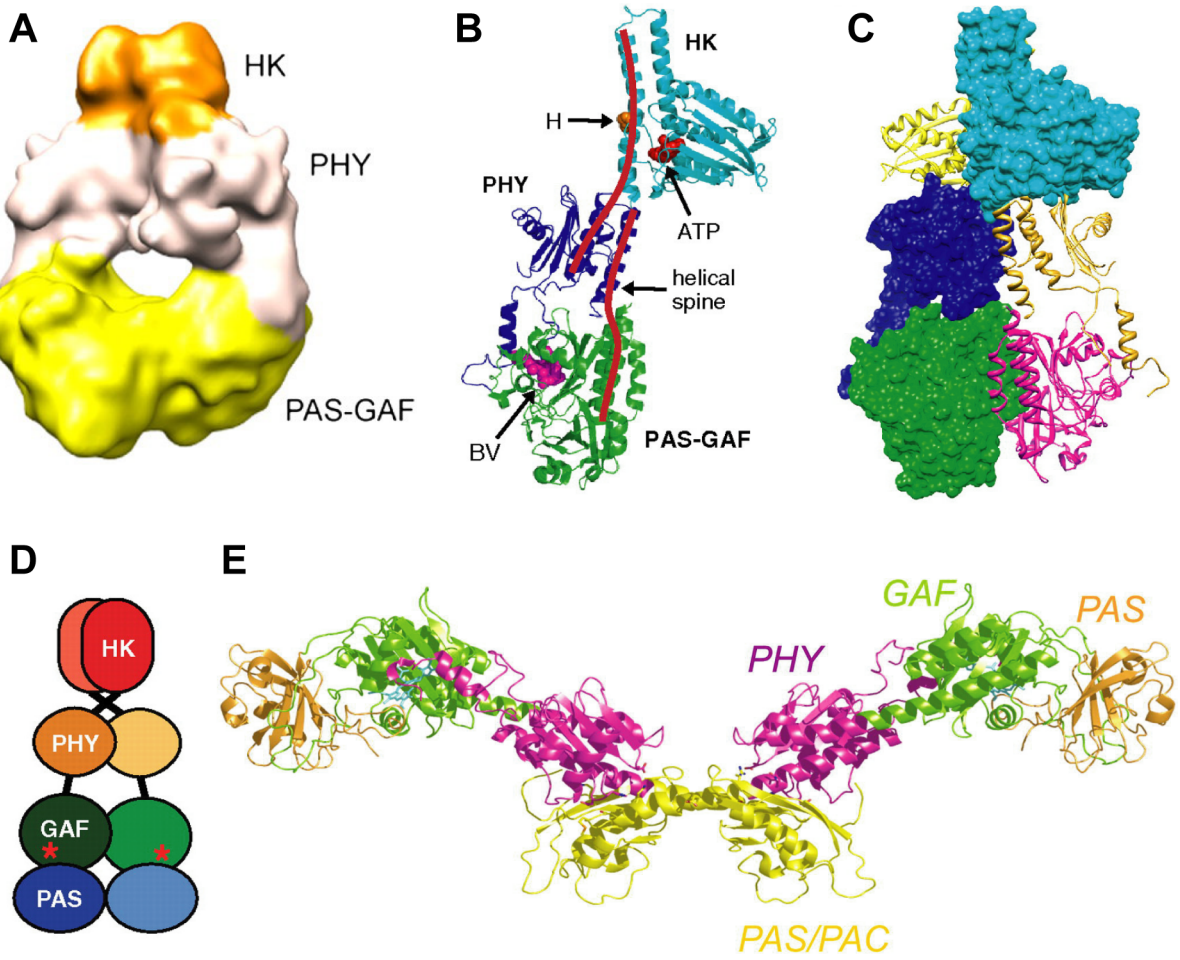

Figure 6.14: Parallel and antiparallel arrangements in phytochrome structures. **A:** Surface view on the 3D cryoEM density map of *Dr*BphP full length protein. The location of the PAS/GAF, PHY and HK domains are colored yellow, white and orange, respectively. Figure A-D are obtained from Ref.[87]. **B/C:** Model derived from docking of known crystal structures to the cryoEM map. **B:** *Dr*BphP monomer. The PAS/GAF, PHY and HK domains are displayed in green, blue and cyan, respectively. The positions of BV, the ATP-binding site and the conserved histidine residue for trans-phosphorylation are highlighted. The long α-helical linkers are shown as "helical spine" highlighted by a red line. **C:** *Dr*BphP dimer with one monomer in surface view. The HK domain is located at the opposite side of the α-helix which is shown as a simplification in **D**. The asterisks represent the binding pocket of the BV chromophore. **E:** Structure of the *Rp*BphP1 dimer (figure from Ref.[69]). The PAS, GAF, PHY and PAS/PAC domains are displayed in orange, green, magenta and yellow. The monomers are entangled near the PHY-PAS/PAC interface. Dimerization is promoted by the PAS/PAC domain.

the conformation of the PHY domain deviates from crystallographically determined structures as it comprises a 30° rotation possibly caused by a hinge in the connecting α-helix and leading to the central hole. As a crystal structure of the *Dr*BphP PHY domain is not available the PHY domain of *Pa*BphP was used for docking which might cause the structural differences. On the other hand this effect could reflect the flexibility of the GAF-PHY connecting α-helix[84] which could be an important feature for the *in vivo* domain arrangement and therefore might be important for signaling. The overall structure shows that each monomer forms an elongated, slightly bent conformation and twists around the other monomer in a parallel, right-handed fashion (Fig. 6.14 B)[87]. The dimerization interface involves all domains and comprises two long overlapping α-helices between GAF-PHY and PHY-HK, respectively, that were predicted also by *Yang et al.*[11]. The HK domains are twisted around each other as they are located at the opposite side of the long α-helix compared to the photosensory module (Fig. 6.14 C, D)[87]. Given these structural informations a model for HK-phytochromes was proposed[172]: upon illumination reorientation of the bilin induces conformational changes within the protein environment that involve rearrangements of the GAF domains relative to each other by modifying their dimerization interface and relative to the PHY domains by altering the tongue contact. These conformational changes are transmitted *via* the long α-helices to affect the HK domains in reorientation of the phosphoacceptor histidine relative to the ATP-binding catalytic site which enables trans-phosphorylation. Also the binding affinity of the response regulator could be altered thus allowing the intermolecular phosphotransfer[172]. This hypothesis could be an explanation for the conservation of the B-ring propionate-interacting arginine residues in phytochromes with HK effector domains as they could affect the dimerization interface because they are in close proximity of the helix bundle.

Interestingly, an engineered PAS-GAF construct of *Dr*BphP where the stabilizing interactions in the dimer interface are removed and which is therefore monomeric, allows photoconversion to P_{fr} that is inhibited in the wild type construct caused by the missing PHY domain. The authors suggest that in the truncated *Dr*BphP construct the dimerization inhibits photoconversion that is overcome in the native structure by the PHY domain. This is caused by the relief of the constraints from the helix packing at the dimer interface which allows more degrees of freedom[152].

The first phytochrome structure including most of the effector module is from the bathy-BphP *Rp*BphP1[69]. The protein contains a PAS/PAC domain and a novel two-helix output sensor (HOS) domain. *Rp*BphP1 forms a complex with the transcriptional repressor *Rp*PpsR2 after photoconversion in P_r that requires the HOS domain. In the crystal structure the monomers form an antiparallel dimer where the dimerization interface does not involve the photosensory module but just the effector domains (Fig. 6.14 E). Thereby, the antiparallel arrangement is crucial for HOS domain activation[69]. This proves that

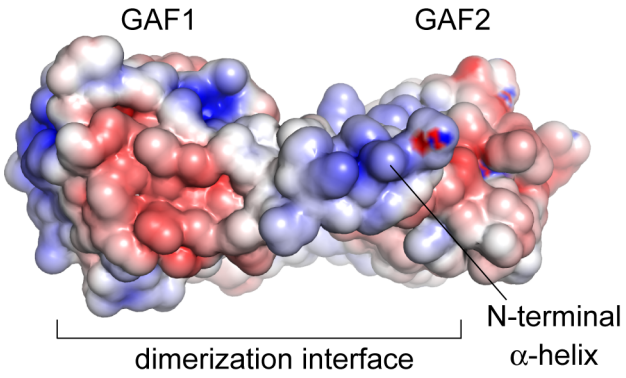

Figure 6.15: Electrostatic surface potential of *Syn*Cph2(1-2) (±5 kT/e; ion strength (+1/-1): 0.15, (+2/-2): 0; ion radius (+1): 2.0, (-1): 1.8, (+2/-2): 2.0; grid size: x=y=z= -1; 10 grid points/$Å^2$) at the dimerization interface. Negative and positive potentials on the surface are shown in red and blue, respectively.

phytochromes do not necessarily dimerize in the photosensory module but comply the requirements of their effector modules. Interestingly, as shown for *Dr*BphP [87] and proposed for *Pa*BphP [11] also *Rp*BphP1 comprises a helical spine of two long overlapping α-helices [69].

The structure of *Rp*BphP shows that the antiparallel monomer arrangement in the crystal structure of *Syn*Cph2(1-2) could be not just a crystallization artifact but indeed the physiological conformation for signaling. Also in the GGDEF-EAL domain containing protein FimX, a regulator of twitching motility in *Pseudomonas aeruginosa*, that is a high-affinity receptor for c-di-GMP as both its GGDEF and EAL domain are degenerated, elongated antiparallel dimer organization determined by SAXS measurements can be observed. The GGDEF-EAL module is not involved in dimerization that is mediated by the N-terminal REC and PAS domains [173]. Given these structural insights the antiparallel arrangement of *Syn*Cph2(1-2) may be of physiological relevance. The electrostatic surface potential at the dimerization interface of *Syn*Cph2(1-2) (Fig. 6.15) reveals opposing positive and negative batches in the interface that fit nicely upon dimerization. Also the degree of conservation (Fig. 6.17) observed in the interface area is high, suggesting that the helix bundle in the crystal structure might have a relevance *in vivo*. Besides the mainly monomeric quaternary structure of *Syn*Cph2(1-2) the elution profile of size exclusion chromatography shows a distinct dimeric state, next to minor peaks of oligomeric arrangements [138].

6.4.4 The tongue region - a highway for signaling?

In our experiments we could see that the $W^G/_A G$, PRxSF and WxE motifs in the tongue region, that are conserved in Group I and Group II phytochromes, are crucial for formation of the P_{fr} state [139], whereby the bulky aromatic character of the tryptophan residues is

important. In bathy-BphPs the PRxSF motif exhibits an inverted orientation; instead of the arginine residue, Ser-385 points towards the chromophore and hydrogen bonds to the aspartate of the DIP motif. Furthermore, the positions of the conserved tryptophan residues are inverted in bathy-BphPs. The structural differences in the tongue region of phytochromes with P_r or P_{fr} ground states (Ref.[139]: Fig. 7A) are also given in the stem region as they comprise a β-sheet or an α-helix in this region, respectively. Interestingly, *Syn*Cph2(1-2) comprises an increased α-helical content upon photoconversion in P_{fr}; in addition the hydrodynamic diameter of the protein is enlarged[138]. Also for PhyA from oat a 3% increase of the α-helical content in P_{fr} is detected *via* CD spectroscopy. Upon binding of a monoclonal antibody to the N-terminus the effect is repressed[174]. For PhyA from pea the same increase can be observed[175]. Comparing these findings with the structure of *Syn*Cph1 this effect does not surprise as the N-terminus is situated in close proximity of the tongue region and an antibody would easily affect a structural rearrangement of the latter. As in *Syn*Cph2(1-2) the N-terminal PAS domain is missing this leads to the conclusion that the increase of the α-helical content in *Syn*Cph2(1-2) is very likely associated with the tongue region.

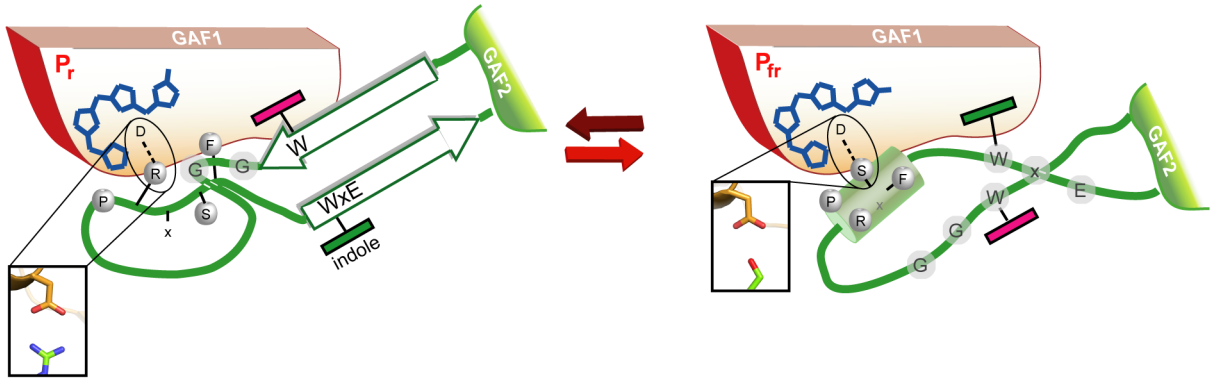

Figure 6.16: Model for conformational changes within the tongue region during photoconversion (figure from Ref.[139]). Upon red-light illumination the aspartate - arginine salt bridge between the GAF1 domain and the tongue (inlet) is broken. The tip of the tongue refolds and induces a disordering in the β-sheet stalk region while the tryptophan motifs are switched and the new aspartate - serine hydrogen bond (inlet) is formed.

Given all these findings we created a model for the conformational changes of the tongue region *via* tryptophan switch during photoconversion from P_r to P_{fr}[139] (Fig. 6.16). Upon illumination with red light the $Z \rightarrow E$ isomerization of the chromophore triggers structural changes. The aspartate-arginine salt bridge between the GAF1 domain and the tongue is broken *via* a swap of the anchor-like tryptophan residues from the $W^G/_A G$ and WxE motifs. The tongue is refolded as the β-sheets are rearranged and an α-helical structure evolves. Upon these reorganizations the PRxSF motif is inverted and a new GAF1-tongue-connecting hydrogen bond between aspartate and serine is formed (Fig.

6.16).

As the tryptophan-switch model is also based on the P_{fr} structures of bathy-BphPs it is possible that the P_{fr} structure of P_r-ground state phytochromes differs. On the one hand there must be a structural difference because the latter do not exhibit a dark-adapted P_{fr} state. On the other hand the P_{fr} CD spectra of bathy-BphPs and non-bathy phytochromes deviate, but this can be assigned to the type of bound chromophore and the D-ring orientation[136] (Section 6.3.3). As the relevance of the conserved residues is underlined by mutagenesis studies[138,139,166] the differences in bathy- and non-bathy phytochromes very likely do not affect the changes described in the model and it might be true for both phytochrome classes.

Supposedly, the structural rearrangements in the tongue region affect the C-terminal α-helix that connects the GAF2 and GGDEF domains. An alignment of Group II phytochromes (used proteins according to alignment in Ref.[139]) reveals a conservation pattern for *Syn*Cph2(1-2) that is shown in Fig. 6.17 in the crystal structure. Apart from the chromophore surroundings also the helices which are involved in the helix bundle in the dimer show a high grade of conservation. In the GAF2 domain many amino acids in the central β-sheet are conserved, the role of this conservation pattern is elusive at the moment. In the region from the tongue to the C-terminus only a few amino acids are conserved in all considered Group II phytochromes, which are highlighted in Fig. 6.18. Besides Trp-369,

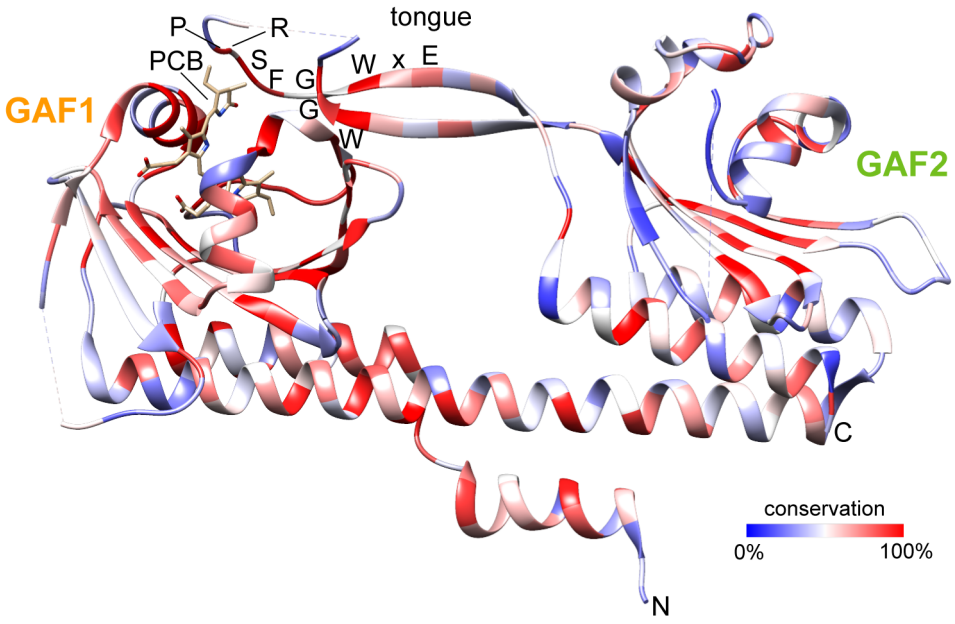

Figure 6.17: Conservation of the *Syn*Cph2(1-2) amino acids in relation to Cph2-like Group II phytochromes (used proteins according to Ref.[139]: Fig. 5) as presented with the Chimera program[176]. The degree of conservation is indicated by a color code in which 0% and 100% conserved amino acids are displayed in blue and red, respectively.

Gly-371, Pro-382, Ser-385 and Trp-389 of the $W^{G}/_{A}G$, PRxSF and WxE motifs in the tongue region only two more residues are conserved: Leu-406 and an additional tryptophan residue Trp-399. This residue and its orientation is also conserved in *Syn*Cph1 and in the bathy-BphPs *Pa*BphP and *Rp*BphP1 (Fig. 6.18). As in bathy-BphPs the loop region, where the residue is situated, is shifted towards the GAF1 domain and might affect the proceeding α-helix, this tryptophan residue could have a role in signal transduction as anchor of its secondary structure element.

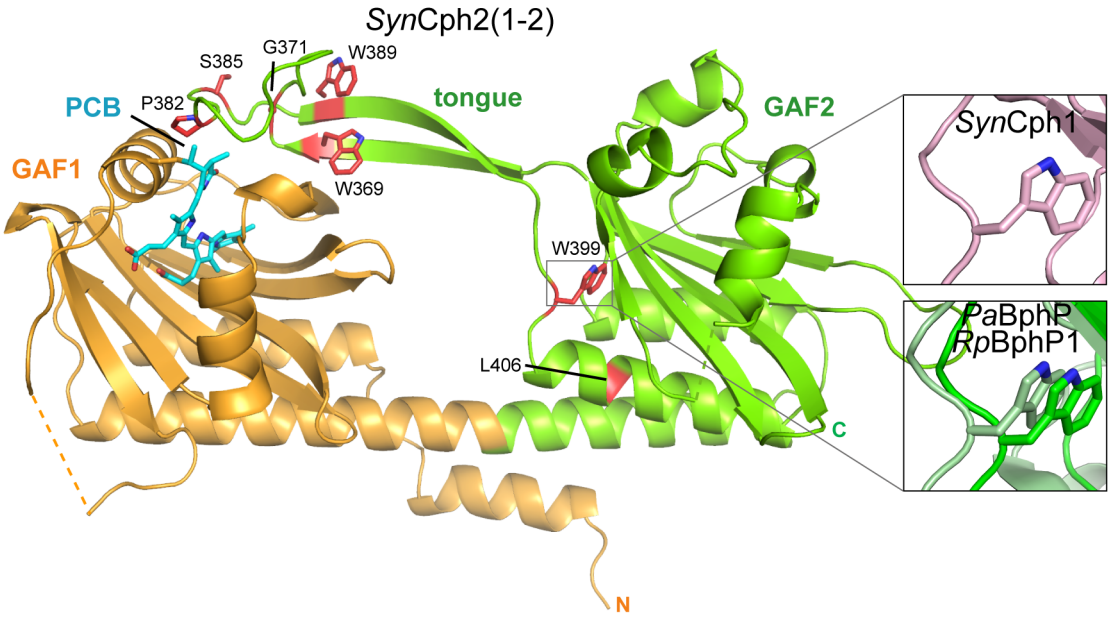

Figure 6.18: Amino acids from the tongue region to the C-terminus in *Syn*Cph2(1-2) that are conserved in all considered PAS-less phytochromes (Fig. 6.17). GAF1, GAF2 and PCB are displayed in orange, green and cyan, respectively. The conserved amino acids are shown in stick presentation and are highlighted in red. The inlets on the right side show the conserved tryptophan residue Trp-399 in *Syn*Cph1 (violet), *Pa*BphP (green) and *Rp*BphP1 (pale green).

A change in the position of the GAF2 domain after photoconversion due to the flexible long α-helical linker is possible and might have further effects on the C-terminal helix. For *Syn*Cph1 it could be shown that in the parallel dimer upon photoconversion the neighboring PHY domains move closer together whereas in the monomers the PHY and HK domains move further apart which brings the HK domain in an active conformation [177].

Suggesting that like in *Dr*BphP [87] the effector domains of *Syn*Cph2 are connected to GAF2 *via* a long α-helix, the signal transduction could proceed *via* multiple structural rearrangements. In the BLUF-EAL protein YcgF the domain connecting α-helix is supposed to move relative to the domain surface of BLUF upon photoactivation and either controls the access to the c-di-GMP binding site or the dimeric association of the EAL domain [178]. In the *Avena sativa* phototropin 1 it could be shown that covalent attachment of FMN to the LOV2 domain under illumination triggers a conformational change that results in

the unfolding of an α-helix located outside of the domain (Jα-helix)[179], a crucial event in the regulation of kinase signaling in phototropin[180]. Such an unfolding of the α-helix could explain that after photoconversion the PHY and HK domains in *Syn*Cph1 are further apart[177]. Nevertheless, this has not been observed in phytochromes, yet. On the other hand similar characteristics have been shown for a putative class III adenylyl cyclase from *Mycobacterium tuberculosis* that comprises a catalytic and a regulatory domain that are connected *via* a long α-helix. This helix is partly unfolded from the inhibited to the active state thus rotating the catalytic domains to form two catalytic sites in the dimer[181] (Fig. 6.19 A). Interestingly, the crystal structure of the human phosphodiesterase PDE2 (Fig. 6.19 B), which is composed of a GAF-GAF bidomain and the catalytic domain, resembles closely the cryo-EM structure of *Dr*BphP[87] in the GAF-GAF arrangement

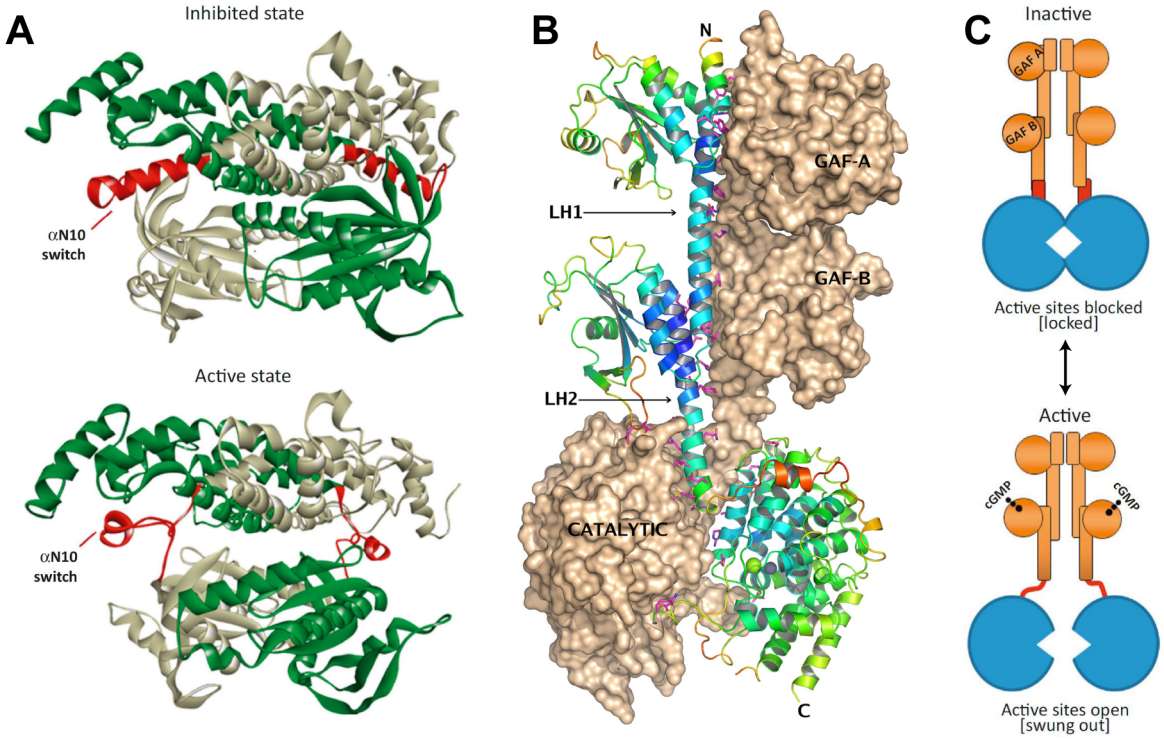

Figure 6.19: Examples of proteins that use partially unfolding of helices for signaling. **A:** Adenylate cyclase Rv1264 unfolds an α-helix upon activation. In the dimeric structure the two-domain monomers are shown in green and gray, respectively. The domains are connected *via* the αN10 switch which unfolds and is shown in red (Figure from Ref.[182], adapted from[181]). **B:** Dimeric crystal structure of the cyclic nucleotide phosphodiesterase 2. The first monomer is shown in ribbon presentation colored by crystallographic B-factor, blue = low, red = high; the second monomer is displayed in surface presentation. The long connecting α-helices are indicated as LH1 and LH2 (Figure from Ref.[183]). **C:** Model of the PDE-2 activation. In the inactive state the active sites are blocked; upon binding of cGMP to GAF2 the connecting α-helix (red) partly unfolds whereby the catalytic domains can rearrange thus leading to accessibility of the active sites. GAF domains and the catalytic domain are shown in orange and blue, respectively (Figure from Ref.[182]).

(GAF-PHY in *Dr*BphP) as well as in the two interdomain-connecting long α-helices. Interestingly, the α-helical linker between GAF2 and the catalytic domain is supposed to be partly unfolded upon cGMP-binding to GAF2 which results in an accessibility of the active sites[182,183] (Fig. 6.19 C). The same mechanism could be attributed to HK-phytochromes like *Syn*Cph1 that demand parallel dimerization for signaling and for other phytochromes like *Syn*Cph2 where an unfolding might result in an rearrangement of the effector domains thus activating them.

6.4.5 Signaling in CBCRs

Signaling in CBCRs cannot be mediated by a PHY domain as they function as GAF-only photoreceptors. In the known CBCR crystal structures the monomer orientation differs. *An*PixJ and *Te*PixJ (*15E*) form parallel dimers building a helix bundle in the dimerization interface like in phytochromes[122]. On the other hand in the *Te*PixJ (*15Z*) structure an antiparallel arrangement is observed[123,184]. The recently published NMR structures of *Te*PixJ in the *15Z*- and *15E*-state (PDB codes 2M7U and 2M7V, respectively) comprise a monomeric protein suggesting that the contacts between the GAF domains are insufficient to maintain the dimer organization in solution[184].

Like in phytochromes[69,87] the C-terminal α-helix of the GAF domain in *An*PixJ and *Te*PixJ is continuously connected to the helix of the neighboring domain as indicated by secondary structure predictions[122]. As long helices are suggested to transmit signals over long distances[11] this feature of signaling could be an ubiquitous feature in GAF-containing photoreceptors.

For *Te*PixJ it is supposed that any motion affecting the helix is crucial for signal transduction[184]. On the one hand this could be accomplished by the observed displacement of the β-sheet in *Te*PixJ during *15Z* $\rightarrow$ *15E* photoconversion caused by the release of one β-strand. This could affect the mobility and positioning of the N- and C-terminal α-helices because they are coupled to a pair of β-strands[184]. On the other hand a structural reorganization can be observed upon photoconversion as a β-strand is converted into a flexible region and a 3_{10}-helix. This disrupts an arginine - glutamate salt bridge between the β-strand and the N-terminal α-helix which could alter the mobility of this helix[184]. The refolding event of the secondary structures reminds of the signal transduction in LOV photoreceptors[179] (Section 6.4.4). This process could loosen the constraints on the flanking HAMP domains in *Te*PixJ by an axial rotation of the helix bundles[184]. HAMP domains were shown to transmit a intramolecular signal *via* an axial rotation of a helix bundle in its dimerization interface[185].

We were able to show that the GAF-GGDEF construct of *Syn*Cph2(5-6) can produce c-di-GMP in a light-dependent manner[145]. The mechanism of intramolecular signal

transduction involving long interdomain α-helices seems plausible if the GAF domain is followed directly by or is situated directly after an effector domain. However, CBCRs often contain multiple copies of chromophore-binding GAF domains in a row in front of the effector module[186]. AphC from *Nostoc* sp. PCC 7120 contains three GAF domains in its photosensory module, whereby GAF1 and GAF3 are chromophore-binding domains and exhibit P_r / P_{fr} and P_r / P_o photochemistry, respectively[116]. Although GAF1 is photochemically active as stand-alone domain, it is likely that GAF1-2 comprise a Group II phytochrome as GAF2 contains the WAG and PRxSF motif as well as the tryptophan residue of the WxE motif. In this study it was shown that both, GAF1 and GAF3, affect the activity of the C-terminal HK module. The *15E*-GAF1 / *15E*-GAF3-state exhibits the highest rate of autophosphorylation activity, *15E*-GAF1 / *15Z*-GAF3 shows intermediate activity and the *15Z*-GAF1 / *15Z*-GAF3-state is the least active state[116]. In this context it is possible that the GAF domains are positioned on a long α-helical spine, composed of a helix bundle with overlapping long interdomain α-helices, which is influenced by each single GAF domain. Thereby, a signal reaches the effector domain that is an integrated result of the different GAF signals. This would represent an immense fine-tuning effect on the output module in CBCRs.

6.4.6 Impact of the *Syn*Cph2 signaling on *Synechocystis* phototaxis

We could show that *Syn*Cph2(5-6) produces c-di-GMP in the GGDEF2 domain under blue light conditions. This results in *Synechocystis* cells that do not move towards blue light, whereas *cph2*-deficient cells ($\triangle$*cph2*) comprise positive phototaxis under these conditions[145]. In comparison to *Syn*Cph2(5-6), *Syn*Cph2(1-4) does not exhibit such a clear phenotype. However, an impact on the growth of *Synechocystis* cells by *Syn*Cph2 was shown, as *cph2*-deficient cells comprised reduced growth under red light conditions[103] thus implying that the P_{fr} state is indeed the signaling state in *Syn*Cph2(1-2).

*Syn*Cph2(5-6) fails to replace the full length protein under white light conditions as the mutant remains immobile because of the blue light content in the light. A coproduction of *Syn*Cph2(5-6) and *Syn*Cph2(1-4) in $\triangle$*cph2*-cells restores the wild type phenotype under white light that shows positive phototaxis. Apparently, *Syn*Cph2(1-4) counteracts the inhibitory activity of *Syn*Cph2(5-6) thus proving that its EAL domain is indeed active and degrades c-di-GMP[145]. The GGDEF1 domain on the other hand is catalytically inactive as it contains mutations in the residues essential for catalysis.

The domain architecture of *Syn*Cph2 and the fact that GGDEF and EAL domains are usually located at the C-terminus of sensory domains[92] indicate that it is a hybrid of a Group II phytochrome with C-terminal GGDEF*-EAL domains and a CBCR-GAF domain followed by a GGDEF domain. Interestingly, the single modules can be found

in other cyanobacterial species. The CBCR-GGDEF modules are in at least 17 gene products C-terminal in different multi-domain proteins but can be also found as stand-alone proteins[145]. The *Syn*Cph2(1-4) module is not so widely spread in cyanobacteria as *Syn*Cph2(5-6). It can be found in at least six other gene products, three of them with the same domain architecture as *Syn*Cph2, three others as stand-alone proteins. As in two cyanobacteria, *Microcoleus vaginatus* FGP-2 and *Oscillatoria* sp. PCC 6505 both modules of *Syn*Cph2 are found in two different gene products[145], it can be assumed that *Syn*Cph2 may be a Rosetta stone protein. The latter describes the effect that when two or more proteins that are encoded separately in the genome also appear as fusion proteins, either in the same or in some other organism, such fusion proteins (Rosetta stone proteins) indicate a possible interaction of the single proteins[187,188]. For the modules of *Syn*Cph2 this has not been shown, yet. On the other hand the activity of both counter-acting EAL and GGDEF domains would help to level the c-di-GMP concentration in the direct environment of the protein therefore comprising a wavelength-dependent fine-tuning of the c-di-GMP level. It also seems plausible, that in a post-translational step the full-length protein is cleaved to achieve two functional modules. For the BV-binding BphP BphG1 from *Rhodobacter sphaeroides*, a PAS-GAF-PHY-GGDEF-EAL protein, it could be shown that it comprises light-independent PDE activity. As recombinantly expressed in *E. coli*, BphG1 undergoes partial cleavage into a PAS-GAF-PHY-GGDEF module and in an EAL domain that retains its PDE activity. Interestingly, the other module without the EAL domain now shows light-dependent DGC activity. Whether the cleavage of the EAL domain occurs also in the native host *R. sphaeroides* has still to be tested[189].

The *Syn*Cph2(1-4) module contains both, a GGDEF* and an EAL domain. The combination of c-di-GMP producing and degrading domains within one protein is well known[95]. Thereby one domain often is catalytically inactive as in *Syn*Cph2 and has different tasks. The GGDEF*-EAL protein CC3396 from *Caulobacter crescentus* with an catalytically inactive GGDEF domain exhibits PDE activity. Instead of DGC activity the GGDEF* domain has a regulatory function and binds GTP to in response activate the PDE activity of the subsequent EAL domain[99]. This mechanism would be also plausible for the *Syn*Cph2(1-4) module.

6.5 Photoconversion - a one-way street for phytochromes

As in other phytochromes[37] we could show that the photoconversion in *Syn*Cph2(1-2) is a unidirectional process as in the $P_{fr} \rightarrow P_r$ reaction other intermediates than in the $P_r \rightarrow P_{fr}$ are passed[166]. Based on our findings of the photocycle intermediates as well as the results of other groups and suggesting that the photocycles of Group I and Group II phytochromes are not essentially different a possible photocycle of *Syn*Cph2(1-2) is proposed

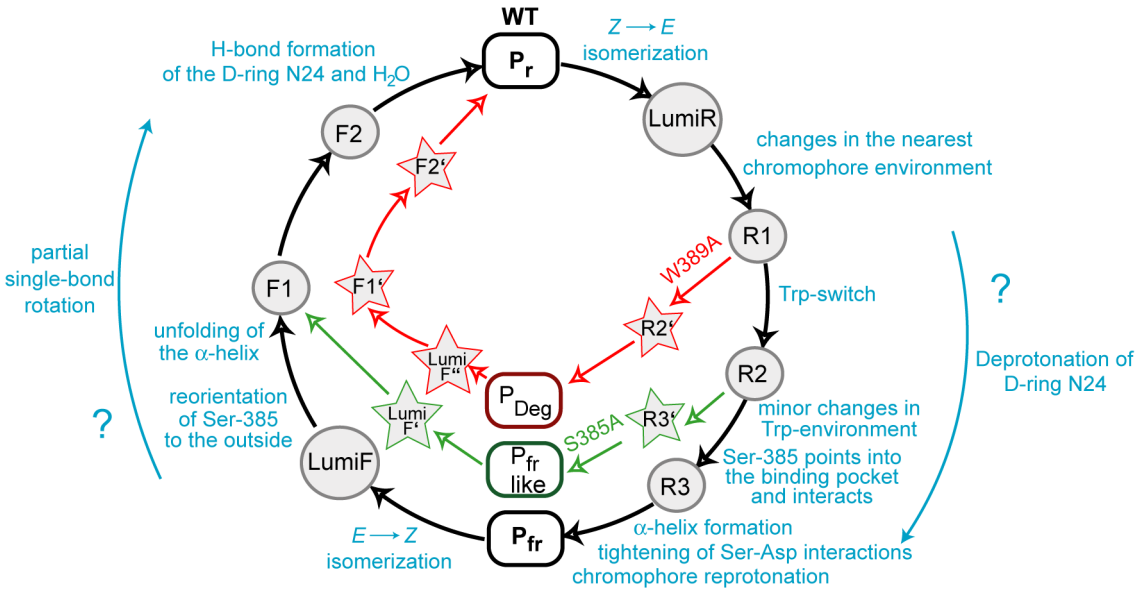

Figure 6.20: Proposed photocycle of *Syn*Cph2(1-2) (black lines), similar in Ref.[166]. Rounded rectangles highlight P_r, P_{fr} and P_{fr}-like states, circles the intermediates. The differing intermediates of the S385A and W389A mutants are shown as green and red stars, respectively. Colored arrows indicate deviations of the wild type photocycle caused by the mutation. The structural changes presumably occurring during the formation of an intermediate or the final state are shown in blue. The blue arrows with the question mark indicate that it is not possible to assign the deprotonation or single bond rotation to the R2 / R3 or F1 / F2 formation, respectively.

here (Fig. 6.20).

Upon red light illumination of P_r the chromophore undergoes a $Z \rightarrow E$ isomerization and the Lumi-R state is built. The next intermediate R1 is reached, where the changes compared to P_r just extend from the chromophore to its nearest environment as the tongue region seems not to be affected in these intermediates[166]. In intermediate R2 the first changes in the tongue region occur, as an alanine substitution of Trp-389 is not able to reach a native R2 intermediate (Fig. 6.20). As the phenylalanine mutation can restore wild type-like behavior and underlines the importance of the bulky aromatic character of this residue, it can be assumed that the previously supposed tryptophan switch triggers the formation of the R2 intermediate. Either during transition in R2 or in R3 the chromophore is deprotonated at the D-ring nitrogen N24 with a water molecule as proton receptor[37]. On the other hand in *At*BphPI it could be shown that the aspartate of the DIP motif is essential for this deprotonation because in the D197A mutant no transient proton exchange of the chromophore can be observed[163]. As the S385A mutant affects the formation of intermediate R3[166] it can be assumed that the changes in the tongue region extend to the tongue's tip in this intermediate. Presumably the orientation of the serine residue is changed and it points into the binding pocket. Eventually it is already participating in the

hydrogen bond network that also involves Asp-79. Given that the W389F mutant exhibits an increased lifetime of this intermediate minor changes in the tryptophan environment might also occur in this intermediate. Interestingly, *Arabidopsis thaliana* and *zea maize* PhyA and PhyB possess a phenylalanine residue at the tryptophan position implying, that these minor changes are not affecting photoconversion.

During the transition of R3 to P_{fr} in pea PhyA the α-helical content increases, that is observed in phytochromes during photoconversion into P_{fr} [175]. As the α-helix in the tongue region of bathy-BphP structures involves the serine residue (which is also predicted for *Syn*Cph1, Fig. 6.7) it can be assumed that the reorganization of the tongue's secondary structure is a process that extends from the formation of R3 to P_{fr} and is divided in at least two steps. At first the serine is oriented towards the chromophore, whereas in the second step the α-helix is built, supposedly tightening the serine - aspartate interactions. During the R3 $\rightarrow$ P_{fr} transition the chromophore is reprotonated on N24 under involvement of the DIP aspartate [37] and/or of His-130 [161,163]. Given the quantum yield of photoconversion of 0.12 in *Syn*Cph2(1-2) [138] only 12% of the energy is used for P_{fr} formation.

In the $P_{fr} \rightarrow P_r$ photoconversion already the early intermediate Lumi-F resembles the P_r state and displays only minor subsequent absorption changes [166]. In the $P_{fr} \rightarrow$ Lumi-F transition the $E \rightarrow Z$ double bond isomerization occurs. The decrease of the α-helical content in pea PhyA is observed earlier as in the forward reaction, namely during the Lumi-F $\rightarrow$ F1 transition [175]. The S385A mutant of *Syn*Cph2(1-2) affects only the Lumi-F and not the following states thus suggesting that in F1 the orientation of the serine residue has already changed towards the opposite site of the chromophore binding pocket. During transition in F1 or F2 the partial single bond rotation at C14-C15 takes place involving the break of the D-ring nitrogen N24 - DIP-aspartate interaction [37]. The cryo-trapped L1 state in the $P_{fr} \rightarrow P_r$ photoconversion of *Pa*BphP could be identified as Lumi-F; here the single-bond rotation already occurred and the N24 - aspartate hydrogen bond is broken [86] suggesting that this process occurs earlier in photoconversion than expected or that the assignment of the structure is wrong. In the F2 $\rightarrow P_r$ conversion the hydrogen bond of the D-ring nitrogen to a water molecule is established [37]. The quantum yield of the $P_{fr} \rightarrow P_r$ photoconversion is 0.19 and thus higher as for the forward reaction [138].

6.6 *Syn*Cph2 sensing color - an unusual phytochrome?

*Syn*Cph2, assuming that it is not cleaved post-translationally, is a protein that can sense red, far red, blue and green light [138,145] as well as supposedly UV-A light [107]. This makes *Syn*Cph2 a "color-sensing" protein that can level c-di-GMP concentrations according to the light qualities [145]. The N-terminal *Syn*Cph2(1-2) module comprises red / far red photochemistry like canonical phytochromes [138] and conserves structural requirements like

the tongue region and the long domain-connecting α-helix[139]. It can therefore be assumed as minimal model for plant phytochromes.

It is rather unusual for a phytochrome to be associated with another photosensory module. Other rare examples of the latter is *Ac*Phy3, a protein from the fern *Adiantum capillus-veneris* that comprises a N-terminal phytochrome module that shows P_r / P_{fr} photoconversion and a C-terminal phototropin-like module that involves two LOV domains and is supposed to sense blue light[190]. As homologous genes of the latter have been identified in other ferns, the gene family was named "neochrome"[40]. Another example for color-sensing phytochromes is the PYP-phytochrome Ppr from *Rhodospirillum cectenum.* It contains a N-terminal photoactive yellow protein (PYP) domain, a central phytochrome photosensory module and a C-terminal HK domain. The N-terminal domain of Ppr covalently attaches the blue-light absorbing PYP-chromophore 4-hydroxycinnamic acid and exhibits a photocycle that is spectrally similar to PYP but kinetically slower[191]. The phytochrome module attaches BV and the full length protein exhibits a mixed PYP-phytochrome spectrum[192].

AphC from *Nostoc* sp. PCC 7120 is a HK that triggers the cAMP signaling cascade dependent on red and far red light[193]. It contains three N-terminal GAF domains whereby GAF1 and GAF3 are able to bind a chromophore[116]. As GAF2 comprises conserved tongue motifs, AphC is presumably like *Syn*Cph2, a hybrid of a Group II phytochrome and a CBCR GAF domain. The autophosphorylation activity of the HK domain was shown to be dependent from the photostate of both chromophore-binding domains[116] (Subsection 6.4.5).

6.7 Applications of GAF-containing photoreceptors

Using light in the infrared region is attractive for applications in life sciences, because most autofluorescence, scattering as well as absorption from lipids, water and heme can be mostly avoided thus allowing imaging through thick tissue and in live animals[152]. Accordingly, fluorescent proteins, biosensors or optogenetic constructs in synthetic biology (Fig. 6.21) should preferably comprise fluorescence or action spectra in this wavelength range[194]. As phytochromes meet these requirements par excellence they represent an interesting target for bioengineering. Thereby, their use as permanently fluorescent proteins is the most accomplished application.

Engineering of near-infrared fluorescent phytochromes involves several strategies to inhibit photoconversion, namely the stabilization of the P_r conformation of the chromophore and thereby hindrance of the $Z \rightarrow E$ isomerization from the excited state. Moreover, the destabilization of the chromophore after photoisomerization and thereby increasing the back-flipping from Lumi-R* to P_r* is used to increase the fluorescence. Additionally,

the decrease of the deprotonation rate of the chromophore is applied[152]. For example the incorporation of a non-native chromophore like PEB increases the fluorescence yield as well as mutations like Y176H in *Syn*Cph1[157]. The truncation of the PHY domain and introduction of amino acid substitutions also enhance fluorescence properties[194] like in Wi-Phy, a monomeric PAS-GAF construct of *Dr*BphP with mutations in the dimerization interface as well as in the DIP aspartate and a tyrosine residue in the D-ring environment[152]. It could be shown that the same construct but without the tyrosine substitution can be used as infrared-fluorescent protein in mammalian cells and mice where it spontaneously incorporates BV, derived from heme breakdown in the organism[195]. The PAS-GAF construct with various amino acid substitutions iRFP of *Rp*BphP2 from *Rhodopseudomonas palustris* was analyzed by RR and molecular dynamics simulations. Compared to the wild type protein the tilt angle of the chromophore D-ring in iRFP compared to ring C is increased, accompanied by a loss of hydrogen bond interactions of the ring D carbonyl. Also the number of water molecules in the binding pocket is decreased[196].

Phytochromes can also be used as fluorescent biosensors taking advantage of the multidomain organization, the possibility to change the spectral characteristics *via* altering the chromophore or by changing the tertiary structure[194]. Therefore, they can be used in the detection of redox potentials, metal ions or of protein-protein interactions. The mechanism for sensing redox potentials depends on the reversibility of chromophore attachment to phytochromes as it can compete with the formation of a disulfide bond with an additionally introduced cysteine substitution. Metal ion detection occurs *via* coordination of the bilin chromophore and the ion which alters the spectral and fluorescent characteristics[194]. A mercury ion BphP-based biosensor is already available that uses the high binding affinity of mercury ions to cysteines thus inhibiting BV binding[197]. For the detection of protein-protein interactions the phytochrome PAS and GAF domains can be used as split-based biosensors where the domains are on two separate polypeptide chains, each associated with one possible interaction partner, respectively. Upon association of the interaction partners the PAS and GAF domains come into close contact, BV can be assembled and the protein complex starts to fluoresce[194]. The function of such a split near-infrared biosensor based on *Rp*BphP2 could be shown in *HeLa* cells and even in living mice[198].

The third application for phytochromes in bioengineering is their use in optogenetics[199]. The latter term describes the usage of photoreceptors to control biological processes in mammalian cells and tissues[194]. In contrast to phytochromes[194] flavin-binding proteins are well established as optogenetic tools, for example a phototropin LOV domain was fused to Rac1, a key GTPase regulating actin cytoskeletal dynamics in metazoan cells. It sterically blocks Rac1 interactions until irradiation unwounds the domain-linking α-helix. Illumination is thus able to induce cell motility and controls the direction of cell move-

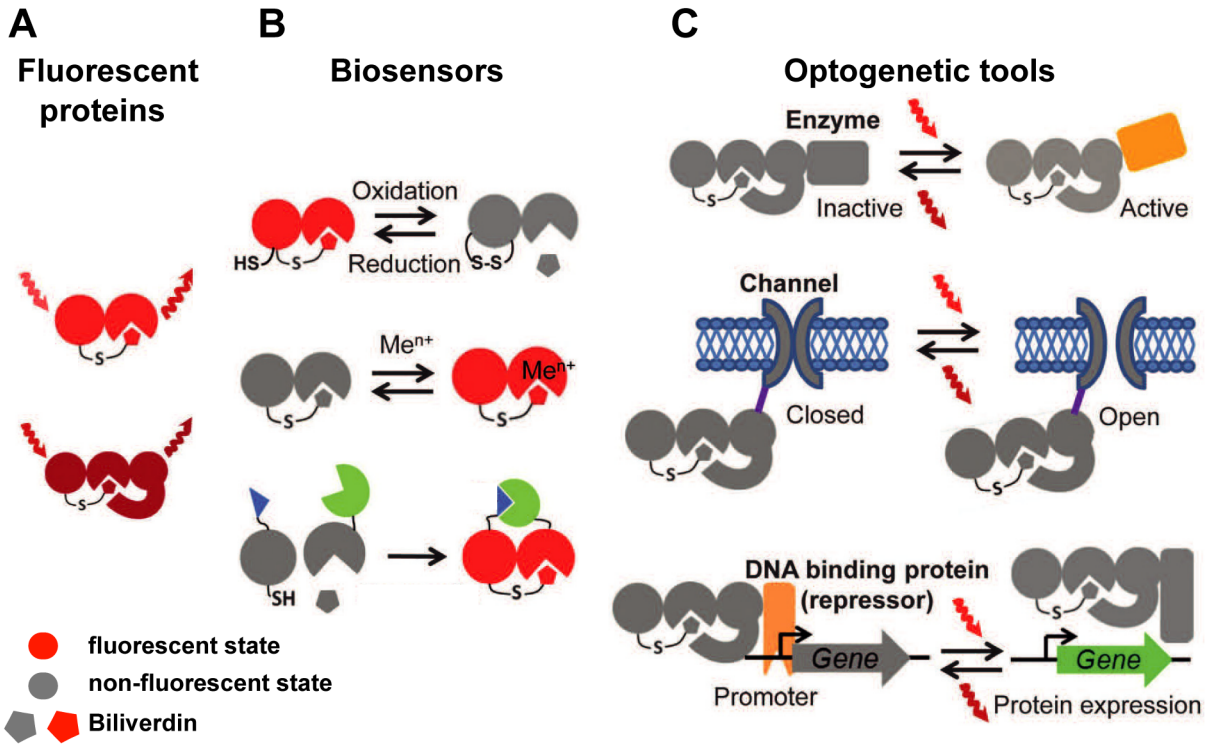

Figure 6.21: Possible applications for phytochromes **A:** Fluorescent proteins of two (PAS-GAF) or three domains (PAS-GAF-PHY), the arrows indicate irradiation and fluorescence, respectively. **B:** Two-domain (PAS-GAF) biosensors for detection of the redox potential (**above**), metal ions (**middle**) and of protein interactions by a split biosensor (**below**). **C:** Optogenetic tools to control enzymatic activity (**above**), the opening and closing of ion channels (**middle**) and the gene expression by regulating the interactions between a DNA repressor and a gene promoter (**below**). Red and far red arrows indicate irradiation with red and far red light, respectively. Red and gray symbols refer to a fluorescent and non-fluorescent state (figure modified from Ref.[194]).

ment[200]. For phytochromes at least two applications in optogenetics are known. The photosensory module of *Syn*Cph1 was fused to the HK region of EnvZ of *E. coli*. The linker region was engineered in length and the HK activity could be controlled by red light thus regulation the expression of a reporter gene in *E. coli*[201]. In another system the red light-regulated interaction of PhyB and PIF3 is used to control gene expression as each one is fused to one half of a protein, the DNA-binding and transactivation domains of GAL4. Co-localization upon red light illumination leads to transcriptional activation[202].

*Syn*Cph2 has not been used in bioengineering, yet. Due to its blue-shifted absorbance compared to other phytochromes[138] it is not so suitable for applications in tissues where infrared light is favorable[194]. Another problem for the production in other organisms or tissues is the supply of the chromophore. In humans for example BV is available because of the heme breakdown[195], in bacterial systems as *E. coli* the co-expression of a HO is required[194]. The production of PCB is in need of even one more enzymes thus complicating

the expression in other organisms and makes BphPs more attractive targets.

For applications in optogenetics on the other hand *Syn*Cph2 might be a suitable target. In comparison to canonical phytochromes it comprises only two domains to gain functional red / far red photochemistry. On the other hand, CBCRs exhibit an even smaller photosensory module consisting of one single domain and are highly fluorescent. GAF3 from the RGS protein from *Synechocystis* sp. displays a two-fold higher fluorescence quantum yield than *Syn*Cph2(1-2) [138,203]. In this context, the small size and the high spectral diversity make CBCRs attractive targets for bioengineering. Nevertheless, *Syn*Cph2 could be useful as a optogenetic tool in bacteria. Here, the chromophore production can be achieved *via* including an additional plasmid that contains HO1 and PcyA genes. In combination with the blue light-sensitive LOV domain fusion proteins, chimeras with the photosensory domains of *Syn*Cph2 and effector domains could provide a wavelength-tunable and therefore very sensitive control of gene-expression or other biological processes.

7 Outlook

In this work we provide a spectroscopical and structural characterization of *Syn*Cph2(1-2). We were able to illuminate the role of the tongue region in the stabilization of the P_{fr} state and in signal transduction. Our model of a Trp-switch in the tongue region during photoconversion is based on structural, spectroscopical and mutagenesis data and could be confirmed in the kinetical studies. Nevertheless, a direct proof of a tongue movement and reorganization of the secondary structure elements in the stem region of the tongue is still elusive. Here, for further insights, different experiments are possible. The most convincing would be a crystal structure of a non-bathyphytochrome in the P_{fr} state. For *Syn*Cph2(1-2) a locked P_{fr} state would be applicable that can be achieved for example *via* crosslinking the reorganized tongue and the GAF1 domain after photoconversion by a disulfide bridge or possible click chemistry reactions. The role and position of the tryptophan residues of the conserved $W^G/_A G$ and WxE motifs during photoconversion can be illuminated *via* NMR spectroscopy where the shift of the tryptophans in a ^{15}N-labelled *Syn*Cph2(1-2) could reveal the change in solvent accessibility and chemical environment. Also the reaction of possible indole-specific reagents could provide insights into the accessibility of the tryptophan residues upon photoconversion. Various cross linkers within the tongue region and their effect on spectroscopical characteristics may give hints to a possible shift or drift of the different sections within the tongue. The question, whether Ser-385 points into the binding pocket after photoconversion in P_{fr} like in the bathy-BphP structures can be addressed by an assay with a S385C mutant where in P_{fr} iodoacetamide is added that covalently binds to the thiol group of the cysteine and can be proved for example by mass spectrometry.

The difference between bathyphytochromes and non-bathyphytochromes is still elusive. The role of the additionally conserved residues in bathy-BphPs in contrast to other phytochromes is unclear. It would be very interesting to generate swap-variants of *Syn*Cph2(1-2) that contain the tongue region of bathyphytochromes. This experiment would show, if the tongue suffices to establish a P_{fr} ground state or whether additional characteristics of the BV-binding site are essential.

Besides the tongue-region the further mechanism of intramolecular signaling should be addressed in the future. The influence of the conserved tryptophan residue in the loop region subsequent of the tongue can be analyzed by mutagenesis. As this residue might not affect the spectral characteristics, although it may participate in signal transduction,

a soluble *Syn*Cph2(1-4) protein should be established. With this module it will be possible to illuminate the role of the C-terminal helix in *Syn*Cph2(1-2) and its presumed conformational changes within photoconversion like unfolding, rotation, reorientation or any other mechanism to transfer the light-signal to the effector domains, as the degradation of c-di-GMP can be monitored.

A crystal structure of the N-terminal module of *Syn*Cph2 with the effector domains will contribute in increasing the knowledge about signal transduction from sensor to effector domains. Also for the C-terminal photosensory module of *Syn*Cph2 a crystal structure including the EAL or GGDEF2 domain would help to illuminate signal transduction in CBCRs as only structures of the single CBCR GAF domains exist. It is intriguing, to find out the mechanism of signaling in CBCRs and compare it to phytochromes.

Another starting point for *Syn*Cph2(1-2) is its application in optogenetics. Here, phytochromes play just a minor role at the moment but have the potential to be an excellent tool.

8 References

[1] Williams, D. (Retrieved 2013-08-23) (1. July 2013) Sun fact sheet, NASA. *http://nssdc.gsfc.nasa.gov/planetary/factsheet/sunfact.html*.

[2] I.A.E.A., (Retrieved 2013-08-23) Power Reactor Information System (PRIS). *http://www.iaea.org/pris/*.

[3] Kopp, G., and Lean, J. L. (2011) A new, lower value of total solar irradiance: Evidence and climate significance. *Geophys. Res. Lett. 38*, 1–7.

[4] Olson, J. M. (2006) Photosynthesis in the archean era. *Photosynth. Res. 88*, 109–117.

[5] Heintzen, C. (2012) Plant and fungal photopigments. *WIREs Membr. Transp. Signal. 1*, 411–432.

[6] Purcell, E. B., and Crosson, S. (2008) Photoregulation in prokaryotes. *Curr. Opin. Microbiol. 11*, 168–178.

[7] Rockwell, N. C., Su, Y. S., and Lagarias, J. C. (2006) Phytochrome structure and signaling mechanisms. *Annu. Rev. Plant Biol. 57*, 837–858.

[8] Rockwell, N. C., and Lagarias, J. C. (2010) A brief history of phytochromes. *Chem. Phys. Chem. 11*, 1172–1180.

[9] Butler, W. L., Norris, K. H., Siegelman, H. W., and Hendricks, S. B. (1959) Detection, assay, and preliminary purification of the pigment controlling photoresponsive development of plants. *Proc. Natl. Acad. Sci. U.S.A. 45*, 1703–1708.

[10] Essen, L. O., Mailliet, J., and Hughes, J. (2008) The structure of a complete phytochrome sensory module in the Pr ground state. *Proc. Natl. Acad. Sci. U.S.A. 105*, 14709–14714.

[11] Yang, X., Kuk, J., and Moffat, K. (2008) Crystal structure of Pseudomonas aeruginosa bacteriophytochrome: Photoconversion and signal transduction. *Proc. Natl. Acad. Sci. U.S.A. 105*, 14715–14720.

[12] Wagner, J. R., Brunzelle, J. S., Forest, K. T., and Vierstra, R. D. (2005) A light-sensing knot revealed by the structure of the chromophore-binding domain of phytochrome. *Nature 438*, 325–331.

[13] Wagner, J. R., Zhang, J., Brunzelle, J. S., Vierstra, R. D., and Forest, K. T. (2007) High resolution structure of Deinococcus bacteriophytochrome yields new insights into phytochrome architecture and evolution. *J. Biol. Chem. 282*, 12298–12309.

[14] Yoshihara, S., Katayama, M., Geng, X., and Ikeuchi, M. (2004) Cyanobacterial phytochrome-like PixJ1 holoprotein shows novel reversible photoconversion between blue- and green-absorbing forms. *Plant Cell Physiol. 45*, 1729–1737.

[15] Aravind, L., and Ponting, C. P. (1997) The GAF domain: an evolutionary link between diverse phototransducing proteins. *Trends Biochem. Sci. 22*, 458–459.

[16] Montgomery, B. L., and Lagarias, J. C. (2002) Phytochrome ancestry: sensors of bilins and light. *TPS 7*, 357–366.

[17] Martinez-Argudo, I., Little, R., and Dixon, R. (2004) Role of the amino-terminal GAF domain of the NifA activator in controlling the response to the antiactivator protein NifL. *Mol. Microbiol. 52*, 1731–1744.

[18] Möglich, A., Ayers, R. A., and Moffat, K. (2009) Structure and signaling mechanism of Per-ARNT-Sim domains. *Structure 17*, 1282–1294.

[19] Vreede, J., van der Horst, M. A., Hellingwerf, K. J., Crielaard, W., and van Aalten, D. M. F. (2003) PAS domains: common structure and common flexibility. *J. Biol. Chem. 278*, 18434–18439.

[20] Hefti, M. H., Françoijs, K.-J., de Vries, S. C., Dixon, R., and Vervoort, J. (2004) The PAS fold. *Eur. J. Biochem. 271*, 1198–1208.

[21] Ho, Y.-S. J., Burden, L. M., and Hurley, J. H. (2000) Structure of the GAF domain, a ubiquitous signaling motif and a new class of cyclic GMP receptor. *EMBO J. 19*, 5288–5299.

[22] Yoon, J.-M., Hahn, T.-R., Cho, M.-H., Jeon, J.-S., Bhoo, S. H., and Kwon, Y.-K. (2008) The PHY domain is required for conformational stability and spectral integrity of the bacteriophytochrome from Deinococcus radiodurans. *Biochem. Bioph. Res. Co. 369*, 1120–1124.

[23] Oka, Y., Matsushita, T., Mochizuki, N., Suzuki, T., Tokutomi, S., and Nagatani, A. (2004) Functional analysis of a 450-amino acid N-terminal fragment of phytochrome B in arabidopsis. *Plant Cell 16*, 2104–2116.

[24] Scheer, H., and Zhao, K. H. (2008) Biliprotein maturation: the chromophore attachment. *Mol. Microbiol. 68*, 263–276.

[25] Eriksen, N. (2008) Production of phycocyanin-a pigment with applications in biology, biotechnology, foods and medicine. *Appl. Microbiol. Biotechnol. 80*, 1–14.

[26] Sekar, S., and Chandramohan, M. (2008) Phycobiliproteins as a commodity: trends in applied research, patents and commercialization. *J. Appl. Phycol. 20*, 113–136.

[27] Kohchi, T., Mukougawa, K., Frankenberg, N., Masuda, M., Yokota, A., and Lagarias, J. C. (2001) The Arabidopsis HY2 gene encodes phytochromobilin synthase, a ferredoxin-dependent biliverdin reductase. *Plant Cell 13*, 425–436.

[28] Frankenberg, N., Mukougawa, K., Kohchi, T., and Lagarias, J. C. (2001) Functional genomic analysis of the HY2 family of ferredoxin-dependent bilin reductases from oxygenic photosynthetic organisms. *Plant Cell 13*, 965–978.

[29] Dammeyer, T., Bagby, S. C., Sullivan, M. B., Chisholm, S. W., and Frankenberg-Dinkel, N. (2008) Efficient phage-mediated pigment biosynthesis in oceanic cyanobacteria. *Curr. Biol. 18*, 442–448.

[30] Alvey, R. M., Biswas, A., Schluchter, W. M., and Bryant, D. A. (2011) Effects of modified phycobilin biosynthesis in the cyanobacterium Synechococcus sp. strain PCC 7002. *J. Bacteriol. 193*, 1663–1671.

[31] Chen, Y.-R., Su, Y.-S., and Tu, S.-L. (2012) Distinct phytochrome actions in nonvascular plants revealed by targeted inactivation of phytobilin biosynthesis. *Proc. Natl. Acad. Sci. U.S.A. 109*, 8310–8315.

[32] Kelly, J. M., and Lagarias, J. C. (1985) Photochemistry of 124-kilodalton Avena phytochrome under constant illumination in vitro. *Biochemistry 24*, 6003–6010.

[33] Holzwarth, A. R. In *The light reactions*; Barber, J., Ed.; Elsevier, Amsterdam, 1987; Chapter Picosecond fluorescence spectroscopy and energy transfer in photosynthetic antenna pigments, pp 95–157.

[34] Braslavsky, S. E., Gärtner, W., and Schaffner, K. (1997) Phytochrome photoconversion. *Plant Cell Environ. 20*, 700–706.

[35] Gärtner, W. (2012) Kurt Schaffner: from organic photochemistry to photobiology. *Photochem. Photobiol. Sci. 11*, 872–880.

[36] Rohmer, T., Lang, C., Bongards, C., Gupta, K. B. S. S., Neugebauer, J., Hughes, J., Gärtner, W., and Matysik, J. (2010) Phytochrome as molecular machine: revealing chromophore action during the Pfr –> Pr photoconversion by magic-angle spinning NMR spectroscopy. *J. Am. Chem. Soc. 132*, 4431–4437.

[37] Song, C., Rohmer, T., Tiersch, M., Zaamen, J., Hughes, J., and Matysik, J. (2013) Solid-state NMR spectroscopy to probe photoactivation in canonical phytochromes. *Photochem. Photobiol. 89*, 259–273.

[38] Mroginski, M. A., Murgida, D. H., and Hildebrandt, P. (2007) The chromophore structural changes during the photocycle of phytochrome: a combined resonance raman and quantum chemical approach. *Acc. Chem. Res. 40*, 258–266.

[39] Gärtner, W., and Braslavski, S. E. In *Photoreceptors and light signaling*; Batschauer, A., Ed.; Royal Society of Chemistry, Cambridge, UK, 2004; Chapter The phytochromes: spectroscopy and function, pp 137–180.

[40] Hughes, J. (2013) Phytochrome cytoplasmic signaling. *Annu. Rev. Plant Biol. 64*, 377–402.

[41] Smith, H. (2000) Phytochromes and light signal perception by plants - an emerging synthesis. *Nature 407*, 585–591.

[42] Krall, L., and Reed, J. W. (2000) The histidine kinase-related domain participates in phytochrome B function but is dispensable. *Proc. Natl. Acad. Sci. 97*, 8169–8174.

[43] Casal, J. J. (2013) Photoreceptor signaling networks in plant responses to shade. *Annu. Rev. Plant Biol. 64*, 403–427.

[44] Kreslavski, V. D., Carpentier, R., Klimov, V. V., and Allakhverdiev, S. I. (2009) Transduction mechanisms of photoreceptor signals in plant cells. *J. Photochem. Photobiol. C: Photochem. Rev. 10*, 63–80.

[45] Quail, P. H. (1997) An emerging molecular map of the phytochromes. *Plant Cell Environ. 20*, 657–665.

[46] Casal, J. J., Davis, S. J., Kirchenbauer, D., Viczian, A., Yanovsky, M. J., Clough, R. C., Kircher, S., Jordan-Beebe, E. T., Schäfer, E., Nagy, F., and Vierstra, R. D. (2002) The serine-rich N-terminal domain of oat phytochrome A helps regulate light responses and subnuclear localization of the photoreceptor. *Plant Physiol. 129*, 1127–1137.

[47] Wada, M., and Skimazaki, K. In *Light sensing in plants*; Iino, M., Ed.; The Botanical Society of Japan, Springer-Verlag, 2005.

[48] Yeh, K. C., and Lagarias, J. C. (1998) Eukaryotic phytochromes: light-regulated serine/threonine protein kinases with histidine kinase ancestry. *Proc. Natl. Acad. Sci. U.S.A. 95*, 13976–13981.

[49] Chen, M., and Chory, J. (2011) Phytochrome signaling mechanisms and the control of plant development. *Trends Cell Biol. 21*, 664–671.

[50] Chen, M. (2008) Phytochrome nuclear body: an emerging model to study interphase nuclear dynamics and signaling. *Curr. Opin. Plant Biol. 11*, 503–508.

[51] Chen, M., Schwab, R., and Chory, J. (2003) Characterization of the requirements for localization of phytochrome B to nuclear bodies. *Proc. Natl. Acad. Sci. 100*, 14493–14498.

[52] Bae, G., and Choi, G. (2008) Decoding of light signals by plant phytochromes and their interacting proteins. *Annu. Rev. Plant Biol. 59*, 281–311.

[53] Leivar, P., and Quail, P. H. (2011) PIFs: pivotal components in a cellular signaling hub. *Trends Plant Sci. 16*, 19–28.

[54] Fankhauser, C., Yeh, K.-C., Lagarias, J. C., Zhang, H., Elich, T. D., and Chory, J. (1999) PKS1, a substrate phosphorylated by phytochrome that modulates light signaling in Arabidopsis. *Science 284*, 1539–1541.

[55] Neuhaus, G., Bowler, C., Kern, R., and Chua, N.-H. (1993) Calcium/calmodulin-dependent and -independent phytochrome signal transduction pathways. *Cell 73*, 937–952.

[56] Jaedicke, K., Lichtenthäler, A. L., Meyberg, R., Zeidler, M., and Hughes, J. (2012) A phytochrome - phototropin light signaling complex at the plasma membrane. *Proc. Natl. Acad. Sci. 109*, 12231–12236.

[57] Rodriguez-Romero, J., Hedtke, M., Kastner, C., Müller, S., and Fischer, R. (2010) Fungi, hidden in soil or up in the air: light makes a difference. *Annu. Rev. Microbiol. 64*, 585–610.

[58] Bahn, Y. S., Xue, C., A., I., Rutherford, J. C., Heitman, J., and Cardenas, M. E. (2007) Sensing the environment: lessons from fungi. *Nat. Rev. Microbiol. 1*, 57–69.

[59] Blumenstein, A., Vienken, K., Tasler, R., Purschwitz, J., Veith, D., Frankenberg-Dinkel, N., and Fischer, R. (2005) The Aspergillus nidulans phytochrome FphA represses sexual development in red light. *Curr. Biol. 15*, 1833–1838.

[60] Brandt, S., von Stetten, D., Günther, M., Hildebrandt, P., and Frankenberg-Dinkel, N. (2008) The fungal phytochrome FphA from Aspergillus nidulans. *J. Biol. Chem. 283*, 34605–34614.

[61] Stock, A. M., Robinson, V. L., and Goudreau, P. N. (2000) Two-component signal transduction. *Annu. Rev. Biochem. 69*, 183–215.

[62] Purschwitz, J., Müller, S., and Fischer, R. (2009) Mapping the interaction sites of Aspergillus nidulans phytochrome FphA with the global regulator VeA and the White Collar protein LreB. *Mol. Genet. Genomics 281*, 35–42.

[63] Davis, S. J., Vener, A. V., and Vierstra, R. D. (1999) Bacteriophytochromes: Phytochrome-like photoreceptors from nonphotosynthetic eubacteria. *Science 286*, 2517–2520.

[64] Giraud, E., and Verméglio, A. (2008) Bacteriophytochromes in anoxygenic photosynthetic bacteria. *Photosynth. Res. 97*, 141–153.

[65] Giraud, E., Fardoux, J., Fourrier, N., Hannibal, L., Gentry, B., Bouyer, P., Dreyfus, B., and Verméglio, A. (2002) Bacteriophytochrome controls photosystem synthesis in anoxygenic bacteria. *Nature 417*, 202–205.

[66] Bhoo, S. H., Davis, S. J., Walker, J., Karniol, B., and Vierstra, R. D. (2001) Bacteriophytochromes are photochromic histidine kinases using a biliverdin chromophore. *Nature 414*, 776–779.

[67] Jaubert, M., Lavergne, J., Fardoux, J., Hannibal, L., Vuillet, L., Adriano, J.-M., Bouyer, P., Pignol, D., Giraud, E., and Verméglio, A. (2007) A singular bacteriophytochrome acquired by lateral gene transfer. *J. Biol. Chem. 282*, 7320–7328.

[68] Karniol, B., Wagner, J. R., Walker, J. M., and Vierstra, R. D. (2005) Phylogenetic analysis of the phytochrome superfamily reveals distinct microbial subfamilies of photoreceptors. *Biochem. J. 392*, 103–116.

[69] Bellini, D., and Papiz, M. Z. (2012) Structure of a bacteriophytochrome and light-stimulated protomer swapping with a gene repressor. *Structure 20*, 1436–46.

[70] Dixit, R., and Suseela, M. (2013) Cyanobacteria: potential candidates for drug discovery. *A. van Leeuw. J. Microb. 103*, 947–961.

[71] Tan, L. T. (2007) Bioactive natural products from marine cyanobacteria for drug discovery. *Phytochemistry 68*, 954–979.

[72] Berla, B. M., Saha, R., Immethun, C. M., Maranas, C. D., Moon, T. S., and Pakrasi, H. (2013) Synthetic biology of cyanobacteria: unique challenges and opportunities. *Front. Microbiol. 4*, 1–14.

[73] Hughes, J., Lamparter, T., Mittmann, F., Hartmann, E., Gärtner, W., Wilde, A., and Börner, T. (1997) A prokaryotic phytochrome. *Nature 386*, 663.

[74] Stanier, R. Y., Kunisawa, R., Mandel, M., and Cohen-Bazire, G. (1971) Purification and properties of unicellular blue-green algae (order Chroococcales). *Bacteriol. Rev. 35*, 171–205.

[75] Vernotte, C., Picaud, M., Kirilovsky, D., Olive, J., Ajlani, G., and Astier, C. (1992) Changes in the photosynthetic apparatus in the cyanobacterium Synechocystis sp. PCC 6714 following light-to-dark and dark-to-light transitions. *Photosynth. Res. 32*, 45–57.

[76] Anderson, S. L., and McIntosh, L. (1991) Light-activated heterotrophic growth of the cyanobacterium Synechocystis sp. strain PCC 6803: a blue-light-requiring process. *J. Bacteriol. 173*, 2761–2767.

[77] Jorissen, H., Quest, B., Remberg, A., Coursin, T., Braslavsky, S. E., Schaffner, K., Tandeau de Marsac, N., and Gärtner, W. (2002) Two independent, light-sensing two-component systems in a filamentous cyanobacterium. *Eur. J. Biochem. 269*, 2662–2671.

[78] Lamparter, T., Esteban, B., and Hughes, J. (2001) Phytochrome Cph1 from the cyanobacterium Synechocystis PCC6803. *FEBS J. 268*, 4720–4730.

[79] Sharda, S., Shah, R., and Gärtner, W. (2007) Domain interaction in cyanobacterial phytochromes as a prerequisite for spectral integrity. *Eur. Biophys. J. 36*, 815–821.

[80] Quest, B., Hübschmann, T., Sharda, S., Tandeau de Marsac, N., and Gärtner, W. (2007) Homologous expression of a bacterial phytochrome. *FEBS J. 274*, 2088–2098.

[81] Hahn, J., Strauss, H. M., Landgraf, F. T., Gimenez, H. F., Lochnit, G., Schmieder, P., and Hughes, J. (2006) Probing protein-chromophore interactions in Cph1 phytochrome by mutagenesis. *FEBS J. 273*, 1415–1429.

[82] Psakis, G., Mailliet, J., Lang, C., Teufel, L., Essen, L.-O., and Hughes, J. (2011) Signaling kinetics of cyanobacterial phytochrome Cph1, a light regulated histidine kinase. *Biochemistry 50*, 6178–6188.

[83] Yang, X., Stojkovic, E. A., Kuk, J., and Moffat, K. (2007) Crystal structure of the chromophore binding domain of an unusual bacteriophytochrome, RpBphP3, reveals residues that modulate photoconversion. *Proc. Natl. Acad. Sci. U.S.A. 104*, 12571–12576.

[84] Mailliet, J., Psakis, G., Feilke, K., Sineshchekov, V., Essen, L. O., and Hughes, J. (2011) Spectroscopy and a high-resolution crystal structure of Tyr263 mutants of cyanobacterial phytochrome Cph1. *J. Mol. Biol. 413*, 115–127.

[85] Yang, X., Kuk, J., and Moffat, K. (2009) Conformational differences between the Pfr and Pr states in Pseudomonas aeruginosa bacteriophytochrome. *Proc. Natl. Acad. Sci. 106*, 15639–15644.

[86] Yang, X., Ren, Z., Kuk, J., and Moffat, K. (2011) Temperature-scan cryocrystallography reveals reaction intermediates in bacteriophytochrome. *Nature 479*, 428–432.

[87] Li, H., Zhang, J., Vierstra, R. D., and Li, H. (2010) Quaternary organization of a phytochrome dimer as revealed by cryoelectron microscopy. *Proc. Natl. Acad. Sci. U.S.A. 107*, 10872–10877.

[88] Ulijasz, A. T., Cornilescu, G., von Stetten, D., Kaminski, S., Mroginski, M. A., Zhang, J., Bhaya, D., Hildebrandt, P., and Vierstra, R. D. (2008) Characterization of two thermostable cyanobacterial phytochromes reveals global movements in the chromophore-binding domain during photoconversion. *J. Biol. Chem. 283*, 21251–21266.

[89] Park, C. M., Kim, J. I., Yang, S. S., Kang, J. G., Kang, J. H., Shim, J. Y., Chung, Y. H., Park, Y. M., and Song, P. S. (2000) A second photochromic bacteriophytochrome from Synechocystis sp. PCC 6803: spectral analysis and down-regulation by light. *Biochemistry 39*, 10840–10847.

[90] Cornilescu, G., Ulijasz, A. T., Cornilescu, C. C., Markley, J. L., and Vierstra, R. D.

(2008) Solution structure of a cyanobacterial phytochrome GAF domain in the red-light-absorbing ground state. *J. Mol. Biol. 383*, 403–413.

[91] Ulijasz, A. T., Cornilescu, G., Cornilescu, C. C., Zhang, J., Rivera, M., Markley, J. L., and Vierstra, R. D. (2010) Structural basis for the photoconversion of a phytochrome to the activated Pfr form. *Nature 463*, 250–254.

[92] Römling, U., Gomelsky, M., and Galperin, M. Y. (2005) C-di-GMP: the dawning of a novel bacterial signalling system. *Mol. Microbiol. 57*, 629–639.

[93] Ross, P., Weinhouse, H., Aloni, Y., Michaeli, D., Weinberger-Ohana, P., Mayer, R., Braun, S., De Vroom, E., Van Der Marel, G. A., Van Boom, J. H., and Benziman, M. (1987) Regulation of cellulose synthesis in Acetobacter xylinum by cyclic diguanylic acid. *Nature 325*, 279–281.

[94] Chan, C., Paul, R., Samoray, D., Amiot, N. C., Giese, B., Jenal, U., and Schirmer, T. (2004) Structural basis of activity and allosteric control of diguanylate cyclase. *Proc. Natl. Acad. Sci. U. S. A. 101*, 17084–17089.

[95] Schirmer, T., and Jenal, U. (2009) Structural and mechanistic determinants of c-di-GMP signalling. *Nat. Rev. Microbiol. 7*, 724–735.

[96] Christen, B., Christen, M., Paul, R., Schmid, F., Folcher, M., Jenoe, P., Meuwly, M., and Jenal, U. (2006) Allosteric control of cyclic di-GMP signaling. *J. Biol. Chem. 281*, 32015–32024.

[97] Dow, J. M., Fouhy, Y., Lucey, J. F., and Ryan, R. P. (2006) The HD-GYP domain, cyclic di-GMP signaling, and bacterial virulence to plants. *Mol. Plant Microbe In. 19*, 1378–1384.

[98] Barends, T. R. M., Hartmann, E., Griese, J. J., Beitlich, T., Kirienko, N. V., Ryjenkov, D. A., Reinstein, J., Shoeman, R. L., Gomelsky, M., and Schlichting, I. (2009) Structure and mechanism of a bacterial light-regulated cyclic nucleotide phosphodiesterase. *Nature 459*, 1015–1018.

[99] Christen, M., Christen, B., Folcher, M., Schauerte, A., and Jenal, U. (2005) Identification and characterization of a cyclic di-GMP-specific phosphodiesterase and its allosteric control by GTP. *J. Biol. Chem. 280*, 30829–30837.

[100] Kumar, M., and Chatterji, D. (2008) Cyclic di-GMP: a second messenger required for long-term survival, but not for biofilm formation, in Mycobacterium smegmatis. *Microbiology 154*, 2942–2955.

[101] Hickman, J. W., and Harwood, C. S. (2008) Identification of FleQ from Pseudomonas aeruginosa as a c-di-GMP-responsive transcription factor. *Mol. Microbiol. 69*, 376–389.

[102] Wu, S. H., and Lagarias, J. C. (2000) Defining the bilin lyase domain: lessons from the extended phytochrome superfamily. *Biochemistry 39*, 13487–13495.

[103] Fiedler, B., Broc, D., Schubert, H., Rediger, A., Börner, T., and Wilde, A. (2004) Involvement of cyanobacterial phytochromes in growth under different light qualities and quantities. *Photochem. Photobiol. 79*, 551–555.

[104] Hübschmann, T., Yamamoto, H., Gieler, T., Murata, N., and Börner, T. (2005) Red and far-red light alter the transcript profile in the cyanobacterium Synechocystis sp. PCC 6803: impact of cyanobacterial phytochromes. *FEBS Lett. 579*, 1613–1618.

[105] Wilde, A., Fiedler, B., and Börner, T. (2002) The cyanobacterial phytochrome Cph2 inhibits phototaxis towards blue light. *Mol. Microbiol. 44*, 981–988.

[106] Fiedler, B., Börner, T., and Wilde, A. (2005) Phototaxis in the cyanobacterium Synechocystis sp. PCC 6803: role of different photoreceptors. *Photochem. Photobiol. 81*, 1481–1488.

[107] Moon, Y.-J., Kim, S. Y., Jung, K.-H., Choi, J.-S., Park, Y. M., and Chung, Y.-H. (2011) Cyanobacterial phytochrome Cph2 is a negative regulator in phototaxis toward UV-A. *FEBS Lett. 585*, 335–340.

[108] Narikawa, R., Fukushima, Y., Ishizuka, T., Itoh, S., and Ikeuchi, M. (2008) A novel photoactive GAF domain of cyanobacteriochrome AnPixJ that shows reversible green/red photoconversion. *J. Mol. Biol. 380*, 844–855.

[109] Hirose, Y., Shimada, T., Narikawa, R., Katayama, M., and Ikeuchi, M. (2008) Cyanobacteriochrome CcaS is the green light receptor that induces the expression of phycobilisome linker protein. *Proc. Natl. Acad. Sci. 105*, 9528–9533.

[110] Ishizuka, T., Narikawa, R., Kohchi, T., Katayama, M., and Ikeuchi, M. (2007) Cyanobacteriochrome TePixJ of Thermosynechococcus elongatus harbors phycoviolobilin as a chromophore. *Plant Cell Physiol. 48*, 1385–1390.

[111] Ishizuka, T., Kamiya, A., Suzuki, H., Narikawa, R., Noguchi, T., Kohchi, T., Inomata, K., and Ikeuchi, M. (2011) The cyanobacteriochrome, TePixJ, isomerizes its own chromophore by converting phycocyanobilin to phycoviolobilin. *Biochemistry 50*, 953–961.

[112] Rockwell, N. C., Njuguna, S. L., Roberts, L., Castillo, E., Parson, V. L., Dwojak, S., Lagarias, J. C., and Spiller, S. C. (2008) A second conserved GAF domain cysteine is required for the blue/green photoreversibility of cyanobacteriochrome Tlr0924 from Thermosynechococcus elongatus. *Biochemistry 47*, 7304–7316.

[113] Terauchi, K., Montgomery, B. L., Grossman, A. R., Lagarias, J. C., and Kehoe, D. M. (2004) RcaE is a complementary chromatic adaptation photoreceptor required for green and red light responsiveness. *Mol. Microbiol. 51*, 567–577.

[114] Scott, J. W., Hawley, S. A., Green, K. A., Anis, M., Stewart, G., Scullion, G. A., Norman, D. G., and Hardie, D. G. (2004) CBS domains form energy-sensing modules

whose binding of adenosine ligands is disrupted by disease mutations. *J. Clin. Invest. 113*, 274–284.

[115] Rockwell, N. C., Ohlendorf, R., and Möglich, A. (2013) Cyanobacteriochromes in full color and three dimensions. *Proc. Natl. Acad. Sci. 110*, 806–807.

[116] Chen, Y., Zhang, J., Luo, J., Tu, J.-M., Zeng, X.-L., Xie, J., Zhou, M., Zhao, J.-Q., Scheer, H., and Zhao, K.-H. (2012) Photophysical diversity of two novel cyanobacteriochromes with phycocyanobilin chromophores: photochemistry and dark reversion kinetics. *FEBS J. 279*, 40–54.

[117] Ohmori, M. et al. (2001) Characterization of genes encoding multi-domain proteins in the genome of the filamentous nitrogen-fixing cyanobacterium Anabaena sp. strain PCC 7120. *DNA Res. 8*, 271–284.

[118] Kehoe, D. M., and Gutu, A. (2006) Responding to color: the regulation of complementary chromatic adaptation. *Annu. Rev. Plant Biol. 57*, 127–150.

[119] Ikeuchi, M., and Ishizuka, T. (2008) Cyanobacteriochromes: a new superfamily of tetrapyrrole-binding photoreceptors in cyanobacteria. *Photochem. Photobiol. Sci. 7*, 1159–1167.

[120] Yoshihara, S., Suzuki, F., Fujita, H., Geng, X. X., and Ikeuchi, M. (2000) Novel putative photoreceptor and regulatory genes required for the positive phototactic movement of the unicellular motile cyanobacterium Synechocystis sp. PCC 6803. *Plant Cell Physiol. 41*, 1299–1304.

[121] Yoshihara, S., Geng, X., Okamoto, S., Yura, K., Murata, T., Go, M., Ohmori, M., and Ikeuchi, M. (2001) Mutational analysis of genes involved in pilus structure, motility and transformation competency in the unicellular motile cyanobacterium Synechocystis sp. PCC6803. *Plant Cell Physiol. 42*, 63–73.

[122] Narikawa, R., Ishizuka, T., Muraki, N., Shiba, T., Kurisu, G., and Ikeuchi, M. (2013) Structures of cyanobacteriochromes from phototaxis regulators AnPixJ and TePixJ reveal general and specific photoconversion mechanism. *Proc. Natl. Acad. Sci. U.S.A. 110*, 918–923.

[123] Burgie, E. S., Walker, J. M., Philipps, G. N. J., and Vierstra, R. D. (2013) A photolabile thioether linkage to phycoviolobilin provides the foundation for the blue/green photocycles in DXCF-cyanobacteriochromes. *Structure 21*, 88–97.

[124] Narikawa, R., Kohchi, T., and Ikeuchi, M. (2008) Characterization of the photoactive GAF domain of the CikA homolog (SyCikA, Slr1969) of the cyanobacterium Synechocystis sp. PCC 6803. *Photochem. Photobiol. Sci. 7*, 1253–1259.

[125] Hirose, Y., Narikawa, R., Katayama, M., and Ikeuchi, M. (2010) Cyanobacteriochro-

me CcaS regulates phycoerythrin accumulation in Nostoc punctiforme, a group II chromatic adapter. *Proc. Natl. Acad. Sci. 107*, 8854–8859.

[126] Rockwell, N. C., Martin, S. S., Feoktistova, K., and Lagarias, J. C. (2011) Diverse two-cysteine photocycles in phytochromes and cyanobacteriochromes. *Proc. Natl. Acad. Sci. 108*, 11854–11859.

[127] Ma, Q., Hua, H.-H., Chen, Y., Liu, B.-B., Krämer, A. L., Scheer, H., Zhao, K.-H., and Zhou, M. (2012) A rising tide of blue-absorbing biliprotein photoreceptors - characterization of seven such bilin-binding GAF domains in Nostoc sp. PCC7120. *FEBS J. 279*, 4095–4108.

[128] Rockwell, N. C., Martin, S. S., Gulevich, A. G., and Lagarias, J. C. (2012) Phycoviolobilin formation and spectral tuning in the DXCF cyanobacteriochrome subfamily. *Biochemistry 51*, 1449–1463.

[129] Enomoto, G., Hirose, Y., Narikawa, R., and Ikeuchi, M. (2012) Thiol-based photocycle of the blue and teal light-sensing cyanobacteriochrome Tlr1999. *Biochemistry 51*, 3050–3058.

[130] Wu, S.-H., McDowell, M. T., and Lagarias, J. C. (1997) Phycocyanobilin is the natural precursor of the phytochrome chromophore in the green alga Mesotaenium caldariorum. *J. Biol. Chem. 272*, 25700–25705.

[131] Lamparter, T. (2004) Evolution of cyanobacterial and plant phytochromes. *FEBS Lett. 573*, 1–5.

[132] Brücker, G., Mittmann, F., Hartmann, E., and Lamparter, T. (2005) Targeted site-directed mutagenesis of a heme oxygenase locus by gene replacement in the moss Ceratodon purpureus. *Planta 220*, 864–874.

[133] Quest, B., and Gärtner, W. (2004) Chromophore selectivity in bacterial phytochromes. *Eur. J. Biochem. 271*, 1117–1126.

[134] Vuillet, L., Kojakinovic, M., Zappa, S., Jaubert, M., Adriano, J.-M., Fardoux, J., Hannibal, L., Pignol, D., Verméglio, A., and Giraud, E. (2007) Evolution of a bacteriophytochrome from light to redox sensor. *EMBO J. 26*, 3322–3331.

[135] Anders, K. Strukturelle und funktionelle Analyse von Phytochromen des Cph2-Typs. M.Sc. thesis, Philipps-University Marburg, 2008.

[136] Rockwell, N. C., Shang, L., Martin, S. S., and Lagarias, J. C. (2009) Distinct classes of red/far-red photochemistry within the phytochrome superfamily. *Proc. Natl. Acad. Sci. U.S.A. 106*, 6123–6127.

[137] Song, C., Psakis, G., Lang, C., Mailliet, J., Gärtner, W., Hughes, J., and Matysik, J. (2011) Two ground state isoforms and a chromophore D-ring photoflip triggering

extensive intramolecular changes in a canonical phytochrome. *Proc. Natl. Acad. Sci. U.S.A. 108*, 3842–3847.

[138] Anders, K., von Stetten, D., Mailliet, J., Kiontke, S., Sineshchekov, V. A., Hildebrandt, P., Hughes, J., and Essen, L.-O. (2011) Spectroscopic and photochemical characterization of the red-light sensitive photosensory module of Cph2 from Synechocystis PCC 6803. *Photochem. Photobiol. 87*, 160–173.

[139] Anders, K., Daminelli-Widany, G., Mroginski, M. A., von Stetten, D., and Essen, L.-O. (2013) Structure of the cyanobacterial phytochrome 2 photosensor implies a tryptophan switch for phytochrome signaling. *J. Biol. Chem. 288*, 35714–35725.

[140] Marshall, J., Cronin, T. W., and Kleinlogel, S. (2007) Stomatopod eye structure and function: a review. *Arth. Struct. & Dev. 36*, 420 – 448.

[141] Marshall, J., and Oberwinkler, J. (1999) Ultraviolet vision: The colourful world of the mantis shrimp. *Nature 401*, 873–874.

[142] Sineshchekov, V. A. (1995) Photobiophysics and photobiochemistry of the heterogeneous phytochrome system. *Biochim. Biophys. Acta 1228*, 125–164.

[143] Giraud, E., Zappa, S., Vuillet, L., Adriano, J.-M., Hannibal, L., Fardoux, J., Berthomieu, C., Bouyer, P., Pignol, D., and Verméglio, A. (2005) A new type of bacteriophytochrome acts in tandem with a classical bacteriophytochrome to control the antennae synthesis in Rhodopseudomonas palustris. *J. Biol. Chem. 280*, 32389–32397.

[144] Savakis, P. Spektroskopische und funktionelle Charakterisierung einer lichtgeschalteten Diguanylatzyklase aus Synechocystis sp. M.Sc. thesis, Philipps-University Marburg, 2010.

[145] Savakis, P., De Causmaecker, S., Angerer, V., Ruppert, U., Anders, K., Essen, L.-O., and Wilde, A. (2012) Light-induced alteration of c-di-GMP level controls motility of Synechocystis sp. PCC 6803. *Mol. Microbiol. 85*, 239–251.

[146] Stanek, M., and Grubmayr, K. (1998) Protonated 2,3-dihydrobilindiones-models for the chromophores of phycocyanin and the red-absorbing form of phytochrome. *Chem. Eur. J. 4*, 1653–1659.

[147] Borucki, B. (2006) Proton transfer in the photoreceptors phytochrome and photoactive yellow protein. *Photochem. Photobiol. Sci. 5*, 553–566.

[148] Margulies, L., and Stockburger, M. (1979) Spectroscopic studies on model compounds of the phytochrome chromophore. Protonation and deprotonation of biliverdin dimethyl ester. *J. Am. Chem. Soc. 101*, 743–744.

[149] Göller, A. H., Strehlow, D., and Hermann, G. (2005) The excited-state chemistry of phycocyanobilin: a semiempirical study. *Chem. Phys. Chem. 6*, 1259–1268.

[150] Hirose, Y., Rockwell, N. C., Nishiyama, K., Narikawa, R., Ukaji, Y., Inomata, K., Lagarias, J. C., and Ikeuchi, M. (2013) Green/red cyanobacteriochromes regulate complementary chromatic acclimation via a protochromic photocycle. *Proc. Natl. Acad. Sci. 110*, 4974–4979.

[151] Song, C., Psakis, G., Kopycki, J., Lang, C., Matysik, J., and Hughes, J. (2014) The D-ring, not the A-ring, rotates in Synechococcus OS-B' phytochrome. *J. Biol. Chem. 289*, 2552–2562.

[152] Auldridge, M. E., Satyshur, K. A., Anstrom, D. M., and Forest, K. T. (2012) Structure-guided engineering enhances a phytochrome-based infrared fluorescent protein. *J. Biol. Chem. 287*, 7000–7009.

[153] Jones, D. T. (1999) Protein secondary structure prediction based on position-specific scoring matrices. *J. Mol. Biol. 292*, 195–202.

[154] Karniol, B., and Vierstra, R. D. (2003) The pair of bacteriophytochromes from Agrobacterium tumefaciens are histidine kinases with opposing photobiological properties. *Proc. Natl. Acad. Sci. 100*, 2807–2812.

[155] Dammeyer, T., and Frankenberg-Dinkel, N. (2008) Function and distribution of bilin biosynthesis enzymes in photosynthetic organisms. *Photochem. Photobiol. Sci. 7*, 1121–1130.

[156] Cornejo, J., and Beale, S. (1997) Phycobilin biosynthetic reactions in extracts of cyanobacteria. *Photosynth. Res. 51*, 223–230.

[157] Fischer, A. J., and Lagarias, J. C. (2004) Harnessing phytochrome's glowing potential. *Proc. Natl. Acad. Sci. U.S.A. 101*, 17334–17339.

[158] Fischer, A. J., Rockwell, N. C., Jang, A. Y., Ernst, L. A., Waggoner, A. S., Duan, Y., Lei, H., and Lagarias, J. C. (2005) Multiple roles of a conserved GAF domain tyrosine residue in cyanobacterial and plant phytochromes. *Biochemistry 44*, 15203–15215.

[159] Hu, W., Su, Y.-S., and Lagarias, J. C. (2009) A light-independent allele of phytochrome B faithfully recapitulates photomorphogenic transcriptional networks. *Mol. Plant 2*, 166–182.

[160] Hughes, J. (2010) Phytochrome three-dimensional structures and functions. *Biochem. Soc. Trans. 38*, 710–716.

[161] Wagner, J. R., Zhang, J., von Stetten, D., Günther, M., Murgida, D. H., Mroginski, M. A., Walker, J. M., Forest, K. T., Hildebrandt, P., and Vierstra, R. D. (2008) Mutational analysis of Deinococcus radiodurans bacteriophytochrome reveals key amino acids necessary for the photochromicity and proton exchange cycle of phytochromes. *J. Biol. Chem. 283*, 12212–12226.

[162] Zhang, J., Stankey, R. J., and Vierstra, R. D. (2013) Structure-guided engineering of plant phytochrome B with altered photochemistry and light signaling. *Plant Physiol. 161*, 1445–1457.

[163] Von Stetten, D., Seibeck, S., Michael, N., Scheerer, P., Mroginski, M. A., Murgida, D. H., Krauss, N., Heyn, M. P., Hildebrandt, P., Borucki, B., and Lamparter, T. (2007) Highly conserved residues Asp-197 and His-250 in Agp1 phytochrome control the proton affinity of the chromophore and Pfr formation. *J. Biol. Chem. 282*, 2116–2123.

[164] Oka, Y., Matsushita, T., Mochizuki, N., Quail, P. H., and Nagatani, A. (2008) Mutant screen distinguishes between residues necessary for light-signal perception and signal transfer by phytochrome B. *PLoS Genet. 4*, e1000158.

[165] Shang, L. X., Rockwell, N. C., Martin, S. S., and Lagarias, J. C. (2010) Biliverdin amides reveal roles for propionate side chains in bilin reductase recognition and in holophytochrome assembly and photoconversion. *Biochemistry 49*, 6070–6082.

[166] Anders, K., Gutt, A., Gärtner, W., and Essen, L.-O. (2014) Late intermediates of the red-light sensor Cph2 from Synechocystis sp. show role of tongue motifs in photoconversion. *J. Biol. Chem. submitted on 03.03.2014*, unpublished.

[167] Baker, N. A., Sept, D., Joseph, S., Holst, M. J., and McCammon, J. A. (2001) Electrostatics of nanosystems: Application to microtubules and the ribosome. *Proc. Natl. Acad. Sci. 98*, 10037–10041.

[168] Dolinsky, T. J., Nielsen, J. E., McCammon, J. A., and Baker, N. A. (2004) PDB2PQR: an automated pipeline for the setup of Poisson-Boltzmann electrostatics calculations. *Nucleic Acids Res. 32*, W665–W667.

[169] Gong, W., Hao, B., and Chan, M. K. (2000) New mechanistic insights from structural studies of the oxygen-sensing domain of Bradyrhizobium japonicum FixL. *Biochemistry 39*, 3955–3962.

[170] Diensthuber, R., Bommer, M., Gleichmann, T., and Möglich, A. (2013) Full-length structure of a sensor histidine kinase pinpoints coaxial coiled coils as signal transducers and modulators. *Structure 21*, 1127–1136.

[171] Wang, C., Sang, J., Wang, J., Su, M., Downey, J. S., Wu, Q., Wang, S., Cai, Y., Xu, X., Wu, J., Senadheera, D. B., Cvitkovitch, D. G., Chen, L., Goodman, S. D., and Han, A. (2013) Mechanistic insights revealed by the crystal structure of a histidine kinase with signal transducer and sensor domains. *PLoS Biol. 11*, e1001493.

[172] Vierstra, R. D., and Zhang, J. J. (2011) Phytochrome signaling: solving the Gordian knot with microbial relatives. *TPS 16*, 417–426.

[173] Navarro, M. V. A. S., De, N., Bae, N., Wang, Q., and Sondermann, H. (2009) Structural analysis of the GGDEF-EAL domain-containing c-di-GMP receptor FimX. *Structure 17*, 1104–1116.

[174] Chai, Y. G., Song, P. S., Cordonnier, M. M., and Pratt, L. H. (1987) A photoreversible circular dichroism spectral change in oat phytochrome is suppressed by a monoclonal antibody that binds near its N-terminus and by chromophore modification. *Biochemistry 26*, 4947–4952.

[175] Song, P.-S., C., Park, M. H., and Furuya, M. (1997) Chromophore: apoprotein interactions in phytochrome A. *Plant Cell Environ. 20*, 707–712.

[176] Pettersen, E. F., Goddard, T. D., Huang, C. C., Couch, G. S., Greenblatt, D. M., Meng, E. C., and Ferrin, T. E. (2004) UCSF Chimera - a visualization system for exploratory research and analysis. *J. Comput. Chem. 25*, 1605–1612.

[177] Heyes, D. J., Khara, B., Sakuma, M., Hardman, S. J. O., O'Cualain, R., Rigby, S. E. J., and Scrutton, N. S. (2012) Ultrafast red light activation of Synechocystis phytochrome Cph1 triggers major structural change to form the Pfr signalling-competent state. *PLoS ONE 7*, 1–13.

[178] Schroeder, C., Werner, K., Otten, H., Krätzig, S., Schwalbe, H., and Essen, L. O. (2008) Influence of a joining helix on the BLUF domain of the YcgF photoreceptor from Escherichia coli. *ChemBioChem 9*, 2463–2473.

[179] Harper, S. M., Neil, L. C., and Gardner, K. H. (2003) Structural basis of a phototropin light switch. *Science 301*, 1541–1544.

[180] Harper, S. M., Christie, J. M., and Gardner, K. H. (2004) Disruption of the LOV-Jalpha helix interaction activates phototropin kinase activity. *Biochemistry 43*, 16184–16192.

[181] Tews, I., Findeisen, F., Sinning, I., Schultz, A., Schultz, J. E., and Linder, J. U. (2005) The structure of a pH-sensing mycobacterial adenylyl cyclase holoenzyme. *Science 308*, 1020–1023.

[182] Schultz, J. E., and Natarajan, J. (2013) Regulated unfolding: a basic principle of intraprotein signaling in modular proteins. *Trends Biochem. Sci. 38*, 538–545.

[183] Pandit, J., Forman, M. D., Fennell, K. F., Dillman, K. S., and Menniti, F. S. (2009) Mechanism for the allosteric regulation of phosphodiesterase 2A deduced from the X-ray structure of a near full-length construct. *Proc. Natl. Acad. Sci. 106*, 18225–18230.

[184] Cornilescu, C. C., Cornilescu, G., Burgie, E. S., Markley, J. L., Ulijasz, A. T., and Vierstra, R. D. (2014) Dynamic structural changes underpin photoconversion of a blue/green cyanobacteriochrome between its dark and photoactivated states. *J. Biol. Chem. 289*, 3055–3065.

[185] Ferris, H. U., Dunin-Horkawicz, S., Hornig, N., Hulko, M., Martin, J., Schultz, J. E., Zeth, K., Lupas, A. N., and Coles, M. (2012) Mechanism of regulation of receptor histidine kinases. *Structure 20*, 56–66.

[186] Rockwell, N. C., Martin, S. S., and Lagarias, J. C. (2012) Red/green cyanobacteriochromes: sensors of color and power. *Biochemistry 51*, 9667–9677.

[187] Veitia, R. (2002) Rosetta Stone proteins: "chance and necessity"? *Genome Biol. 3*, 1001.1–1001.3.

[188] Date, S. V. In *Bioinformatics*; Keith, J., Ed.; Methods in Molecular Biology; Humana Press, 2008; Vol. 453; pp 169–180.

[189] Tarutina, M., Ryjenkov, D. A., and Gomelsky, M. (2006) An unorthodox bacteriophytochrome from Rhodobacter sphaeroides involved in turnover of the second messenger c-di-GMP. *J. Biol. Chem. 281*, 34751–34758.

[190] Nozue, K., Kanegae, T., Imaizumi, T., Fukuda, S., Okamoto, H., Yeh, K.-C., Lagarias, J. C., and Wada, M. (1998) A phytochrome from the fern Adiantum with features of the putative photoreceptor NPH1. *Proc. Natl. Acad. Sci. 95*, 15826–15830.

[191] Jiang, Z., Swem, L. R., Rushing, B. G., Devanathan, S., Tollin, G., and Bauer, C. E. (1999) Bacterial photoreceptor with similarity to photoactive yellow protein and plant phytochromes. *Science 285*, 406–409.

[192] Chung, Y. H., Masuda, M., and Bauer, C. E. (2007) Purification and reconstitution of PYP-phytochrome with biliverdin and 4-hydroxycinnamic acid. *Methods Enzymol. 422*, 184–189.

[193] Okamoto, S., Kasahara, M., Kamlya, A., Nakahira, Y., and Ohmori, M. (2004) A phytochrome-like protein AphC triggers the cAMP signaling induced by far-red light in the cyanobacterium Anabaena sp. strain PCC7120. *Photochem. Photobiol. 80*, 429–433.

[194] Piatkevich, K. D., Subach, F. V., and Verkhusha, V. V. (2013) Engineering of bacterial phytochromes for near-infrared imaging, sensing, and light-control in mammals. *Chem. Soc. Rev. 42*, 3441–3452.

[195] Shu, X., Royant, A., Lin, M. Z., Aguilera, T. A., Lev-Ram, V., Steinbach, P. A., and Tsien, R. Y. (2009) Mammalian expression of infrared fluorescent proteins engineered from a bacterial phytochrome. *Science 324*, 804–807.

[196] Velazquez Escobar, F., Hildebrandt, T., Utesch, T., Schmitt, F. J., Seuffert, I., Michael, N., Schulz, C., Mroginski, M. A., Friedrich, T., and Hildebrandt, P. (2014) Structural parameters controlling the fluorescence properties of phytochromes. *Biochemistry 53*, 20–29.

[197] Gu, Z., Zhao, M., Sheng, Y., Bentolila, L. A., and Tang, Y. (2011) Detection of mercury ion by infrared fluorescent protein and its hydrogel-based paper assay. *Anal. Chem. 83*, 2324–2329.

[198] Filonov, G., and Verkhusha, V. (2013) A near-infrared BiFC reporter for in vivo imaging of protein-protein interactions. *Chem. Biol. 20*, 1078–1086.

[199] Möglich, A., and Moffat, K. (2010) Engineered photoreceptors as novel optogenetic tools. *Photochem. Photobiol. Sci. 9*, 1286–1300.

[200] Wu, Y. I., Frey, D., Lungu, O. I., Jaehrig, A., Schlichting, I., Kuhlman, B., and Hahn, K. M. (2009) A genetically encoded photoactivatable Rac controls the motility of living cells. *Nature 461*, 104–108.

[201] Levskaya, A., Chevalier, A. A., Tabor, J. J., Simpson, Z. B., Lavery, L. A., Levy, M., Davidson, E. A., Scouras, A., Ellington, A. D., Marcotte, E. M., and Voigt, C. A. (2005) Engineering Escherichia coli to see light. *Nature 438*, 441–442.

[202] Shimizu-Sato, S., Huq, E., Tepperman, J. M., and Quail, P. H. (2002) A light-switchable gene promoter system. *Nat. Biotechnol. 20*, 1041–1044.

[203] Zhang, J., Wu, X.-J., Wang, Z.-B., Chen, Y., Wang, X., Zhou, M., Scheer, H., and Zhao, K.-H. (2010) Fused-gene approach to photoswitchable and fluorescent biliproteins. *Angew. Chem. Int. Ed. 49*, 5456–5458.

[204] Evans, K., Fordham-Skelton, A., Mistry, H., Reynolds, C., Lawless, A., and Papiz, M. (2005) A bacteriophytochrome regulates the synthesis of LH4 complexesin Rhodopseudomonas palustris. *Photosynth. Res. 85*, 169–180.

[205] Litts, J. C., Kelly, J. M., and Lagarias, J. C. (1983) Structure-function studies on phytochrome. Preliminary characterization of highly purified phytochrome from Avena sativa enriched in the 124-kilodalton species. *J. Biol. Chem. 258*, 11025–31.

[206] Tasler, R., Moises, T., and Frankenberg-Dinkel, N. (2005) Biochemical and spectroscopic characterization of the bacterial phytochrome of Pseudomonas aeruginosa. *FEBS J. 272*, 1927–1936.

[207] Yoshihara, S., Shimada, T., Matsuoka, D., Zikihara, K., Kohchi, T., and Tokutomi, S. (2006) Reconstitution of blue-green reversible photoconversion of a cyanobacterial photoreceptor, PixJ1, in phycocyanobilin-producing Escherichia coli. *Biochemistry 45*, 3775–3784.

9 Appendix

9.1 Absorbance maxima of GAF-containing photoreceptors

Table 9.1: Spectroscopically characterized GAF-containing photoreceptors with their Group affiliation, chromophore and the absorbance maxima as well as names of their *15Z*- and *15E*-states. The term "Bathyp." in the Group description refers to bathyphytochromes which have the P_{fr}/ *15E*-state as ground state.

Organism	**Protein**	**Group**	λ_{max} ***15Z***	λ_{max} ***15E***	**Chromophore**	**Ref.**
Synechocystis sp. PCC 6803	*Syn*Cph2(1-2)	II	644 nm, P_r	695 nm, P_{fr}	PCB	[138]
Synechocystis sp. PCC 6803	*Syn*Cph1(1-3)	I	654 nm, P_r	702 nm, P_{fr}	PCB	[81]
Rhodopseudomonas palustris	*Rp*BphP1	I, Bathyp.	682 nm, P_r	757 nm, P_{fr}	BV	[204]
Rhodopseudomonas palustris	*Rp*BphP2	I	710 nm, P_r	750 nm, P_{fr}	BV	[143]
Rhodopseudomonas palustris	*Rp*BphP3	I	705 nm, P_r	650 nm, P_{nr}	BV	[143]
Bradyrhizobium ORS278	*Br*BphP1	I, Bathyp.	676 nm, P_r	752 nm, P_{fr}	BV	[65]
Bradyrhizobium ORS278	*Br*BphP3	I	610 nm, P_o	670 nm, P_r	PCB	[67]
Deinococcus radiodurans	*Dr*BphP	I	698 nm, P_r	750 nm, P_{fr}	BV	[66]
Avena sativa	124 kDa Phy from etiolated seedlings	I	668 nm, P_r	730 nm, P_{fr}	PΦB	[205]
Calothrix sp. PCC 7601	CphA	I	663 nm, P_r	707 nm, P_{fr}	PCB	[79]

Organism	**Protein**	**Group**	λ_{max} ***15Z***	λ_{max} ***15E***	**Chromo-phore**	**Ref.**
Synechocystis sp. PCC 6803	*Syn*Cph2(1-2)	II	644 nm, P_r	695 nm, P_{fr}	PCB	[138]
Calothrix sp. PCC 7601	CphB	I	704 nm, P_r	750 nm, P_{fr}	BV	[79]
Pseudomonas aeruginosa	*Pa*BphP	I, Bathyp.	700 nm, P_r	754 nm, P_{fr}	BV	[206]
Synechococcus sp. OS-B'	*Sy*B-Cph1(1-2)	II	630 nm, P_r	704 nm, P_{fr}	PCB	[88]
Synechocystis sp. PCC6803	*Syn*Cph2(5-6)	III	417 nm, P_b	525 nm, P_g	PCB PVB	[144,145]
Thermosynecho-coccus elongatus	*Te*PixJ	III	428 nm, P_b	529 nm, P_g	PVB	[123]
Thermosynecho-coccus elongatus	Tlr0924	III	434 nm, P_b	538 nm, P_g	PVB	[112]
Nostoc sp. PCC 7120	All1688	III	414 nm, P_b	560 nm, P_g	PCB	[127]
Nostoc sp. PCC 7120	All2239	III	414 nm, P_b	586 nm, P_g	PCB	[127]
Nostoc sp. PCC 7120	Alr3356	III	408 nm, P_b	598nm, P_o	PCB	[127]
Nostoc sp. PCC 7120	All3691-GAF2	III	408 nm, P_b	490 nm, P_g	PVB	[127]
Nostoc sp. PCC7120	All1280-GAF2	III	413 nm, P_b	560 nm, P_g	PCB PVB	[127]
Nostoc sp. PCC 7120	Alr1966-GAF2	III	428 nm, P_b	514 nm, P_g	PCB PVB	[127]
Nostoc sp. PCC 7120	Alr2279	III	424 nm, P_b	534 nm, P_g	PCB PVB	[127]
Synechocystis sp. PCC 6803	*Sy*PixJ	III	410 nm, P_b	535 nm, P_g	PCB	[207]
Nostoc sp. PCC 7120	*An*PixJ-GAF2	III	648 nm, P_r	543 nm, P_g	PCB	[108]
Nostoc punctiforme	*Np*AF142g2	III	650 nm, P_r	532 nm, P_g	PCB	[186]
Nostoc punctiforme	*Np*R4776g2	III	652 nm, P_r	538 nm, P_g	PCB	[186]

Organism	Protein	Group	λ_{max} **15Z**	λ_{max} **15E**	Chromophore	Ref.
Synechocystis sp. PCC 6803	*Syn*Cph2(1-2)	II	644 nm, P_r	695 nm, P_{fr}	PCB	[138]
Nostoc punctiforme	*Np*F2854g3	III	656 nm, P_r	546 nm, P_g	PCB	[186]
Nostoc punctiforme	*Np*R5113g2	III	650 nm, P_r	528 nm, P_g	PCB	[186]
Nostoc punctiforme	*Np*R3784	III	652 nm, P_r	554 nm, P_g	PCB	[186]
Synechocystis sp. PCC 6803	*Sy*CcaS	III	538 nm, P_g	672 nm, P_r	PCB	[109]
Fremyella diplosiphon	RcaE	III	532 nm, P_g	661 nm, P_r	PCB	[150]
Nostoc punctiforme ATCC29133	Ccas	III	536 nm, P_g	672 nm, P_r	PCB	[125]
Nostoc sp. PCC 7120	AphC-GAF1	III	635 nm, P_r	685 nm, P_{fr}	PCB	[116]
Nostoc sp. PCC 7120	AphC-GAF2	III	645 nm, P_r	595 nm, P_o	PCB	[116]
Synechocystis sp. PCC 6803	*Sy*CikA	III	402 nm, P_v	566 nm, P_y	PCB	[124]

9.2 Crystal and NMR structures of GAF-containing photoreceptors

Table 9.2: Phytochrome and CBCR crystal and NMR structures in the PDB data base until 24.02.2014.

Protein	Organism	Photostate	Resolution	Domains	PDB code	Year of Deposition
Phytochromes						
*Dr*BphP	*Deinococcus radiodurans*	P_r	2.50 Å	PAS-GAF	1ZTU	2005
*Dr*BphP Y307S	*Deinococcus radiodurans*	P_r	2.15 Å	PAS-GAF	2O9B	2007
*Dr*BphP Y307S	*Deinococcus radiodurans*	P_r	1.45 Å	PAS-GAF	2O9C	2007

Protein	Organism	Photostate	Resolution	Domains	PDB code	Year of Deposition
*Dr*BphP D207H, Y307S	*Deinococcus radiodurans*	P_r	1.72 Å	PAS-GAF	3S7P	2011
*Dr*BphP D207H, Y307S	*Deinococcus radiodurans*	P_r	1.24 Å	PAS-GAF	3S7O	2011
*Dr*BphP D207H, Y307S, alternative His207 conformation	*Deinococcus radiodurans*	P_r	2.45 Å	PAS-GAF	3S7N	2011
*Dr*BphP monomeric F145S, D207H, Y263F, L311E, L314E	*Deinococcus radiodurans*	P_r	1.75 Å	PAS-GAF	3S7Q	2012
*Dr*BphP, monomeric	*Deinococcus radiodurans*	P_r	1.70 Å	PAS-GAF	4IJG	2013
*Pa*BphP	*Pseudomonas aeruginosa*	P_{fr}	2.90 Å	PAS-GAF-PHY	3C2W	2008
*Pa*BphP Q188L	*Pseudomonas aeruginosa*	Mixed P_r/P_{fr}	2.97 Å	PAS-GAF-PHY	3IBR	2009
*Pa*BphP Q188L	*Pseudomonas aeruginosa*	Mixed P_r/P_{fr}	2.85 Å	PAS-GAF-PHY	3G6O	2009
*Pa*BphP	*Pseudomonas aeruginosa*	P_{fr}	2.55 Å	PAS-GAF-PHY	3NHQ	2011
*Pa*BphP intermediate L1 $P_{fr}\rightarrow P_r$	*Pseudomonas aeruginosa*	intermediate L1	2.80 Å	PAS-GAF-PHY	3NOP	2012
*Pa*BphP intermediate L2 $P_{fr}\rightarrow P_r$	*Pseudomonas aeruginosa*	intermediate L2	2.70 Å	PAS-GAF-PHY	3NOT	2012
*Pa*BphP intermediate L3 $P_{fr}\rightarrow P_r$	*Pseudomonas aeruginosa*	intermediate L3	3.0 Å	PAS-GAF-PHY	3NOU	2012
*Rp*BphP3	*Rhodopseudomonas palustris*	P_r	2.20 Å	PAS-GAF	2OOL	2007

Protein	Organism	Photostate	Resolution	Domains	PDB code	Year of Deposition
*Rp*BphP1	*Rhodopseudomonas palustris*	P_{fr}	2.90 Å	PAS-GAF-PHY-PAS	4GW9	2012
*Rp*BphP2	*Rhodopseudomonas palustris*	P_r	1.79 Å	PAS-GAF	4EO4	2012
*Sy*B-Cph1	*Synechococcus* sp.	P_r	Solution NMR	GAF1	2K2N	2008
*Sy*B-Cph1	*Synechococcus* sp.	P_r	Solution NMR	GAF1	2KOI	2009
*Sy*B-Cph1	*Synechococcus* sp.	P_{fr}	Solution NMR	GAF1	2KLI	2009
*Sy*B-Cph1 refined	*Synechococcus* sp.	P_{fr}	Solution NMR	GAF1	2LB5	2011
*Sy*B-Cph1 refined	*Synechococcus* sp.	P_r	Solution NMR	GAF1	2LB9	2011
*Syn*Cph1	*Synechocystis* sp. PCC 6803	P_r	2.21 Å	PAS-GAF-PHY	2VEA	2008
*Syn*Cph1 Y263F	*Synechocystis* sp. PCC 6803	P_r	1.95 Å	PAS-GAF-PHY	3ZQ5	2011
*Syn*Cph2(1-2)	*Synechocystis* sp. PCC 6803	P_r	2.60 Å	GAF1-GAF2	4BWI	2013
CBCRs						
*An*PixJ	*Anabaena* (*Nostoc*) sp. PCC 7120	*15Z*	1.80 Å	GAF2	3W2Z	2013
*Te*PixJ	*Thermosynechococcus elongatus*	*15E*	2.00 Å	GAF	3VV4	2013
*Te*PixJ	*Thermosynechococcus elongatus*	*15Z*	2.42 Å	GAF	4FOF	2013
*Te*PixJ with PVB	*Thermosynechococcus elongatus*	*15E*	1.77 Å	GAF	4GLQ	2013

Protein	**Organism**	**Photostate**	**Resolution**	**Domains**	**PDB code**	**Year of Deposition**
*Te*PixJ	*Thermosynechococcus elongatus*	*15Z*	Solution NMR	GAF	2M7U	2014
*Te*PixJ	*Thermosynechococcus elongatus*	*15E*	Solution NMR	GAF	2M7V	2014

9.3 Abbreviations

Å	Ångström
*An*PixJ	CBCR from *Anabaena* (*Nostoc*) sp.
*At*BphP1	Bacteriophytochrome 1 from *Agrobacterium tumefaciens*
Bathy-BphP	Bathy-bacteriophytochrome
BLUF	Sensors of Blue-light using FAD
BphP	Bacteriophytochrome
BV	Biliverdin
CBCR	Cyanobacteriochrome
CBS	Domain in cystathionine beta-synthases
CCA	Complementary chromatic adaption
CD	Circular dichroism spectroscopy
C-di-GMP	Cyclic diguanylate
cGMP	Cyclic guanosine monophosphate
COP1	Constitutive photomorphogenic 1
Cph2	Cyanobacterial phytochrome 2
CphB	Cyanobacterial phytochrome B
CRY	Cryptochromes
DBV	Dihydrobiliverdin
DGC	Diguanylate cyclase
Dph	Diatom phytochromes
*Dr*BphP	Bacteriophytochrome from *Deinococcus radiodurans*
EAL	Output domain with the conserved amino acid motif Glu/Ala/Leu
FAD	Flavin adenine dinucleotide
FHL	FHY1-like
FhlA	Formate hydrogen lyase transcription activator
FHY1	Far red elongated hypocotyl 1
FMN	Flavin mononucleotide
Fph	Fungal phytochromes
GAF	cGMP phosphodiesterase /adenyl cyclase / FhlA
GGDEF	output domain with the conserved amino acid motif Gly/Gly/Asp/Glu/Phe
GMP	Guanosine monophosphate
GTP	Guanosine triphosphate
HAMP	domain in HKs, adenyl cyclases, methyl-accepting proteins and phosphatases
HD-GYP	Effector domain with the conserved amino acids His/Asp and Gly/Tyr/Pro
HFR1	Long hypocotyl in far red 1
HK	Histidine kinase

HO1	Heme oxygenase
HOS	2-helix-output sensor
HPt	Histidine-containing phophotransfer protein
HY2	biliverdin reductase
HY5	Long hypocotyl
I_P	Primary inhibition site
I_S	Secondary inhibition site
LAF1	Long after far red light 1
LreB	Light response B
LOV	Light oxygen voltage domain
MBV	Mesobiliverdin
MCP	Methyl-accepting chemotaxis protein domain
5,10-MTHF	5,10-Methenyltetrahydrofolat
NDPK2	Nucleoside phosphate dikinase 2
NLS	Nuclear localization signal
NMR	Nuclear magnetic resonance
NTE	N-terminal extension
*Pa*BphP	Bacteriophytochrome from *Pseudomonas aeruginosa*
PAS	Per-ARNT (Aryl hydrocarbon receptor nuclear transporter)-Sim
P_b	blue light-absorbing conformation
PCB	Phycocyanobilin
PCD	Photosensory core domain
PcyA	PCB:ferredoxin oxidoreductase
PDE	Phosphodiesterase
PEB	Phycoerythrobilin
P_{fr}	Far red light-absorbing phytochrome conformation
P_g	green light-absorbing conformation
pGpG	Dinucleotide 5´-phosphoguanylyl-(3´-5´)-guanosine
PHY	phytochrome domain
Phy	phytochrome
PIF	Phytochrome interacting factor
PIL	PIF3-like protein
PKS1	phytochrome kinase substrate 1
P_{nr}	Near-red light-absorbing phytochrome conformation
P_o	Orange light-absorbing phytochrome conformation
PΦB	Phytochromobilin
P_r	Red light-absorbing phytochrome conformation
PUB	Phycourobilin

P_v	violet light-absorbing conformation
PVB	Phycoviolobilin
P_y	yellow light-absorbing conformation
PYP	Photoactive yellow protein
REC	Response regulator receiver domain (also RR)
r.m.s.	root mean square
*Rp*BphP1	Bacteriophytochrome 1 from *Rhodopseudomonas palustris*
RR	Response regulator receiver domain (also REC)
RR	Resonance Raman spectroscopy
*Syn*Cph1	Cyanobacterial phytochrome 1 from *Synechocystis* sp. PCC 6803
*Syn*Cph2	Cyanobacterial phytochrome 2 from *Synechocystis* sp. PCC 6803
*Te*PixJ	CBCR from *Thermosynechococcus elongatus*
TIM	Triosephosphate isomerase
TPcR	10-thio-phycocyanorubin
TPvR	10-thio-phycoviolorubin
UV-B	Ultraviolet-B
UVR8	UV resistance locus 8
VeA	Velvet A

9.4 Amino acids

amino acid	3-Letter code	1-Letter code
Alanine	Ala	A
Arginine	Arg	R
Asparagine	Asn	N
Aspartic acid	Asp	D
Cysteine	Cys	C
Glutamic acid	Glu	E
Glutamine	Gln	Q
Glycine	Gly	G
Histidine	His	H
Isoleucine	Ile	I
Leucine	Leu	L
Lysine	Lys	K
Methionine	Met	M
Phenylalanine	Phe	F
Proline	Pro	P
Serine	Ser	S
Threonine	Thr	T
Tryptophan	Trp	W
Tyrosine	Tyr	Y
Valine	Val	V

10 Acknowledgements

First I would like to thank Prof. Dr. Lars-Oliver Essen for giving me the opportunity to write my PhD thesis in his group about a fascinating and inspiring project. It was a pleasure for me to be able to present my work on international conferences and discuss my results with other scientists from all over the world.

I thank Prof. Dr. Alfred Batschauer, who was willing to do the second evaluation of my PhD thesis and Prof. Dr. Norbert Hampp for being in my PhD committee.

Dr. Uwe Linne, Dr. Jo Mailliet, Dr. David von Stetten, Dr. Vitaly A. Sineshchekov, Prof. Dr. Peter Hildebrandt, Prof. Dr. Jon Hughes, Prof. Dr. Annegret Wilde, Dr. Grazia Daminelli-Widany, Prof. Dr. Maria Andrea Mroginski, Alexander Gutt and Prof. Dr. Wolfgang Gärtner I want to thank for all the experiments and fruitful cooperations.

I thank the students Anne Nöll, Michael Kock, Kathrin Hnida, Maximilian Reuter, Silke von Horsten, Jakub Gunera, Tobias Seitz, Franka Schreiner and Jana Lorenz for their work and their contribution to the project. Furthermore, I would like to thank Sven De Causmaecker, Veronika Angerer, Philipp Savakis and Silke von Horsten whose diploma or master thesis I supervised, for a great time and their contributions to the phytochrome project. In addition, I thank Silke von Horsten as well as Dr. Yann Geisselbrecht and Philipp Savakis for reading the manuscript.

Especially Veronika Angerer, Petra Gnau, Silke von Horsten, Michael Kock, Prof. Dr. Lars-Oliver Essen and Ellen Essen I would like to thank for their great support in difficult times over the last two years.

My extraordinary colleagues from the Essen group, I want to thank for an enjoyable and memorable time. Working in such a nice atmosphere with all the serious, interesting, funny and not exclusively academic discussions was a pleasure to me. I really had a great time and also enjoyed activities outside the lab as well as our seminars in alpine environment. The social cohesion is our strength and I hope that the group will keep its spirit.

In the end, I would like to thank my mother and my dearest friends who inexhaustibly support me on all my steps of life.